2016

Protein Regulators of Phosphoinositides as Promoters of Cancer Metastasis

Caitlin Anne Sengelaub

PROTEIN REGULATORS OF PHOSPHOINOSITIDES AS PROMOTERS OF CANCER METASTASIS

A Thesis Presented to the Faculty of

The Rockefeller University

in Partial Fulfillment of the Requirements for

the degree of Doctor of Philosophy

by

Caitlin Anne Sengelaub

June 2016

PROTEIN REGULATORS OF PHOSPHOINOSITIDES AS PROMOTERS OF CANCER METASTASIS

Caitlin Anne Sengelaub, Ph.D.

The Rockefeller University 2016

Metastasis, the spread of cancer cells from a primary tumor to a distal organ, represents the predominant cause of mortality in patients with solid tumors. However, the molecular mechanisms underpinning this multistep progression are poorly defined. Successful metastasis requires a cancer cell to acquire multiple capabilities, including the ability to migrate, invade, and co-opt the microenvironment in the distal organ for colonization. Many of these phenotypes require the actions of a family of lipids called phosphoinositides (PIs). Although structurally small molecules and minor components of the cellular lipidome, PIs are critical mediators of many cellular processes through their localization, abundance, and recruitment of effector proteins. The actions of PIs are orchestrated by PI regulator proteins that bind to or act upon each PI. Identifying and characterizing PI regulator proteins that promote metastasis could elucidate novel cellular pathways and enable the development of therapeutic approaches targeting mechanisms unique to metastatic disease.

In this thesis, I describe work delineating the molecular mechanisms of three PI regulator proteins in promoting breast cancer metastasis. These proteins were initially identified as putative targets of the metastasis suppressor miRNAs, miR-126 and miR-335. We identify PITPNC1 as amplified in nearly half human breast cancers, and

overexpressed in metastatic melanoma, breast, and colon cancer. Biochemical and cell-biological experiments reveal that PITPNC1 binds to phosphatidyl inositol 4-phosphate (PI4P) in the Golgi. Through this binding, PITPNC1 recruits RAB1B to the Golgi, which in turn recruits GOLPH3. GOLPH3 facilitates elongation of the Golgi structure, enhancing vesicular release. Through this pathway, PITPNC1 increases the secretion of a set of pro-angiogenic and pro-invasive proteins including ADAM10, FAM3C, HTRA1, MMP1, and PDGFA.

In the second half of this thesis, I characterize the molecular mechanism of PTPRN2 and PLCβ1 in driving breast cancer metastasis by enhancing cellular migration. I find that increased expression of PTPRN2 and PLCβ1 associates with human metastatic relapse. PTPRN2 and PLCβ1 enzymatically reduce plasma membrane phosphatidyl inositol 4,5-bisphosphate (PI(4,5)P2) through two independent mechanisms. Reduction of plasma membrane PI(4,5)P2 abundance releases the PI(4,5)P2-binding protein cofilin from its membrane-bound inactive state into the cytoplasm. Cytoplasmic cofilin binds and severs actin, generating free barbed ends in actin filaments and inducing actin polymerization. PTPRN2 and PLCβ1-mediated actin remodeling dynamics increase cellular migration, a key metastatic phenotype.

ACKNOWLEDGEMENTS

The work described in this thesis would not have been possible without the time, effort, and support of many individuals. I would like to thank my advisor Sohail Tavazoie, for conceiving of these projects and providing tremendous resources and support in pursuing them. Sohail's enthusiasm for cancer biology and scientific research is contagious and motivated me to dive into a field in which I had no prior training, for which I am very grateful. Thank you for your mentorship and for creating an environment where I was free to pursue my hypotheses.

I am extremely fortunate to have conducted part of this work in collaboration with a previous postdoctoral fellow in the laboratory, Dr. Nils Halberg. Nils patiently and carefully taught me the vast majority of the techniques used in this research. His fearless attitude and tenacity have greatly benefitted my graduate training and this research.

Many thanks to Dr. Howard Hang and Dr. Sandy Simon for their help while serving on my Faculty Advisory Committee. I am grateful for their support and insight in guiding these projects. Thank you to Dr. Timothy Chan for serving as my external examiner at my thesis defense.

I am very grateful to present members of the Tavazoie laboratory for creating a collegial and encouraging laboratory environment. I am especially indebted to Dr. Claudio Alarcon and Dr. Hani Goodarzi for their vast scientific knowledge, advice, and troubleshooting help. Thanks to Dr. Lisa Fish, Dr. Hyeseung Li, Dr. Jiamin Loo, Zander Nguyen, Dr. Kim Png, and Raissa Tanqueco and for their help in collecting reagents,

advice with protocols, and camaraderie. Thanks also to our laboratory's administrator, Emily Mandel, for her swift and kind support with all logistical matters. Special thanks Kristina Navrazhina, a previous undergraduate in the laboratory, for allowing me to hone my teaching abilities on her and for flawlessly performing several of the experiments in this thesis.

I would like to thank Dr. Henrik Molina in the Rockefeller Proteomics Resource Center for his assistance with mass spectrometry and SILAC, as well as for the many hours he spent teaching me mass spectrometry sample preparation and analyzing data from mass spectrometry experiments. Thanks also to Dr. Allison North, Dr. Kaye Thomas, and Dr. Pablo Ariel in the Rockefeller Bio-Imaging Resource Center for their assistance with confocal microscopy, and to Dr. Kunihiro Uryu for his assistance with electron microscopy.

Thanks to Cris Rosario, Kristen Cullen, Marta Delgado, and Emily Harms in the Dean's Office for all of their efforts in supporting the Rockefeller graduate program and their commitment to the graduate students.

Thank you to my family—Dr. Lisa Kurz, Dr. Dale Sengelaub, Dr. Cara Wellman, and Jack Sengelaub—with whom I could not have done this without. Your love, humor, and encouragement have always propelled me forward. I am exceptionally grateful for my Mom's tireless and clever editing as well as my Dad's meticulous proofreading. This thesis is 100-fold better thanks to them.

Finally, I would like to thank Joshua Horwitz, who has provided intellectual insight, technical assistance, moral support, and boundless love throughout the execution of this work. Science is lucky to have him, and so am I.

TABLE OF CONTENTS

LIST OF FIGURES

LIST OF TABLES

CHAPTER I: INTRODUCTION

Breast Cancer in the United States: Subtyping and Staging

The American Cancer Society estimates that more than 230,000 new cases of invasive breast cancer will be diagnosed in women in the United States in 2015, making breast cancer the most common type of cancer among women in the United States. It is estimated that one in eight women in the U.S. will develop invasive breast cancer during her lifetime. Breast cancer is the second most common cancer-related cause of death among women after lung cancer, with approximately 40,000 deaths per year. Breast cancer can also afflict men although with a 100-fold lower incidence rate. An estimated 2,300 men will be diagnosed with breast cancer in 2015 and 400 will die from breast cancer. Additionally, approximately 60,000 women will be diagnosed with carcinoma in situ (CIS), a non-invasive form of breast cancer with a survival rate of essentially 100% (The American Cancer Society, 2015).

Breast cancer is defined as neoplastic growth in the epithelial cells of the lobules and ducts in the breast. Brest cancer is clinically heterogeneous disease with many histopathological subtypes identified. The most common histopathological presentation is invasive ductal carcinoma, which represents 50-80% of breast cancer cases (Polyak, 2011). Other less common subtypes include lobular carcinoma, tubular carcinoma, mucinous carcinoma, medullary carcinoma, and inflammatory breast cancer. Histological typing alone has proven to be a poor prognostic marker for survival and metastatic relapse in patients (Ellis et al., 1992), indicating a role for molecular drivers of breast

cancer progression that are independent of the morphological features of the tumor as defined by these subtypes.

Advances in cellular expression profiling using high-throughput microarray-based technology enabled the identification of molecular subtypes of breast cancer with improved prognostic ability and prediction of effective treatment. Based on these studies, four major subtypes have been identified and are now utilized in clinical diagnosis: luminal-A, luminal-B, *HER2* amplified, and basal-like (Perou et al., 2000; Sorlie et al., 2001; Sotiriou and Pusztai, 2009). Luminal subtypes A and B are characterized by their expression of the estrogen receptor and/or progesterone receptor, and comprise approximately 70% of diagnosed malignancies (Sotiriou and Pusztai, 2009) . An estimated 30% of patients with luminal B tumors also overexpress HER2. The luminal A subtype is less proliferative than the luminal B subtype as measured by Ki67 staining, and consequently patients whose tumors are luminal B subtype have a poorer prognosis (Cheang et al., 2009).

HER2 amplified tumors exhibit high expression of HER2 and low expression of the estrogen and progesterone receptors. They represent approximately 15% of invasive breast cancers, and have a poorer prognosis than the luminal subtypes (Slamon et al., 1987). Due to genomic amplification, breast cancers may have 25-50 copies of the HER2 gene resulting in 40-100-fold increases in HER2 protein levels (Kallioniemi et al., 1992; Venter et al., 1987). *HER2* encodes the human epidermal growth factor receptor, an oncogene that when overexpressed promotes tumorigenesis through several pathways including inducing mitosis and preventing apoptosis leading to deregulated cellular

proliferation, disrupting cell adhesion and polarity, and enhancing invasive capacity (Moasser, 2007).

Basal-like tumors are characterized by high expression of basal epithelial genes and basal cytokeratins and low expression of estrogen receptor, progesterone receptor, and *HER2*. The basal subtype is correlated with mutations in the *BRCA1* gene, a tumor-suppressor gene involved in the repair of DNA double-strand breaks (Rakha and Ellis, 2009). Basal-like tumors grow at a more rapid rate than other types, and are more likely to occur in women under age 50. Additionally these tumors are more likely to present as a higher histological grade indicating that the cancer cells are dividing more rapidly (higher mitotic index), are poorly differentiated, and show marked morphological variation from normal breast cells. Basal-like tumors are characterized as triple-negative breast cancer (TNBC) when they are negative for immunohistochemical expression of the estrogen receptor, progesterone receptor, and *HER2*. TNBC represent 12-17% of women diagnosed with breast cancer (Foulkes et al., 2010).

Breast cancer is diagnosed as four stages. Stages I through III are characterized by the size of the tumor and whether the tumor has spread to nearby lymph nodes. Stage IV is characterized as the spread of the tumor to a distant organ, or the process of metastasis. The five-year survival rate for women diagnosed with breast cancer varies widely depending on the tumor stage at diagnosis. According to the National Cancer Institute's Surveillance, Epidemiology, and End Results (SEER) data, the five-year relative survival rate for breast cancer when the tumor is confined to the primary site is approximately 99%. When the tumor has spread to regional lymph nodes, the survival rate decreases to 72-90%, depending on tumor size and number of cancer-positive lymph nodes. However,

when the cancer has metastasized to a distal site, the survival rate drops dramatically to 22% (National Cancer Institute, 2015). For the vast majority of breast cancer-related deaths, it is not the primary tumor but the occurrence of distal metastasis that is the primary cause of death.

Treatments for Breast Cancer

Current treatment for breast cancer depends upon the subtype and stage at diagnosis. Primary therapy for breast cancer involves surgical removal of the tumor, unless the tumor is too large to be surgically resected. Adjuvant therapies are then administered to prevent cancer recurrence, and these include radiation therapy and chemotherapy. Additional adjuvant therapies are targeted depending on the breast cancer molecular subtype. For breast cancers with overexpression of the estrogen or progesterone receptors, endocrine therapy is administered that specifically targets these receptors. Endocrine therapy primarily comprises two classes: selective estrogen receptor modulators and aromatase inhibitors. Selective estrogen receptor modulators such as tamoxifen bind the estrogen receptor competitively and prevent binding by estrogens, inhibiting cancer cell growth. Tamoxifen administration reduces the relative risk of death from breast cancer by 30% (Yeo et al., 2014). Aromatase inhibitors reduce estrogens by blocking the aromatase enzyme from producing estrogens. As with the selective estrogen receptor modulators, aromatase inhibitors reduce cancer cell growth by lowering the amount of estrogens that reaches the cancer cell (Smith and Dowsett, 2003). For patients whose tumors exhibit *HER2* amplification, the primary targeted adjuvant therapy is trastuzumab. Trastuzumab, marketed as Herceptin, is a monoclonal antibody

that binds to the HER receptors to inhibit their ability to induce cellular growth and progression. Trastuzumab slow disease progression and reduces the risk of death from breast cancer by 20% in patients (Slamon et al., 2001).

There are currently no targeted biological therapeutics for women with TNBC. Given their low expression of estrogen and progesterone receptors, these tumors to not respond to endocrine therapy. Approximately 20% of women with TNBC will respond to chemotherapy, however the majority shows no response (Foulkes et al., 2010). TNBC patients with BRCA gene mutations may benefit from poly-ADP ribose polymerase (PARP) inhibitors. Cells with BRCA mutations are highly sensitive to PARP activity, a base-excision enzyme in DNA double-strand break repair. Addition of PARP inhibitors to these cells induces chromosomal instability and results in apoptosis (Farmer et al., 2005). Various PARP inhibitor compounds are currently undergoing clinical trials in breast cancer patients. Identifying additional genes that are critical for TNBC tumor growth and disease progression has the potential to identify novel targeted therapeutics for this patient population.

Since metastasis is the predominant cause of mortality in breast cancer patients, identifying therapeutic targets of metastatic progression represents an unmet clinical need of high importance.

Molecular Mechanisms of Metastasis

In order to treat or prevent the process of metastasis, it is necessary to understand the molecular mechanisms of metastasis and determine key mediators of metastatic progression. Metastasis requires a cascade of steps, each requiring distinct phenotypes and molecular capacities of a cancer cell. A cancer cell in the primary tumor must migrate out of the primary tumor site, intravasate into the vasculature, survive in the blood vessels, arrest in capillary beds, extravasate out of the vasculature, and inhabit a distal organ. Each step in the metastatic cascade is highly inefficient and may be rate-limiting, such that only an estimated 0.01% of all disseminated cancer cells ultimately successfully colonize a secondary site (Fidler, 1970).

The primary tumor is composed of a heterogeneous population of cells, likely driven by the selective pressure placed on the tumor, such as lack of nutrients, lack of oxygen, or low pH in combination with the genetic instability frequently present within cancer cells. Genetic instability in cancer cells can be due to mutations in DNA repair proteins, telomeric dysfunction, or abnormal mitosis (Chiang and Massague, 2008), and this increases the frequency of alterations that produce varied cellular phenotypes. Cancer cells must be able to overcome many barriers in order to survive and grow, such as the ability to sustain proliferation, resist cell death, evade the immune system, and induce angiogenesis (Hanahan and Weinberg, 2011). However, in addition to these capabilities to survive in the primary tumor, metastatic cells must possess additional abilities in order to metastasize. The molecular and phenotypic variation in the primary tumor cells produces a subpopulation of cells capable of completing the metastatic cascade.

The first step of the metastatic cascade requires that a cancer overcome cell-intrinsic and cell-extrinsic barriers to leave the primary tumor site. Metastatic cancer cells exhibit reduced cellular adhesion, a necessary quality for a cancer cell to leave the tumor colony. This reduced cellular adhesion is often a result of a loss of E-cadherin, a transmembrane protein that tethers cells together forming junctions (Perl et al., 1998). Additionally, cancer cells may recruit stromal cells, which secrete proteinases capable of cleaving cell-adhesion integrins, enabling cancer cells to dissociate from the primary tumor (Kessenbrock et al., 2010).

Another phenotype that is required for metastasis in increased migratory capacity, enabling cancer cells to traffic throughout the body. Through advances in *in vivo* imaging of invasive cancer cells it was noted that cancer cells migrate at high speed along collagen fibers in the extracellular matrix, and this phenotype correlated with the metastatic capacity of these cells (Condeelis and Segall, 2003). The enhanced migratory capacity of cancer cells is mediated by changes in the actin cytoskeleton, cell adhesion contact disassembly, and factors in the microenvironment that induce signal transduction (Condeelis et al., 2005). Cancer cells migrate towards growth factors, a process known as chemotaxis. For example, tumor-associated macrophages secrete epidermal growth factor (EGF), which stimulates cancer cell migration by binding to the EGF receptor and inducing actin polymerization and motility (Wyckoff et al., 2004). The RHO family of small GTPases have also been shown to be necessary for cancer cell motility. Both RHO and RAC proteins have been identified as overexpressed in various cancers, and this overexpression correlates with worse patients outcomes (Sahai and Marshall, 2002).

In addition to migration, metastatic cells must also be able to invade through tissue in order to metastasize. Cancer cells need to overcome components of the tumor microenvironment that act to limit invasion, such as the extracellular matrix and basement membrane. The extracellular matrix (ECM) is composed of proteoglycans, and fibers such as collagens, elastins, fibronectins, and glycoproteins such as laminins. The basement membrane is layers of ECM that separate the endothelium from deeper tissues. Invasive cancer cells form membrane protrusions called invadopodia to move through the ECM and penetrate the basement membrane to gain access to the vasculature. Invadopodia formation is mediated by WASP proteins and the Arp2/3 protein complex, which are required for invasion in breast cancer cells (Gligorijevic et al., 2012). Invasive cancer cells degrade the extracellular matrix by secreting proteinases, such as matrix metalloproteinase 1 (MMP1). The degradation of the ECM is also facilitated by MMPs secreted by stromal cells including tumor-associated macrophages and fibroblasts (Kessenbrock et al., 2010). The degradation of the ECM by cancer cells and the ability to coordinate cellular migration and invasion are necessary features for cancer cells to begin the metastatic process.

Once cancer cells have migrated away from the primary tumor site and invaded through the ECM, they next invade into the vasculature, a process called intravasation. Cancer cells must then survive in the circulation, where they are subjected to sheering forces as part of hemodynamic flow. During travel through the circulation, cancer cells are not adhered to the ECM, a condition that triggers programmed cell death in normal cells (a mechanism referred to as anoikis). Cancer cells are able to resist anoikis, although the mechanism of this ability is not yet described. Additionally, cancer cells have been

found to bind to platelets. Binding to platelets protects cancer cells from turbulent blood flow and shields these cells from immune surveillance (Nash et al., 2002). These mechanisms enhance the ability of metastatic cells to survive in travel to a secondary site in the organism.

Cancer cells in the circulation frequently arrest in capillary beds, where a subset of cells are able to invade out of the blood vessel in the process of extravasation to arrive at a secondary organ. However, the location of metastatic colonies is not sufficiently explained by blood flow patterns. In early clinical studies of metastasis, it was noted that metastatic nodules form preferentially in specific organs, leading Stephen Paget to propose his "seed and soil" hypothesis, suggesting that cancer cells ("seeds") preferentially grow in specific compatible microenvironments ("soil") (Paget, 1889). The most common sites of breast cancer metastasis are the brain (10%), lung (20%), liver (30%), and bone (40%). However in TNBC, the rates of distal metastasis are higher in the brain and lung (30% and 40%, respectively) and lower in in the bone (10%) (Foulkes et al., 2010). The organ specificity of metastasis for various cancers highlights the importance of the interactions between cancer cells and their microenvironment. The distal organs must facilitate the initial survival of the extravasated cancer cells, and the cancer cells must be able to co-opt this novel organ site for their growth.

In the distal organ, the cancer cells initiate colonies that proliferate to form metastatic nodules, hindering the organ's structure and function until organ failure occurs. However, this process may happen acutely, or cancer cells may enter dormancy for a period of years. Consequently a cancer patient may remain in remission for several years before the onset of metastatic relapse. Patients with *HER2*-amplified tumors or

TNBC tend to relapse within five years, while patients with luminal tumor subtypes demonstrate a constant rate of relapse over 10 to 15 years (Smid et al., 2008). Recent studies have indicated that cancer cells undergo cell cycle arrest upon entering the distal organ and require cell-extrinsic and cell-intrinsic signals to reactivate (Giancotti, 2013). For example, a secreted antagonist of TGFβ ligands, Coco, accumulates on the surface of metastatic cancer cells in the lung and shields them from the inhibitory action of growth-suppressing proteins (Gao et al., 2012).

It is clear from the complexity of the metastatic cascade that the coordinated action of many genes is required for its completion. Full dissection of the molecular mechanisms governing these processes has yet to be achieved, and given the molecular heterogeneity in patients' primary tumors, may involve a multitude of gene pathways each capable of generating a given metastatic phenotype. One mechanism by which cancer cells coordinate the expression of a network of metastatic gene products is post-transcriptional regulation carried out by small noncoding microRNAs.

Regulation of Metastasis by MicroRNAs

MicroRNAs or miRNAs are small noncoding RNAs that are processed through cleavage events to generate 21-26-nucleotide miRNA duplexes (Kim, 2005; Winter et al., 2009). One strand of the miRNA duplex is loaded into the RNA-induced silencing complex (RISC), and the miRNA guides the binding of the RISC complex to messenger RNAs (mRNAs) with sequence complementarity (Liu et al., 2004). Binding of mRNAs by the RISC leads to translational repression, reducing gene and protein expression of a given miRNA's target transcript (Filipowicz et al., 2008). miRNAs may share sequence

complementarity with multiple genes, enabling a single miRNA to regulate the expression of several genes concurrently. Deregulated miRNA expression as a mechanism to modulate the expression of a gene network is an established feature of metastasis in multiple cancers, including breast, colorectal, gastric cancers, melanoma, and hepatocellular carcinoma (Li et al., 2011b; Loo et al., 2015; Pencheva et al., 2012; Tavazoie et al., 2008; Wong et al., 2011).

To identify miRNA regulators of metastasis, poorly metastatic MDA-MB-231 and CN34 breast cancer cell populations were subjected to *in vivo* selection to enrich for subpopulations with the ability to colonize the lungs (Pollack and Fidler, 1982). The resulting LM2 and CNLM1a1 sublines exhibit increased lung metastatic capacity relative to their respective parental populations (Minn et al., 2005; Tavazoie et al., 2008). Small RNA profiling of the *in vivo*-selected highly metastatic breast cancer cells and their poorly metastatic parental cell populations revealed miR-126 and miR-335 as silenced in the highly metastatic sublines. Depletion of these miRNAs increased the metastatic capacity of breast cancer cells while overexpression of either miRNA abrogated metastatic colonization capacity, establishing miR-126 and miR-335 as functional suppressors of breast cancer metastasis. Breast cancer patients whose primary tumors' express low levels of miR-126 and miR-335 have worse overall survival and relapse-free survival compared to patients whose primary tumors' express high levels of these miRNAs (Tavazoie et al., 2008). Interestingly, miR-126 has now been identified as a tumor suppressor miRNA in lung, cervical, pancreatic, colorectal, and gastric cancers as well (Feng et al., 2010; Guo et al., 2008; Hamada et al., 2012; Wang et al., 2008; Yanaihara et al., 2006). miR-335 has also been identified as a suppressor of metastasis in

small cell lung, gastric, and ovarian cancers (Cao et al., 2013; Gong et al., 2014; Yan et al., 2012).

These microRNAs mediate their effects through their downstream gene targets. In highly metastatic breast cancer cells, silencing of these miRNAs de-represses the expression of a set of pro-metastatic genes. miR-126 was demonstrated to repress the expression of *IGFBP2*, *MERTK*, and *PITPNC1*, which enhance metastasis through the recruitment of endothelial cells (Png et al., 2012). miR-335 represses the expression of several pro-metastatic genes, including *SOX4, TNC*, *PTPRN2* and *PLCB1* (Tavazoie et al., 2008). We were intrigued by the finding that three of these putative targets of miR-126 and miR-335, PITPNC1 (phosphatidyl inositol transfer protein cytoplasmic 1), PTPRN2 (phosphotyrosine phosphatase receptor type N 2), and PLCβ1 (phospholipase C beta 1), shared a common functional characterization as regulators of phosphoinositides.

Phosphoinositides in Normal and Metastatic Cell Processes

Phosphoinositides (PIs) are key regulators of many cellular functions in both normal and malignant cells. PIs are the major determinants of membrane identity and regulate membrane trafficking in both normal and disease states (Balla, 2013; Vicinanza et al., 2008). PIs consist of an inositol ring linked to a diacylglycerol backbone through a phosphodiester linkage. These lipids are synthesized in the endoplasmic reticulum by PI synthase enzymes and distributed throughout the cell through vesicular traffic and PI transfer proteins (Agranoff et al., 1958). The function and localization of PIs differ greatly depending on the phosphorylation state of the hydroxyl groups on the inositol ring, which are metabolically interconverted to different phosphorylated states by PI

kinases and PI phosphatases, or reduced to second messengers through PI hydrolyzers. The inositol ring may be phosphorylated at the 3', 4' and 5' positions. Through the advent of novel biochemical and cell-biological methods, the cellular roles of various PIs and their protein regulators in secretion, endocytosis, actin dynamics, and intracellular signaling have begun to be elucidated (Mayinger, 2012). Although the roles of phosphatidyl inositol 5-phosphate (PI5P) and phosphatidyl inositol 3,4-bisphosphate (PI(3,4)P2) are still unclear, functions of the other five PIs have been delineated in multiple pathways as described below. These PIs govern cellular functions through recruiting proteins to specific cellular locations. To modulate these processes, protein regulators of PIs may increase or decrease the abundance of a PI or change the location of a PI.

Phosphatidyl inositol 3-phosphate (PI3P) is mainly located in endosomes where it mediates several steps of endocytic membrane trafficking. Endocytic vesicles fuse with early endosomes that then combine to form multivesicular bodies and then late endosomes. The contents of late endosomes are either sorted for recycling back to the Golgi or sorted for degradation in lysosomes. PI3P recruits proteins involved in endocytic vesicle fusion to early endosomes such as Rab5 and EEA1 (Simonsen et al., 1998). PI3P is phosphorylated to phosphatidyl inositol 3,5-bisphosphate (PI(3,5)P2) in late endosomes by the 5' kinase PIKfyve. PI(3,5)P2 has been implicated in regulating the localization and size of late endosomes and lysosomes, however PI(3,5)P2 effector proteins have yet to be identified (Dove et al., 2009). Therefore both PI(3,5)P2 and PI3P regulate endocytosis, a process which is disrupted in cancer cells. Improper endocytic trafficking of growth receptors can lead to prolonged growth signaling. Improper

endocytosis of cell surface marker leads to loss of cell polarity, a hallmark of tumor cells (Mosesson et al., 2008).

Phosphatidyl inositol 4-phosphate (PI4P) is the most abundant PI within the cell. It is mainly localized in the Golgi, the organelle responsible for vesicular sorting, however a pool of PI4P also exists in the plasma membrane (Balla et al., 2005). The role of PI4P in the plasma membrane is less well described, although PI4P may serve as a precursor for PI(4,5)P2 in the plasma membrane. PI4P is synthesized from PI by PI4-kinases which are present in the *trans* Golgi network (TGN), the Golgi stacks closer to the plasma membrane rather than the *cis* stacks closer to the endoplasmic reticulum (Balla et al., 2002). PI4P is essential for the Golgi's function in exocytosis, as it recruits proteins such as AP-1 and FAPP-2 that are critical for vesicle budding from the TGN (Godi et al., 2004; Wang et al., 2003). Additionally, PI4P maintains Golgi structure through the PI4P-binding protein GOLPH3 linked to the actin cytoskeleton (Dippold et al., 2009). Since secretion is necessary for metastatic invasion, angiogenesis, and remodeling of the metastatic niche, regulation of Golgi PI4P is an important process in metastatic cancer cells.

Phosphatidyl inositol 4,5-bisphosphate (PI(4,5)P2) is present mainly in the plasma membrane where it performs a myriad of functions including membrane trafficking, signaling, and actin dynamics. This lipid has been implicated in regulated exocytosis by recruiting the CAPS protein (calcium-activated protein for secretion) to the plasma membrane where it facilitates secretory vesicle fusion to the plasma membrane. PI(4,5)P2 has also been shown to be involved in clathrin-mediated endocytosis by recruiting the clathrin adaptor protein AP-2, which aids in the formation of clathrin-coated pits

necessary for endocytic vesicle formation. However, PI(4,5)P2 must then be removed from endocytic vesicles after membrane fission or the vesicles become coated with actin and aggregate in the cytoplasm (Brown et al., 2001). PI(4,5)P2 is involved in cellular signaling through its hydrolysis to generate the second messengers diacylglycerol (DAG) and inositol triphosphate (IP3), which activate protein kinase C signal transduction cascades. Additionally PI(4,5)P2 has recently been found to regulate the activity of ion channels and transporters in the plasma membrane, although the mechanism of activation and physiological relevance have yet to be determined (Suh and Hille, 2008). This lipid also regulates actin dynamics by recruiting multiple actin remodeling proteins including cofilin, WASP, and ERM proteins to differentially activate or inhibit their activity. Modulating actin dynamics is required for cancer cell motility. PI(4,5)P2 is also the precursor to phosphatidyl inositol 3,4,5-trisphosphate (PI(3,4,5)P3 or PIP3), a key molecule in cancer cell proliferation.

PIP3 is generated by PI3-kinase when the kinase is activated through extracellular signaling via growth factors, hormones, or cytokines. PIP3 then recruits the kinase Akt to the plasma membrane where Akt is dually phosphorylated and becomes activated. Active Akt phosphorylates many downstream substrates including mTOR, which promotes cell growth and cell cycle progression. Because PIP3 is preferentially generated near sites on the plasma membrane where signaling by extracellular factors has occurred, PIP3 plays a key role in membrane polarization and chemotaxis.

Phosphoinositides and Their Regulators in Cancer and Other Diseases

PIP3 is the best-characterized PI in cancer development and progression. PIP3 and the PI3-kinase signaling pathway effect multiple pro-tumorigenic cellular processes, including cell growth, survival, adhesion, and motility. PIP3 levels are stringently regulated by both PI3-kinase and PTEN, the phosphatase which dephosphorylates PIP3 back to its precursor, PI(4,5)P2. Mutations in PTEN and the alpha catalytic subunit of PI3K (PI3KCA) are among the most common genetic changes in a broad spectrum of cancers including up to 25% of breast cancers, up-regulating the activity of PI3-kinase or abrogating the activity of PTEN to sustain PIP3 signaling (Samuels et al., 2004). Additionally, inhibitory mutations in another PIP3 phosphatase, SHIP1 that dephosphorylates PIP3 to PI(3,4)P2, have been identified in leukemia (Luo et al., 2003). Given the importance of PIP3 signaling in cancer, PI3-kinase represents an attractive target for the development of therapeutic anti-cancer agents (Liu et al., 2009).

Several protein regulators of PI(4,5)P2 have also been implicated in cancer. PI(4,5)P2 is synthesized from PI4P by PIPKI, and mutations in the PIPKIγ isoform have been identified in gastric cancer. Loss of PIP5KIγ activity in these cancer cells reduced PI(4,5)P2 levels and weakened cell-cell junctions, enabling cells to dissociate from the primary tumor as part of the beginning of the metastatic cascade (Yabuta et al., 2002). PI(4,5)P2 is hydrolyzed by the phospholipase C family of enzymes. PLCγ expression is increased in several cancers including breast, colorectal, prostate, and head and neck cancer. PLCγ has been shown to enhance cancer cell motility following stimulation by epidermal growth factor (EGF) in the tumor microenvironment (Bunney and Katan, 2010).

A protein regulator of PI4P, GOLPH3, has also recently been identified as an oncogene. GOLPH3 bridges PI4P and actin, inducing tensile forces that facilitate the elongated ribbon morphology of the Golgi. Interestingly, copy number analysis revealed *GOLPH3* expression is frequently amplified in multiple solid tumor cancers, including one-third of breast cancers and melanomas. Overexpression of GOLPH3 has been shown to enhance cellular proliferation in cancer cells *in vitro*, although the precise mechanism is unclear (Scott et al., 2009). The identification of GOLPH3 as a clinically relevant cancer promoter further underlines the significance of PI4P in mediating cancer phenotypes.

Other pathologies associated with protein regulators of PIs are X-linked, meaning they are inherited through the X chromosome and thus predominantly afflict male offspring of asymptomatic female carriers. These diseases may affect females as well, but much more rarely since both parents must be carriers for the disease to manifest in female offspring. X-linked agammaglobulinemia is disorder that afflicts patients with mutations in their *Btk* gene. The encoded protein, Btk, contains a plekstrin homology (PH) domain that binds to PIP3. Binding to PIP3 activates Btk's kinase activity, enabling it to phosphorylate phospholipase C, which in turn hydrolyzes PI(4,5)P2. Hydrolysis of PI(4,5)P2 generates DAG and IP3, which mediate B cell signaling and maturation (Conley et al., 2000). Patients with mutations in Btk thus do not generate mature B cells, a key immune cell type responsible for the generation of antibodies in response to infection. These patients develop persistent and recurrent infections unless treated with intravenous infusion of immunoglobulin (IVIG).

Oculocerebrorenal syndrome (also called Lowe syndrome) is also an X-linked disorder caused by mutations in the *OCRL1* gene. OCRLI is an inositol polyphosphate-5-phosphatase, which dephosphorylates PI(4,5)P2 to generate PI4P, and loss of this protein leads to elevated PI(4,5)P2 levels. OCRL1 has been demonstrated to localize to clathrin-coated pits and early endosomes, indicating a role for this protein in endocytosis. Additionally, fibroblasts from Lowe syndrome patients show defects in the actin cytoskeleton and consequently impaired cell adhesion and migration. OCRL1 thus impacts multiple aspects of membrane trafficking, which leads to a multifaceted clinical presentation. Patients with Lowe syndrome display kidney function defects, cataracts, glaucoma, hypotonia, and cognitive impairment (Mehta et al., 2014).

Myotubular myopathy and Charcot-Marie-Tooth Neuropathy Type 4 are both caused by mutations in the MTM (myotubular myopathy) family of phosphatases, which dephosphorylate PI3P. Myotubular myopathy is caused by mutations in the *MTM1* gene and manifests as mild to severe skeletal muscle weakness. MTM1 localizes to the PI3P-rich endosomes in cells, but the mechanistic link between the role of MTM1 in endosomal dynamics and muscle degeneration has yet to be determined (Tsujita et al., 2004). Charcot-Marie Tooth (CMT) Neuropathy is caused by mutations in the *MTMR2* gene, and is distinct from the above pathologies through its autosomal inheritance pattern. Patients with CMT exhibit distal muscle weakens and sensory loss due to axonal demyelinating and neurodegeneration. MTMR2 dephosphorylates both PI3P and PI(3,5)P2, although the direct link between these PIs and myelination is unknown.

Phosphoinositide Regulator Proteins as Drivers of Cancer Metastasis

Given the significance of phosphoinositide dysregulation in cancer and other diseases, PI regulator proteins are potent mediators of pathogenesis. We sought to determine the function of three proteins identified as putative targets of metastasis suppressor miRNAs (PITPNC1, PTPRN2, and PLCβ1) in regulating PIs to promote breast cancer metastasis. PITPNC1 is a member of the RdgB (Retinal Degeneration type B) family of PI transfer proteins. This protein family was named after its founding member RdgB when it was discovered that flies with mutations in this gene exhibit impaired response to light and photoreceptor cell degeneration through vesiculation of the rhabdomeric membranes (Harris and Stark, 1977). From these defects, it is postulated that the function of RdgB is to bring PI to the rhabdomeric membranes where it is synthesized to PI(4,5)P2, a key molecule in the light detection pathway (Harris and Stark, 1977). PITPNC1 (also known as RdgBβ) is a much smaller soluble homolog of RdgB, and its function in mammalian cells is unknown.

PTPRN2 was initially identified as an auto-antigen in type I diabetes and is predominantly present in neuroendocrine cells (Lan et al., 1996; Lu et al., 1996; Wasmeier and Hutton, 1996). As a transmembrane protein, PTPRN2 shuttles between secretory vesicles and the plasma membrane. Due to its presence in neurosecretory vesicles, PTPRN2 has been implicated in insulin and neurotransmitter exocytosis, however the precise role of PTPRN2 in the secretory pathway is unknown (Cai et al., 2011). PTPRN2 belongs to the protein tyrosine phosphatase family, but does not exhibit activity against phosphoprotein substrates due to several critical mutations in the PTP

domain (Magistrelli et al., 1996). Recently, PTPRN2 was found to exhibit phosphatidylinositol phosphatase (PIP) activity against PI(4,5)P2 (Caromile et al., 2010).

PLCβ1 belongs to the family of PLC enzymes, which hydrolyze PI(4,5)P2 to generate the second messengers diacylglycerol (DAG) and inositol triphosphate (IP3) (Rhee, 2001). PLCβ1 localizes mainly to the inner leaflet of the plasma membrane, where it is activated by the Gaq family of G proteins, although a subset of the protein is found in the cytoplasm and nucleus (Smrcka et al., 1991; Taylor et al., 1991).

In this thesis, I describe findings toward delineating the molecular mechanisms of these three PI regulator proteins in breast cancer metastasis. Through molecular, biochemical, cell-biological, and *in vivo* experiments as well as analysis of clinical datasets, I describe roles for PITPNC1 in driving metastatic secretion through binding PI4P (Chapters II and III) and for PTPRN2 and PLCβ1 in promoting metastatic migration through modulating PI(4,5)P2 (Chapter IV). In Chapter V, I discuss the biological implications of these findings for metastatic disease.

CHAPTER II: CLINICAL RELEVANCE AND MECHANISTIC CHARCTERIZATION OF PITPNC1 IN METASTASIS

Identification of Multiple Mechanisms of PITPNC1 Regulation in Breast Cancer

We began our mechanistic studies on PITPNC1 by seeking to identify pre- and post-transcriptional mechanisms that augment PITPNC1 expression in highly metastatic breast cancer cells. Kim Png and Nils Halberg had previously identified PITPNC1 as target of miR-126, leading to increased PITPNC1 expression in highly metastatic cells with silenced miR-126 (Png et al., 2012). Nils Halberg and I further identified a second mechanism of post-transcriptional regulation of PITPNC1. We identified several regions of sequence complementarity between the *PITPNC1* coding sequence and the seed sequence of another established metastasis suppressor miRNA in breast cancer, miR-335 (Figure 2.1). This sequence complementarity suggested that miR-335 might also be capable of regulating PITPNC1 expression in breast cancer via miRNA-mediated gene silencing through translational repression.

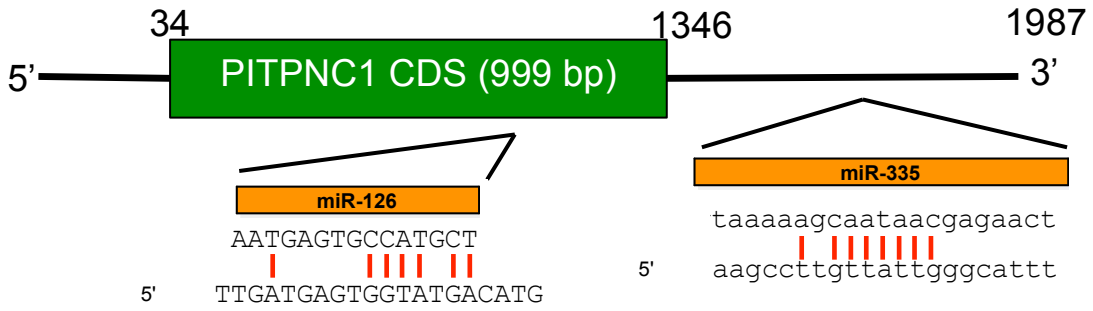

Figure 2.1. Potential miR-126 and miR-335 target sequences in the *PITPNC1* gene. Diagram of the *PITPNC1* gene including 5' untranslated region, *PITPNC1* coding sequences (CDS), and 3' untranslated region (UTR), with regions of complementarity to miR-126 and miR-335 shown.

To test this hypothesis, I performed heterologous luciferase reporter assays wherein the coding sequence (CDS) and 3' untranslated region (3' UTR) of the PITPNC1 gene were cloned into a luciferase reporter vector, and these constructs were transfected into MDA-MB-231 cells. The effect of miR-335 on the expression of its putative target *PITPNC1* was examined by measuring luciferase activity read-out after addition of the luciferase substrate, luciferin. I tested whether decreasing expression of miR-335 by transfecting cells with locked nucleic acid (LNA) targeting miR-335 would increase *PITPNC1*-driven luciferase activity in these cells. Addition of LNA targeting miR-335 did not increase *PITPNC1* CDS-driven luciferase activity compared to addition of a control LNA, however *PITPNC1*-3'UTR-driven luciferase activity increased 1.5-fold (Figure 2.2). These results were consistent with our analysis of putative miRNA target sites in the *PITPNC1* gene (Figure 2.1), which did not reveal miR-335 target sequences with *PITPNC1's* CDS, only within its 3'UTR. This suggests that miR-335 may repress *PITPNC1* translation through binding to *PITPNC1*'s 3'UTR. I performed site-directed mutagenesis to mutate the 8-nucleotide sequence within *PITPNC1*'s 3'UTR complementary to the seed sequence of miR-335. Importantly, mutating the miRNA-complementarity sequence abrogated the miRNA-mediated regulation (Figure 2.2a), consistent with direct targeting of *PITPNC1* by miR-335.

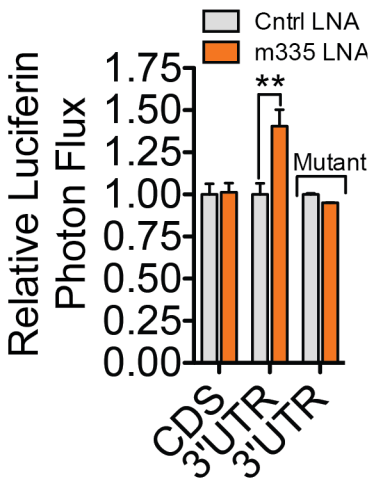

Figure 2.2. miR-335 directly regulates *PITPNC1* through targeting its 3'UTR. Heterologous reporter assays measuring luciferase activity driven off of PITPNC1's wild-type or miR-335 target site mutant CDSs and 3'UTRs in MDA-MB-231 cells treated with LNA targeting miR-335 or control LNA. n = 4. Data are represented as mean ± S.E.M. **p < 0.01.

Given that miRNA silencing reduces translation of a gene target, we next examined PITPNC1 protein levels in breast cancer cells with altered levels of miR-335. Western blot analysis of PITPNC1 in LM2 cells with retroviral-induced overexpression of miR-335 revealed reduced protein levels of PITPNC1 compared to cells overexpressing a control vector (Figure 2.3a). Conversely, MDA-MB-231 cells treated with LNA targeting miR-335 exhibited increased protein levels of PITPNC1 compared to cells treated with control LNA (Figure 2.3b). These complementary experiments indicate that miR-335 regulates the protein level of PITPNC1 in breast cancer cells, and reveal an additional mechanism of post-transcriptional regulation of this gene in breast cancer metastasis.

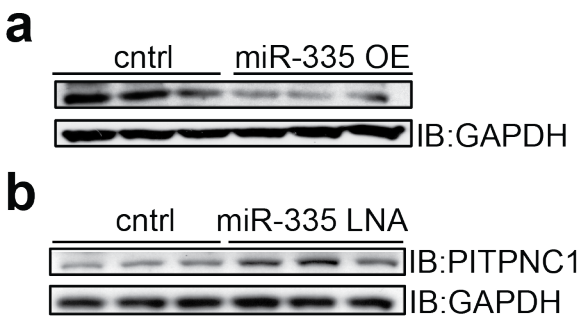

Figure 2.3. miR-335 expression inversely correlates with PITPNC1 protein levels.
a. Western blot analysis of PITPNC1 levels in three biological replicates of LM2 cells overexpressing miR-335 or a control vector.
b. Western blot analysis of PITPNC1 levels in three biological replicates of MDA-MB-231 cells treated with LNA targeting miR-335 or a control LNA.
Western blot analysis of GAPDH was used as the loading control.

Consistent with loss of both miRNA-126 and miRNA-335 in the i*n vivo*-selected highly metastatic derivative sublines, PITPNC1 protein expression is higher in the LM2 and CNLM1a1 cells compared to their poorly metastatic parental populations, MDA-MB-231 and CN34 respectively (Figure 2.4). Together these findings reveal PITPNC1's protein abundance is increased in highly metastatic breast cancer cells in part due to silenced regulation by miR-126 and miR-335.

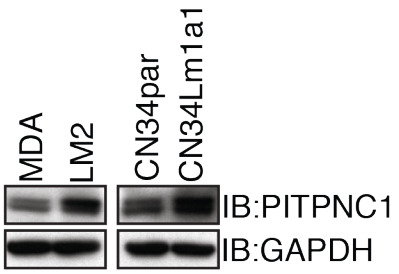

Figure 2.4. PITPNC1 protein abundance in highly metastatic and poorly metastatic breast cancer cells.

Western blot analysis of PITPNC1 levels in MDA-MB-231, LM2, CN34, and CN34LM1a1 cells. Western blot analysis of GAPDH was used a loading control.

Nils Halberg analyzed genomic copy number data from 244 human breast cancer cell lines and tumors from the Broad Institute's Tumorscape (Beroukhim et al., 2010) and found PITPNC1 to be significantly amplified in 46% of these samples ($q = 2.32 \times 10^{-15}$) (Figure 2.5). Copy number variation has been found across many cancers, due mainly to the genomic instability that is an established feature of malignancy (Hanahan and Weinberg, 2011). Thus genomic amplification represents a third mechanism by which breast cancer cells upregulate PITPNC1 expression, further underlining its relevance in breast cancer metastasis.

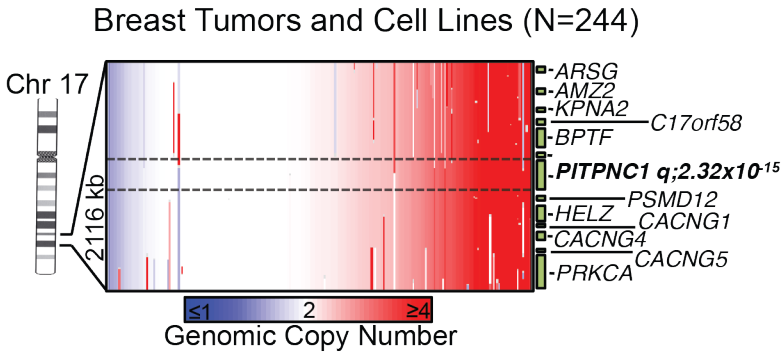

Figure 2.5. Genomic amplification of *PITPNC1* in breast cancer.

Genomic copy number analysis of 244 breast tumors and cell lines. Data from Tumorscape (Beroukhim et al., 2010).

Clinical Relevance of PITPNC1 in Breast Cancer, Colon Cancer, and Melanoma

We next sought to determine if PITPNC1 expression was clinically correlated with breast cancer progression. We measured *PITPNC1* cDNA levels in a commercially available collection of human breast cancers, and found *PITPNC1* expression increased in cancerous tissue relative to normal breast tissue (Figure 2.6a). Consistent with a role for PITPNC1 in promoting metastasis, *PITPNC1* expression increased with breast cancer stage, with the highest expression in stage IV (distal metastasis). Notably, in this dataset and the Tumorscape dataset, *PITPNC1* expression was higher in patients with triple-negative breast cancer (TNBC) (Figure 2.6b, c). Together these date support the conclusion that increased *PITPNC1* expression clinically correlates with breast cancer progression, and may be particularly significant in TNBC.

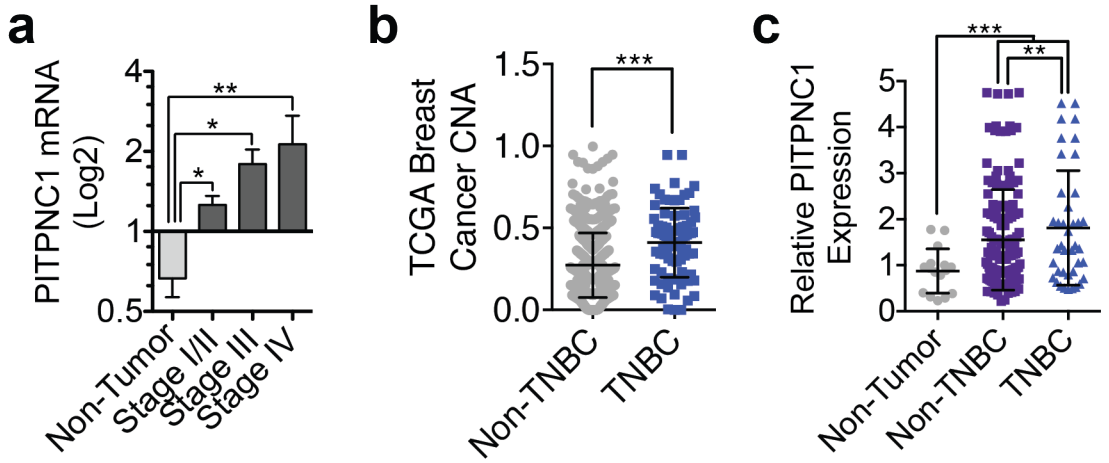

Figure 2.6. *PITPNC1* expression increases with breast cancer stage and correlates with triple-negative breast cancer status.

a. PITPNC1 expression analysis of human breast cancers (stages I-IV) and normal epithelial breast tissue (Non-Tumor) was performed using TissueScan qPCR Array Breast Cancer Panels I, II, and III (Origene).

b, c. Data from Figure 2.5 and (**a**) were segregated based on their status as triple-negative breast cancer (TNBC) or non-TNBC.

Data are represented as mean ± S.E.M. *$p < 0.05$, **$p < 0.01$, ***$p < 0.001$.

Given the data supporting regulation of *PITPNC1* expression by miR-126 and miR-335—two microRNAs that have been established as metastasis suppressors in multiple cancers—we questioned if PITPNC1 was clinically correlated with metastatic progression in other cancer types. *PITPNC1* expression in patients' primary melanoma tumors and primary colorectal tumors was significantly correlated with metastatic progression outcomes, indicating that PITPNC1 may promote metastasis in these cancers in addition to breast cancer (Figure 2.7a, b).

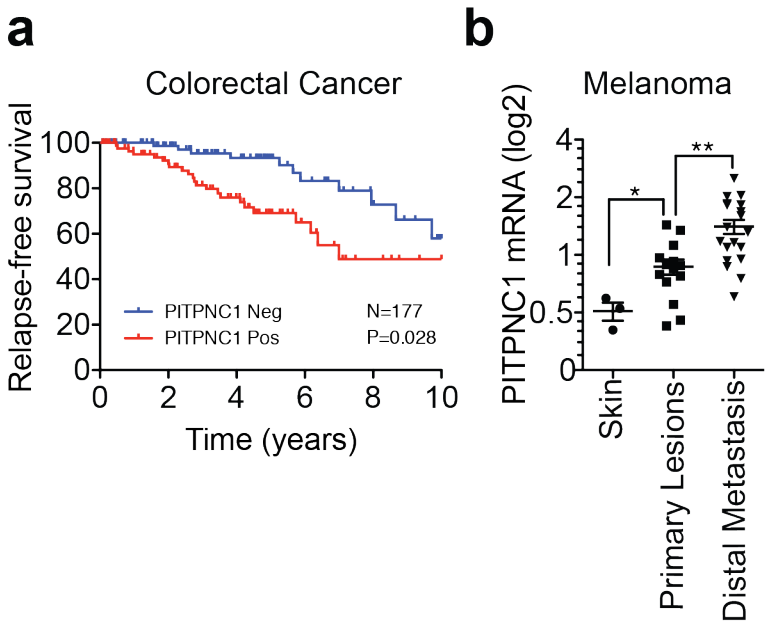

Figure 2.7. Clinical correlation of *PITPNC1* with metastatic outcomes in colorectal cancer and melanoma.

a. Kaplan-Meier curve representing metastasis-free survival cohort of colorectal patients (N=177) as a function of their primary tumor's *PITPNC1* expression levels (Data from GSE17536). Patients whose primary tumors' *PITPNC1* expressions levels were greater or lower than the median for the population were classified as PITPNC1 positive (red) or negative (blue), respectively.

b. *PITPNC1* expression levels in normal skin, patients' primary melanoma lesions, and patients' distal metastatic lesions (Haqq et al., 2005). N = 37. Data are represented as mean ± S.E.M. *$p < 0.05$, **$p < 0.01$.

To determine whether PITPNC1 is a functional promoter of metastasis, we depleted PITPNC1 in highly metastatic cells, injected these cells into the tail vein of NOD SCID mice, and measured the ability of these cells to colonize the lungs. Png and Halberg previously performed this assay in the highly metastatic derivative LM2 breast cancer cells, and found that depletion of PITPNC1 significantly reduced the ability of these cells to colonize the lungs (Png et al., 2012). Halberg and I depleted PITPNC1 using short hairpin RNA-mediated gene silencing in an additional highly metastatic derivative breast cancer cell line, CNLM1a1, and again found that PITPNC1 expression was necessary for these cells to maximally colonize the lungs of mice (Figure 2.8a, b).

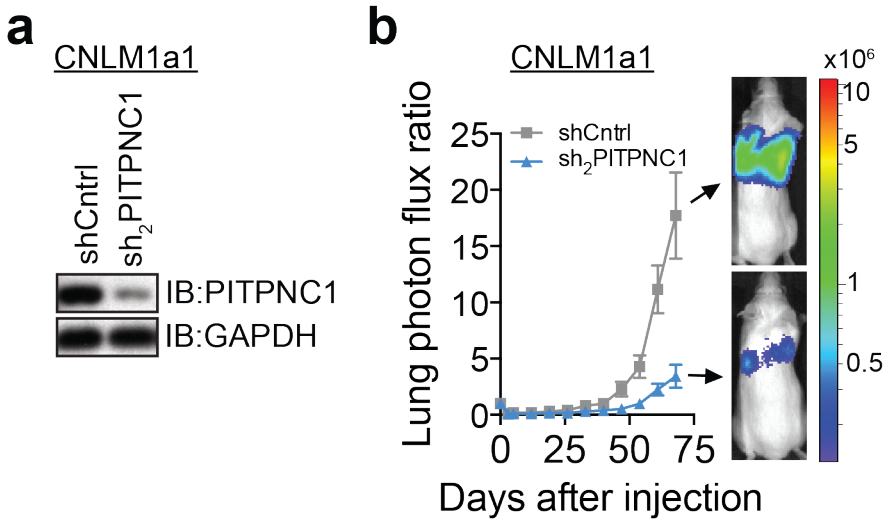

Figure 2.8. Functional validation of PITPNC1 in breast cancer metastasis.
a. Western blot analysis of PITPNC1 levels in CNLM1a1 cells expressing a short hairpin targeting PITPNC1 or a control hairpin. GAPDH was used as a loading control.
b. Bioluminescence imaging quantification of lung colonization by 40,000 CNLM1a1 cells as in (**a**). N=5 mice/group. Error bars represent SEM.

The LM2 and CNLM1a1 cell lines are derived from cells collected from human breast cancer patients, so the metastatic assays must be performed in an immunodeficient

background. We tested the role PITPNC1 in a syngeneic mouse model of spontaneous breast cancer metastasis by depleting PITPNC1 in highly metastatic murine breast cancer cells, 4T1. 4T1 cells were *in vivo*-selected for the ability to spontaneously metastasize to the lungs of mice and form metastatic colonies (Aslakson and Miller, 1992). PITPNC1 knockdown in 4T1 cells also reduced the ability of these cells to metastasize in immunocompetent mice, indicating that PITPNC1's effects are independent of the immune capacity of the host (Figure 2.9a, b). These findings establish PITPNC1 as a robust mediator of breast cancer metastasis.

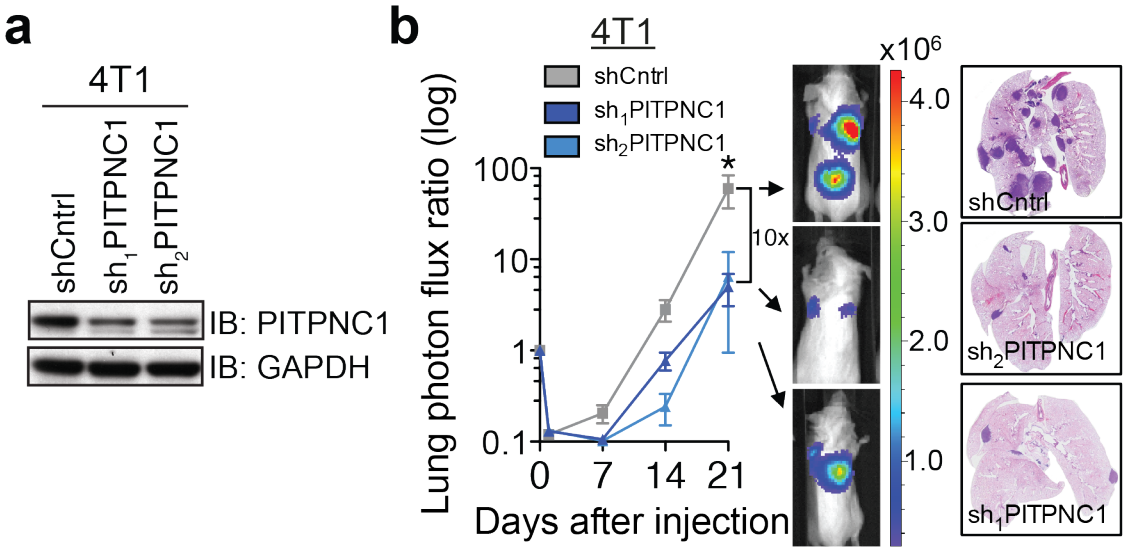

Figure 2.9. PITPNC1 drives metastasis in a syngeneic model of breast cancer metastasis.

a. Western blot analysis of PITPNC1 levels in murine 4T1 cells transduced with short hairpins targeting PITPNC1 or a control hairpin. Western blot analysis of GAPDH was used as a loading control.

b. Bioluminescence imaging quantification of lung metastatic colonization by 50,000 4T1 breast cancer cells expressing a control or PITPNC1 targeting hairpins. N=5/group. Right, representative lung histology. Data are represented as mean ± S.E.M. *$p < 0.05$.

To functionally validate the role of PITPNC1 in colorectal cancer and melanoma, we performed similar *in vivo* metastasis assays. For colorectal cancer, we depleted PITPNC1 in the high metastatic colon cancer subline LS-174T-LvM3, derived from the LS-174T human colon cancer cell line (Loo et al., 2015). This cell line possesses a mutated form of the KRAS oncogene, which is mutated in 35-50% of colon cancers and thus is relatively representative of human colorectal cancer (Wilson et al., 2010). Since colorectal cancer predominantly metastasizes to the liver, these cells were injected intrasplenically and liver colonization was measured. LS-174T-LvM3 with PITPNC1 depletion exhibited 15-fold reduced liver metastasis capacity compared to LS-174T-LvM3 control cells (Figure 2.10a, b).

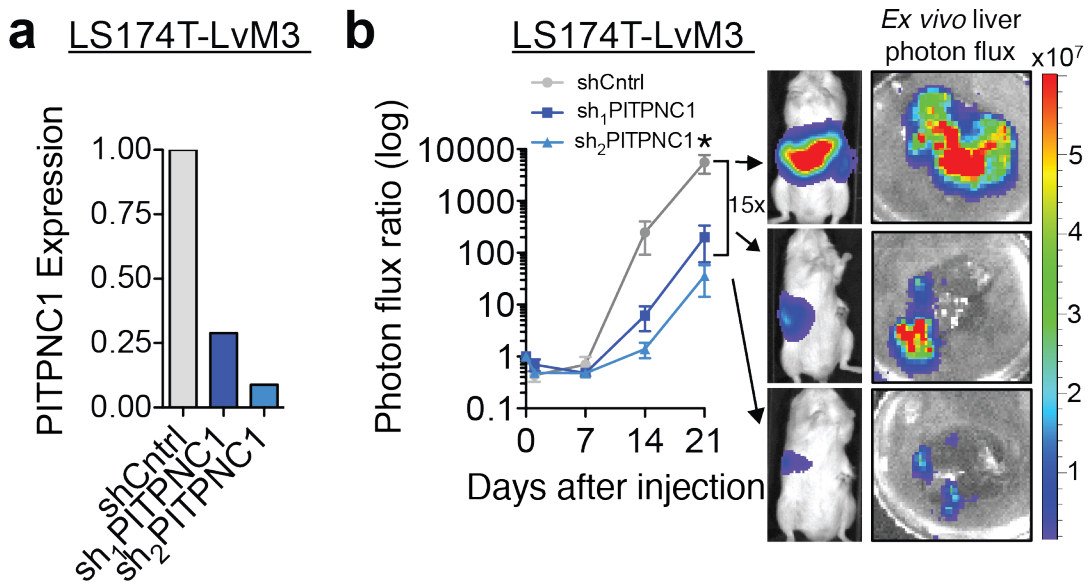

Figure 2.10. Functional validation of PITPNC1 as driver of colorectal cancer metastasis.

a. LS174T-LvM3 colon cancer cells were transduced with a control hairpin or hairpins targeting PITPNC1. *PITPNC1* expression levels were determined by qRT-PCR.

b. Bioluminescence imaging quantification of liver colonization by 80,000 cells in (**a**). Right, luciferase signal from *ex vivo* livers at day 21. N=6/group. Data are represented as mean ± S.E.M. *$p < 0.05$.

To test the role of PITPNC1 in melanoma metastasis, we depleted PITPNC1 in the highly metastatic MeWo melanoma line (Pencheva et al., 2012) and tested the ability of these cells to metastasize to the lungs. These cells were injected via the tail vein, and MeWo cells with PITPNC1-knockdown showed 8-fold reduced lung colonization capacity compared to control cells (Figure 2.11a, b). Together these data indicate PITPNC1 is functionally required in colorectal cancer and melanoma metastasis.

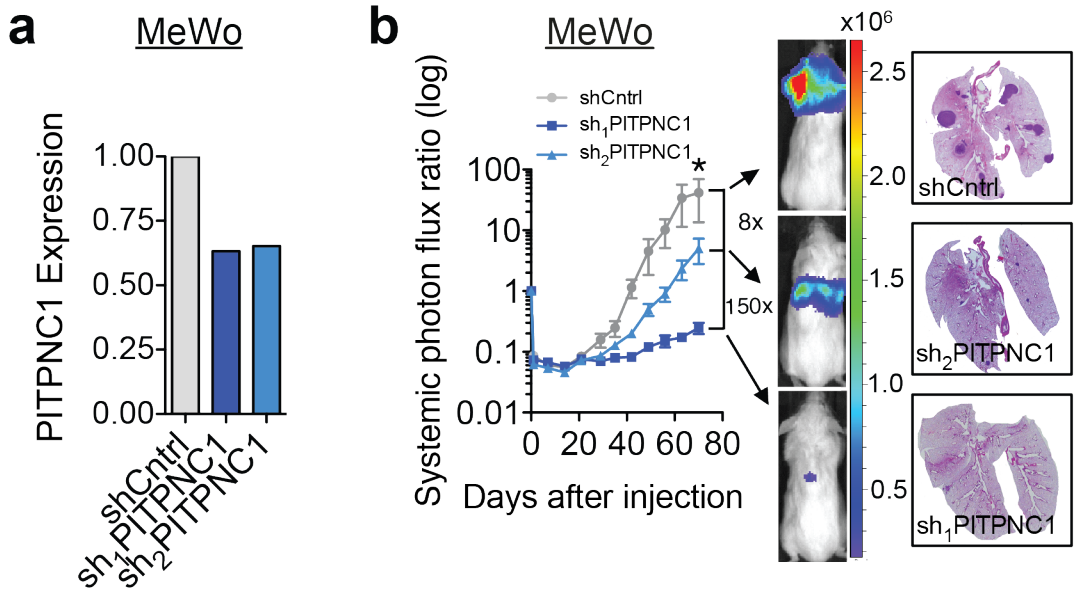

Figure 2.11. Functional validation of PITPNC1 as driver of melanoma metastasis. **a.** MeWo melanoma cells were transduced with lentivirus expressing a control hairpin or hairpins targeting PITPNC1. *PITPNC1* expression levels were determined by qRT-PCR. **b.** Bioluminescence imaging quantification of lung colonization by 40,000 cells in (**a**). Right, representative lung histology. N=5/group. Data are represented as mean ± S.E.M. *$p < 0.05$.

Identification of the Metastatic Phenotypes Mediated by PITPNC1

To investigate the mechanism by which PITPNC1 promotes metastasis, we next sought to determine the metastatic phenotypes it governs. Png and Halberg previously demonstrated that depletion of PITPNC1 in LM2 cells significantly inhibited *in vitro* invasion of these cells though Matrigel, a gelatinous protein mixture that mimics the extracellular matrix in tissue. Invasion is a necessary feature of highly metastatic cells, as they must possess the capacity to invade through surrounding tissue, extravasate from the primary site, and intravasate at a secondary site (Chiang and Massague, 2008). Additionally, Png and Halberg found that depletion of PITPNC1 in LM2 cells significantly reduced the ability of these cells to recruit endothelial cells (Png et al., 2012). Recruitment of endothelial cells is a necessary precursor for the formation of new blood vessels to supply nutrients to the tumor. However, Png and Halberg found that recruiting endothelial cells aided in tumor growth at early stages of colonization, prior to vasculature development, indicating that endothelial interaction may play a role in metastatic initiation as well.

I tested the role of PITPNC1 in these metastatic phenotypes in several other cell lines to confirm that PITPNC1 was required for these processes in multiple cancers. Depletion of PITPNC1 using two independent short hairpin RNAs in CNLM1a1, HCC-1806, BT-549, and 4T1 breast cancer cells all reduced the ability of these cells to invade through Matrigel and recruit endothelial cells compared to cells transduced with a control hairpin (Figure 2.12a, b). These human breast cancer cell lines all represent TNBC, consistent with our clinical findings for a role for PITPNC1 in driving TNBC. The requirement for PITPNC1 expression in these metastatic phenotypes was also observed in

melanoma and colon cancer cells. PITPNC1 depletion in Mewo-LM2 melanoma cells and 6513-LvM3B cells, a colon cancer cell line *in vivo*-selected for liver metastatic capacity, reduced their invasive and endothelial recruitment capacities (Figure 2.12a, b).

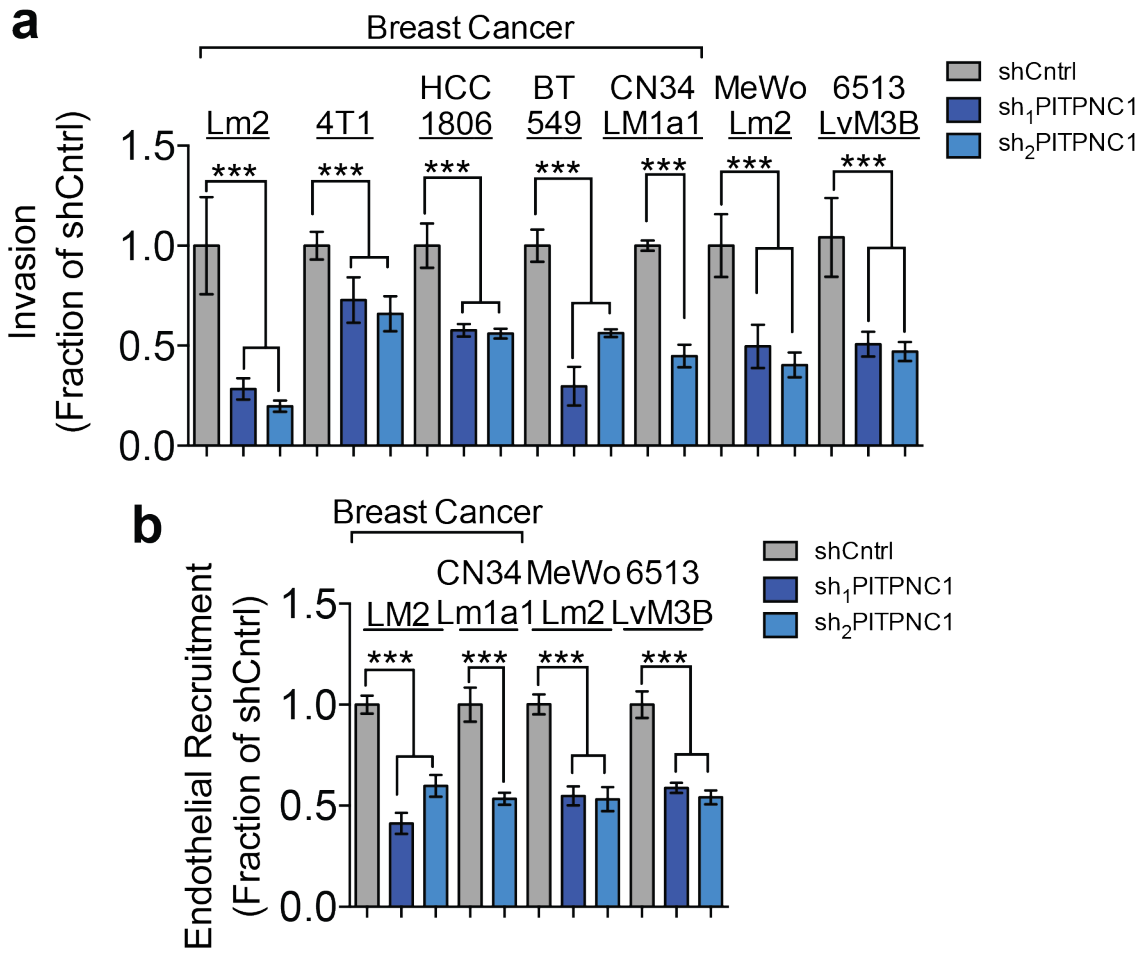

Figure 2.12. PITPNC1 promotes Matrigel invasion and endothelial recruitment in multiple cancer types.

a. Matrigel invasion by 50,000 LM2, 4T1, HCC-1806, BT-549, CN34LM1a1, MeWo or LS174T-LvM3 cells expressing short hairpins targeting PITPNC1 or a control hairpin. Data normalized to control group values. N=4/group.

b. Trans-well recruitment of 80,000 human umbilical vein endothelial cells (HUVEC) by cancer cells as in (**a**). Data normalized to control group values. N=4/group.

Data are represented as mean ± S.E.M. ***p < 0.001.

Depletion of PITPNC1 did not affect two additional metastatic phenotypes, *in vitro* migration and proliferation. Cancer cells frequently demonstrate increased motility (Condeelis et al., 2005), thus we tested *in vitro* migration by allowing breast, colon, and melanoma cancer cells to migrate through a porous trans-well membrane. Depletion of PITPNC1 did not affect the migratory capacity of breast, melanoma, or colon cancer cells (Figure 2.13), indicating that the inhibitory effects we find in the Matrigel invasion assay are not due to decreased migratory capacity of PITPNC1-knockdown cells, but instead due to an inability to breakdown the Matrigel to enable movement—a process which requires secreted factors.

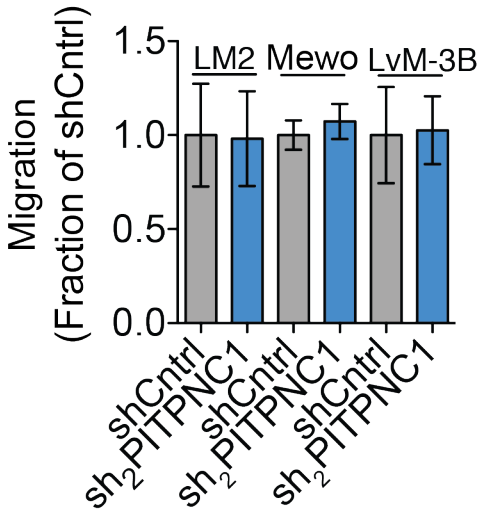

Figure 2.13. PITPNC1 is not required for migration capacity in multiple cancer types.

Trans-well migration of 20,000 LM2, MeWo, or LS174T-LvM3 cells expressing PITPNC1 knockdown or control hairpin. Values were normalized to those of shControl cells. N=4/group. Error bars represent S.E.M.

Additionally, the effects of PITPNC1-knockdown on *in vivo* metastasis, invasion, and endothelial recruitment are not due to decreased proliferation, as these cells display

similar growth rates to control cells (Png et al., 2012) (Figure 2.14a-c). These findings reveal that the phenotypic effects of PITPNC1 depletion are selective and do not result from reduced cellular viability.

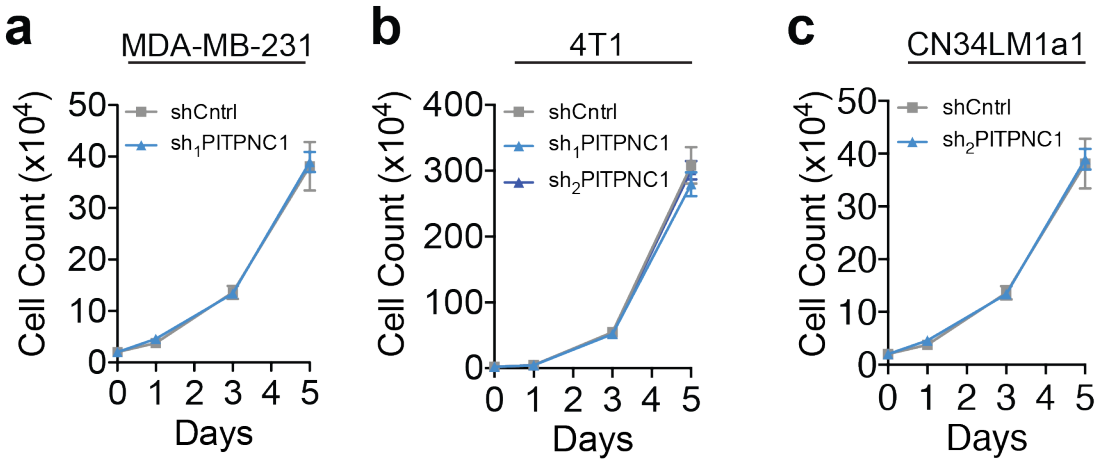

Figure 2.14. Depletion of PITPNC1 does not affect cellular proliferation.
a-c. Proliferation of 20,000 MDA-MB-231 (**a**), 4T1 (**b**), and CN34LM1a1 (**c**) cells expressing short hairpins targeting PITPNC1 or a control hairpin. N=3/group. Error bars represent S.E.M.

Since depletion of PITPNC1 in highly metastatic cells revealed this gene as necessary for maximal metastasis, invasion, and endothelial recruitment capacities, we questioned if increased expression of PITPNC1 in poorly metastatic cells was sufficient to augment these phenotypes. Indeed, overexpression of PITPNC1 in MDA-MB-231 cells was sufficient to enhance *in vitro* invasion and endothelial recruitment, as well as metastatic colonization (Figure 2.15a-c). Therefore, PITPNC1 is both necessary and sufficient for metastatic capacity.

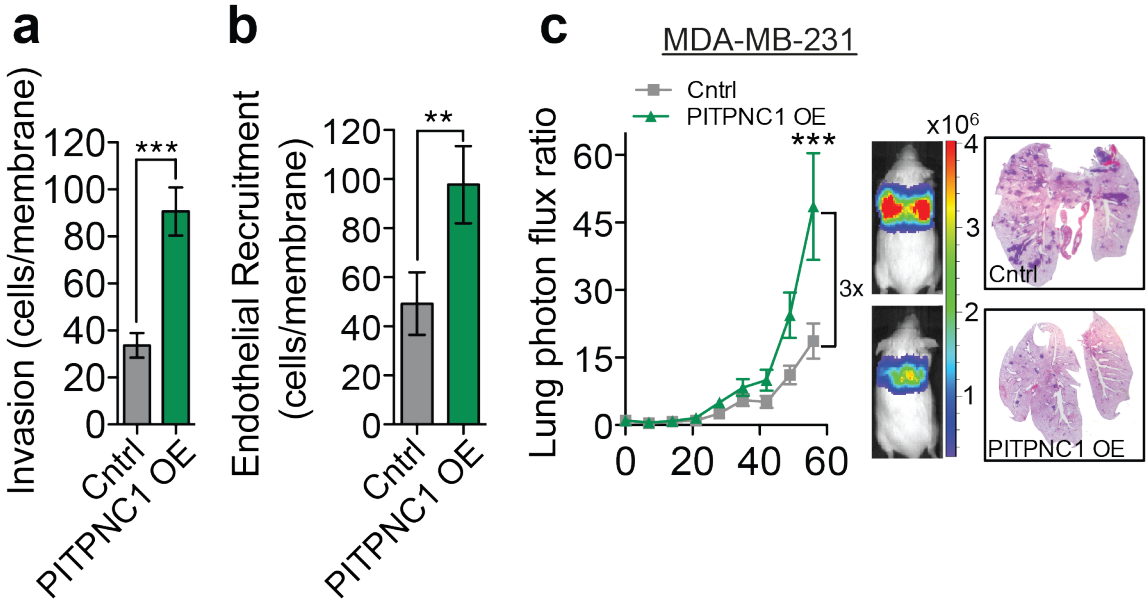

Figure 1.15. PITPNC1 is sufficient to promote breast cancer metastasis.

a, b. 50,000 MDA-MB-231 cells transduced with PITPNC1 overexpression or a control vector were subjected to the Matrigel invasion assay (**a**) and endothelial recruitment assay (**b**). N = 4/group.

c. Bioluminescence imaging quantification of lung colonization by 40,000 cells in (**a**). N = 6/group. Right, representative lung histology.

Data are represented as mean ± S.E.M. **p < 0.01, ***p < 0.001.

Characterization and Mechanistic Role of PITPNC1's Lipid-Binding Activity

To elucidate the molecular mechanism by which PITPNC1 regulates metastatic colonization, we sought to determine the role of its phosphatidyl inositol transfer protein (PITP) lipid-binding and transferring domain. This N-terminal domain comprises approximately 80% of the PITPNC1 protein, with the remainder composed of a C-terminal unstructured tail. To perform lipid biochemistry experiments with PITPNC1, I first expressed and purified recombinant PITPNC1 protein using an *E. Coli* IPTG-induced expression system. Although PITPNC1 was not expressed at high levels in the *E.*

Coli, I was able to collect sufficient protein by expressing a GST-tagged fusion protein and purifying the protein using glutathione-based affinity purification (Figure 2.16a).

To identify PITPNC1's lipid substrate, Halberg first performed a lipid-overlay assay in which a broad range of lipids were spotted on a membrane and blotted with purified recombinant PITPNC1 protein. Bound PITPNC1 was detected using an anti-GST antibody. These lipid-blot assays revealed that PITPNC1 binds most strongly to Phosphatidyl inositol 4-phosphate (PI4P), with weaker binding to PIs containing a single phosphate head group, namely phosphatidyl inositol 3-phosphate (PI3P) and phosphatidyl inositol 5-phosphate (PI5P) (Figure 2.16b). To test this interaction in a more physiological context, Halberg then conducted a vesicular pull-down experiment. In this experiment, liposomes that contain the PI of interest are incubated with recombinant PITPNC1 protein. The liposomes mimic the membranes in which these lipids would be located in the cell, and thus binding is more biologically relevant compared to isolated lipids. Following incubation, the liposomes are pelleted and the fraction of PITPNC1 protein bound to liposomes is compared to the fraction of PITPNC1 protein remaining in the supernatant (unbound protein). Consistent with the lipid overlay assay, PITPNC1 was found to bind to vesicles containing PI4P to a greater extent than to those containing PI3P, PI5P, phosphatidyl inositol 3,4-bisphosphate (PI(3,4)P2), or phosphatidic acid (PA) (Figure 2.16c).

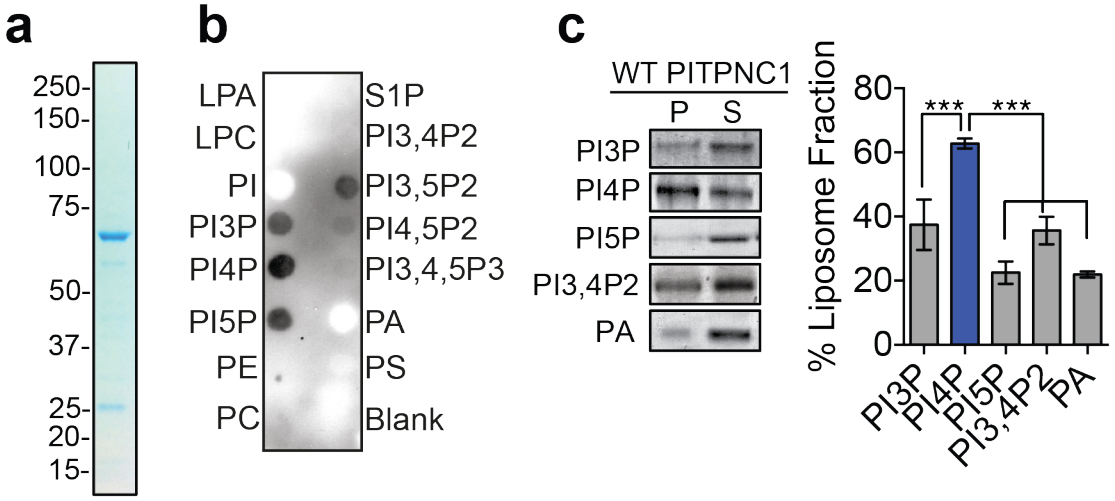

Figure 2.16. PITPNC1 binds to PI4P *in vitro*.

a. Gel electrophoresis of GST-tagged recombinant PITPNC1 protein stained with colloidal blue (predicted molecular weight: 68 kD).

b. Lipid overlay assay. Lipid-bound recombinant PITPNC1-GST was detected with anti-GST antibody. The experiment was repeated 3 times.

c. Vesicle pull-down assay of recombinant PITPNC1 using vesicles containing PI3P, PI4P, PI5P, PI(3,4)P2, or PA. Pelleted vesicle fraction (P) and supernatant fraction (S) were subjected to 1-D gel electrophoresis. Right, densitometry analysis of gel image indicating percent of total PITPNC1 in pelleted fraction. N=3/group. Data are represented as mean ± S.E.M. ***$p < 0.001$.

Having observed lipid binding towards PI4P in the above biochemical experiments, we next sought to verify the physiological relevance of this binding. I performed immunofluorescence microscopy experiments to elucidate the cellular localization of PITPNC1 in breast cancer cells and determine if lipid-binding activity is necessary for this localization. I observed that GFP-tagged PITPNC1 displays diffuse cytoplasmic staining as previously described (Takano et al., 2003), but intriguingly

showed most intense staining in perinuclear regions that co-stained with p230, a marker of the trans Golgi network (TGN) (Figure 2.17a). The Golgi is the sorting hub for vesicles traveling to the plasma membrane or endosomal compartments, and these functions are dependent on resident PI4P (Mayinger, 2012). Although some PI4P is localized to the plasma membrane as well, the TGN is the predominant location of PI4P in the cell. Additionally, co-staining of PITPNC1 and PI4P using the PI4P-specific PH-domain of FAPP1 confirmed that PITPNC1 accumulates in PI4P-positive areas of the Golgi (Figure 2.17b). This data supported our hypothesis derived through biochemical experiments that PITPNC1 binds PI4P *in vivo*.

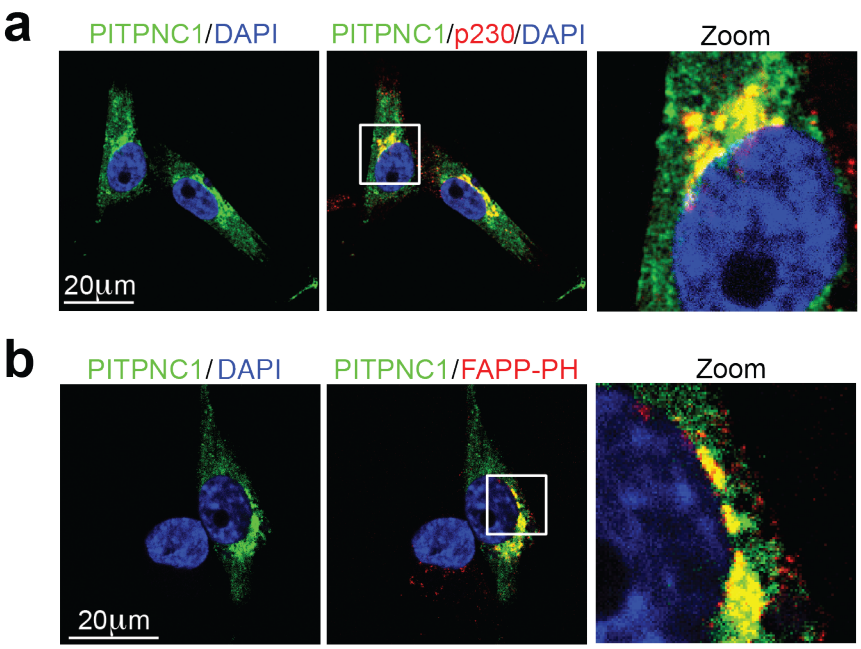

Figure 2.17. PITPNC1 co-localizes with *trans* Golgi and PI4P markers.

a. MDA-MB-231 cells expressing GFP-tagged PITPNC1 (green) co-stained with anti-p230 antibody (red) and 4',6-diamidino-2-phenylindole (DAPI, blue) were analyzed by immunofluorescence microscopy.

b. MDA-MB-231 cells expressing GFP-tagged PITPNC1 (green) co-stained with DAPI (blue), and FAPP-PH for the detection of PI4P (red).

To further validate PIPTNC1's binding of PI4P, we sought to abrogate lipid-binding capacity by mutating the PITP domain. Previous studies have shown that the T59E and N90F mutations of PITPα, another PITP domain family member that binds PI and phosphatidylcholine *in vitro*, inhibits lipid binding (Milligan et al., 1997; Tilley et al., 2004; Yoder et al., 2001). Although the PITP domains of PITPα and PITPNC1 are only approximately 40% similar overall, homology analysis revealed these residues are conserved across these PITP domains (Figure 2.18a). I performed site-directed mutagenesis of the corresponding residues in PITPNC1 (T58 and N88) to generate putative lipid-binding mutants forms of PITPNC1. These lipid-bindings mutants forms were expressed at equivalent levels with wild-type PITPNC1, such that any effects observed were due to lipid-binding activity rather than protein expression level (Figure 2.18b). We verified that these mutations abrogated lipid-binding capacity in the vesicular pull-down assay. Both mutations revealed reduced ability of recombinant PITPNC1 to bind PI4P-containing vesicles (Figure 2.18c).

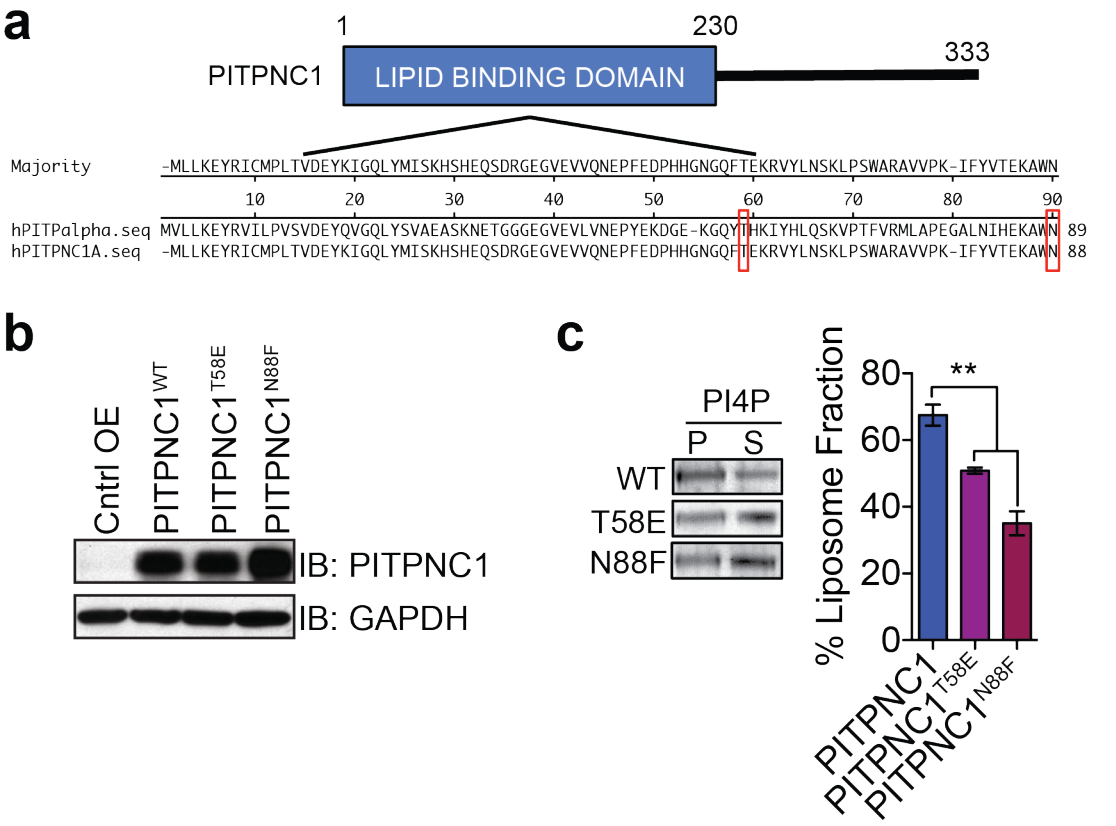

Figure 2.18. Mutations of PITPNC1 T58 and N88 abrogate lipid-binding capacity.

a. Diagram of PITPNC1 isoform A protein structure. Sequence alignment of PITPα (top) and PITPNC1A (bottom) indicating conserved threonine and asparagine residues in the lipid-binding domain.

b. Western blot analysis of PITPNC1 levels in MDA-MB-231 cells transduced with $PITPNC1^{WT}$, $PITPNC1^{T58E}$, and $PITPNC1^{N88F}$. GAPDH was used a loading control.

c. Vesicle pull-down assay of recombinant wild-type or mutant PITPNC1 using vesicles containing PI4P. Pelleted vesicle fraction (P) and supernatant fraction (S) were subjected to 1-D gel electrophoresis. Right, densitometry analysis of gel image indicating percent of total PITPNC1 in pelleted fraction. N=3/group. Data are represented as mean ± S.E.M. $^{**}p < 0.01$.

To determine if PI4P binding was required for Golgi localization of PITPNC1, I then expressed Flag-tagged wild-type or lipid-binding mutant PITPNC1 in breast cancer

cells and performed immunofluorescence analysis between PITPNC1-Flag and the Golgi marker Giantin. These studies revealed that PITPNC1^{N88F} showed reduced localization to the Golgi compared to PITPNC1^{WT}, indicating that Golgi localization is dependent upon PI4P binding (Figure 2.19).

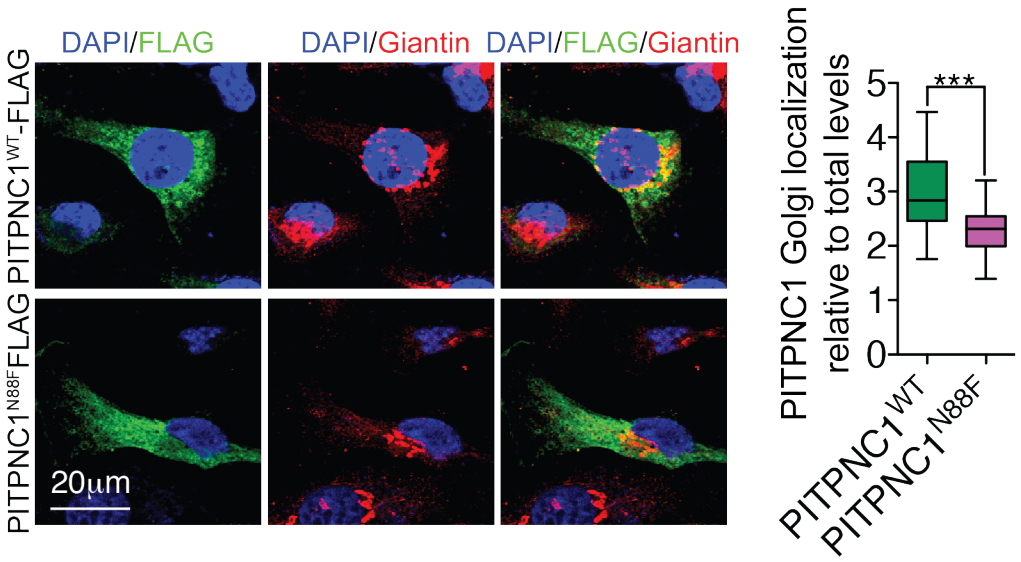

Figure 2.19. PITPNC1's ability to bind PI4P is required for its Golgi localization. MDA-MB-231 cells with stable expression of Flag-tagged wild-type or N88F mutant PITPNC1 co-stained with anti-Flag and anti-Giantin were analyzed by immunofluorescence microscopy. The intensity of Flag immunoreactivity in areas positive for Giantin was considered as the Golgi signal. The Golgi signal was normalized to total cellular levels of PITPNC1 to control for differences in expression levels among individual cells. N=30/group. The upper and lower bars in box and whiskers plots show minimum and maximum data points. ***$p < 0.001$.

We next asked if PI4P binding is required for the pro-metastatic phenotypes mediated by PITPNC1. I overexpressed either wild-type or the two lipid binding mutant forms of PITPNC1 in MDA-MB-231 cells and found that PITPNC1^{WT}, but neither of the lipid binding mutants, was sufficient to promote Matrigel invasion and endothelial

recruitment (Figure 2.20a, b). Similarly, neither PITPNC1^{N88F} nor PITPNC1^{T58E} were sufficient to increase metastatic colonization, suggesting that PITPNC1's lipid binding activity is required for metastasis (Figure 2.20c).

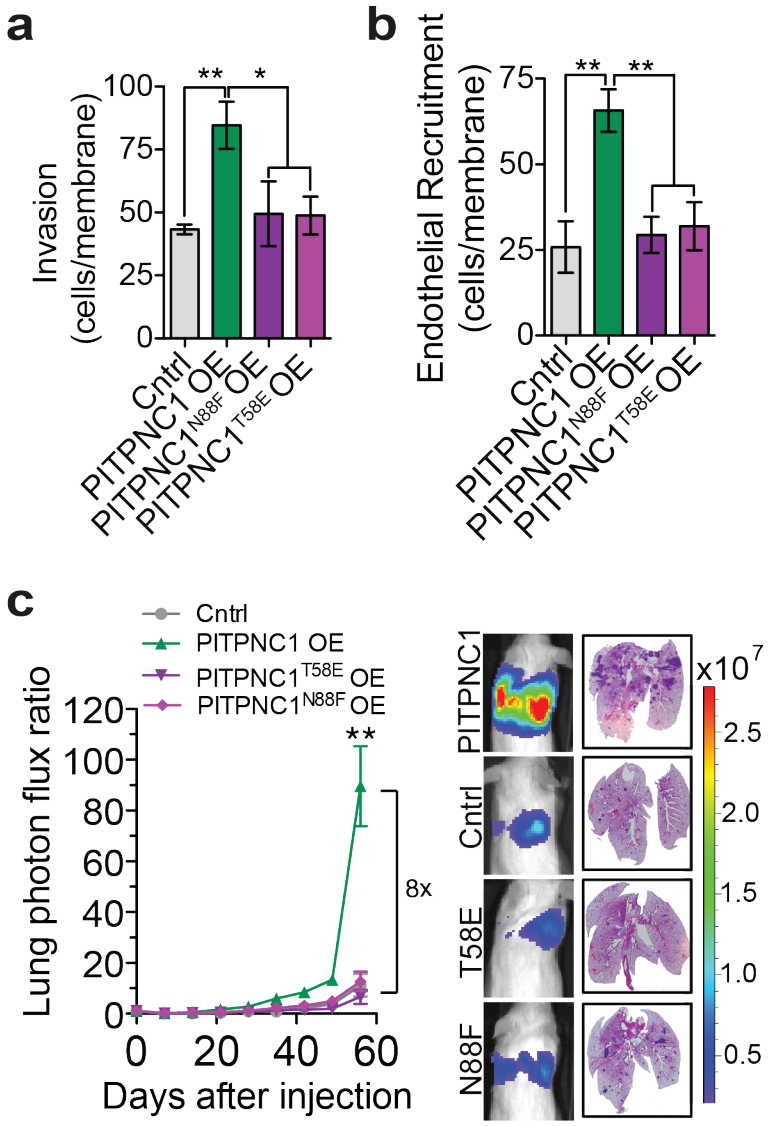

Figure 2.20. PITPNC1's lipid binding domain is required for metastasis.

a, b. 50,000 MDA-MB-231 cells expressing PIPTNC1^{WT}, PITPNC1^{T58E}, PITPNC1^{N88F}, or control vector were subjected to the Matrigel invasion assay (**a**) and endothelial recruitment assay (**b**). N=4/group. Data are represented as mean ± S.E.M.

c. Bioluminescence imaging plot by 40,000 MDA-MB-231 cells in (**a**). N=6/group. Right, representative lung histology. *p < 0.05, **p < 0.01.

To further support our findings in a complementary experiment, we asked if reducing TGN PI4P levels would change the localization of PITPNC1 and abrogate its promotion of metastatic phenotypes. To decrease TGN PI4P levels, I transfected breast cancer cells with a TGN-localized PI4P phosphatase Sac1K2A, previously developed for this purpose (Rohde et al., 2003). The Sac1K2A construct localized exclusively to the Golgi in breast cancer cells (Figure 2.21a), and its expression significantly reduced TGN PI4P levels (Figure 2.21b). In accordance with PITPNC1 binding to TGN PI4P, expression of Sac1K2A significantly reduced PITPNC1-Flag localization to the Golgi (Figure 2.22a). Consistent with a required role for TGN PI4P in PITPCN1 function, reduction of PI4P by Sac1K2A abrogated the ability of PITPNC1 overexpression to enhance invasion and endothelial recruitment (Figure 2.22b, c). Overall, these findings reveal that the interaction between PI4P and PITPNC1 in the TGN is required for PITPNC1's promotion of metastasis.

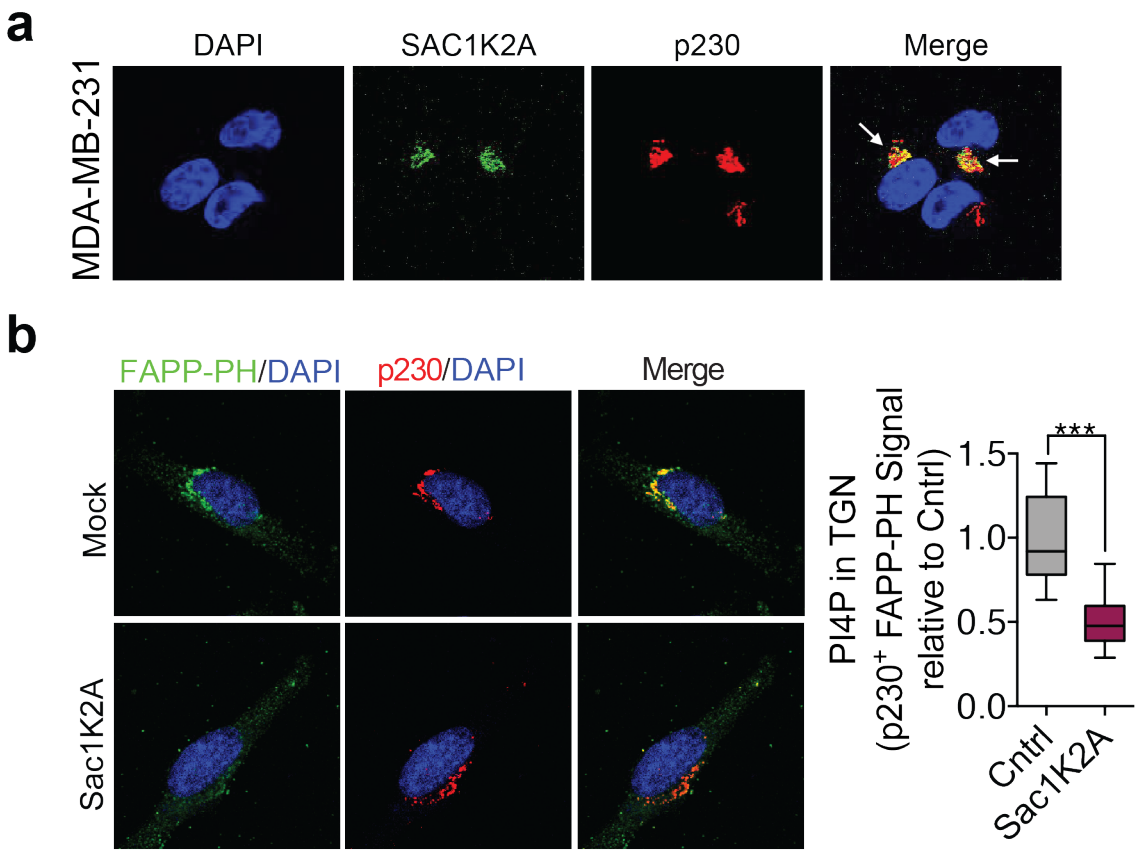

Figure 2.21. Use of Sac1K2A to selectively deplete Golgi PI4P.

a. MDA-MB-231 were transfected with GFP-SAC1K2A and subjected to immunofluorescence analysis for GFP, p230 (red) and DAPI (blue) 48 hours post-transfection. Arrows indicate signal overlap between GFP and the trans-Golgi marker p230.

b. MDA-MB-231 cells were transfected with Sac1K2A and subjected to immunofluorescence analysis for FAPP-PH (green), p230 (red), and DAPI (blue). Right, quantification of PI4P in the Golgi as measured by FAPP-PH signal in p230-postive areas. N = 30/group. The upper and lower bars in box and whiskers plots show minimum and maximum data points. ***$p < 0.001$.

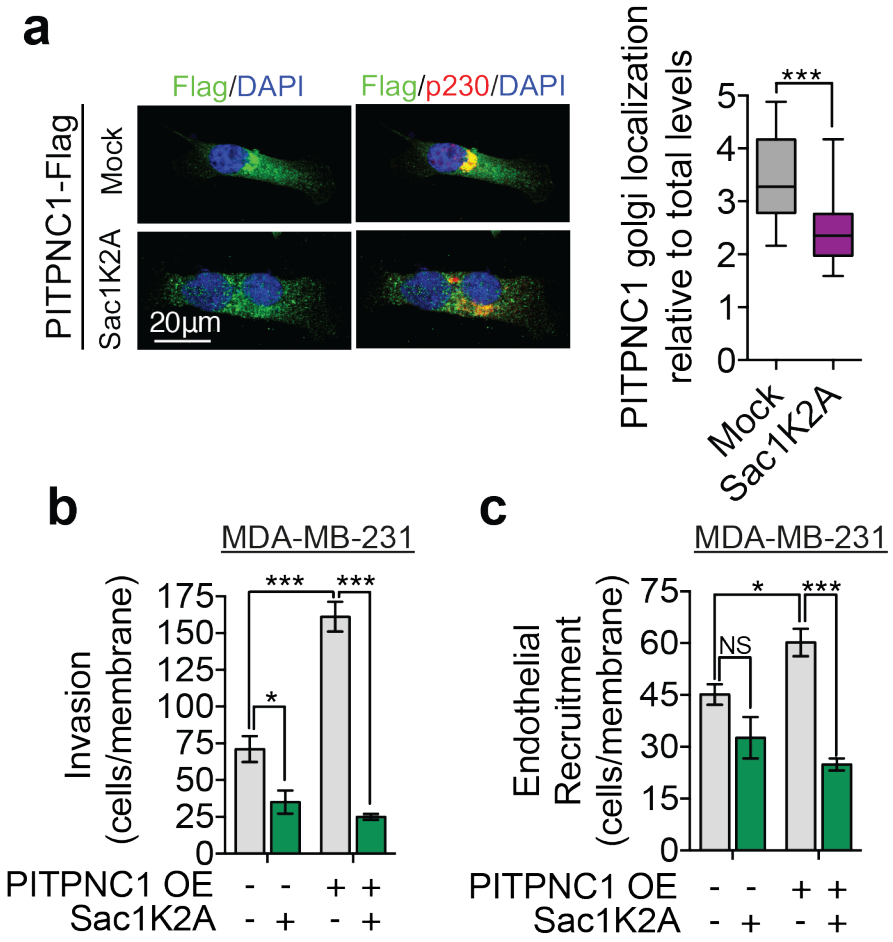

Figure 2.22. Golgi PI4P is required for PITPNC1-mediated invasion and endothelial recruitment.

a. MDA-MB-231 cells expressing PITPNC1-Flag were transfected with Sac1K2A or mock transfected and subjected to immunofluorescence analysis for Flag (green), p230 (red), and DAPI (blue). The intensity of Flag immunoreactivity in areas positive for p230 was considered as the PITPNC1 Golgi signal. The Golgi signal was normalized to total cellular levels of PITPNC1 to control for differences in expression levels among individual cells. N=30/group.

b, **c**. MDA-MB-231 cells overexpressing PITPNC1 or a control vector were transfected with Sac1K2A or mock transfected and subjected to the Matrigel invasion assay (**b**) and endothelial recruitment assay (**c**). N = 4/group.

Data are represented as mean ± S.E.M. The upper and lower bars in box and whiskers plots show minimum and maximum data points. *p < 0.05, ***p < 0.001.

Functional Significance of PITPNC1's Binding partners, 14-3-3 and RAB1B

To gain further mechanistic insights into the cellular function of PITPNC1, we next sought to identify potential PITPNC1 binding proteins. To accomplish this, I expressed Flag-tagged PITPNC1 in MDA-MB-231 breast cancer cells and performed immunoprecipitation of the Flag epitope followed by in-solution trypsin digestion and mass spectrometry quantification. Mass spectrometry revealed several proteins that were significantly bound to PITPNC1 (Figure 2.23). Our findings were validated by the inclusion of the previously identified binding partners of PITPNC1, the 14-3-3 proteins (Garner et al., 2011). Additionally, we identified a novel binding partner for PITPNC1, the small GTPase RAB1B.

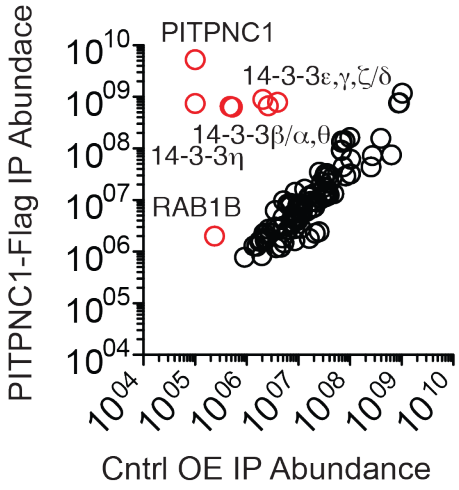

Figure 2.23. PITPNC1 co-immunoprecipitates with 14-3-3 proteins and RAB1B. Lysates from MDA-MB-231 cells expressing Flag-tagged PITPNC1 or control vector were subjected to immunoprecipitation by anti-Flag beads. The eluate was trypsin digested in solution and the liquid chromatography-tandem mass spectrometry (LC-MS/MS) spectra were analyzed by label free quantification. Comparison proteins in the empty vector condition (horizontal axis) and the PITPNC1-Flag condition (vertical axis) revealed PITPNC1, several 14-3-3 protein forms, and RAB1B to be significantly different ($p < 0.05$) between the two samples. N=3/group.

We first investigated the role of 14-3-3 proteins in PITPNC1-mediated metastasis. The 14-3-3 proteins are scaffolding proteins able to bind many functionally diverse signaling proteins. 14-3-3 proteins are involved in a multitude of cellular processes including signal transduction, apoptosis, and cell cycle control (Fu et al., 2000). 14-3-3 was found to bind phosphorylated PITPNC1 on serine-274 and serine-299. This binding shielded a PEST degradation sequence within PITPNC1, thus preventing the protein from being degraded (Garner et al., 2011). The previous studies of PITPNC1-14-3-3 interaction were performed in COS-7 cells, a monkey kidney cell line. To verify that PITPNC1 binds 14-3-3 through phosphorylated S274 and S299 in breast cancer cells, I performed site-directed mutagenesis to mutate the putative phosphorylated serine residues to the non-phosphorylatable alanine residues (Figure 2.24). Western blot analysis of immunoprecipitated PITPNC1^{WT} and PITPNC1$^{S274A, S299A}$ protein from breast cancer cell lysate confirmed that the interaction of PITPNC1 and 14-3-3 proteins is dependent on serine phosphorylation, as the non-phosphorylatable mutant did not co-immunoprecipitate with 14-3-3 (Figure 2.24).

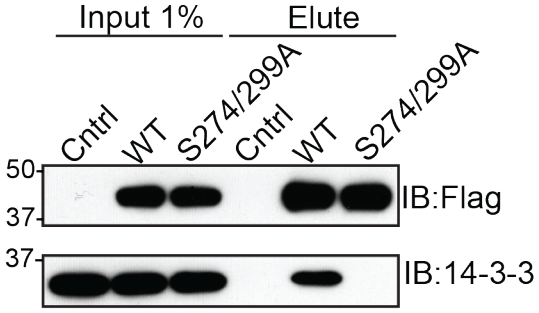

Figure 2.24. 14-3-3 binding to PITPNC1 requires phosphorylated serine residues. Western blot analysis of input and immunoprecipitated Flag-tagged PITPNC1^{WT} and PITPNC1$^{S274A/299A}$ from MDA-MB-231 cells using anti-Flag and anti-14-3-3 antibodies.

We next asked if binding of 14-3-3 was required for the metastatic function of PITPNC1. I transduced cells with retroviral stable overexpression of either PITPNC1^{WT}, PITPNC1$^{S274A, S299A}$, or a control vector and found that only PITPNC1^{WT} was sufficient to promote invasion and endothelial recruitment (Figure 2.25a, b). As expected, these effects are likely explained by the shorter half-life of the PITPNC1$^{S274A, S299A}$ (Figure 2.25c). The significantly shorter half-life of the mutant protein generates a reduced steady-state quantity of PITPNC1 protein in these cells compared to overexpression of wild-type protein, and thus decreased metastatic capacity.

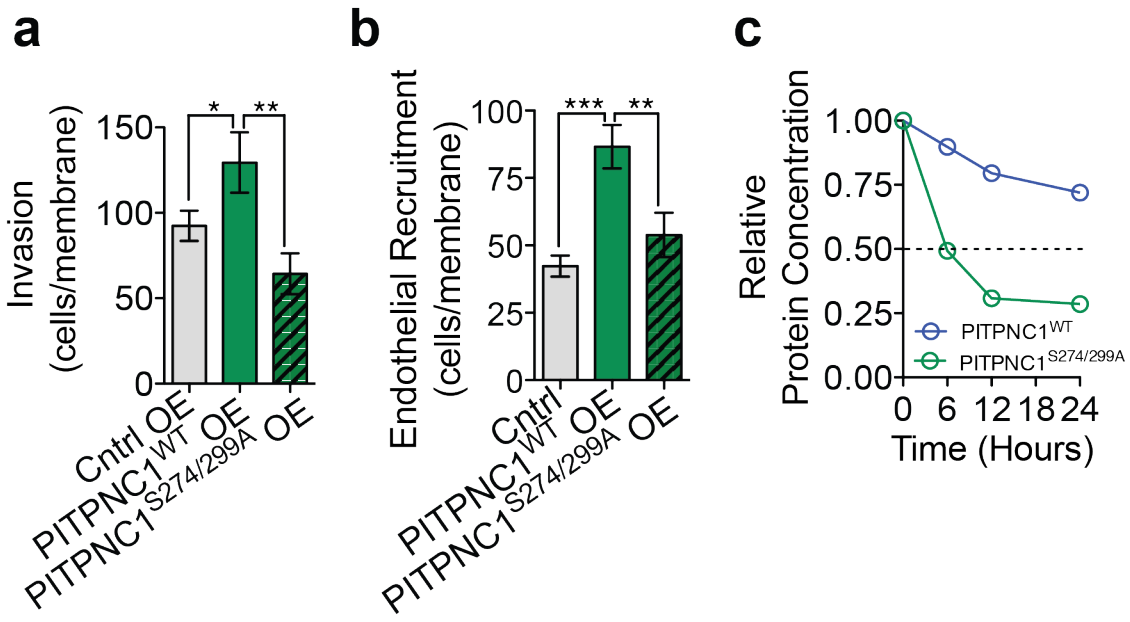

Figure 2.25. 14-3-3 binding is required for PITPNC1's phenotypes and stability.
a, b. MDA-MB-231 cells expressing empty control vector, wild-type PITPNC1, or S274A/299A mutant PITPNC1 were subjected to invasion (**a**) and endothelial recruitment assays (**b**). N=4/group. Data are represented as mean ± S.E.M. *$p < 0.05$, **$p < 0.01$ ***$p < 0.001$.
c. The half-lives of wild-type PITPNC1 and S274A/299A mutant PITPNC1 in MDA-MB-231 cells were determined by treating cells with 100μg/ml cycloheximide over 24 hours and analyzing PITPNC1 protein abundance in cellular lysates by western blotting.

We next turned our attention to the novel PITPNC1 binding partner identified in our screen, RAB1B. I verified that PITPNC1 co-immunoprecipitates with RAB1B by western blot analysis (Figure 2.26a). Additionally, by conducting immunofluorescence experiments Halberg found that PITPNC1-Flag and RAB1B co-localize predominantly in the Golgi region of the breast cancer cells (Figure 2.26b). RAB1B is known to localize to the TGN and is required for proper Golgi structure and function (Dugan et al., 1995; Haas et al., 2007; Plutner et al., 1991).

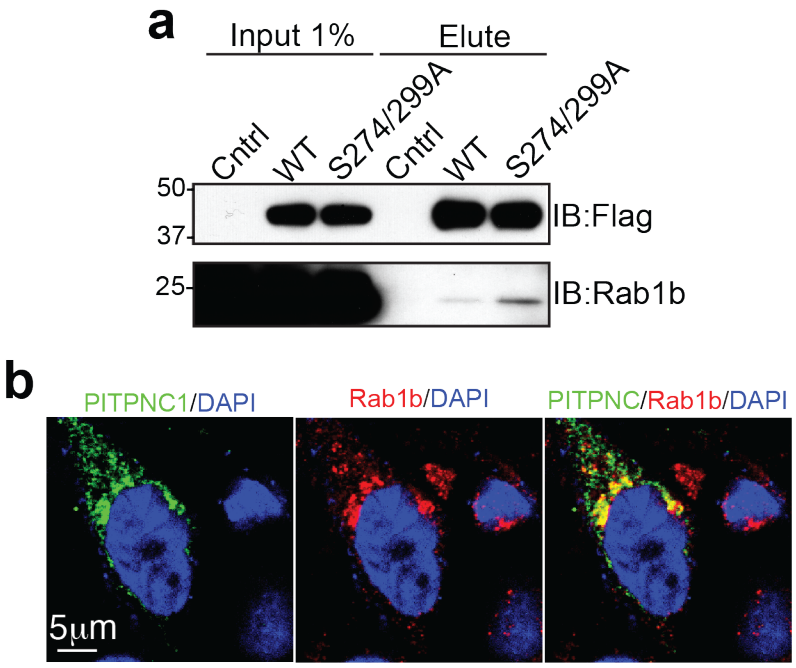

Figure 2.26. RAB1B binds to and co-localizes with PITPNC1.

a. Western blot analysis of input and immunoprecipitated Flag-tagged PITPNC1^{WT} and PITPNC1$^{S274A/299A}$ from MDA-MB-231 cells using anti-Flag and anti-RAB1B antibodies. **b.** MDA-MB-231 cells in (**a**) were immunostained for Flag (Green), RAB1B (red), and DAPI (blue).

Depletion of RAB1B has been previously found to cause vesiculation and breakdown of the Golgi structure, impairing secretion. Given our finding that PITPNC1 localization to the Golgi is required for its ability to promote metastasis, and that RAB1B regulate Golgi function, we next investigated whether PITPNC1 promotes metastasis by enhancing the abundance of RAB1B in the Golgi. Immunofluorescence analysis revealed a 2-fold reduction of endogenous RAB1B in the TGN upon knockdown of PITPNC1, without a change in the total cellular RAB1B protein levels as measured by western blot analysis of whole cell lysate (Figure 2.27a, b). Conversely, over-expression of wild-type PITPNC1 led to a significant increase in RAB1B localized to the Golgi (Figure 2.27c). Consistent with PITPNC1's ability to bind PI4P as requisite for its Golgi localization, lipid-binding mutant PITPNC1 did not increase localization of RAB1B to the Golgi (Figure 2.27c).

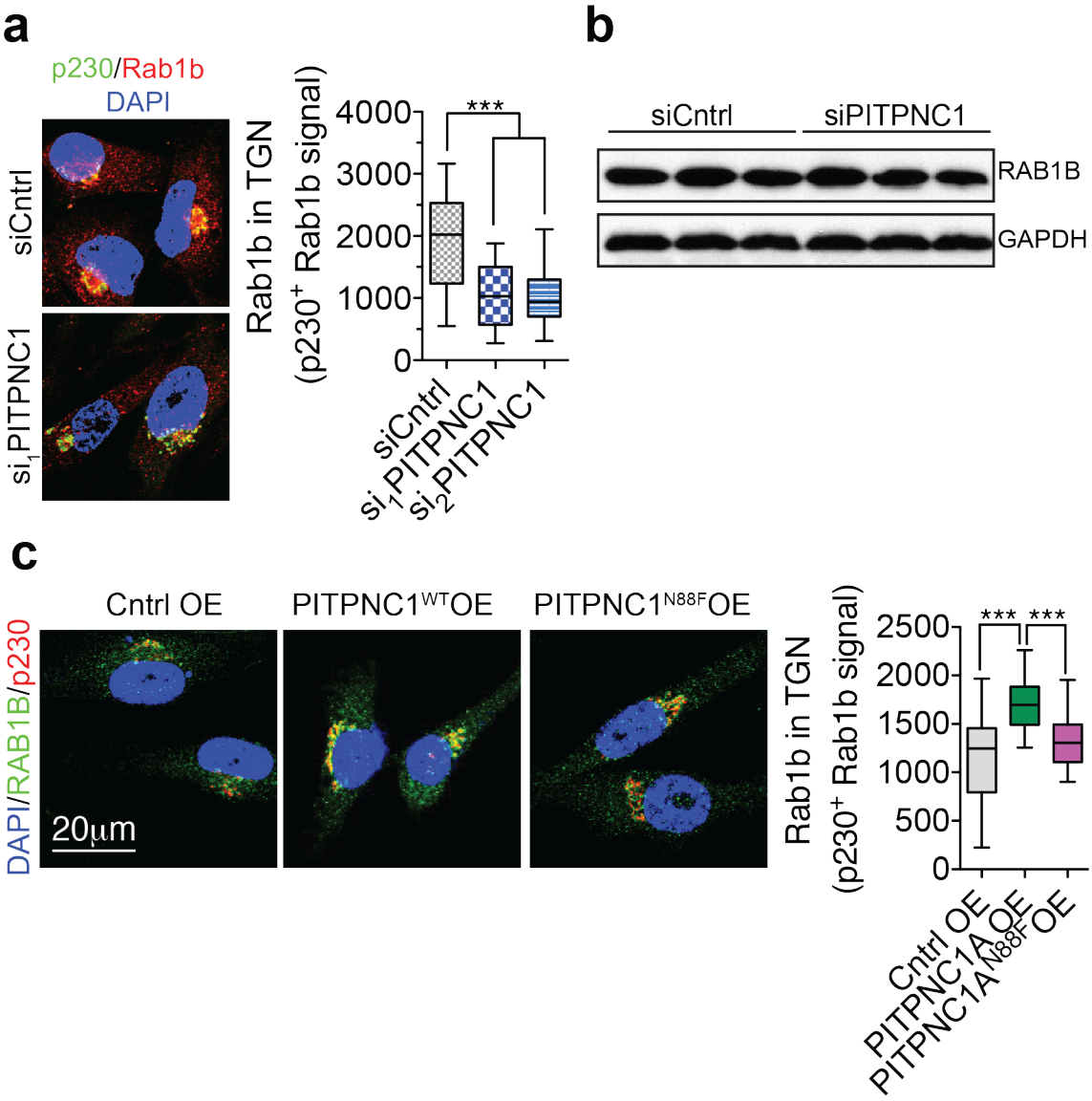

Figure 2.27. PITPNC1 recruits RAB1B to the Golgi.

a. LM2 breast cancer cells transfected with two independent siRNAs targeting PITPNC1 or a control siRNA were analyzed by immunofluorescence for RAB1B (red), p230 (green), and DAPI (blue). Right, quantification of RAB1B signal in the *trans* Golgi network (TGN) as marked by p230-positive areas. N=30/group.

b. Western blot analysis of RAB1B levels in whole cell lysate from LM2 cells in (**a**).

c. MDA-MB-231 cells overexpressing PITPNC1^{WT} or PITPNC1^{N88F} were analyzed by immunofluorescence microscopy as in (**a**). N=30/group. The upper and lower bars in box and whiskers plots show minimum and maximum data points. ***$p < 0.001$.

These above findings suggest that PITPNC1 regulates RAB1B Golgi localization to drive metastasis. To functionally test this relationship, we performed epistasis experiments wherein we depleted RAB1B in the setting of PITPNC1 overexpression (Figure 2.28a). Depletion of RAB1B strongly inhibited PITPNC1-mediated enhancement of Matrigel invasion and endothelial recruitment abilities (Figure 2.28b, c). Notably, depletion of RAB1B reduced these metastatic capacities more strongly in the setting of PITPNC1 overexpression than in control cells, indicating that the effects of RAB1B on these metastatic phenotypes are downstream of PITPNC1, rather than via a separate pathway. These epistasis and co-localization experiments support a pathway in which RAB1B acts as a downstream effector of PITPNC1-mediated metastasis.

Taken together, our findings identify PITPNC1 as a promoter of metastasis in melanoma, breast, and colon cancer through enhancing invasion and endothelial recruitment phenotypes. PITPNC1 binds to PI4P in the Golgi, recruiting its binding partner RAB1B to the Golgi. The role of the RAB1B/PITPNC1 protein complex in the Golgi and in driving metastasis will be further explored in Chapter III.

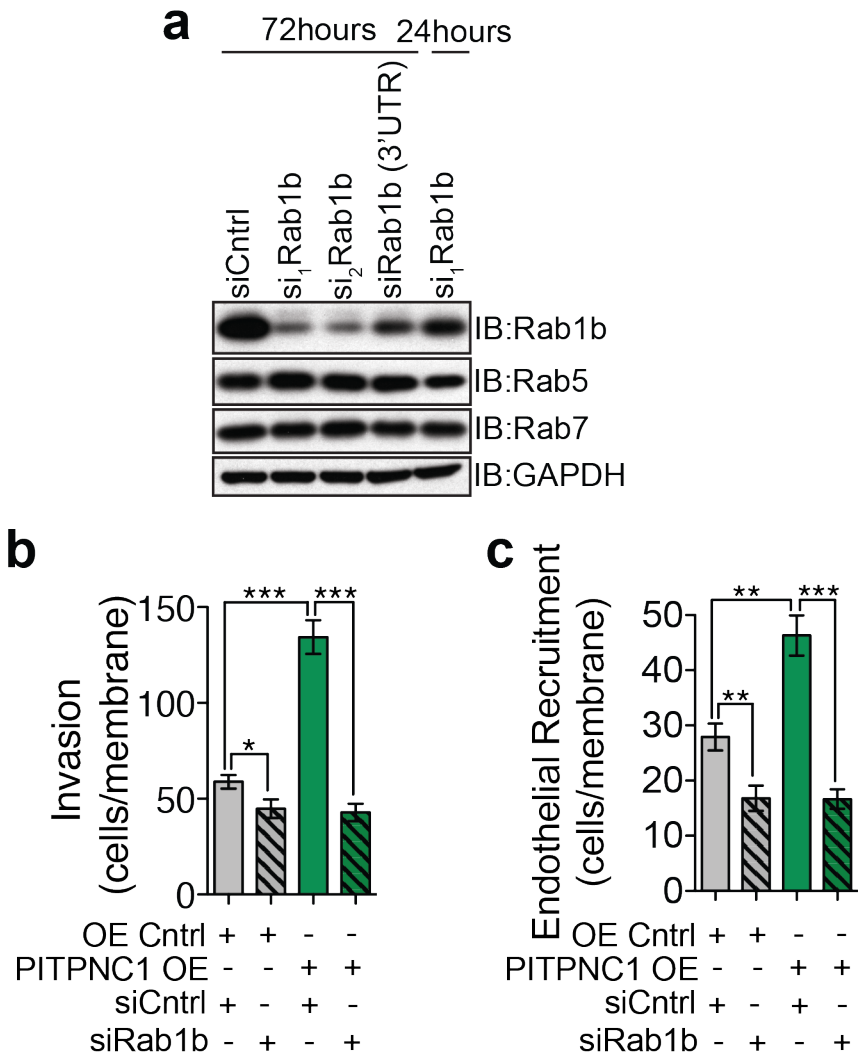

Figure 2.28. RAB1B is required for PITPNC1-mediated invasion and endothelial recruitment phenotypes.

a. Western blot analysis of RAB1B, RAB5, and RAB7 levels in LM2 cells transfected with 3 independent siRNAs targeting RAB1B either 72 hours or 24 hours post-transfection. GAPDH was used as a loading control. siRNA depletion of RAB1B was specific for RAB1B as expression levels of Rab5 and Rab7 were unchanged.

b, c. Matrigel invasion (**b**) and endothelial recruitment (**c**) by MDA-MB-231 cell overexpressing control vector or PITPNC1. 48 hours prior to the experiments both the control and PITPNC1-overexpressing cells were transfected with control siRNA or siRNA targeting RAB1B. N=4/group. Data are represented as mean ± S.E.M. **p < 0.01, ***p < 0.001.

CHAPTER III: CHARACTERIZATION AND FUNCTIONAL INSIGHTS INTO METASTATIC SECRETION REGULATED BY PITPNC1

Mechanism of Action of PITPNC1-RAB1B Complex in Metastatic Secretion

Through immunofluorescence, biochemical, and cell-biological experiments, we established a critical role for Golgi-localized RAB1B and PITPNC1 in driving metastasis. To identify the direct molecular effects between this protein complex, the Golgi, and metastasis, we first explored the role of PITPNC1 and RAB1B on Golgi structure and function.

Several studies have established a direct link between normal structure of the Golgi's membrane-bound stacks and proper Golgi secretory function. Addition of Brefeldin A, an antibiotic which blocks endoplasmic reticulum-to-Golgi transport induces fragmentation of the Golgi ribbon structure and leads to improper localization of secretory cargo (Fujiwara et al., 1988). Similarly, after addition of actin depolymerizing toxins such as cytochalasin D and latrunculin B, cells exhibit Golgi fragmentation and halted secretion (Lazaro-Dieguez et al., 2006). While a fragmented and diffuse Golgi inhibits secretion, an excessively condensed Golgi structure also prevents optimal vesicular budding. In actively secreting cells, enhanced vesicular budding results in an extension of the TGN as visualized by electron microscopy and immunofluorescence (Dippold et al., 2009). This extension is due to the protein GOLPH3, which bridges PI4P in the TGN to MYO18A, an actin cytoskeletal protein, inducing tensile forces on the

Golgi. The elongated Golgi structure facilitates vesicular budding and subsequently augmented secretion (Dippold et al., 2009).

The regulated release of secreted factors is known to orchestrate multiple steps of the metastatic cascade. Work by previous members of the laboratory has supported this requirement for metastatic secretion in multiple cancer types. Png and Halberg previously identified IGFBP2 and MERTK as proteins secreted by highly metastatic breast cancers to recruit endothelial cells and enhance metastasis (Png et al., 2012). Work by Jiamin Loo revealed highly metastatic colorectal cancer cells secrete creatine kinase brain-type (CKB) to augment metabolic energetics and enhance liver metastasis, although this protein is not secreted through the classical secretory pathway (Loo et al., 2015). We questioned whether highly metastatic cells would display changes in Golgi morphology consistent with their requirements for optimal secretion. We performed immunofluorescence experiments to compare Golgi extension between poorly metastatic parental cell populations and their *in vivo*-selected highly metastatic derivative sublines. Remarkably, we found that in breast, colon, and melanoma cancer, the highly metastatic sublines exhibited significantly increased Golgi length compared to the poorly metastatic parental cell population (Figure 3.1). This identifies a correlation between metastatic capacity and Golgi morphology and supports a role for extended Golgi structure and increased secretion in enhanced metastatic capacity.

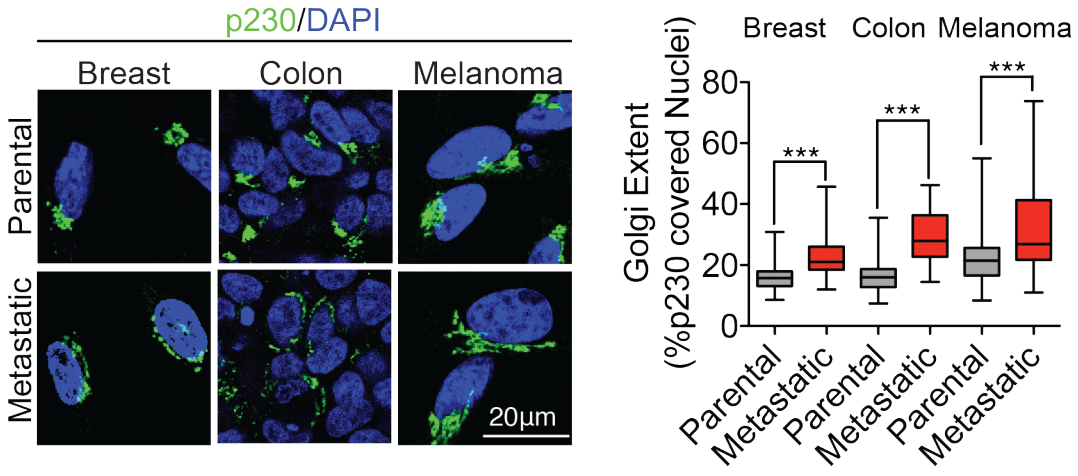

Figure 3.1. Golgi extension correlates with metastatic capacity in multiple cancer types.

Highly metastatic derivatives of the poorly metastatic MDA-MB-231 breast, LS174T colon, and MeWo melanoma cancer cells developed previously (Loo et al., 2015; Minn et al., 2005; Pencheva et al., 2012) and their parental cell populations were immunostained for p230 and DAPI. Golgi extent was quantified as the fraction of the nucleus circumference that was covered by p230-positive Golgi signal. N=40/group. Upper and lower bars in box and whiskers plots show minimum and maximum data points. ***$p < 0.001$.

Previous studies have identified an essential role for RAB1B in maintaining Golgi structure and thus secretory function (Haas et al., 2007; Romero et al., 2013). Similar to previous findings, Halberg observed that breast cancer cells acutely depleted of RAB1B exhibited a condensed Golgi structure compared to control cells by immunofluorescence (Figure 3.2a). In a time course experiment, extended depletion of RAB1B generated complete Golgi breakdown and fragmentation (Figure 3.2b).

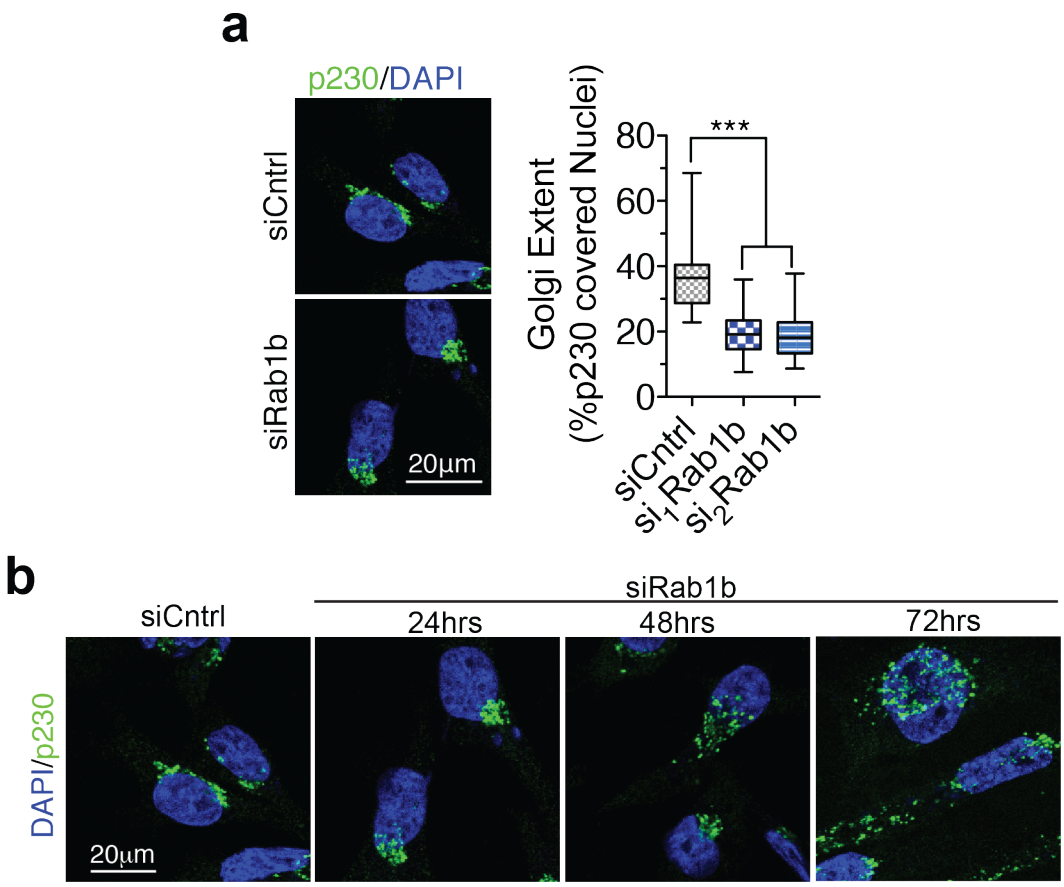

Figure 3.2. RAB1B is required for proper Golgi morphology.

a. LM2 cells transfected with either control or siRNAs targeting RAB1B were immunostained for p230 (green) and DAPI (blue) 24 hours post-transfection. Golgi extent was quantified as the fraction of the nucleus circumference covered by p230 positive Golgi signal. N= 40/group. Data are represented as mean ± S.E.M. ***$p < 0.001$.

b. Immunofluorescence images of cells in (**a**). Cells were imaged 24 hours, 48 hours, and 72 hours post-transfection.

I next questioned if PITPNC1 also regulates such Golgi morphology. I conducted immunofluorescence experiments on breast cancer cells with acute depletion of PITPNC1 and observed a similar condensation of the Golgi structure (Figure 3.3a). We further confirmed this immunofluorescence data with ultrastructural data. Transmission electron microscopy experiments performed by Kunihiro Uryu in The Rockefeller University

Electron Microscopy Facility also revealed a condensed Golgi morphology in cells with acute PITPNC1 depletion (Figure 3.3b).

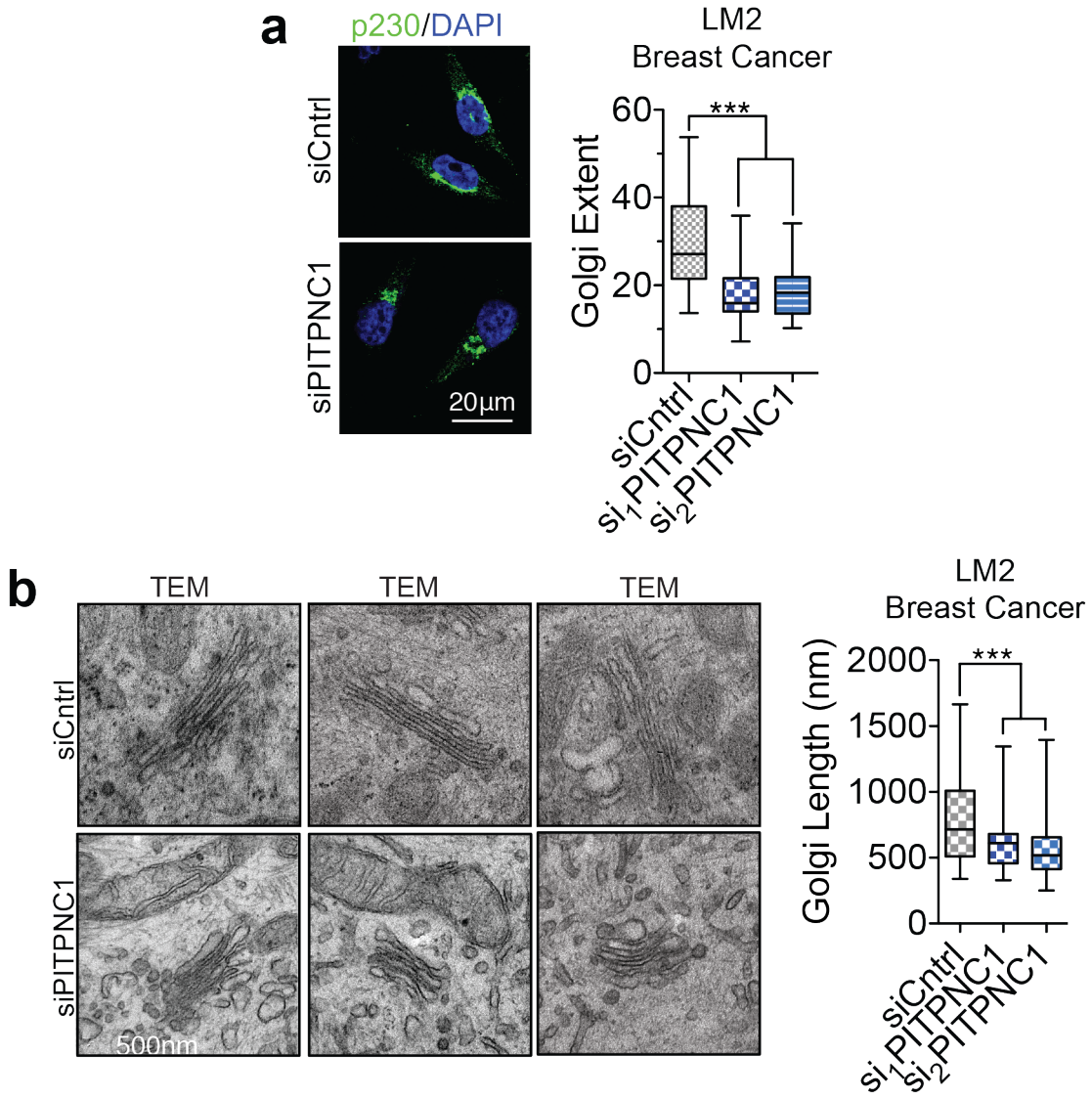

Figure 3.3. PITPNC1 is required for the extended ribbon Golgi morphology.

a. Golgi extent was analyzed by immunofluorescence in LM2 breast cancer cells transfected with siRNAs targeting PITPNC1 or a control siRNA. N=50/group.

b. Golgi structure was analyzed in transmission electron microscopy (TEM) images of LM2 cells transfected with siRNAs targeting PITPNC1 or a control siRNA. N=50/group. Upper and lower bars in box and whiskers plots show minimum and maximum data points. ***$p < 0.001$.

Notably, these effects were not restricted to breast cancer cells, as depletion of PITPNC1 in the MeWo melanoma cells and LvM-3B metastatic colon cancer cells also reduced Golgi extent compared to control cells (Figure 3.4). These results suggest that PITPNC1 regulates Golgi morphology in multiple cancer types.

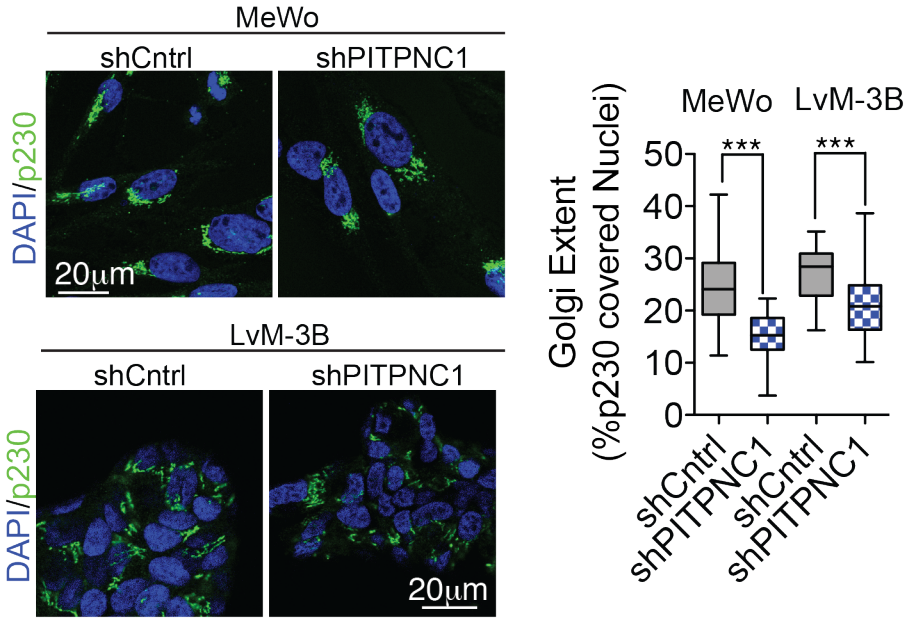

Figure 3.4. PITPNC1 regulates Golgi morphology in multiple cancer types. MeWo melanoma cells and LS174T-LvM3 colon cancer cells were transduced with a short hairpin targeting PITPNC1 or a control hairpin and immunostained for p230 (green) and DAPI (blue). Right, quantification of Golgi extent. N=25/group. Upper and lower bars in box and whiskers plots show minimum and maximum data points. ***$p < 0.001$.

Conversely, breast cancer cells with PITPNC1 overexpression displayed an extended Golgi morphology by both electron microscopy and immunofluorescence, similar to that seen in actively secreting cells (Figure 3.5a-c). However, the lipid-binding mutant form of PITPNC1, PITPNC1^{N88F}, was unable to elongate the Golgi structure (Figure 3.5a, b). This indicates that PITPNC1's role in Golgi structure is dependent upon its localization to the Golgi through binding PI4P in the TGN. Together these effects led

us to hypothesize that PITPNC1 and RAB1B may promote metastasis via mediating Golgi morphology and consequently secretory capacity.

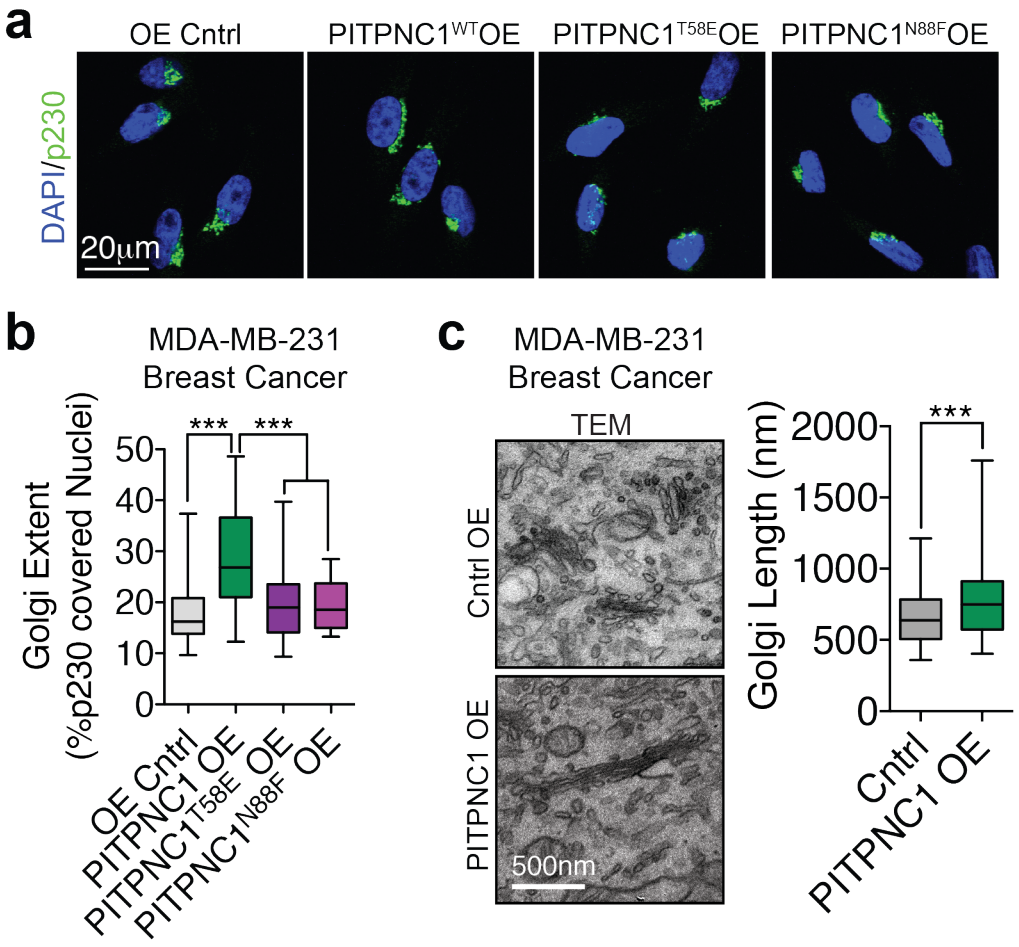

Figure 3.5. PITPNC1 promotes Golgi extension.

a. MDA-MB-231 breast cells overexpressing control vector, wild-type, T58E, or N88F mutant forms of PITPNC1 were immunostained for p230 (green) and DAPI (blue).

b. Quantification of Golgi extent in cells from (**a**). N=20/group.

c. TEM images of MDA-MB-231 cells overexpressing PITPNC1 or a control vector. N=50/group.

Upper and lower bars in box and whiskers plots show minimum and maximum data points. ***$p < 0.001$.

We next sought to investigate how the PITPNC1-RAB1B complex regulates Golgi structure. Given that Golgi extension requires binding of GOLPH3 to Golgi PI4P, we speculated that PITPNC1-RAB1B may induce Golgi elongation through increasing Golgi PI4P levels. Indeed, RAB1B has been previously shown to recruit the PI4-kinase PI4KA (also known as PI4KIIIα) from the plasma membrane to the TGN, which increases local PI4P abundance (Dumaresq-Doiron et al., 2010; Monetta et al., 2007). To determine whether PI4P levels in the TGN were mediated by PITPNC1, we performed co-immunofluorescence imaging experiment using p230 to mark the TGN and FAPP1-PH to mark PI4P. Quantification of these images revealed that PITPNC1 depletion significantly reduced TGN PI4P abundance, whereas PITPNC1 overexpression significantly increased TGN PI4P levels (Figure 3.6a, b). We further confirmed this result by repeating these experiments using a PI4P-specific antibody in place of the PH domain (Figure 3.6c). These findings suggest that TGN PI4P abundance is governed by PITPNC1 in cancer cells.

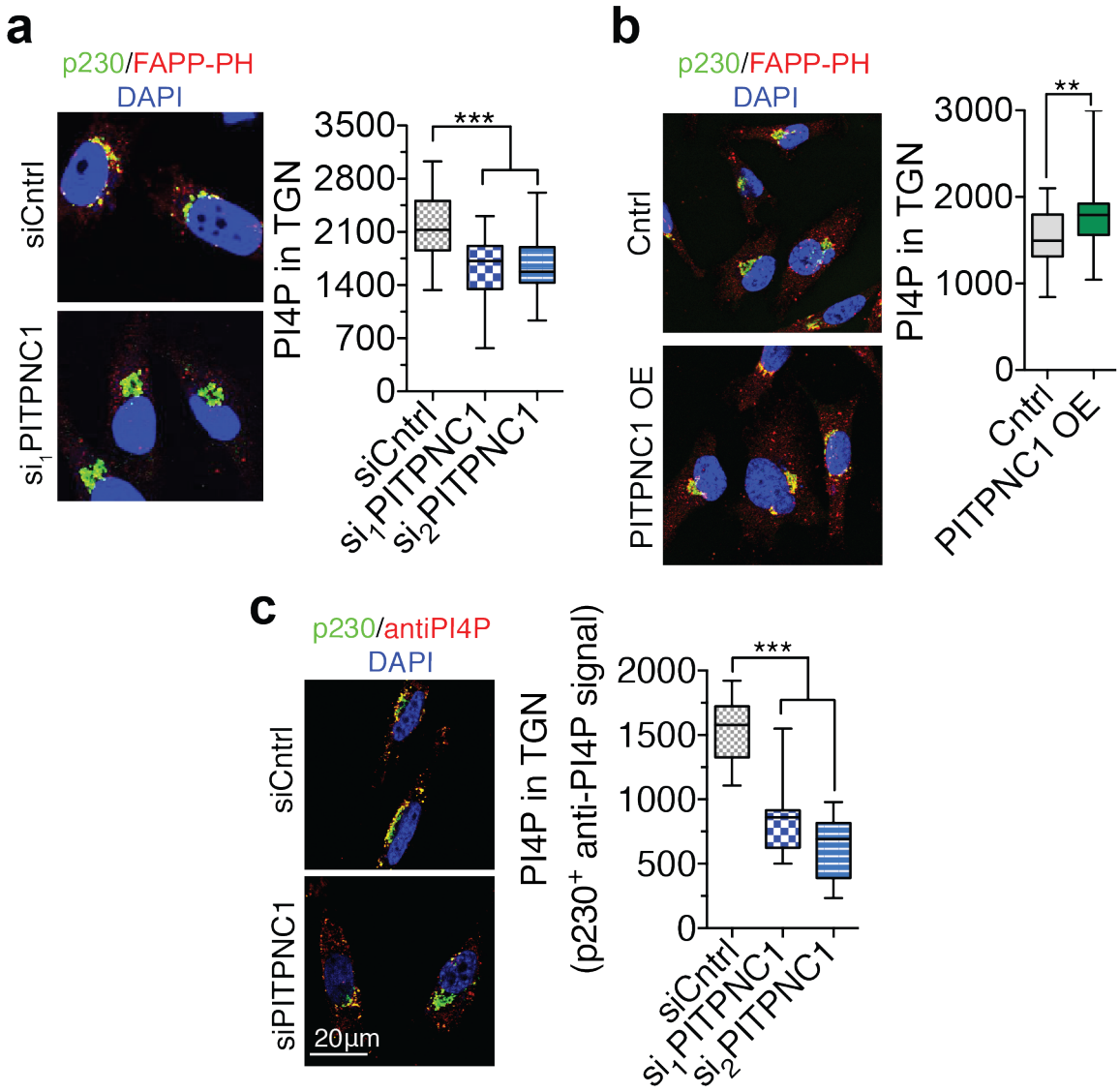

Figure 3.6. PITPNC1 governs PI4P abundance in the Golgi.

a, b. LM2 cells transfected with siRNAs targeting PITPNC1 or a control siRNA (**a**) or MDA-MB-231 cells overexpressing PITPNC1 or control vector (**b**) were stained for PI4P using FAPP-PH domain (red), p230 (green) and DAPI (blue). PI4P levels in the Golgi were quantified as mean fluorescence intensity of FAPP1-PH signal in p230-positive regions. N=50/group.

c. LM2 cells as in (**a**) were immunostained for PI4P using anti-PI4P antibody (red), p230 (green), and DAP1 (blue). N=40/group.

Upper and lower bars in box and whiskers plots show minimum and maximum data points. **p < 0.01, ***p < 0.001.

To further explore whether PI4KA was the kinase responsible for the observed increase in PI4P levels in the breast cancer cells, we performed epistatic experiments with the four PI4Ks expressed in mammalian cells: PI4K2A, PI4K2B, PI4KB, and PI4KA. Unlike PI4KA, PI4K2A, PI4KB, and PI4K2B are all constitutively Golgi-resident PI4-kinases (Balla, 2013). I depleted each of these kinases using siRNA specific to each kinase and found that depletion of PI4K2A and PI4KB dramatically reduced the ability of cancer cells to invade through Matrigel in both PITPNC1 overexpression cells and control cells (Figure 3.7). This suggests that both of these kinases are critical for general Golgi function, but that this effect is independent of PITPNC1. Depletion of PI4K2B revealed a minimal effect on either control cells or cells with PITPNC1 overexpression. The negligible effect of depleting PI4K2B is likely due to its much lower kinase activity compared to PI4K2A and PI4KB (Balla, 2013), and thus is not likely to be involved in PITPNC1-mediated secretion. However, depletion of PI4KA entirely ablated the effects of PITPNC1-induced invasion but did not affect the invasive capacity of control cells (Figure 3.7). Taken together, these findings suggest that PI4KA is recruited to the Golgi from either the cytoplasm or plasma membrane by PITPNC1-RAB1B to increase TGN PI4P and facilitate secretion.

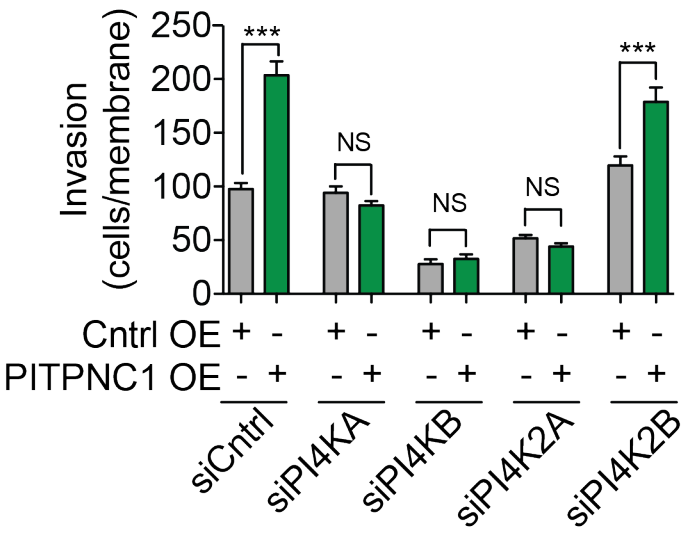

Figure 3.7. Modulation of PI4K isoforms in PITPNC1-mediated invasion. MDA-MB-231 cells overexpressing PITPNC1 or a control vector were transfected with siRNA targeting PI4KA, PI4KB, PI4K2A, PI4K2B, or a control siRNA and subjected to the Matrigel invasion assay. N=4/group. Data are represented as mean ± S.E.M. ***p < 0.001.

Our model predicts that increased PI4P levels in the TGN driven by PITPNC1-RAB1B would recruit additional GOLPH3 to the Golgi, allowing for increased Golgi extension and metastatic secretion. We tested this hypothesis by quantifying the amount of GOLPH3 in the Golgi by immunofluorescence analysis. Depletion of either PITPNC1 or RAB1B led to a 2-fold reduction in GOPH3 abundance in the Golgi, as measured by p230-positive areas of the cell (Figure 3.8a). These changes in localization were not due to changes in GOLPH3 expression, as protein levels in whole cell lysate were unchanged (Figure 3.8b). Correspondingly, overexpression of PITPNC1 correlated with an increase in GOLPH3 Golgi levels (Figure 3.8c).

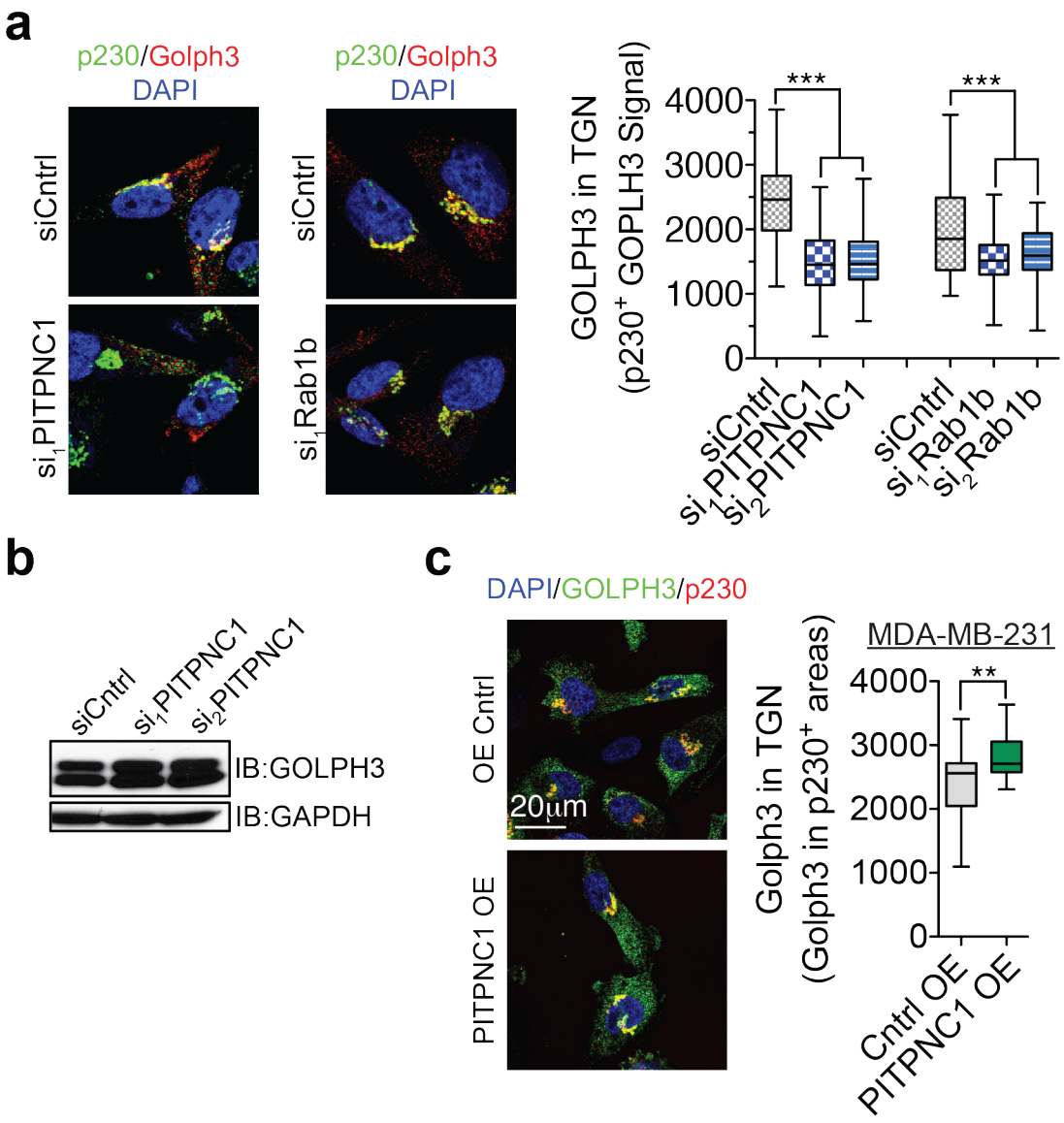

Figure 3.8. The PITPNC1-RAB1B complex recruits GOLPH3 to the Golgi.

a. LM2 cells transfected with either control siRNA or siRNAs targeting PITPNC1 or RAB1B were immunostained for endogenous GOLPH3 and p230. Right, quantification of GOLPH3 levels in the *trans*-Golgi. N=40/group.

b. Western blot analysis of GOLPH3 levels in whole cell lysate from LM2 cells transfected with siRNA targeting PITPNC1 or a control siRNA.

c. MDA-MB-231 cells expressing PITPNC1 or control vector were analyzed for *trans*-Golgi GOLPH3 levels as in (**a**). Upper and lower bars in box and whiskers plots show minimum and maximum data points. **p < 0.01, ***p < 0.001.

We next asked if PITPNC1-dependent recruitment of GOLPH3 to the Golgi is required for PITPNC1-mediated phenotypes. I depleted GOLPH3 using siRNA, and verified the efficiency of knockdown by western blot analysis (Figure 3.9a). Knockdown of GOLPH3 reversed the extended Golgi phenotype induced by PITPNC1 overexpression by 63% (Figure 3.9b).

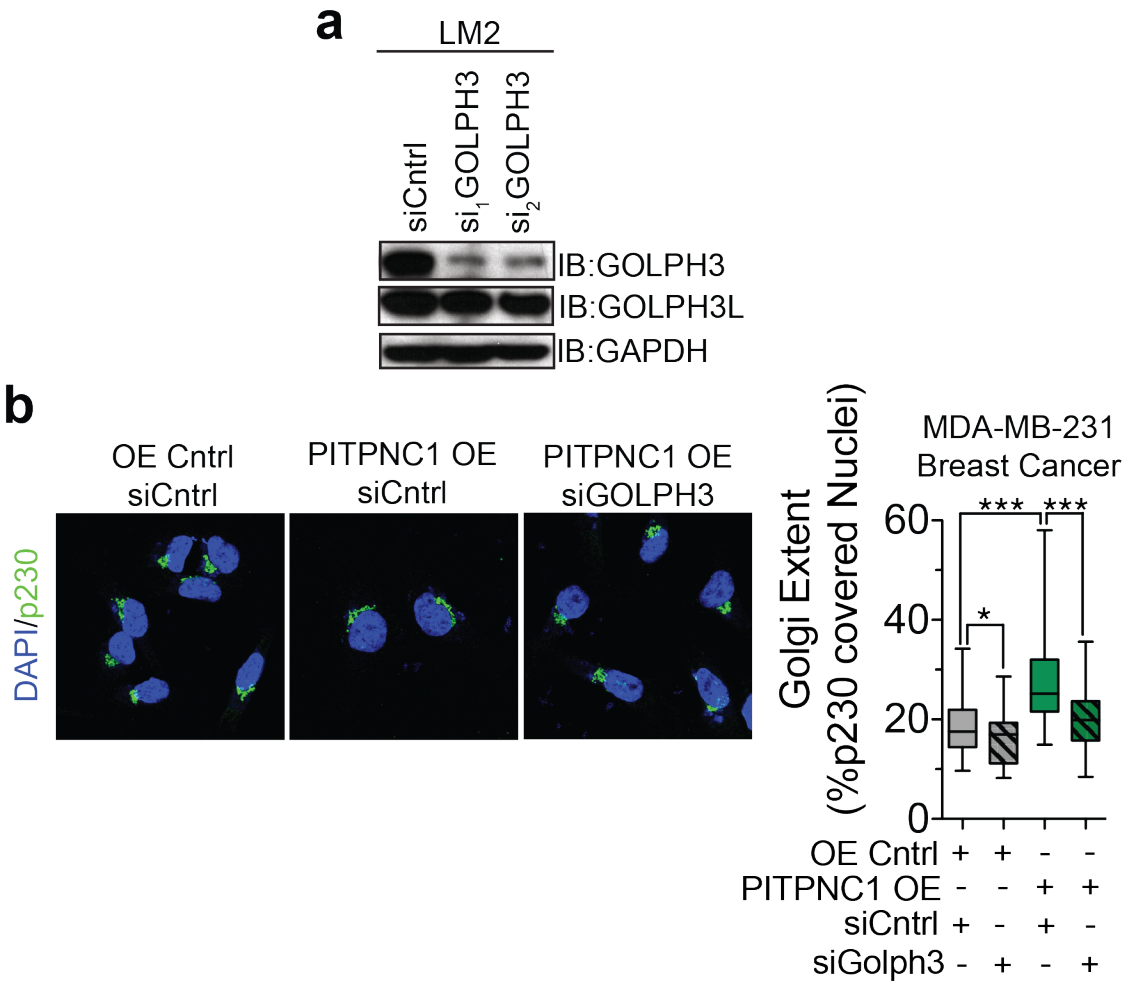

Figure 3.9. GOLPH3 is necessary for PITPNC1-mediated Golgi extension.

a. Western blot analysis of GOLPH3 and GOLPH3L levels in LM2 cells transfected with siRNAs targeting GOLPH3 or a control siRNA. GADPH is used as loading control.

b. MDA-MB-231 cells transfected with GOLPH3 siRNA or control siRNA in the setting of PITPNC1 or control overexpression were immunostained for p230 (green) and DAPI (blue). Right, analysis of Golgi extent. N=30/group. Upper and lower bars in box and whiskers plots show minimum and maximum data points. *p<0.05, ***p < 0.001.

Lastly, we performed epistasis experiments to confirm that GOLPH3 is functionally downstream of PITPNC1's pro-metastatic phenotypes. Depletion of GOLPH3 abrogated PITPNC1-mediated increases in invasion and endothelial recruitment capacities, indicating GOLPH3 is required for PITPNC1's promotion of these effects (Figure 3.10a, b). Depletion of GOLPH3 in control cells also reduced the ability of these cells to invade and recruit endothelial cells but to a significantly lesser extent than in PITPNC1 overexpression cells, verifying that these effects are dependent upon PITPNC1.

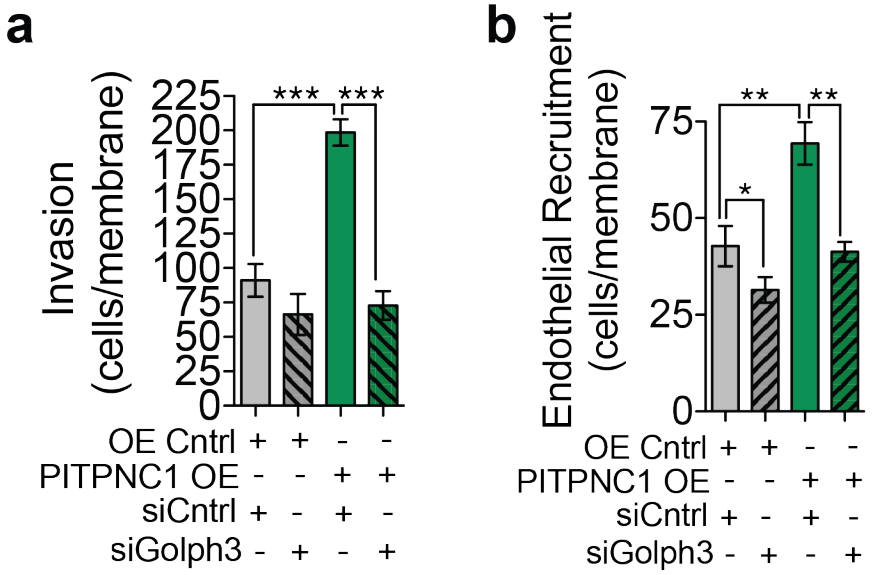

Figure 3.10. GOLPH3 is required for PIPTNC1-mediated metastatic phenotypes. **a, b.** MDA-MB-231 cells were transfected with GOLPH3 siRNA or control siRNA in the setting of control or PITPNC1 overexpression and subjected to the invasion (**a**) and endothelial recruitment (**b**) assays. N=4/group. Data are represented as mean ± S.E.M. $^{**}p < 0.01$, $^{***}p < 0.001$.

We have demonstrated that PITPNC1 recruits RAB1B to the Golgi, which in turn recruits PI4KA. Increased TGN-localized PI4KA increases PI4P TGN levels, recruiting

GOPLPH3 to the TGN to induce Golgi extension. Given the effects of PITPNC1 depletion and overexpression on the structure of the Golgi network, the role of RAB1B in regulating Golgi structure and secretion, and that Golgi extension reflects enhanced vesicular release, we speculated that PITPNC1's pro-metastatic effects are mediated through increased secretory capacity. We previously demonstrated that PITPNC1 promotes cancer cell invasion and endothelial recruitment. These phenotypes both require the secretion of specific factors: proteases for successful invasion and chemoattractants for successful recruitment of endothelial cells. Additionally, cancer cell secretion has been established as necessary in other steps of the metastatic cascade, including immune evasion and metastatic niche colonization (Joyce and Pollard, 2009; Psaila and Lyden, 2009). This model is also consistent with previous work by Png and Halberg identifying PITPNC1 as an upstream effector of secreted IGFBP2 in breast cancer metastasis (Png et al., 2012).

To test whether PITPNC1 expression directly impacted cancer cell secretion, I performed a set of Golgi exit assay experiments (Bonazzi et al., 2005). In this assay, cells are placed at 20°C to halt secretion. Cells are then placed back at 37°C and secretion resumes. Vesicular release is tracked by fixing and staining cells at various time points after the return to 37°C. I conducted this assay by tracking vesicular release by quantifying the amount of PI4P-containing vesicles in the cytoplasm. Since vesicular budding requires PI4P (Hama et al., 1999; Wang et al., 2003), vesicles traveling to the plasma membrane contain PI4P. To demonstrate that PI4P in the cytoplasm marks secreted vesicles, I generated an MMP14-Flag construct to label secretory cargo. MMP14 is a transmembrane matrix metalloproteinase that is sorted through Golgi to the plasma

membrane (Apte et al., 1997). MMP14-Flag and PI4P in the cytoplasm exhibited co-localization, indicating PI4P present in the cytoplasm is predominantly located in secretory vesicles (Figure 3.11).

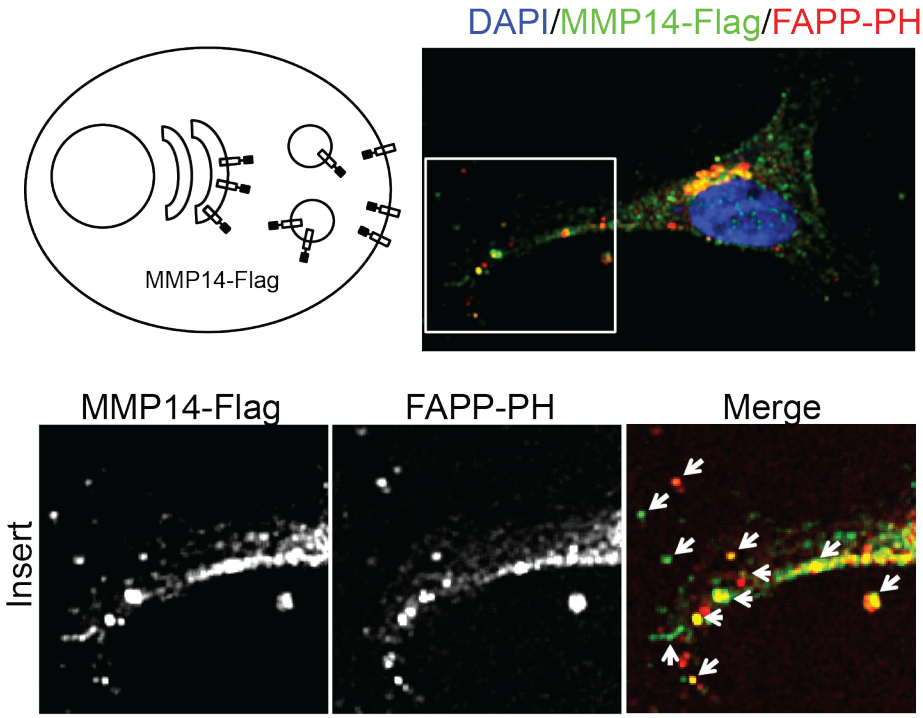

Figure 3.11. Validation of an MMP14-Flag construct to label secretory vesicles. Left, diagram of MMP14-Flag construct labeling secretory vesicles. Right, cancer cells expressing MMP14-Flag were immunostained for DAPI (blue), MMP14-Flag (green), and FAPP-PH (PI4P marker, red). Arrows indicate signal overlap between MMP14-Flag and FAPP-PH.

Interestingly, breast cancer cells with PITPNC1 depletion revealed significantly reduced release of vesicles from the Golgi (Figure 3.12a). Importantly, PITPNC1 overexpression induced increased vesicular release in this assay, consistent with a role for PITPNC1 in driving metastatic secretion (Figure 3.12b). These effects were dependent upon RAB1B, as depletion of RAB1B abrogated the effects of PITPNC1 overexpression on increased vesicular release (Figure 3.12b).

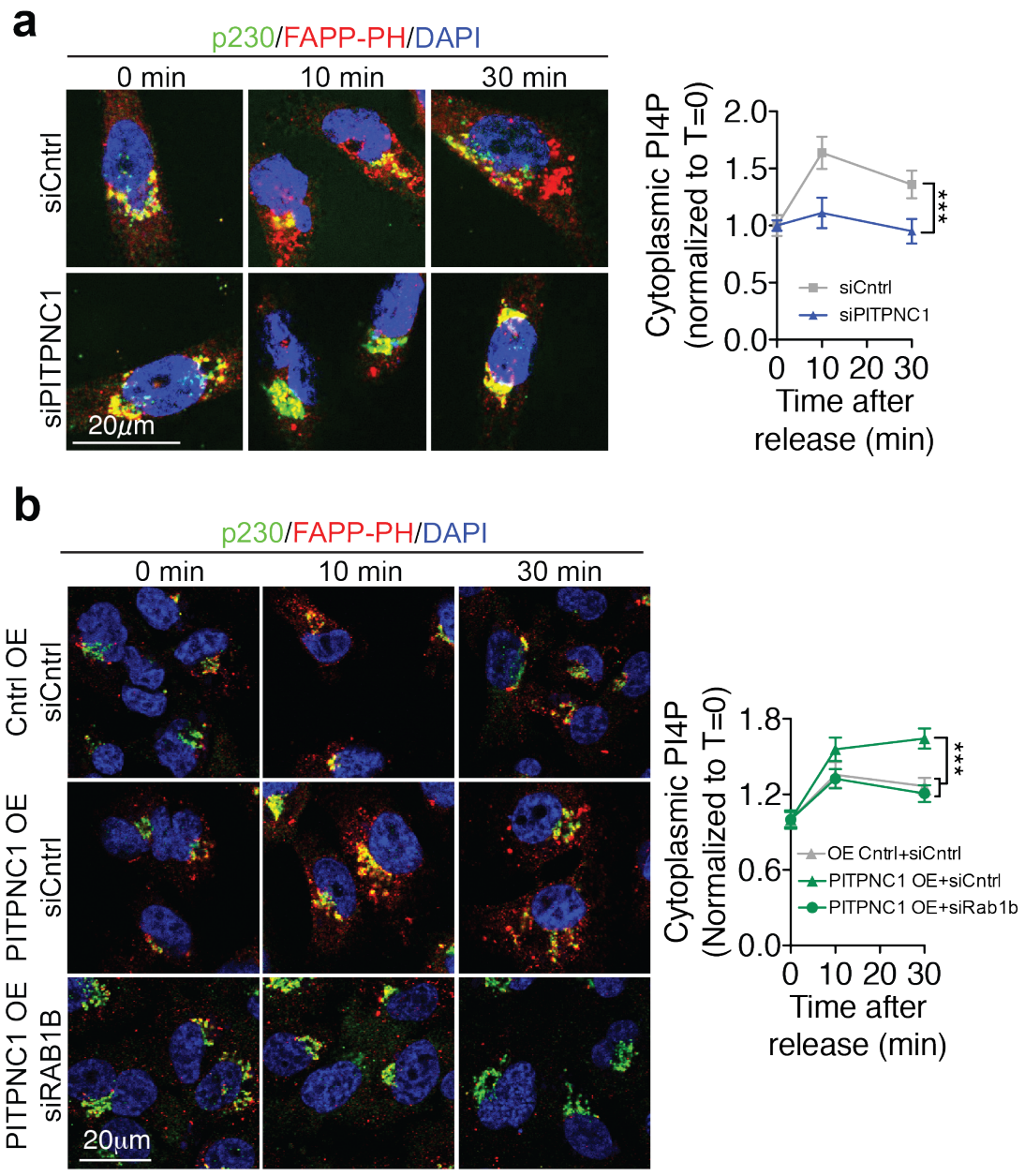

Figure 3.12. PITPNC1 facilitates vesicular secretion.

a, b. Golgi exit assay analysis of LM2 cells transfected with control or PITPNC1-targeting siRNA (**a**) and MDA-MB-231 cells overexpressing PITPNC1 or control vector and transfected with siRNA targeting RAB1B or control siRNA (**b**). Cells were immunostained for PI4P (FAPP-PH, red), p230 (green), and DAPI (blue) at time 0, 10, and 30 minutes. The abundance of PI4P-containing vesicles released to the cytoplasm was determined by subtracting Golgi-localized PI4P from the total cellular PI4P signal. N=10/time point/group. Significance was determined by Fisher's method. ***p<0.001.

Development of a Method to Profile the Secretome of Breast Cancer Cells

We next sought to identify a set of secreted proteins regulated by PITPNC1 and capable of mediating the pro-metastatic effects of PITPNC1. I developed a method to isolate secreted proteins and quantify their relative amounts using stable isotope labeling by amino acids in cell culture (SILAC) and mass spectrometry. We chose to use SILAC since the incorporation of stable isotope-labeled amino acids into proteins allowed for the quantification of small differences in protein amounts. SILAC has previously been used for characterizing the secretome in pancreatic cancer and glioblastoma (Formolo et al., 2011; Gronborg et al., 2006). We were interested in identifying secreted proteins whose secretion changed upon PITPNC1 depletion, thus acting as downstream mediators of metastasis. Utilizing mass spectrometry provides unbiased profiling of all proteins secreted from the cell, enabling identification of novel secreted promoters of metastasis.

Cells secrete proteins in low abundance compared to the overall cellular proteome, and thus it is necessary to maximize secreted protein recovery for mass spectrometry while also minimizing contamination from cytosolic proteins and proteins found in cell culture media. Conditioned media from the cancer cells was collected, concentrated, and subjected to tandem liquid-chromatography mass spectrometry. The initial attempts at this method were performed in media containing fetal bovine serum (FBS), a standard component of cell culture media. However the large quantity of serum proteins interfered with MS analysis by causing incomplete tryptic digestion of secreted proteins (Figure 3.13a). However, the absence of serum in the cell culture media alters cellular processes, including secretion. Prolonged serum starvation leads to cellular death, releasing cellular proteome contents into the media. Contamination of conditioned media

with cytosolic proteins impedes the detection of the low abundance secreted proteins. Given these factors, it was necessary to optimize the time period of serum starvation prior to media collection to maximize secreted protein recovery while minimizing cell death. LM2 cells and CNLM1a cells were cultured in serum-free media for 24 hours, and the number of cells counted every 4 hours (Figure 3.13b). Based on this data, 12 hours was chosen as the duration of serum starvation prior to collection of conditioned media.

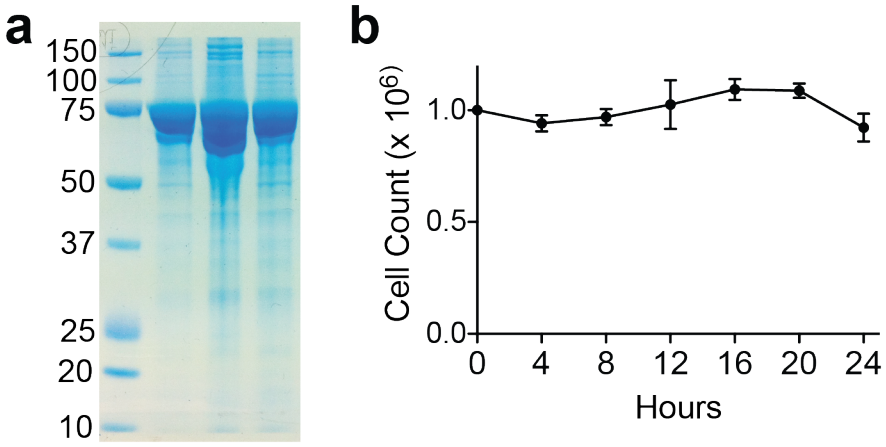

Figure 3.13. Optimization of conditions for cellular secretome profiling.
a. Gel electrophoresis of secreted media collected from MDA-MB-231 cells seeded in triplicate. The prominent band at 75kD corresponds to albumin, a component of FBS.
b. One million MDA-MB-231 cells were seeded in serum-free media and counted every four hours. Data are represented as mean ± S.E.M.

To verify this technique and identify potential pro-metastatic secreted proteins, I first performed secretome analysis on the MDA-MB-231 parental cell line compared to the LM2 metastatic derivative cell line, as well as the CN34 cell line compared to the CNLM1a derivative cell line to identify secreted proteins more abundant in conditioned media collected from the highly metastatic derivative sublines (Table 3.1, 3.2).

Table 3.1. Secretome profiling of LM2 cells compared to MDA-MB-231 cells.

Unique Peptides Identified	Fold Difference (LM2/MDA)	Gene Symbol	Gene Name
20	6.2581	MMP1	Matrix metalloproteinase 1
23	4.4413	COL6A1	Collagen alpha-1(VI) chain
18	3.3526	PSAT1	Phosphohydroxythreonine aminotransferase
5	2.8698	IARS	Isoleucine tRNA ligase
8	2.6846	VIM	Vimentin
9	2.3586	HNRNPC	Heterogeneous nuclear ribonucleoproteins C1/C2
22	2.1874	IQGAP1	p195;Ras GTPase-activating-like protein
4	2.158	PARP1	Poly [ADP-ribose] polymerase 1
14	2.1391	SERPINE2	Glia-derived nexin

Table 3.2. Secretome profiling of CNLM1a1 cells compared to CN34 cells.

Unique Peptides Identified	Fold Difference (CNLM1a1/ CN34)	Gene Symbol	Gene Name
8	167.9701	IGFBP1	Insulin-like growth factor-binding protein 1
6	30.0580	NARC1	Neural apoptosis-regulated convertase 1
12	18.4200	MMP1	Matrix metalloproteinase 1
11	14.9509	MFGE8	Breast epithelial antigen
35	13.2840	VPO1	Vascular peroxidase 1
10	10.6790	PLAT	Tissue-type plasminogen activator
25	8.2782	LAMB2	Laminin subunit beta-2
9	7.8866	CDH4	Cadherin-4
9	6.8671	CKB	Creatine kinase B-type

Of the secretome profiling experiments, only one protein was highly abundant in both the LM2 and CNLM1a1 conditioned media compared to conditioned media from the parental cell populations—MMP1, a matrix metalloproteinase. The MMPs are established regulators of metastasis. MMP activity increases in almost all human cancers compared to non-cancerous surrounding tissue and this activity increase correlates with cancer stage (Egeblad and Werb, 2002). MMPs breakdown extracellular matrix components such as collagens, proteoglycans, and laminins to facilitate cancer cell invasion with the local tissue, intravasation into the circulatory system, and extravasation into a distal organ for metastatic colonization. The identification of MMP1 in the analysis of secreted proteins from the metastatic cell lines validated the developed method for secretome analysis of breast cancer cells. Additional secreted proteins previously demonstrated to promote metastasis include IGFB1, which increases cancer cell proliferation and survival (Vu and Werb, 2000), PLAT, which enhances metastatic invasion through activating plasminogen to degrade the ECM (Andreasen et al., 1997), and CKB, which aids cancer cell energetics (Loo et al., 2015). Components of the ECM that promote cancer cell invasion were also identified, including the collagen COL6A1 (Lu et al., 2012; Naba et al., 2014), and the laminin LAMB2 (Patarroyo et al., 2002).

Optimization of the liquid chromatography/tandem mass spectrometry (LC/MS-MS) protocol by Henrik Molina in The Rockefeller University's Proteomics Resource Center improved the sensitivity of the data collected from the CN34 and CNLM1a1 experiment. In this data set, more proteins were identified (990 proteins compared to 505 proteins in the LM2/MDA experiment) with improved quantification of proteins in the

conditioned media allowing for a broader range of fold difference. We utilized this optimized protocol in all further secretome profiling studies.

Identification and Validation of Secreted Proteins Regulated by PITPNC1

Having validated SILAC and MS for the identification of pro-metastatic secreted proteins, we next sought to identify secreted proteins regulated by PITPNC1 and downstream of PITPNC1-mediated metastasis. PITPNC1-depleted cells and control cells were grown in SILAC media, and conditioned media was collected, concentrated, and subjected to mass spectrometry. Proteomic analysis revealed six proteins that were at least two-fold less abundant in conditioned media from PITPNC1-depleted cells relative to control cells (Figure 3.11a). These proteins were matrix metalloproteinase 1 (MMP1), platelet-derived growth factor A (PDGFA), platelet-derived growth factor receptor L (PDGFRL), A Disintegrin and metalloproteinase domain-containing protein 10 (ADAM10), High temperature requirement protease 1 (HTRA1), and Family with Sequence Similarity 3 (FAM3C, also called ILEI) (Figure 3.14).

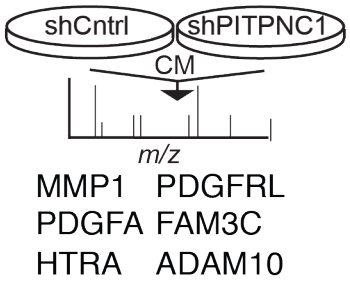

Figure 3.14. Identification of secreted proteins regulated by PITPNC1.
Conditioned media was collected from SILAC-labeled LM2 control and PITPNC1-knockdown cells and subjected to liquid chromatography-mass spectrometry (LC-MS/MS) to identify proteins underrepresented in PITPNC1 knockdown media.

We next verified the reduced abundance of these proteins in secreted media by performing western blot analysis, and confirmed that the protein levels of all of these factors except PDGFRL decreased significantly upon PITPNC1 knockdown (3.15a, b).

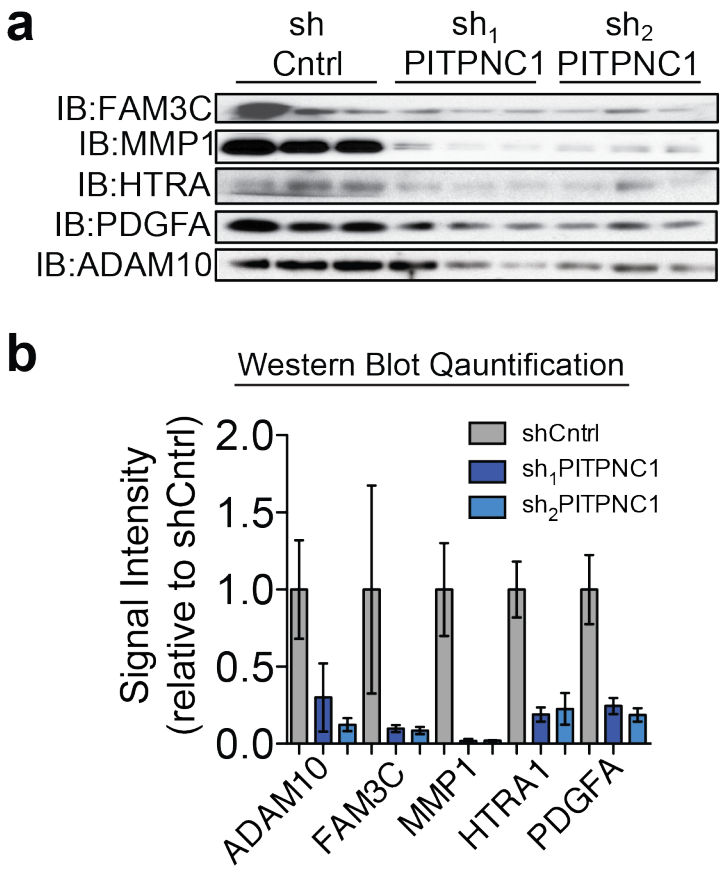

Figure 3.15. PITPNC1-regulated secreted proteins in cellular conditioned media.
a. Western blot analysis for FAM3C, MMP1, HTRA1, PDGFA, and ADAM10 in conditioned media from LM2 cells expressing short hairpins targeting PITPNC1 or a control hairpin.
b. Densitometry analysis of western blots in (**a**).

Importantly, the reduced secretion of these proteins was not due to reduced expression of these proteins. Gene expression levels of FAM3C, MMP1, ADAM10, and PDGFA were not decreased in PIPTNC1-knockdown cells compared to control cells (Figure 3.16a). For HTRA, gene expression was reduced by 50% in PITPNC1 knockdown cells, but its secreted protein level was reduced by 80%, indicating that PITPNC1 in part regulates the secreted level of this protein. However, although the mRNA levels of these genes are unchanged, any post-transcriptional regulation of mRNA could affect intracellular protein levels. To ensure that the differences in secreted protein levels were due to secretion and not differences in intracellular protein levels, I conducted western blot analysis on lysate from control and PITPNC1-depleted cells to measure intracellular protein levels of the secreted factors and found that the levels of MMP1, ADAM, FAM3C, and PDGFA were similar (Figure 3.16b). For HTRA, the intracellular protein level in PITPNC1 knockdown cells was decreased, however this decrease was again less than the reduction in secreted levels consistent with the role of PITPNC1 in secretion of this factor. These findings are consistent with a model wherein these secreted factors are not released from the Golgi upon PITPNC1 knockdown as a consequence of impaired PI4P/GOLPH3 function.

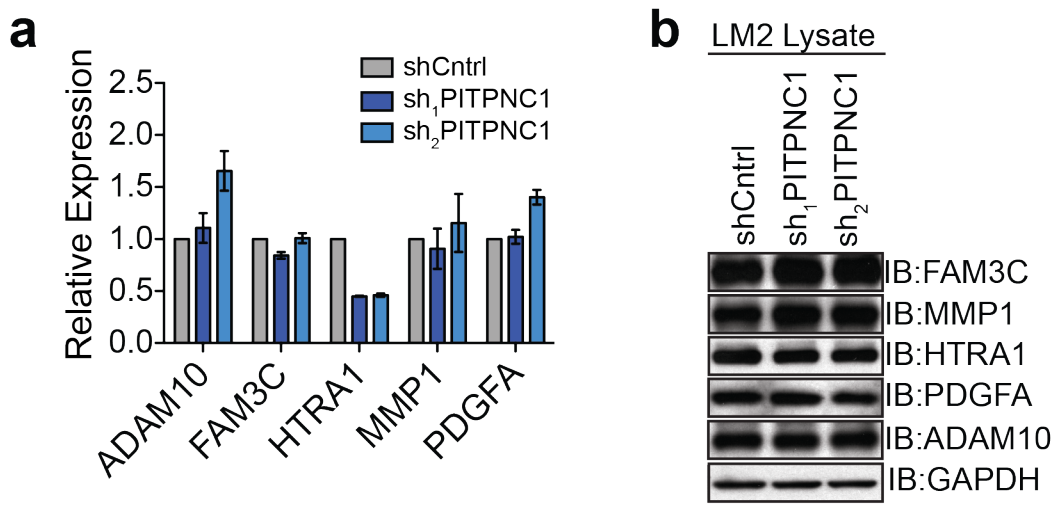

Figure 3.16. Intracellular expression levels of PITPNC1-regulated secreted factors.
a. ADAM10, FAM3C, HTRA1, MMP1, and PDGFA expression levels were determined by qRT-PCR in LM2 cells transduced with short hairpins targeting PITPNC1 or a control vector. N= 3/group. Error bars represent S.E.M.
b. Western blot analysis of FAM3C, MMP1, HTRA1, PDGFA, and ADAM10 in whole cell lysate from cells as in (**a**). Western blot analysis of GAPDH was used as a loading control.

To show that loss of PITPNC1 impaired secretion of one of these specific secreted factors, in I generated a red fluorescent protein (RFP)-tagged version of MMP1 as a marker for metastatic secretion, and tracked localization of this marker in a Golgi exit assay. PITPNC1 depletion significantly reduced MMP1-RFP release from the TGN (Figure 3.17), indicating secretion of MMP1 is impaired in the absence of PITPNC1.

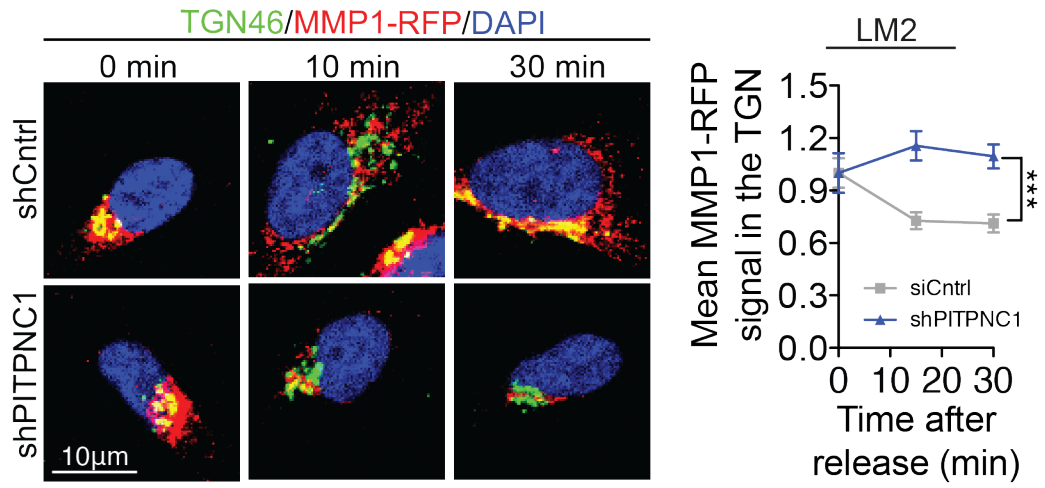

Figure 3.17. PITPNC1 is required for secretion of MMP1.

Golgi exit assay of control and PITPNC1 knockdown cells tracking RFP-labeled MMP1. Cells were immunostained for MMP1-RFP (red), TGN46 (green), and DAPI (blue) at time 0, 10, and 30 minutes. Right, MMP1 signal was analyzed in TGN46-postive regions. N=25/timepoint/group. Significance was determined by Fisher's method. ***$p < 0.001$. Error bars represent S.E.M.

I further verified the role of PITPNC1 in regulating the secretion of these factors by measuring the levels of these proteins in conditioned media collected from control MDA-MB-231 cells and cells overexpressing PITPNC1. Western blot analysis of conditioned media from cells with increased PITPNC1 revealed increased levels of all secreted factors to varying degrees (Figure 3.18a). The intracellular levels of these secreted proteins were unchanged upon overexpression of PITPNC1 (Figure 3.18b). This funding is consistent with our model wherein increased PITPNC1 levels in highly metastatic cells acts to increase only the secretion of these proteins, but not their intracellular levels.

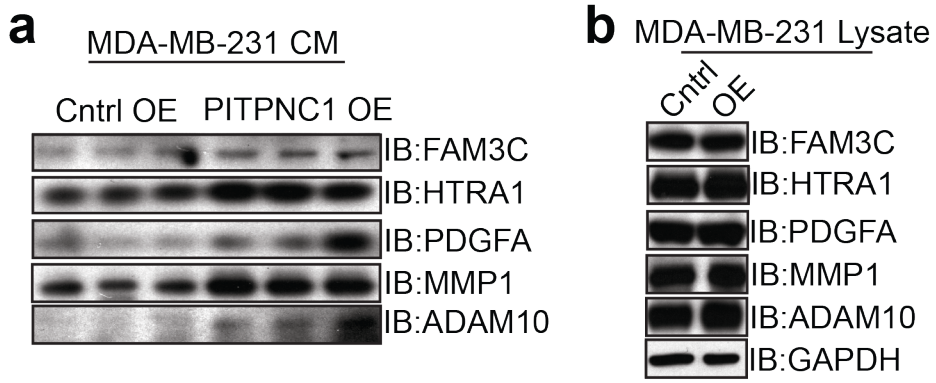

Figure 3.18. PITPNC1 enhances secretion of pro-invasive and pro-angiogenic genes.
a. Western blot analysis for PDGFA, HTRA1, MMP1, ADAM10, and FAM3C in conditioned media from MDA-MB-231 cells overexpressing PITPNC1 or a control vector.
b. Western blot analysis of FAM3C, HTRA1, PDGFA, MMP1, ADAM10, and GAPDH in whole cell lysate from cells as in (**a**). GAPDH was used as a loading control.

Having established that PITPNC1 regulates the secretion of these proteins, we next sought to determine if each of these factors functionally promotes metastatic phenotypes. We depleted each secreted factor individually in PITPNC1-overexpressing cells using lentiviral-based shRNA, and subjected these cells to the invasion and endothelial recruitment assays. Cells with knockdown of each secreted factor reduced the capacity of PITPNC1 overexpression to increase invasion and endothelial recruitment capacities compared to control cells to varying degrees (Figure 3.19a-c). Since each factor was important for this phenotype, this suggests that the breast cancer cells are optimized for maximal invasion and endothelial recruitment capacity through the enhanced secretion of factors that act cooperatively in these processes.

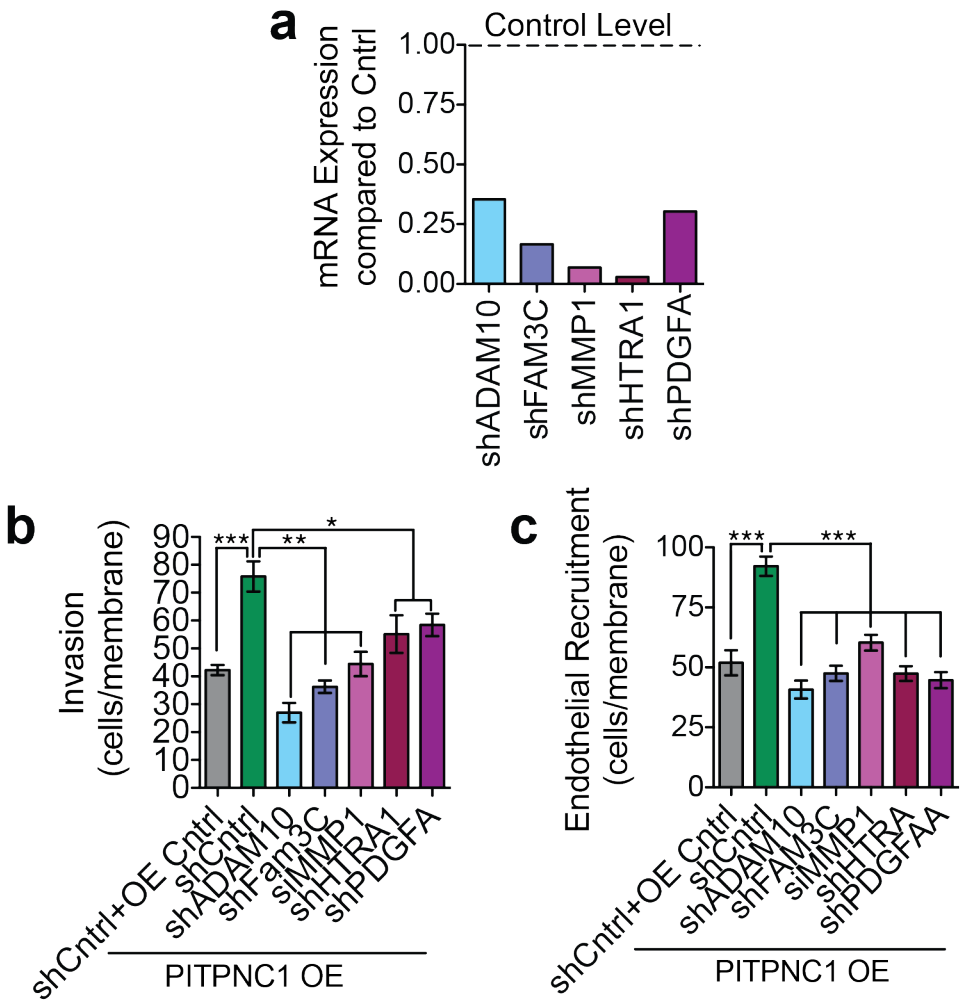

Figure 3.19. PITPNC1-mediated secreted factors are required for invasion and endothelial recruitment phenotypes.

a. MDA-MB-231 cells were transduced with a control shRNA or shRNAs targeting ADAM10, FAM3C, HTRA, PDGFA or a siRNA targeting MMP1 in the setting of PITPNC1 overexpression. Expression levels for each knockdown were measured by qRT-PCR.

b, c. Cells in (**a**) were subjected to the Matrigel invasion assay (**b**) and endothelial recruitment assay (**c**). N=4/group. Data are represented as mean ± S.E.M. *$p < 0.05$, **$p < 0.01$, ***$p < 0.001$.

We further tested the functional significance of these secreted factors in an *in vivo* lung colonization experiment. We depleted each secreted factor in the setting of PITPNC1 overexpression and found that while overexpression of PITPNC1 was significant to increase lung colonization compared to control cells, knockdown of each secreted factor reduced the ability of these cells to form lung metastatic nodules (Figure 3.20). The effects of depleting the secreted factors on invasion, endothelial recruitment, and metastatic colonization indicate that these secreted factors cooperatively impact metastatic progression mediated by PITPNC1. Taken together, these epistatic experiments reveal PITPNC to promote metastasis through increasing the cellular release of ADAM10, FAM3C, HTRA1, MMP1, and PDGFA, which act as secreted pro-metastatic proteins.

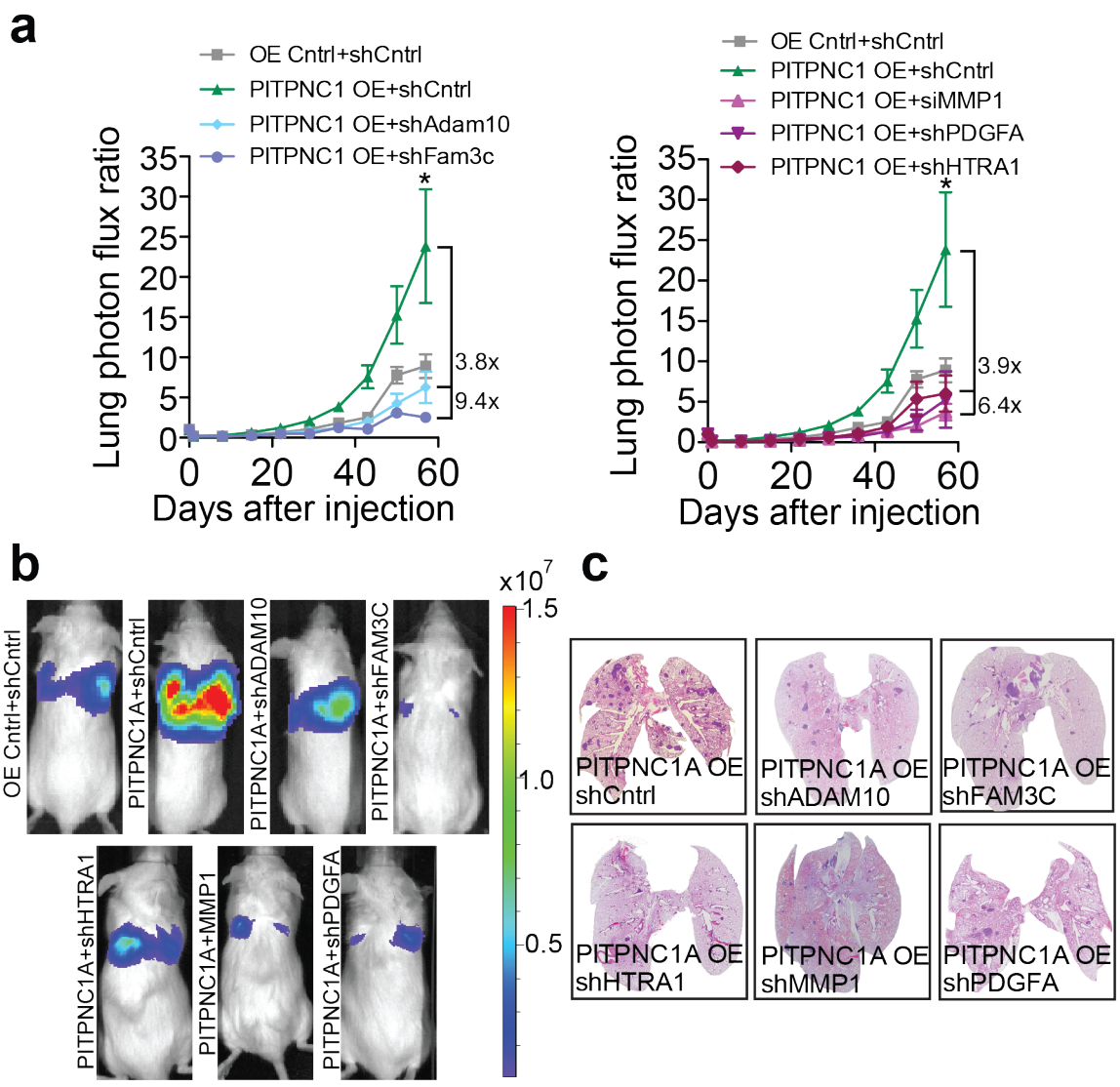

Figure 3.20. PITPNC1 promotes metastasis by facilitating secretion of a set of proteins.

a. Bioluminescence imaging quantification of lung metastatic colonization by 40,000 MDA-MB-231 cells transduced with a control shRNA or shRNAs targeting ADAM10, FAM3C, HTRA, PDGFA or a siRNA targeting MMP1 in the setting of PITPNC1 overexpression. N=6/group. Data are represented as mean ± S.E.M. *p<0.05.

b. Representative bioluminescence images.

c. H&E staining of representative lung sections.

CHAPTER IV: PTPRN2 AND PLCβ1 PROMOTE METASTATIC BREAST CANCER CELL MIGRATION

Functional validation of PTPRN2 and PLCβ1 as Promoters of Metastasis

Given the importance of phosphatidyl inositides (PIs) in regulating cellular processes needed for metastasis and the dramatic effects of PITPNC1 in regulating metastatic secretion (Chapter III), we were interested in identifying the mechanisms of additional protein regulators of other PIs as potential novel drivers of metastasis. We were particularly interested in proteins that regulate PI(4,5)P2, given the role of this lipid in regulating several cellular processes including endocytosis, exocytosis, signal transduction, and cell motility (Balla, 2013; Vicinanza et al., 2008).

Using previously conducted microarray transcriptional profiling of the MDA-MB-231 breast cancer cells and their *in vivo*-selected highly metastatic derivative subline (Minn et al., 2005; Tavazoie et al., 2008) we were intrigued to find two genes, *PTPRN2* and *PLCB1*, that possess known enzymatic activity against PI(4,5)P2 to be both up-regulated in highly metastatic LM2 cells. I validated the up-regulation of these genes in these cells as well as in a second independent breast cancer cell line, CNLM1a1, compared to the parental MDA-MB-231 cell line. Both genes exhibited markedly increased expression in the metastatic CNLM1a1 derivative subline relative the parental CN34 population at both the gene expression and protein levels (Figure 4.1a-d). Additionally, the levels of both proteins were lowest in MCF 10A cells, a mammary epithelial cell line, consistent with the non-invasive and non-tumorigenic characterization of these cells.

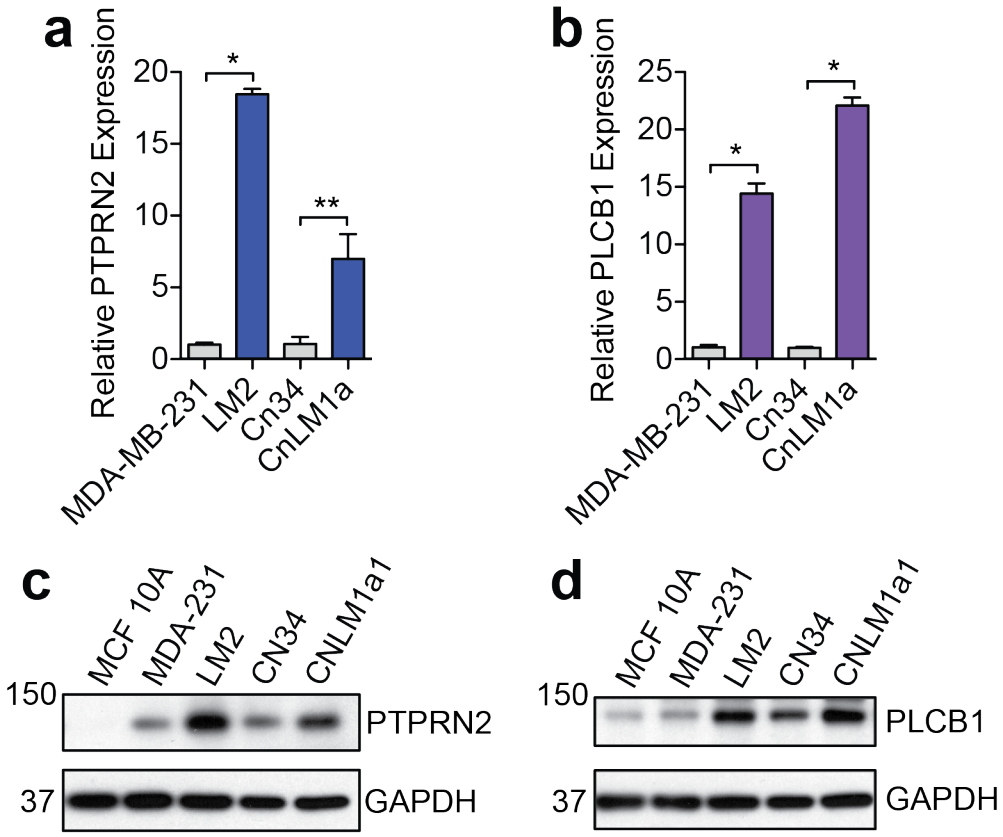

Figure 4.1. PTPRN2 and PLCβ1 expression increases with malignant transformation in breast cell lines.

a, b. *PTPRN2* (**a**) and *PLCB1* (**b**) expression levels were determined by qRT-PCR.

c, d. Western blot analysis of PTPRN2 (**c**) or PLCβ1 (**d**) levels in MCF 10A, MDA-MB-231, LM2, CN34, and CNLM1a1 cells. GAPDH was used as a loading control. Right, densitometry analysis of PTPRN2 or PLCβ1 levels normalized to GAPDH.

*$p < 0.05$, **$p < 0.01$.

I next sought to test the functional significance of this up-regulation in highly metastatic cells by determining if expression of these genes was necessary for breast cancer metastasis. I depleted PTPRN2 or PLCβ1 in highly metastatic LM2 cells and performed tail vein metastatic colonization assays. Knockdown of these genes significantly reduced lung metastatic colonization (Figure 4.2a-d).

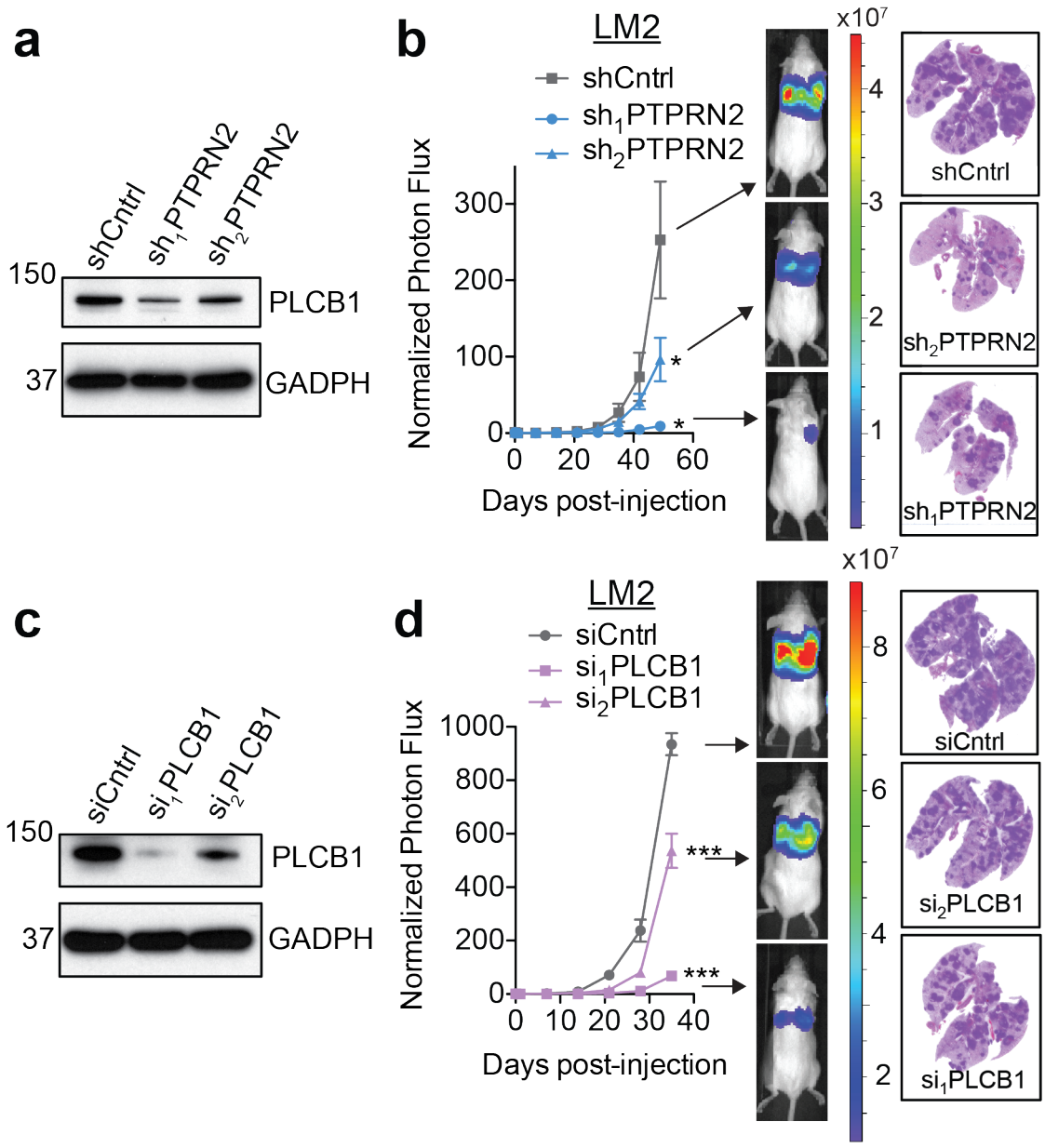

Figure 4.2. Functional validation of PTPRN2 and PLCβ1 as promoters of breast cancer metastasis.

a, c. Western blot analysis of PTPRN2 (**a**) or PLCβ1 (**b**) levels in LM2 cells expressing short hairpins targeting PTPRN2, PLCβ1, or a control hairpin. GAPDH was used as a loading control.

b, d. Bioluminescence imaging quantification of lung colonization by 40,000 LM2 cells as in (**a**, **c**). N=5 mice/group. Right, H&E staining of representative lung sections. Data are represented as mean ± S.E.M. *$p < 0.05$, ***$p < 0.001$.

To show that these effects were not specific to the MDA-MB-231/LM2 system, I depleted PTPRN2 and PLCβ1 in a second highly metastatic derivative subline, CNLM1a1. Depletion of either PTPRN2 or PLCβ1 in the CNLM1a1 cells also decreased the ability of these cells to form lung metastatic nodules (Figure 4.3a, b).

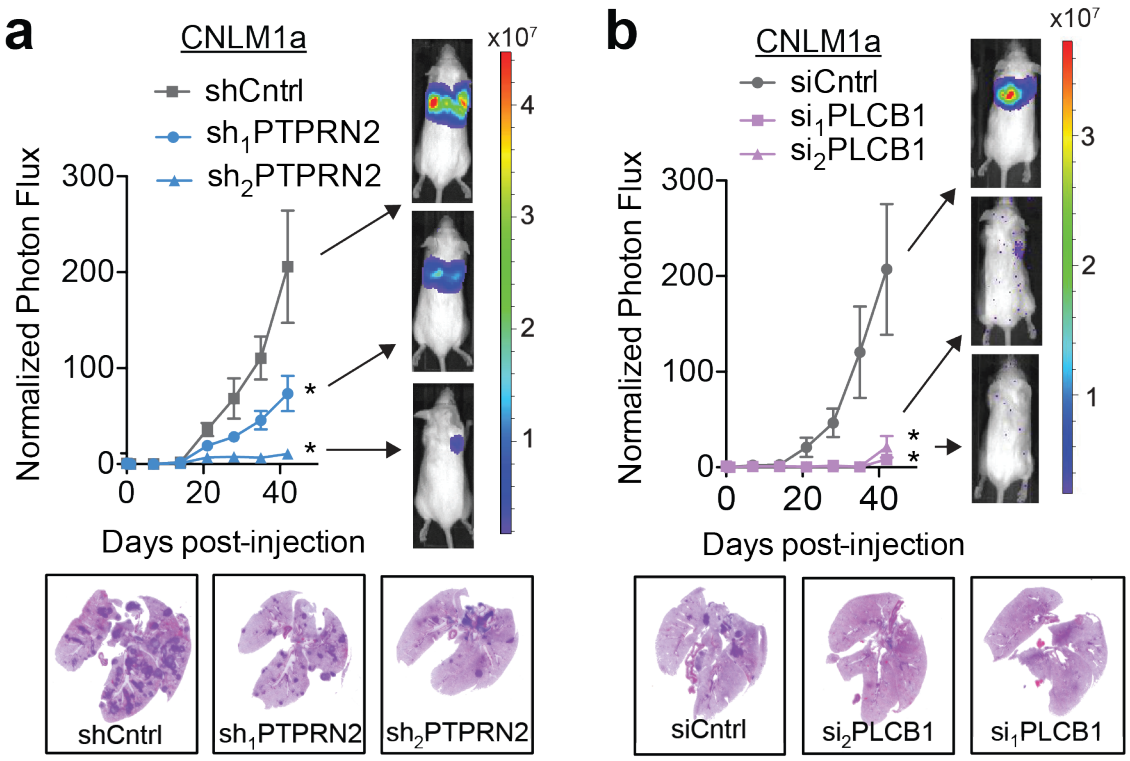

Figure 4.3. Functional validation of PTPRN2 and PLCβ1 in an independent metastatic breast cancer cell line.

a, b. Bioluminescence imaging quantification of lung colonization by 40,000 CNLM1a1 cells with depletion of PTPRN2 (**a**) or PLCβ1 (**b**). N=5 mice/group. Below, H&E staining of representative lung sections. Data are represented as mean ± S.E.M. *p < 0.05.

Interestingly, cells with depletion of either PTPRN2 or PLCβ1 exhibited significantly reduced signal in the lungs of mice as early as 24 hours post-injection compared to control cells (Figure 4.4). This suggests that knockdown of these genes impacts early stages of metastatic progression, such as migration and invasion, rather than later stages of metastatic growth such as angiogenesis (Chiang and Massague, 2008).

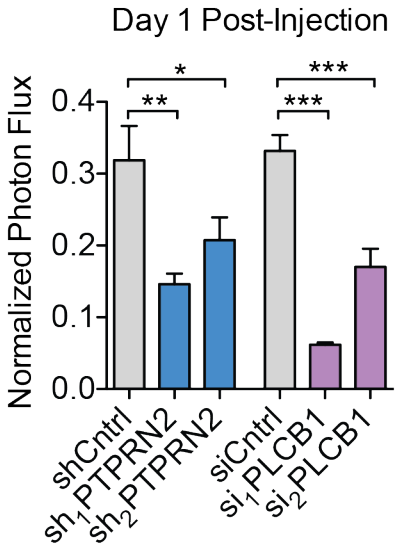

Figure 4.4. Depletion of PTPRN2 or PLCβ1 affects metastatic colonization at early time points.

Bioluminescence imaging quantification of lung colonization one day after injection of 40,000 LM2 cells with knockdown of PTPRN2, PLCβ1, or control cells. Data are represented as mean ± S.E.M. *p < 0.05, **p<0.01, ***p<0.001.

Clinical Significance of PTPRN2 and PLCβ1 in Breast Cancer Metastasis

Having demonstrated the requirement for expression of PTPRN2 and PLCβ1 for breast cancer metastasis, I next asked if expression of the genes correlated with patient outcomes. To investigate the clinical importance of PTPRN2 and PLCβ1 in breast cancer progression, I quantified their expression levels from cDNA samples of patients with

varied stages of breast cancer. Notably, expression levels of both genes increased significantly in tumors of patients with advanced stage IV metastatic disease (Figure 4.5a, b).

I next analyzed data from The Cancer Genome Atlas (TCGA) and found that patients whose primary tumors possessed higher levels of *PTPRN2* and *PLCB1* demonstrated significantly worse overall survival compared to patients whose tumors possessed lower levels of these genes (Cancer Genome Atlas, 2012) (Figure 4.5c). Additionally, *PTPRN2* and *PLCB1* expression correlated with worse distal metastasis-free survival in a second large cohort of breast cancer patients (Figure 4.5d) (Gyorffy et al., 2010). These findings establish PTPRN2 and PLCβ1 as clinically relevant promoters of metastasis in breast cancer.

Figure 4.5. *PTPRN2* and *PLCB1* expression correlates with worse clinical outcomes in breast cancer.

a, b. *PTPRN2* (**a**) and *PLCB1* (**b**) levels were analyzed in human breast cancers (stages I-IV) and normal breast tissue from TissueScan qPCR Array Breast Cancer Panels II and III (Origene, N = 97). Expression levels were normalized to levels in normal tissue for each gene. Data are represented as mean ± S.E.M. *$p < 0.05$, **$p<0.01$.

c. Kaplan-Meier curve representing overall survival of a cohort of breast cancer patients (N = 528) as a function of their primary tumor's *PTPRN2* and *PLCB1* expression levels (data from the TCGA Research Network). Patients whose primary tumors' *PTPRN2* and *PLCB1* expression levels were higher or lower than the median of the population were classified as low (blue) or high (red) expression.

d. Kaplan-Meier curve representing distal metastasis-free survival of a cohort of breast cancer patients (N = 1609) as a function of their primary tumor's *PTPRN2* and *PLCB1* expression levels (Data from KMPlot) Patients' primary tumors' *PTPRN2* and *PLCB1* expression levels were classified as low (blue) or high (red) expression.

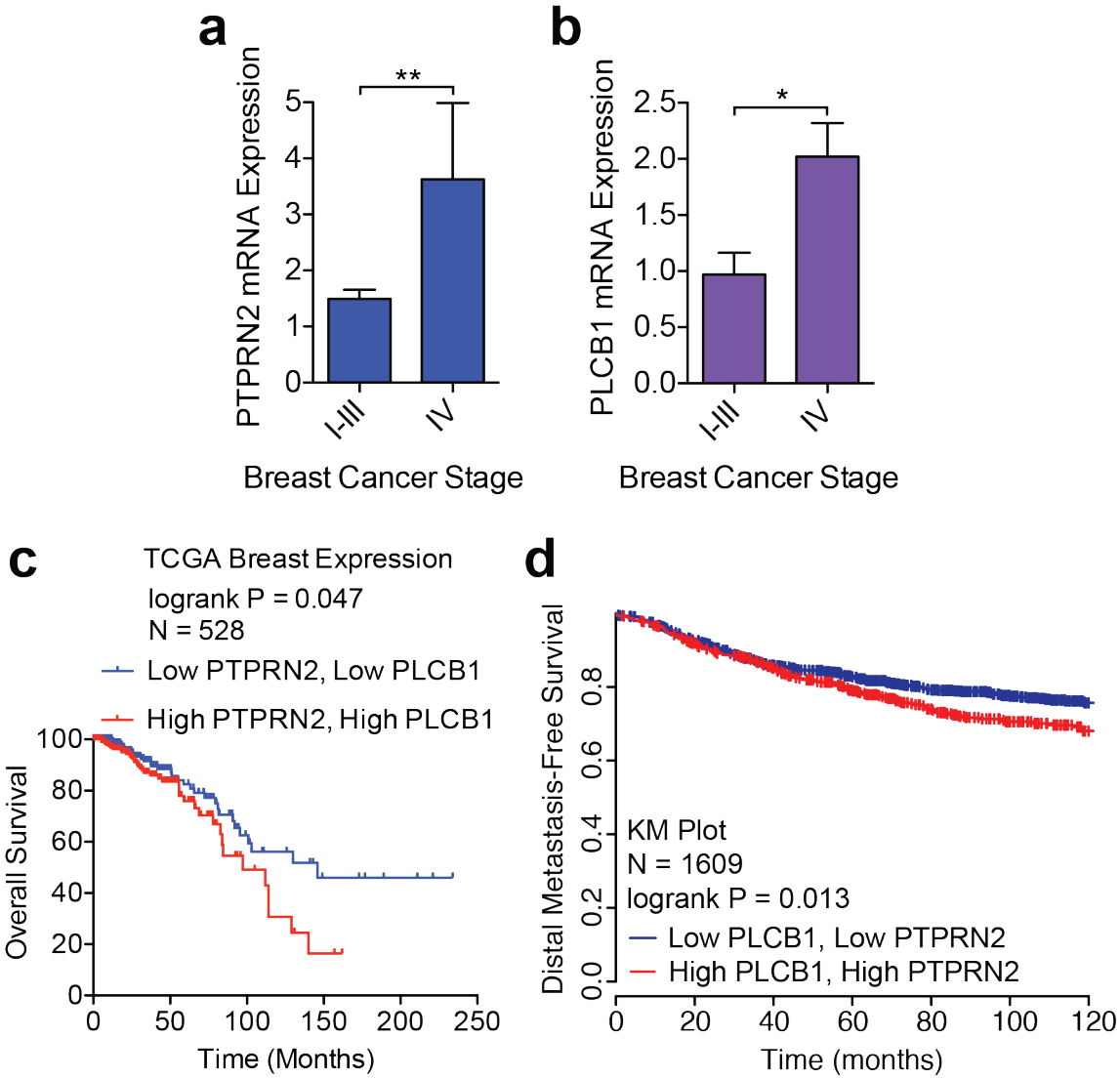
a
PTPRN2 mRNA Expression
**
I-III
IV
Breast Cancer Stage
b
PLCB1 mRNA Expression
*
I-III
IV
Breast Cancer Stage
c
TCGA Breast Expression
logrank P = 0.047
N = 528
Low PTPRN2, Low PLCB1
High PTPRN2, High PLCB1
Overall Survival
Time (Months)
d
Distal Metastasis-Free Survival
KM Plot
N = 1609
logrank P = 0.013
Low PLCB1, Low PTPRN2
High PLCB1, High PTPRN2
Time (months)

Metastatic Phenotypes Mediated by PTPRN2 and PLCβ1

We investigated several cellular metastatic phenotypes to identify the mechanisms by which PTPRN2 and PLCβ1 mediate metastasis. Similar to the action of PITPNC1, depletion of either PTPRN2 or PLCβ1 reduced the ability of cells to invade through Matrigel (Figure 4.6a). However, unlike PITPNC1, cells with knockdown of either gene revealed reduced ability to migrate through a porous trans-well insert in a migration assay (Figure 4.6b). While the requirement for PITPNC1 in invasion was through release of secreted proteases to degrade the Matrigel and enable cell movement, the defects in invasion capacity shown by PTPRN2 and PLCβ1-kncockdown cells appeared to be secondary to a defect in migratory capacity.

To further test a role for PTPRN2 and PLCβ1 in migration, I tested these cells in a scratch assay. Cells with knockdown of either gene and control cells were grown to confluency and a scratch was made through the cell monolayer, clearing the scratch area of cells. Cells were allowed to migrate back into the scratch area. Depletion of either PLCβ1 or PTPRN2 significantly decreased the ability of cells to migrate back into the scratch area over a 24-hour period, confirming the reduced migratory capacity of these cells (Figure 4.6c).

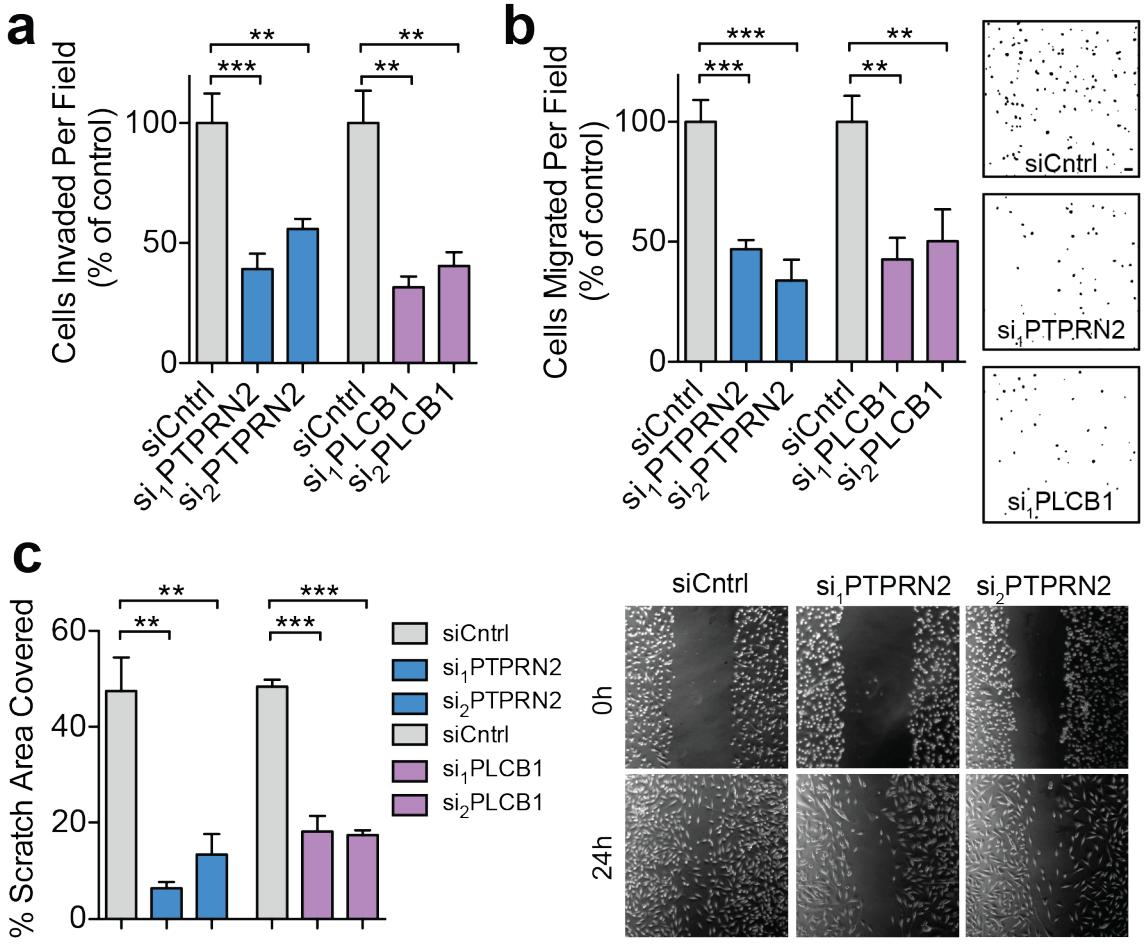

Figure 4.6. PTPRN2 and PLCβ1 are required for metastatic migration and invasion.

a. Matrigel invasion by 50,000 LM2 cells transfected with siRNA targeting PTPRN2, PLCβ1, or control siRNA. Data normalized to control values. N = 6 inserts/group.

b. Migration assay by 100,000 LM2 cells transfected with siRNA targeting PTPRN2, PLCβ1, or control siRNA. Data normalized to control values. N = 6 inserts/group. Right, representative images of the migration assay. Scale bar, 100 μm.

c. Quantification of area covered by cells 24 h after a scratch was made through confluent cells transfected with siRNA targeting PTPRN2, PLCβ1, or control siRNA. N = 5 wells/group. Right, representative images of the scratch assay.

Data are represented as mean ± S.E.M. **p<0.01, ***p<0.001.

To demonstrate that these effects were not limited to LM2 cells, I depleted PTPRN2 or PLCβ1 in four other breast cancer cells: BT-459, CNLM1a1, HCC-1806, and MDA-MB-468, and subjected these cells to the migration assays. Knockdown of either gene significantly reduced metastatic migration (Figure 4.7a-d).

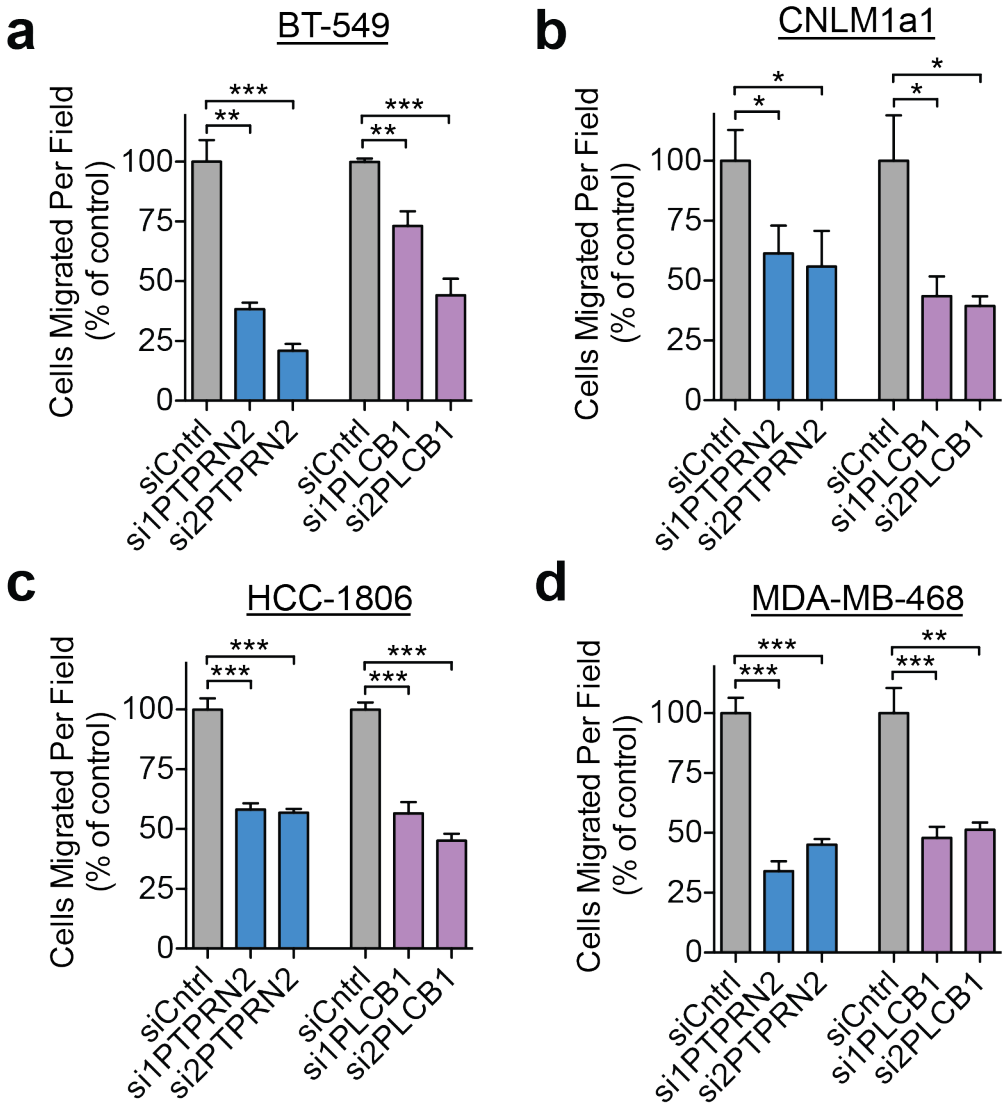

Figure 4.7. PTPRN2 and PLCβ1 are required for metastatic migration in multiple breast cancer cell lines.

a-d. Migration assay by 100,000 BT-549 (**a**), CNLM1a1 (**b**), HCC-1806 (**c**), and MDA-MB-468 (**d**) cells transfected with siRNA targeting PTPRN2, PLCβ1, or control siRNA. N = 5 inserts/group. Data are represented as mean ± S.E.M. *p<0.05, **p<0.01, ***p<0.001.

To ensure that the defects observed in metastatic colonization, Matrigel invasion, and migration capabilities in the setting of PTPRN2 or PLCβ1 knockdown were not due to changes in proliferation capacity of these cells, I conducted a five-day proliferation assay. Cellular growth rates were not affected by either gene in this assay (Figure 4.8a, b). Together these findings indicate that PTPRN2 and PLCβ1 are required for metastatic invasion and migration, and these effects are not secondary to growth defects induced by these genes.

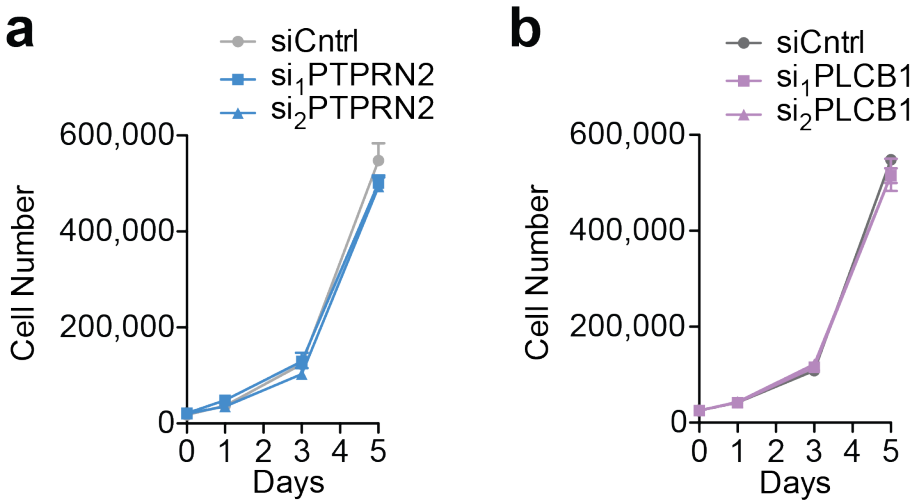

Figure 4.8. Depletion of PTPRN2 or PLCβ1 does not affect cellular proliferation. **a, b.** Proliferation of 20,000 LM2 cells expressing siRNAs targeting PTPRN2 (**a**), PLCβ1 (**b**), or a control hairpin. N=3/group. Error bars represent S.E.M.

Both PTPRN2 and PLCβ1 have been previously demonstrated to possess enzymatic activity for the substrate PI(4,5)P2 (Caromile et al., 2010; Rebecchi and Pentyala, 2000), and we questioned whether this enzymatic activity was necessary for the pro-metastatic effects of PRPN2 or PLCβ1. To test this, I mutated the catalytic domain of each protein to generate enzymatically inactive versions and tested these versions in the metastatic phenotypes. PTPRN2 contains a $C(X)_5R$ catalytic domain common to protein

tyrosine phosphatases (PTPs), where C is the catalytic cysteine (Barford et al., 1998). In canonical PTP domains, the motif also contains an alanine residue (CX**A**XXXR). However, the PTP domain of PTPRN2 contains an aspartic acid residue at this position (CX**D**XXXR), rendering it catalytically inactive against phosphorylated tyrosine resides but enabling its activity to dephosphorylate PI(4,5)P2 (Caromile et al., 2010; Wasmeier and Hutton, 1996). In both conserved PTP domains and PTPRN2's PTP domain, a catalytic cysteine residue mediates the enzymatic phosphate monoester hydrolysis. A previous study had demonstrated that mutation of PTPRN2's catalytic cysteine residue, C945, to a serine residue abrogates the protein's ability to dephosphorylate PI(4,5)P2 (Caromile et al., 2010). Serine is commonly used in mutation of cysteine residues, since it is structurally similar but does not possess nucleophilic activity. The PTP catalytic mechanism involves the formation of a phospho-enzyme intermediate that is hydrolyzed to restore the free enzyme and generates inorganic phosphate, but the cysteine to serine mutation renders this intermediate non-hydrolyzable, trapping the substrate and rendering the enzyme catalytically dead. To dissect the influence of PTPRN2's catalytic activity independent of trapping the substrate or reducing total active enzyme, I instead mutated C945 to an inactive alanine residue. I found that while wild-type PTPRN2 overexpression was sufficient to increase invasion, migration, and metastatic lung colonization in mice, equivalent overexpression PTPRN2C^{945A} was not sufficient to enhance these effects (Figure 4.9a-d). Thus PTPRN2 is sufficient to enhance metastatic capacity and its catalytic activity is required for its promotion of metastatic phenotypes.

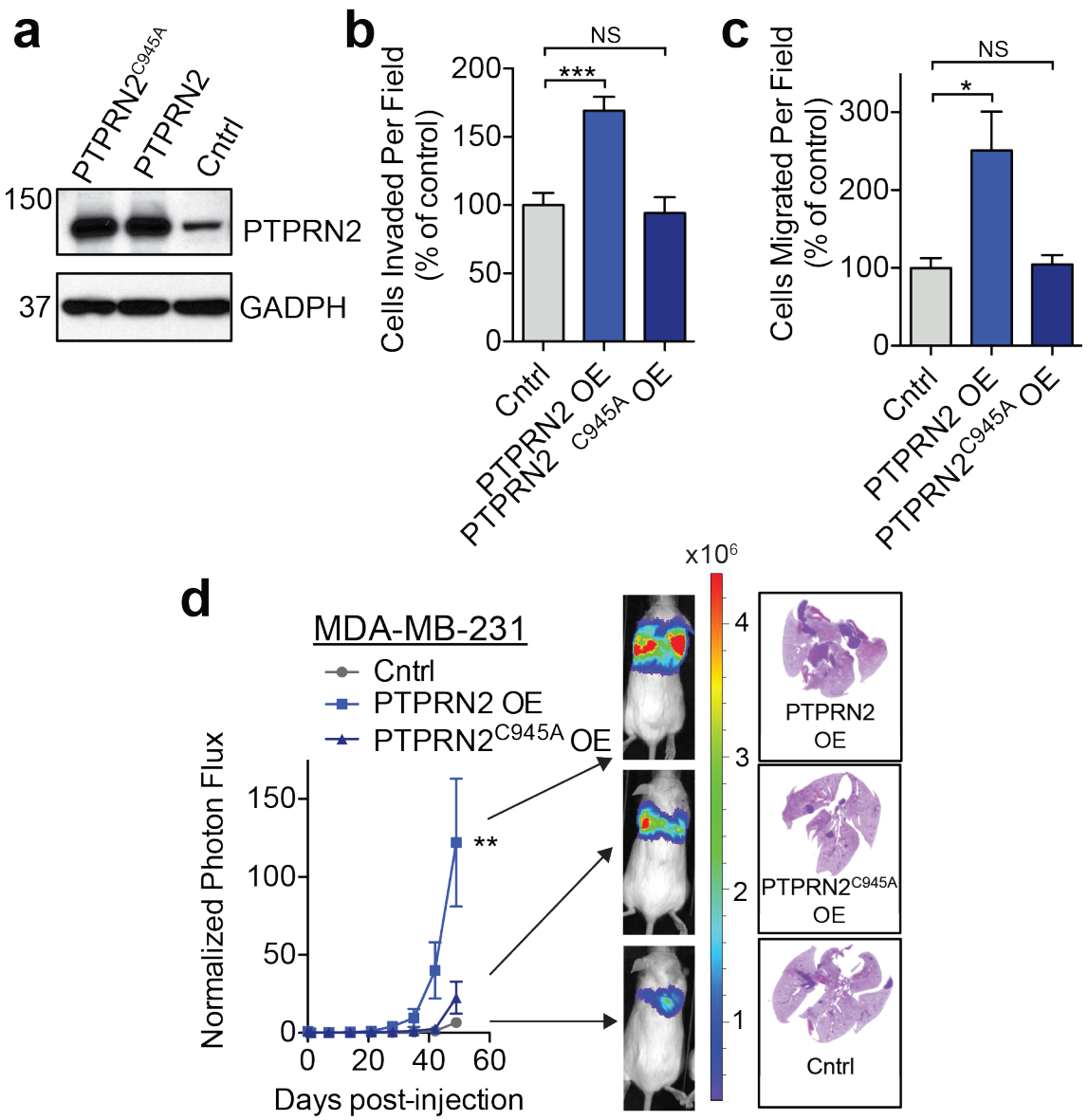

Figure 4.9. PTPRN2's catalytic activity is required for its pro-metastatic effects.

a. Western blot analysis of MDA-MB-231 cells transduced with PTPRN2, PTPRN2^{C945A}, or control vector. GAPDH was used as a loading control.

b, c. Cells in (**a**) were subjected to the Matrigel invasion (**b**) and migration assays (**c**). N = 5 inserts/group.

d. Bioluminescence imaging quantification of lung colonization by 40,000 MDA-MB-231 cells as in (**a**). N = 5 mice/group. Right, representative lung histology.

Data are represented as mean ± S.E.M. *p<0.05, **p<0.01, ***p<0.001.

PLCβ1 contains the high conserved catalytic domain shared by all phospholipase C (PLC) enzymes. The phospholipase mechanism involves hydrolyzing the phosphodiester bond linking the inositol ring (in this case, inositol phosphorylated at the 4' and 5' positions) to the glycerol backbone with two fatty acid chains acylated to it. The mechanism first involves attack by the hydroxyl group on the inositol ring adjacent to the phosphodiester bond, which forms a cyclic intermediate and releases diacyl glycerol, the first product of this reaction. The cyclic intermediate then undergoes nucleophilic attack by a water molecule coordinated by PLC's catalytic histidine, generating inositol triphosphate, the second product of this reaction (Rebecchi and Pentyala, 2000). Mutation of PLCβ1's catalytic histidine residue, H331, has been previously shown to abrogate its ability to hydrolyze PI(4,5)P2 (Ramazzotti et al., 2008). I overexpressed PLCβ1^{H331Q} and PLCβ1^{WT} in the MDA-MB-231 cells, and found that the wild-type enzyme was capable of increasing invasion, migration, and metastasis. However, the catalytically inactive mutant failed to promote these effects (Figure 4.10a-d). These findings establish the enzymatic activity of PLCβ1 as necessary for its pro-metastatic effects.

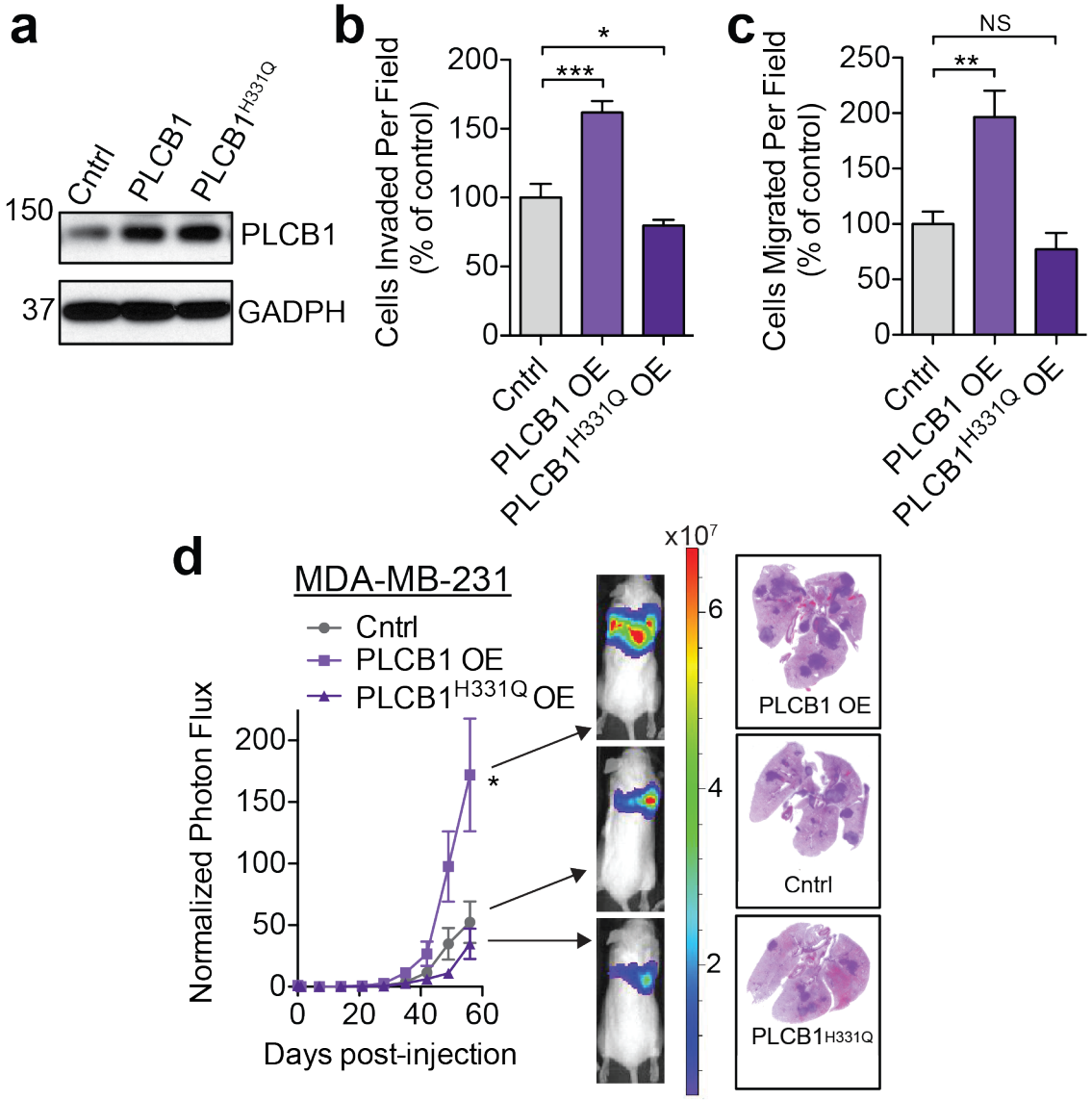

Figure 4.10. PLCβ1's catalytic activity is required for its pro-metastatic effects.

a. Western blot analysis of MDA-MB-231 cells transduced with PLCβ1, PLCβ1^{H331Q}, or control vector. GAPDH was used as a loading control.

b, c. Cells in (**a**) were subjected to the Matrigel invasion (**b**) and migration assays (**c**). N = 5 inserts/group.

d. Bioluminescence imaging quantification of lung colonization by 40,000 MDA-MB-231 cells as in (**a**). N = 5 mice/group. Right, representative lung histology.

Data are represented as mean ± S.E.M. *p<0.05, **p<0.01, ***p<0.001.

Functional characterization of PI(4,5)P2 Levels in Metastatic Migration

Given that the enzymatic activities of both PTPRN2 and PLCβ1 were required to enhance migration and invasion, we next sought to determine the role of their enzymatic substrate (PI(4,5)P2 in metastasis. PI(4,5)P2 is predominantly present in the inner leaflet of the cellular plasma membrane (Martin, 2001; Vicinanza et al., 2008). Interestingly, both PTPRN2 and PLCβ1 also demonstrated prominent localization to the plasma membrane in breast cancer cells (Figure 4.11). A role for PLCβ1 in the nuclei to regulate cellular growth has been previously described, but PLCβ1 did not show nuclear localization in the MDA-MB-231 breast cancer cells, although it did show some cytoplasmic localization. PTPRN2 exhibited additional perinuclear staining in the Golgi region. PTPRN2 is a transmembrane protein, and has been previously observed to be recycled from the plasma membrane to the Golgi, where it is again exported to the plasma membrane.

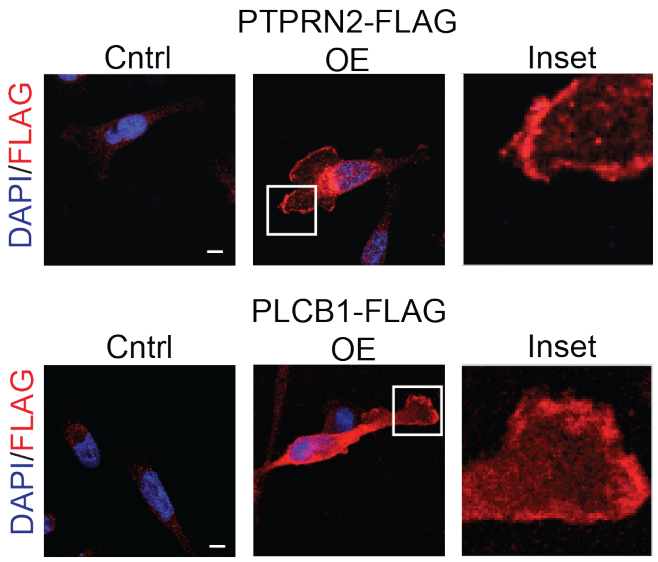

Figure 4.11. PTPRN2 and PLCβ1 localize to the cytoplasm and plasma membrane of breast cancer cells.

Representative images of MDA-MB-231 cells retrovirally transduced with PTPRN2-FLAG, PLCβ1-FLAG, or control vector and immunostained with anti-FLAG (red) and DAPI (blue). Scale bar, 10 μm.

As described above, these enzymes act to reduce the levels of PI(4,5)P2 through two independent mechanisms. PLCβ1 hydrolyzes PI(4,5)P2 to generate IP3 and DAG, while PTPRN2 dephosphorylates the lipid. To determine if these enzymes were affecting the levels of PI(4,5)P2 in breast cancer cells, I first quantified the abundance of PI(4,5)P2 in the plasma membrane of cancer cells using immunofluorescence. I followed an immunocytochemical technique previously demonstrated to accurately reflect changes in PI(4,5)P2 mass (Hammond et al., 2012; Hammond et al., 2009a). This method utilizes a gentle detergent, saponin, and is performed at low temperature to preserve the lipids in the plasma membrane for detection. Consistent with the increased levels of PTPRN2 and PLCβ1 in highly metastatic breast cancer cells and the enzymatic activity of these

proteins against PI(4,5)P2, LM2 cells exhibited lower levels of PI(4,5)P2 in their plasma membranes relative to their less metastatic parental cell population (Figure 4.12).

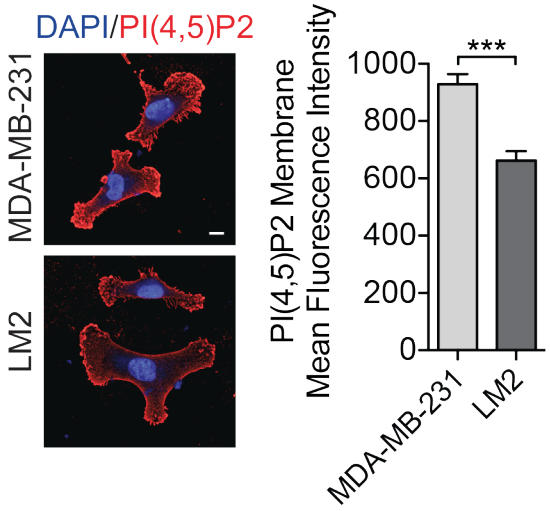

Figure 4.12. Plasma membrane levels of PI(4,5)P2 varies with metastatic capacity. Mean fluorescence intensity of membrane PI(4,5)P2 was analyzed in MDA-MB-231 and LM2 cells immunostained with PI(4,5)P2 antibody (red) and DAPI (blue) using fluorescence microscopy. N = 50 cells/group. Scale bar, 10 μm. Data are represented as mean ± S.E.M. ***p<0.001.

I next tested whether membrane PI(4,5)P2 levels functionally affected metastatic capacity. I added exogenous PI(4,5)P2 to LM2 cells using the PIP carrier system. In this system, a positively charged carrier is incubated with the negatively charged phospholipid to allow the carrier to coordinate the lipid. The carrier-lipid complex is added to cells, and the phospholipid is incorporated into its correct location in the cell (Ozaki et al., 2000). I first confirmed that exogenously added PI(4,5)P2 was incorporated into the inner leaflet of the plasma membrane. Cells were transfected with a construct

encoding the GFP-tagged PH domain of PLCdelta, which binds to PI(4,5)P2 with high affinity. The expression of this construct enables tracking of this lipid within living cells. GFP-PLCdelta-PH showed some membrane localization and diffuse cytoplasmic staining in control cells. In cells treated with exogenous PI(4,5)P2, GFP-PLCdelta-PH showed strongly increased membrane localization (Figure 4.13a). The translocation of the construct to the plasma membrane indicates that exogenous PI(4,5)P2 incorporates into the inner leaflet of the plasma membrane in treated cells.

Addition of exogenous PI(4,5P)2 to the breast cancer cells increased their membrane PI(4,5)P2 levels by 22%, and reduced the ability of the cells to colonize the lungs of mice by 80% compared to cells treated with carrier alone (Figure 4.13b, c). These findings indicate that increased membrane abundance of PI(4,5)P2 reduces metastatic capacity.

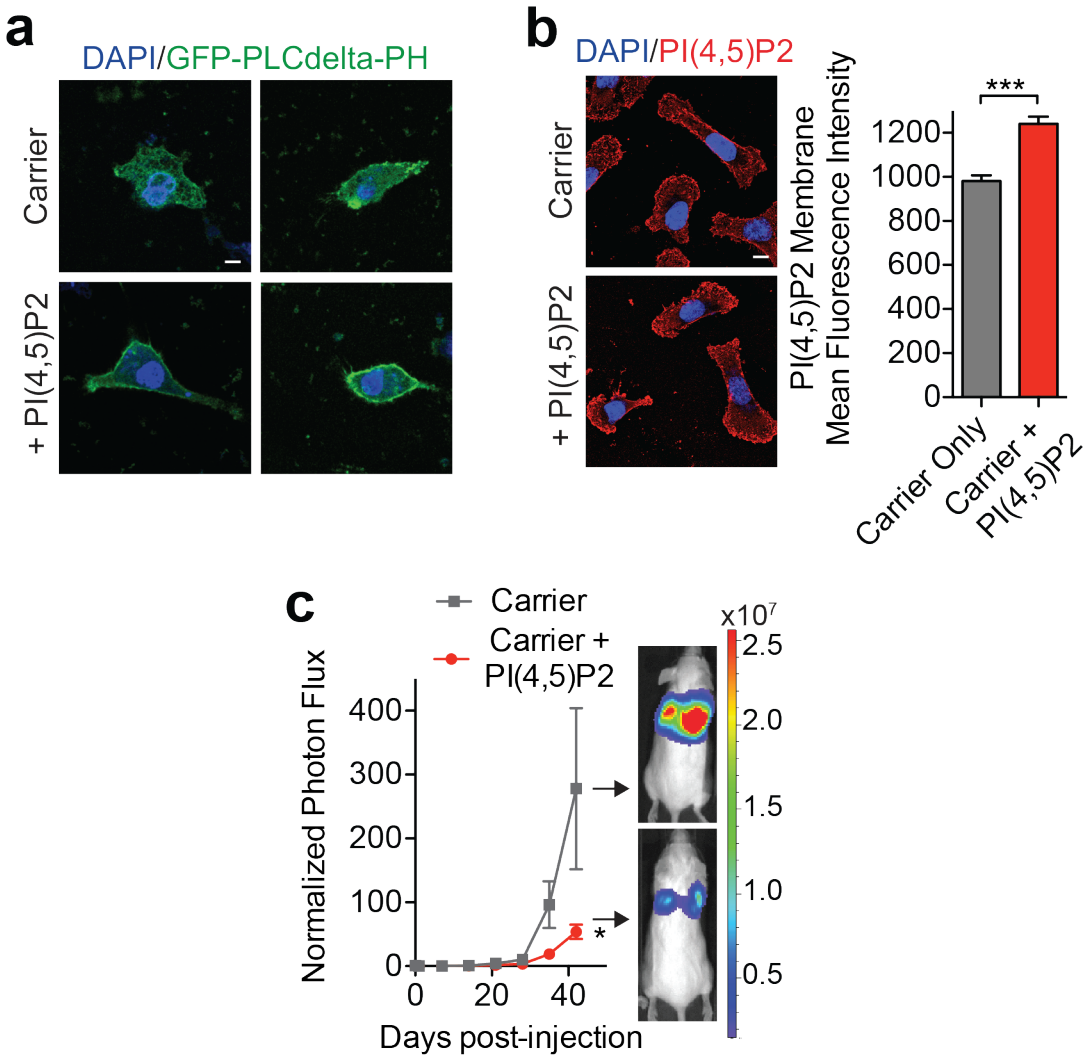

Figure 4.13. Addition of exogenous PI(4,5)P2 abrogates metastatic capacity.

a. MDA-MB-231 cells were transfected with GFP-PLCdelta-PH (green) and treated with carrier incubated with PI(4,5)P2 or carrier alone. Scale bar, 10 μm.

Mean fluorescence intensity of membrane PI(4,5)P2 was analyzed in LM2 cells treated with carrier incubated with PI(4,5)P2 or carrier alone. Cells were immunostained with PI(4,5)P2 antibody (red) and DAPI (blue) and analyzed using fluorescence microscopy. N = 50 cells/group. Scale bar, 10 μm.

b. Bioluminescence imaging quantification of lung colonization by 40,000 LM2 cells treated with carrier incubated with PI(4,5)P2 or carrier alone. Right, H&E staining of representative lung sections. N=6 mice/group.

Data are represented as mean ± S.E.M. *p<0.05, ***p<0.001.

We next asked if PTPRN2 and PLCβ1 enhance metastasis by regulating membrane PI(4,5)P2 levels in breast cancer cells. Consistent with the enzymatic activities of PLCβ1 and PTPRN2 as decreasing the abundance of PI(4,5)P2, overexpression of either enzyme reduced membrane levels of the lipid (Figure 4.14a). Conversely, depleting either enzyme in cancer cells increased the membrane levels of PI(4,5P)2 (Figure 4.14b).

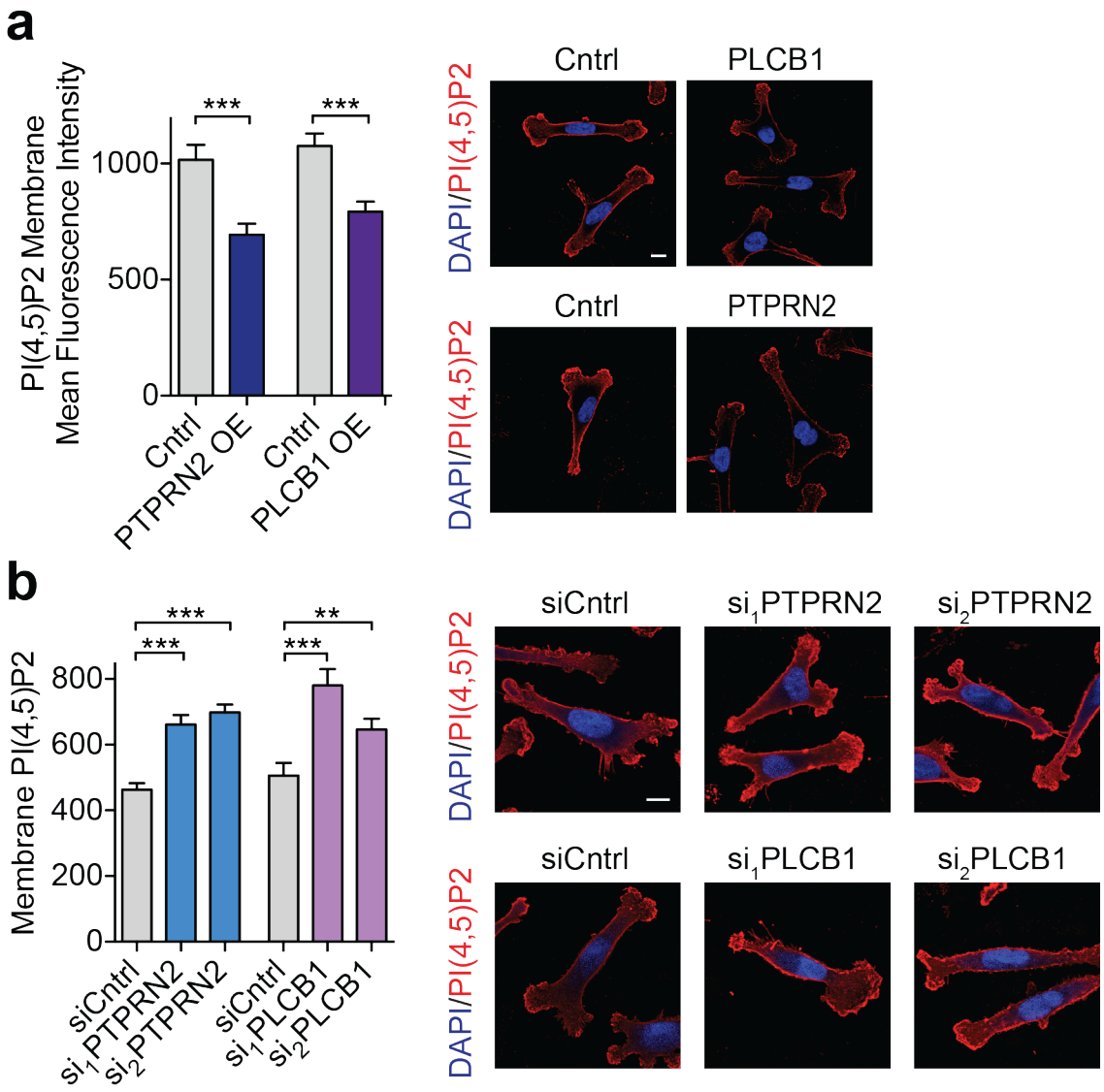

Figure 4.14. PTPRN2 and PLCβ1 modulate PI(4,5)P2 abundance in the plasma membrane.

a, b. MDA-MB-231 cells overexpressing PTPRN2, PLCβ1, or a control vector (**a**) or LM2 cells transfected with siRNA targeting PTPRN2, PLCβ1, or a control siRNA (**b**) were immunostained for PI(4,5)P2 levels and analyzed by fluorescence microscopy. Mean fluorescence intensity of plasma membrane levels of the lipid was quantified. N = 50 cells/group. Right, representative immunofluorescence images of cells stained with anti-PI(4,5)P2 antibody (red) and DAPI (blue). Scale bar, 10 μm.

Data are represented as mean ± S.E.M. **p<0.01, ***p<0.001.

I further confirmed these changes in PI(4,5)P2 abundance by measuring the levels of this lipid using an independent method, a PI(4,5)P2 enzyme-linked immunosorbent assay (ELISA). In this assay, PI(4,5)P2 is extracted from cells, incubated with PI(4,5)P2 detector protein and then added to a PI(4,5)P2-coated plate for competitive binding. A peroxidase-linked secondary detection reagent and colorimetric substrate is used to detect PI(4,5)P2 detector protein bound to the plate. The colorimetric absorbance signal is thus inversely proportional to the amount of lipid extracted (Figure 4.15a). I performed extracted PI(4,5)P2 from cancer cells with overexpression or depletion of PTPRN2 and PLCβ1 and observed changes in PI(4,5)P2 mass consistent with the immunofluorescence data (Figure 4.15b). Together these results suggest that PTPRN2 and PLCβ1 govern the plasma membrane levels of this lipid in breast cancer cells.

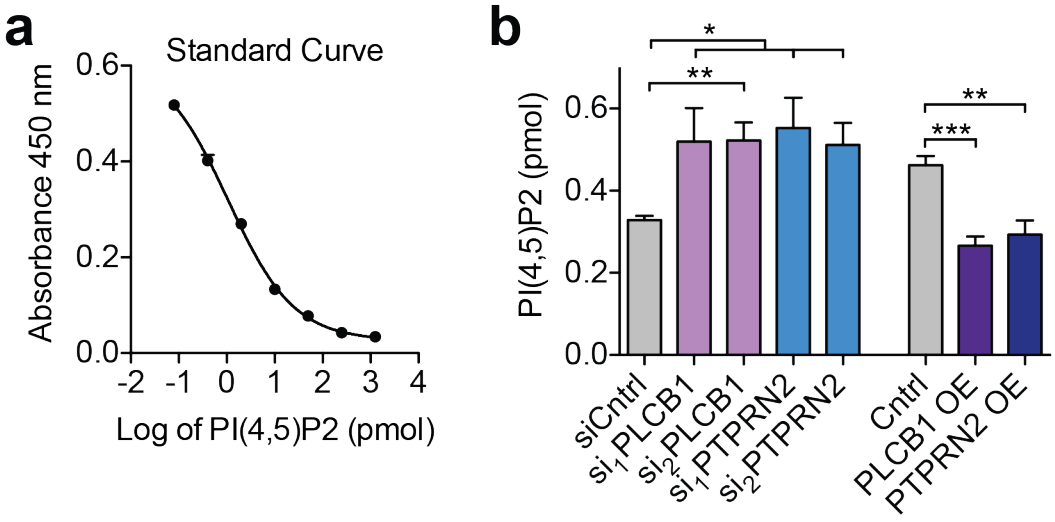

Figure 4.15. PI(4,5)P2 mass quantification upon modulation of PTPRN2 or PLCβ1.
a. ELISA absorbance values were obtained for known concentrations of PI(4,5)P2. The standard curve was generated using non-linear regression analysis.
b 1 x 10^6 LM2 cells with knockdown of PLCB1, PTPRN2, or a control siRNA or MDA-MB-231 cells with overexpression of PLCB1, PTPRN2, or a control vector were subjected to PI(4,5)P2 extraction. Extracted lipid was quantified by ELISA.
Data are represented as mean ± S.E.M. *p<0.05, **p<0.01, ***p<0.001.

I next investigated the functional significance of PI(4,5)P2 plasma membrane levels in metastatic migration, the phenotype mediated by PTPRN2 and PLCβ1. I manipulated the levels of PI(4,5)P2 in cancer cells using two methods. First, I decreased plasma membrane lipid levels to determine whether this could rescue the migratory defect induced by PTPRN2 or PLCβ1 depletion. To selectively deplete plasma membrane PI(4,5)P2, I utilized rapamycin-inducible dimerization constructs previously developed for this purpose (Hammond et al., 2012). In this system, PI(4,5)2 levels are reduced by the enzyme inositol polyphosphate-5-phosphatease (INPP5E), which dephosphorylates the lipid. Cells are transfected with constructs encoding INNP5E fused to FKBP and membrane-inserted protein Lyn11 fused to FRB. Addition of rapamycin induces dimerization of FRB and FKBP, consequently recruiting INPP5E to the plasma membrane. Breast cancer cells transfected with these constructs and treated with rapamycin exhibited reduced plasma membrane PI(4,5)P2 staining compared to cells treated with DMSO (Figure 4.16a). PTPRN2-depleted and PLCβ1-depleted cells, which possess greater levels of plasma membrane PI(4,5)P2, were transfected with these constructs. Addition of rapamycin significantly enhanced their migratory capacity relative to cells treated with DMSO. Control cells treated under the same conditions also exhibited increased migration but to a lesser extent, indicating these effects are partially dependent on PTPRN2 and PLCβ1 (Figure 4.16b, c).

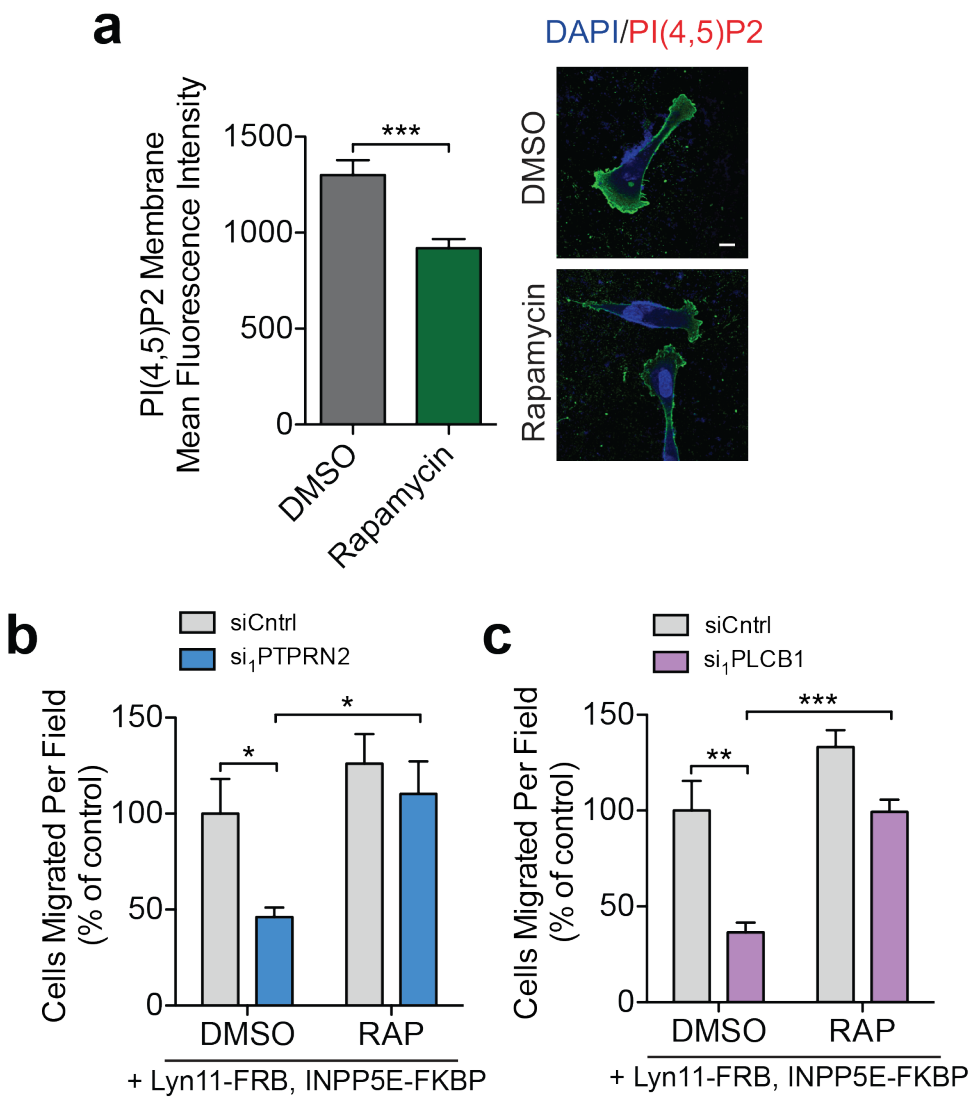

Figure 4.16. Selective depletion of PI(4,5)P2 at the plasma membrane partially rescues PTPRN2 and PLCβ1 depletion.

a. MDA-MB-231 cells transfected with Lyn_{11}-FRB and INPP5E-FKBP, treated with either DMSO or 100 nm rapamycin, and immunostained with anti-PI(4,5)P2 antibody (green) and DAPI (blue). Left, quantification of membrane PI(4,5)P2 mean fluorescence intensity. Right, representative images. N = 50 cells/group. Scale bar, 10 μm.

b, c. LM2 cells transfected with siRNA targeting PTPRN2 (**b**), PLCβ1 (**c**) or a control siRNA were transfected with Lyn_{11}-FRB and INPP5E-FKBP, treated with either DMSO or 100 nm rapamycin and subjected to the migration assay. N = 5 inserts/group.

Data are represented as mean ± S.E.M. *p<0.05, **p<0.01, ***p<0.001.

Given that decreasing plasma membrane PI(4,5)P2 increased migratory capacity, I questioned whether increasing PI(4,5)P2 levels would abrogate the enhanced migratory capacity induced by PTPRN2 or PLCβ1 overexpression. In a complementary set of experiments, I increased levels of the lipid by adding exogenous PI(4,5)P2 to the breast cancer cells (Ozaki et al., 2000). Increasing PI(4,5)P2 prevented the effects of PTPRN2 and PLCβ1 overexpression on migration (Figure 4.17a, b). These effects were specific to PI(4,5)P2, since addition of exogenous PI4P, another lipid present in the plasma membrane (D'Angelo et al., 2008), had no effect on migration capacity for either control cells or cells with overexpression of PTPRN2 or PLCβ1 (Figure 4.17c). These findings establish that PTPRN2/PLCβ1-mediated reduction in plasma membrane PI(4,5)P2 levels correlates with increased metastatic migration capacity.

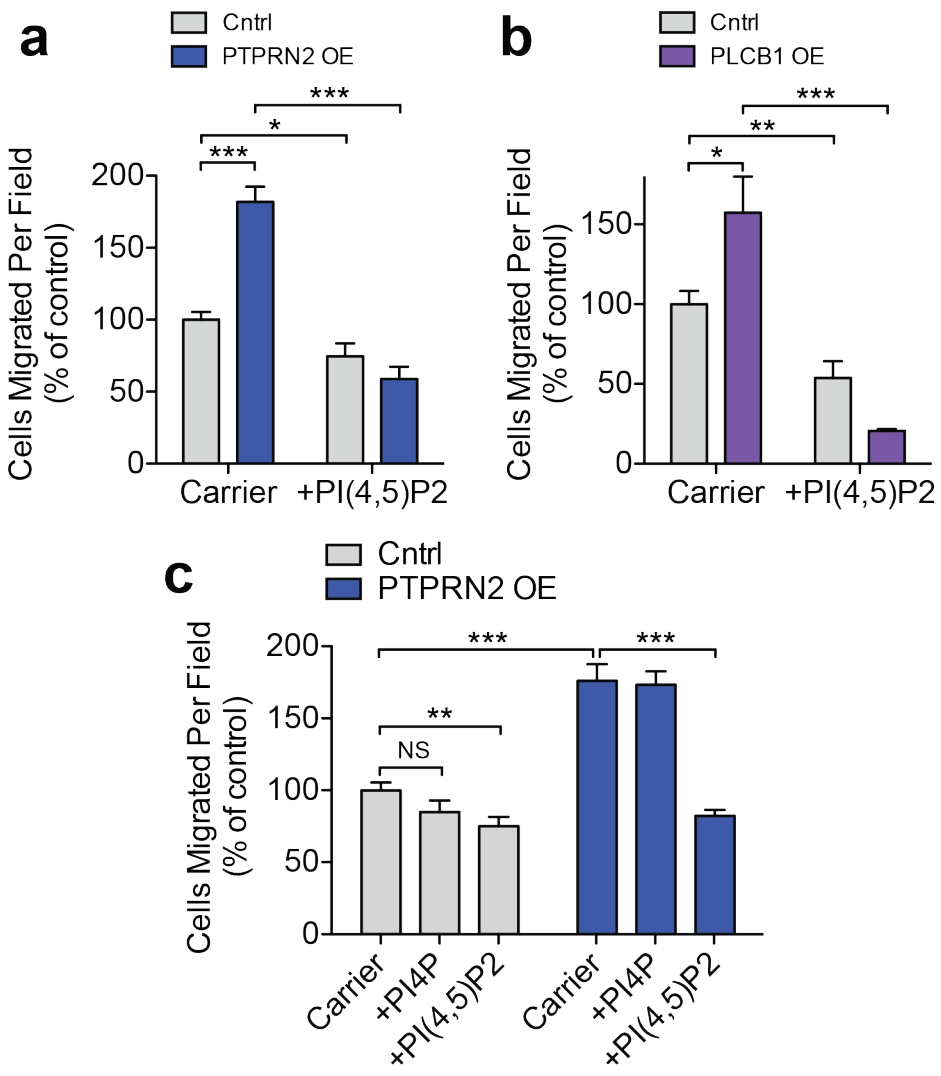

Figure 4.17. Addition of PI(4,5)P2 abrogates PTPRN2 or PLCβ1-mediated metastatic migration.

a, b. MDA-MB-231 cells overexpressing PTPRN2 (**a**), PLCβ1 (**b**) or control vector were treated with carrier alone or carrier incubated with PI(4,5)P2 and subjected to the migration assay. N = 5 inserts/group.

c. MDA-MB-231 cells overexpressing PTPRN2 or a control vector were treated with carrier incubated with PI(4,5)P2, carrier incubated with PI4P, or carrier alone and subjected to the migration assay. N = 5 inserts/group.

Data are represented as mean ± S.E.M. *p<0.05, **p<0.01, ***p<0.001.

Clinical and Functional Studies of PIP5K as a Driver of Metastatic Migration

Based on the importance of PI(4,5)P2 plasma membrane abundance on metastatic capacity, I questioned whether the enzyme that generates this lipid, phosphatidyl inositol 5-phosphate kinase (PIP5K), would also affect metastasis in breast cancer. PIP5K phosphorylates PI4P in the plasma membrane, producing PI(4,5)P2 (van den Bout and Divecha, 2009). Interestingly, breast cancer patients whose tumors exhibited high levels of the three forms of PIPK (PIP5K1A, PIP5K1B, and PIP5K1C) showed dramatically better relapse-free survival and distal metastasis-free survival compared to patients whose tumors expressed low levels of PIP5K (Gyorffy et al., 2010) (Figure 4.18a, b).

I next investigated a role for PIP5K in metastatic phenotypes, I focused on PIP5K1A as it is the dominant isoform in MDA-MB-231 and has been shown to localize to the plasma membrane in membrane ruffles (van den Bout and Divecha, 2009; Yamaguchi et al., 2010). Overexpression of PIP5K1A in LM2 cells reduced the invasion and migration abilities of these cells (Figure 4.18c-e). Taken together, these data suggest that plasma membrane PI(4,5)P2 abundance negatively correlates with metastatic capacity.

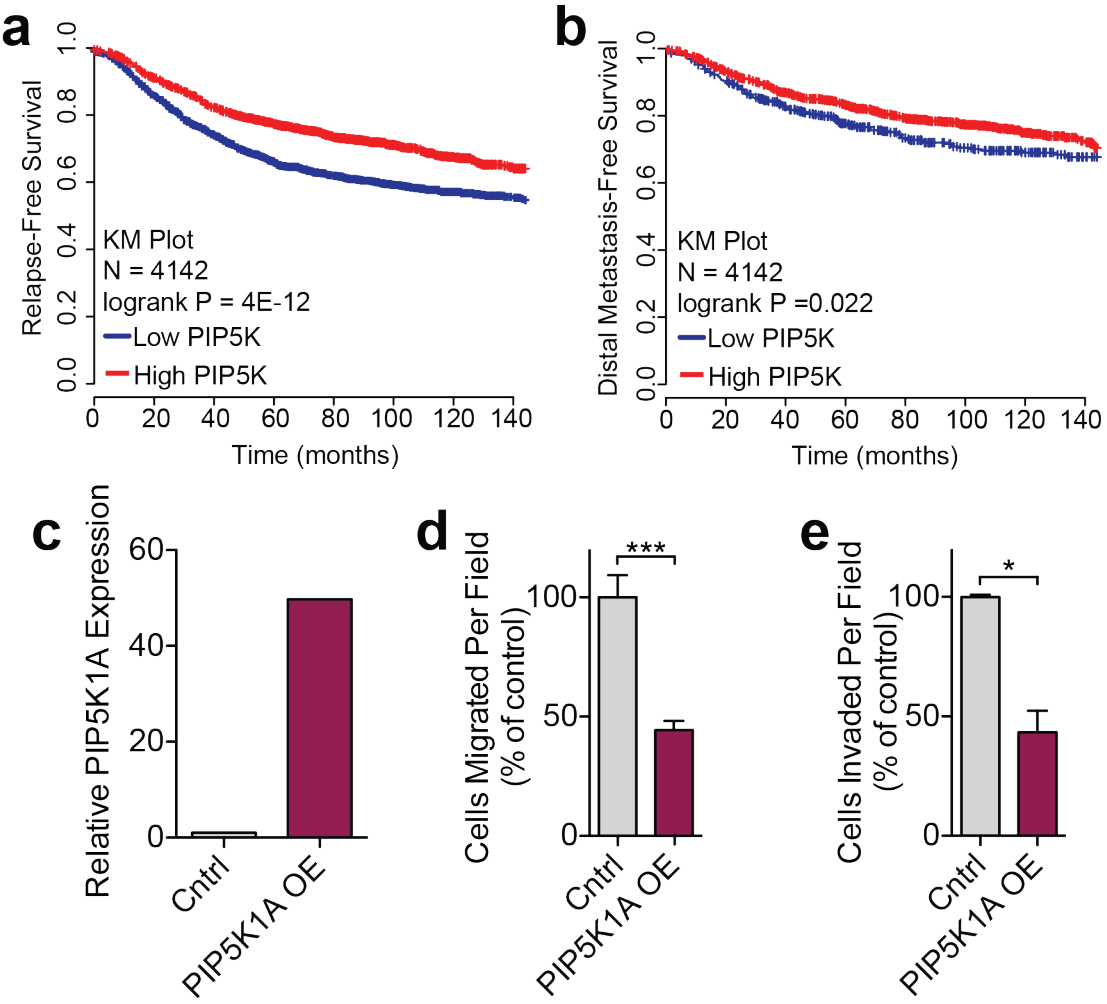

Figure 4.18. PIP5K is a clinically relevant suppressor of metastatic invasion and migration.

a, b. Kaplan-Meier curve representing relapse-free survival (**a**) or distal metastasis free survival (**b**) of a cohort of breast cancer patients as a function of their primary tumor's mean *PIP5K1A*, *PIP5KB*, and *PIP5KC* expression levels. Patients' primary tumors' PIP5K expression levels were classified as low (blue) or high (red) expression.

c. *PIP5K1A* levels in LM2 cells overexpressing PIP5K1A or control vector were measured by qRT-PCR.

d, e. Migration (**c**) and Matrigel invasion (**d**) of LM2 cells overexpressing PIP5K1A or control vector. Data normalized to control values. N = 5 inserts/group.

Data are represented as mean ± S.E.M. *p<0.05, ***p<0.001.

PTPRN2 and PLCβ1 Modulate Cofilin Localization

PI(4,5)P2 regulates cellular processes through binding to effector proteins, either to recruit these proteins to the plasma membrane or to modulate their activity. Given the effects of PTPRN2 and PLCβ1 on metastatic migration through altering PI(4,5)P2 abundance, I questioned whether these effects were mediated through actin dynamics. Multiple proteins involved in actin dynamics are known to be inhibited by plasma membrane PI(4,5)P2 , including gelsolin, profilin, twinfilin, capping proteins, and cofilin (Saarikangas et al., 2010). I first investigated whether any of these genes was clinically significant in breast cancer metastasis. Of these genes, only the increased expression of cofilin was found to significantly correlate with worse distal metastasis-free survival in a cohort of breast cancer patients (Gyorffy et al., 2010) (Figure 4.19a-f). Increased cofilin expression has previously been implicated in breast cancer progression, as well as in oral squamous cellular carcinoma, renal cell carcinoma, and ovarian cancer (Martoglio et al., 2000; Turhani et al., 2006; Unwin et al., 2003; Wang et al., 2007; Wang et al., 2004).

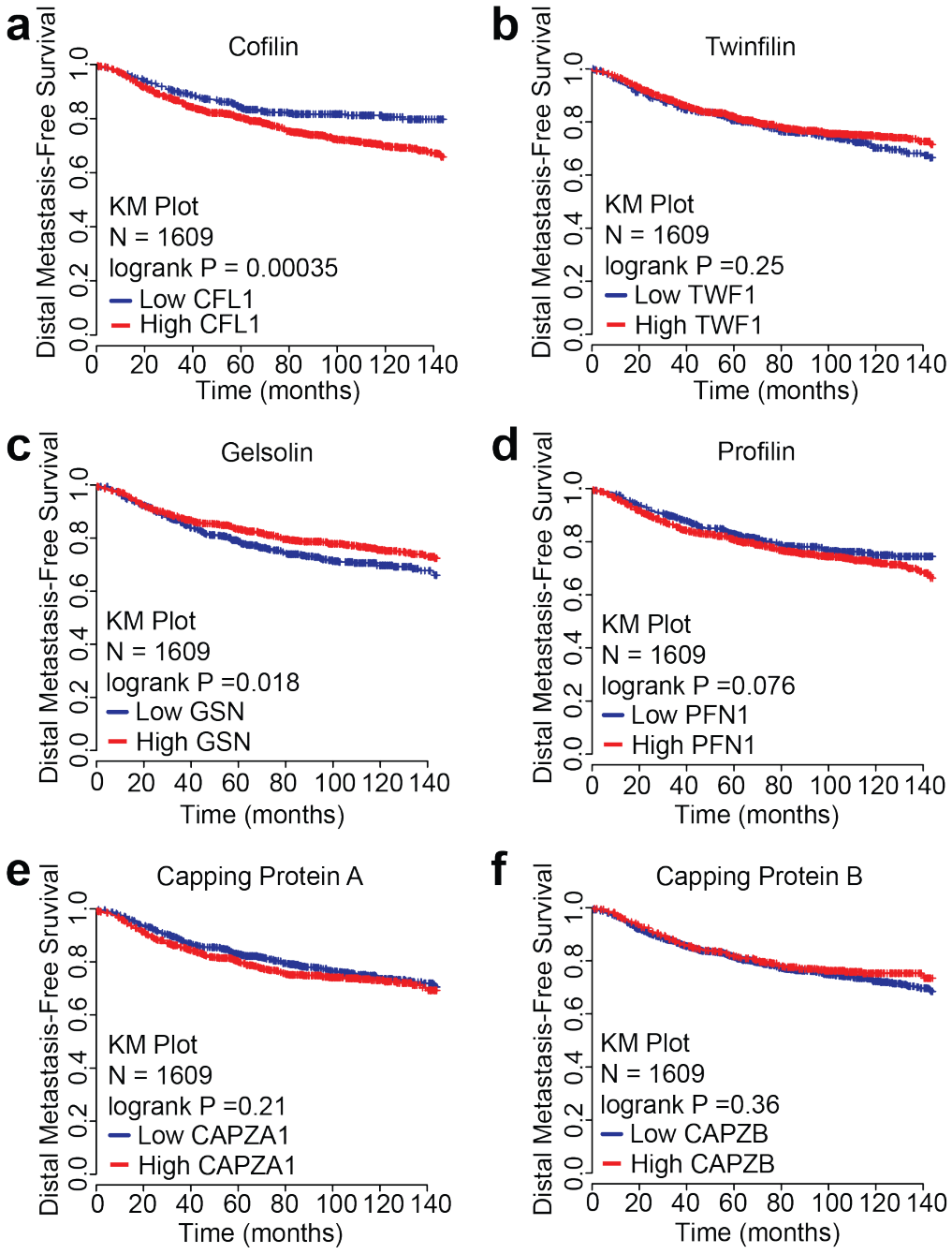

Figure 4.19. Expression of PI(4,5)P2 binding proteins in clinical metastasis-free survival.

a-f. Kaplan-Meier curves representing distal metastasis-free survival of a cohort of breast cancer patients (N = 1609) as a function of their primary tumor's indicated gene expression levels (Data from KMPlot). Patients' primary tumors' indicated gene expression levels were classified as low (blue) or high (red) expression. *CFL1* (**a**), *TWF1* (**b**), *GSN* (**c**), *PFN1* (**d**), *CAPZA1* (**e**), *CAPZB* (**f**).

Cofilin binds to plasma membrane PI(4,5)P2, and this binding prevents cofilin's ability to bind actin (Gorbatyuk et al., 2006; Ojala et al., 2001; Yonezawa et al., 1991). Previous studies have shown that when PI(4,5)P2 is hydrolyzed, cofilin is released from the plasma membrane and acts in the cytoplasm as an actin severing protein to promote migration (Andrianantoandro and Pollard, 2006; Ghosh et al., 2004; van Rheenen et al., 2007). Plasma membrane PI(4,5)P2 levels consequently regulate the localization and activation state of cofilin. Given that PLCβ1 and PTPRN2 alter the levels of plasma membrane PI(4,5)P2, I questioned whether cofilin localization could also change upon depletion or overexpression of PTPRN2 or PLCβ1. Cells depleted of either of these enzymes exhibited higher levels of plasma membrane PI(4,5)P2, and thus would be expected to contain increased levels of membrane-associated cofilin. To test this hypothesis, I sought to purify membrane fractions containing membrane and membrane-associated proteins from cancer cells and quantify the amount of cofilin in these fractions. Western blots from MDA-MB-231 cells showed clean separation between the membrane and cytoplasmic cellular compartments, as epidermal growth factor receptor (EGFR), a transmembrane protein, was present predominantly in the membrane fraction, while tubulin, a component of microtubules in the cytoplasm, was present only in the cytoplasmic fraction (Figure 4.20).

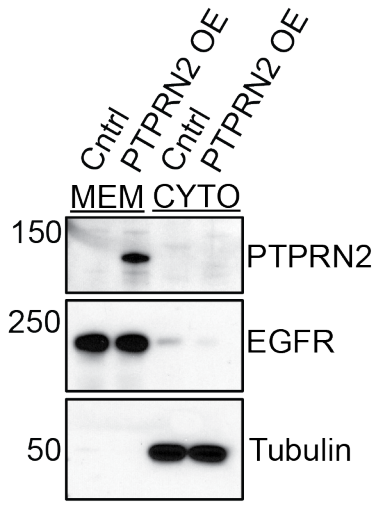

Figure 4.20. Separation of cytoplasmic and membrane proteins.
Membrane and membrane-associated proteins (MEM) and cytoplasmic proteins (CYTO) were collected from MDA-MB-231 cells overexpressing PTPRN2 or a control vector. Protein fractions were subjected to Western blot analysis for PTPRN2, EGFR, and Tubulin.

Having demonstrated effective separation of membrane and cytoplasmic cellular fractions, I next measured membrane cofilin content in the setting of altered PLCβ1 or PTPRN2 expression. Western blot analysis of membrane fractions from metastatic cells depleted of either PLCβ1 or PTPRN2 contained significantly more cofilin (CFL1) protein compared to control cells (Figure 4.21a, b). Conversely, cells overexpressing either of these enzymes contained less cofilin in their membrane fraction relative to control cells (Figure 4.21c, d).

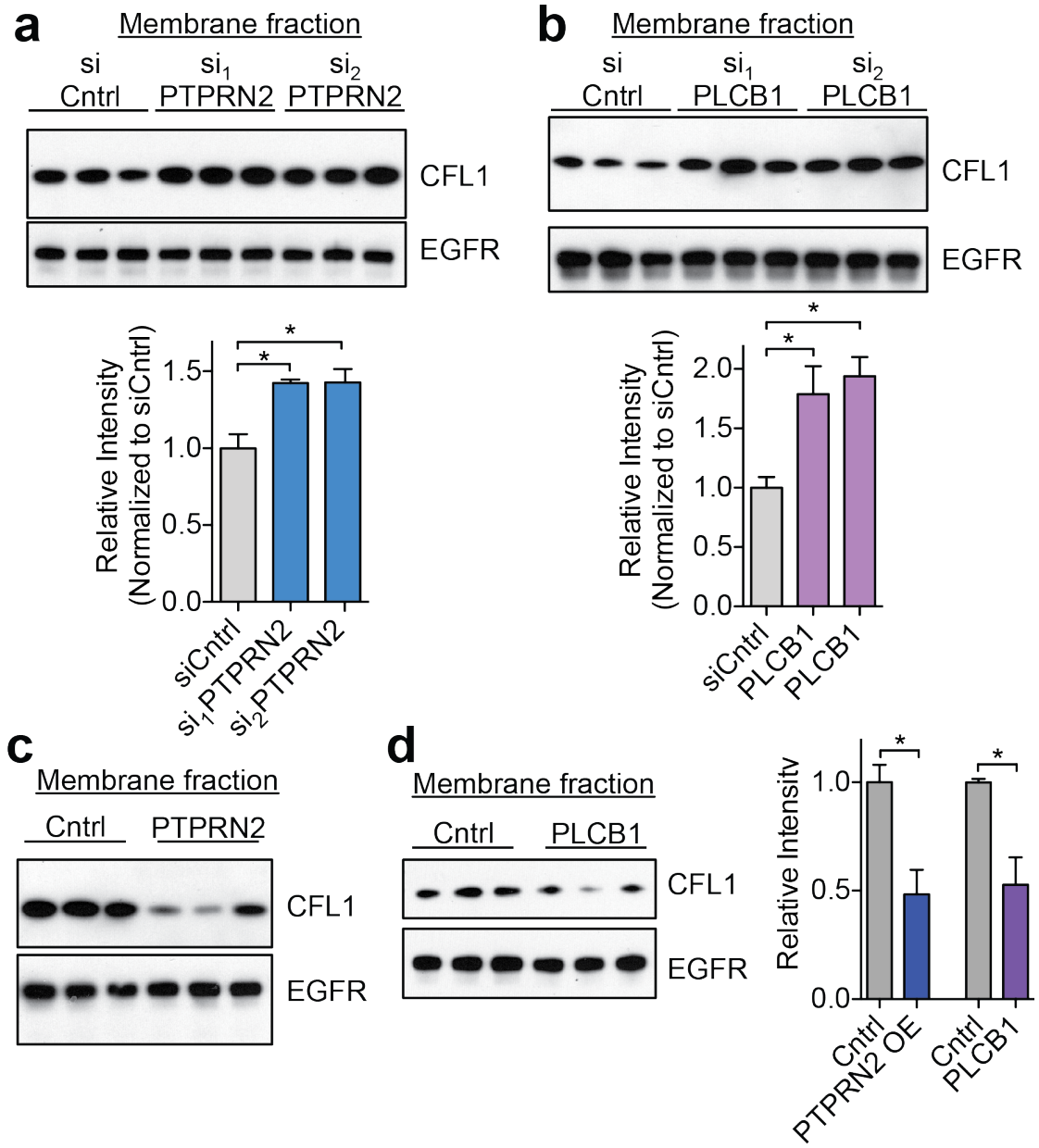

Figure 4.21. PTPRN2 and PLCβ1 regulate the cellular localization of cofilin.

a, b. Membrane and membrane-associated proteins were purified from cells transfected with siRNA targeting PTPRN2 (**a**) or PLCβ1 (**b**) or control siRNA. Fractions were subjected to western blot analysis for CFL1 and EGFR levels. Below, densitometry analysis of CFL1 levels normalized to EGFR levels.

c, d. Membrane and membrane-associated proteins were purified from cells overexpressing PTPRN2 (**c**), PLCβ1 (**d**) or a control vector. Fractions were subjected to western blot analysis for CFL1 and EGFR levels. Right, densitometry analysis of CFL1 levels normalized to EGFR levels. Data are represented as mean ± S.E.M. *p<0.05.

These changes in cofilin membrane quantity were independent of changes in total cofilin protein content, as western blot analysis for cofilin whole cell lysate from these cells revealed no difference in cofilin abundance (Figure 4.22a, b). This indicates that the differences in cofilin membrane quantity were due to changes in cofilin localization rather than changes in cofilin expression upon manipulation of PTPRN2 or PLCβ1 expression levels.

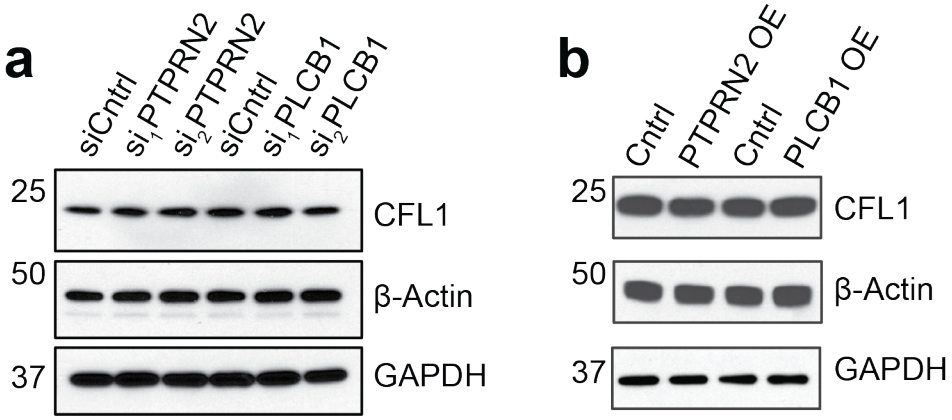

Figure 4.22. Total cofilin and actin protein abundance in cancer cells with modulated PTPRN2 and PLCβ1 expression.

a. Western blot analysis of cofilin and actin in whole cell lysate of LM2 cells transfected with a control siRNA or siRNAs targeting PTPRN2 or PLCβ1.

b. Western blot analysis of cofilin and actin in whole cell lysate of MDA-MB-231 cells overexpressing PTPRN2, PLCβ1, or a control vector.

Western blot analysis of GAPDH was used as a loading control.

To further test the change in cofilin localization upon PTPRN2 or PLCβ1 modulation, I performed immunofluorescence experiments to visualize CFL1 localization. Cells depleted of PTPRN2 or PLCβ1 exhibited significantly increased membrane localization of CFL1 relative to control cells (Figure 4.23a, b). Conversely, overexpression of PTPRN2 or PLCβ1 revealed reduced cofilin membrane localization, and increased cytoplasmic staining (Figure 4.23c). Taken together, these data indicate that PTPRN2 and PLCβ1 act upstream of CFL1 localization. By decreasing plasma membrane PI(4,5)P2 levels, these enzymes reduce cofilin's association with the plasma membrane, increasing the level of cytoplasmic cofilin.

Figure 4.23. Immunofluorescence visualization of cofilin localization governed by PLCβ1 or PTPRN2.

a, b. LM2 cells transfected with siRNA targeting PTPRN2 (**a**), PLCβ1 (**b**), or a control siRNA were immunostained for CFL1 (red) and DAPI (blue). Top, representative images. Bottom, quantification of membrane mean fluorescence intensity of CFL1. N = 50 cells/group. Scale bar, 10 μm.

c. MDA-MB-231 cells overexpressing PTPRN2, PLCβ1, or a control vector were immunostained for CFL1 (red) and DAPI (blue). Left, representative images. Right, quantification of membrane mean fluorescence intensity of CFL1. N = 50 cells/group. Scale bar, 10 μm.

Data are represented as mean ± S.E.M. ***p<0.001.

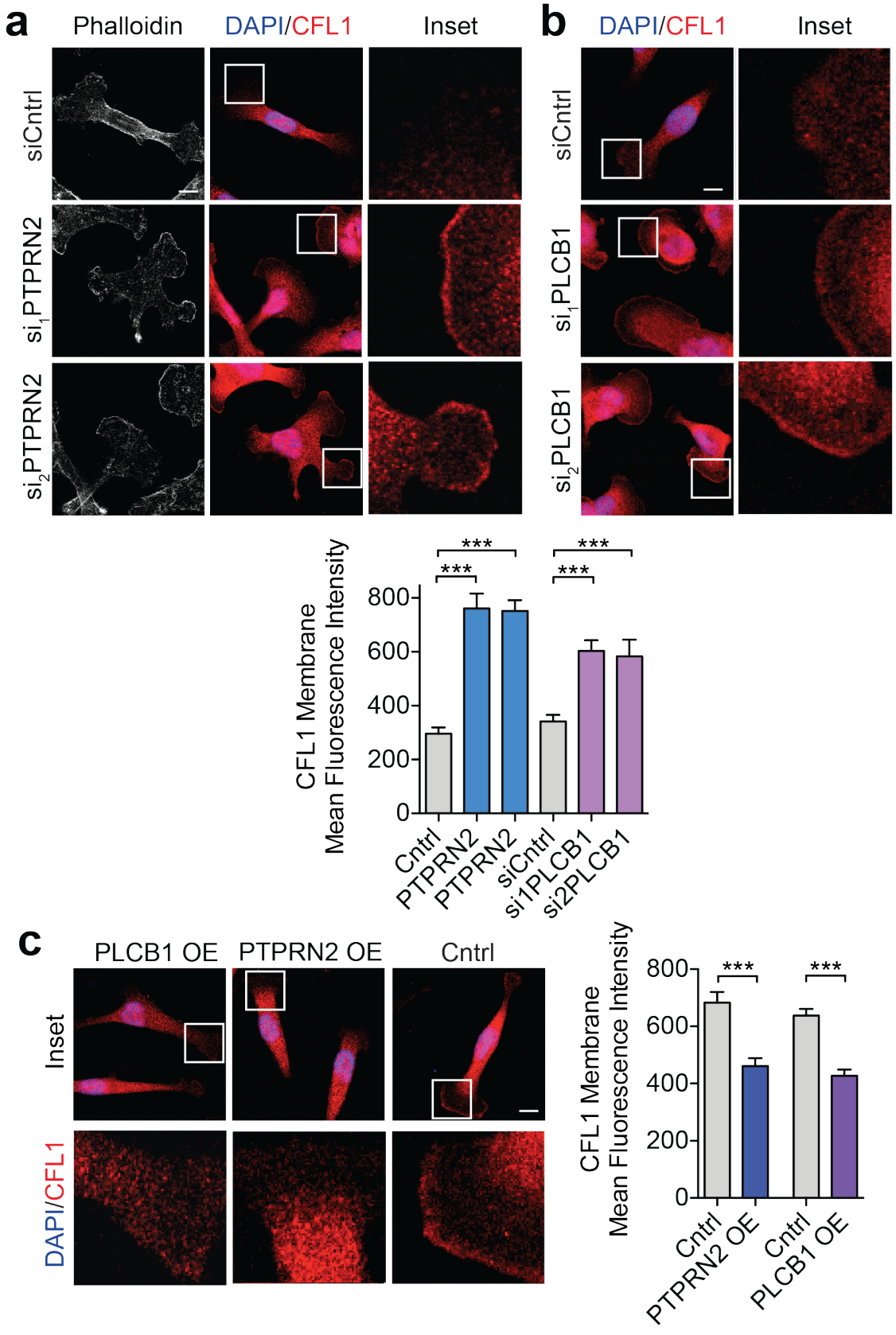
a
Phalloidin
DAPI/CFL1
Inset
siCntrl
si1PTPRN2
si2PTPRN2
b
DAPI/CFL1
Inset
siCntrl
si1PLCB1
si2PLCB1
CFL1 Membrane Mean Fluorescence Intensity
800
600
400
200
0
***
***
***
***
Cntrl
PTPRN2
PTPRN2
siCntrl
si1PLCB1
si2PLCB1
c
PLCB1 OE
PTPRN2 OE
Cntrl
Inset
DAPI/CFL1
CFL1 Membrane Mean Fluorescence Intensity
800
600
400
200
0
***
***
Cntrl
PTPRN2 OE
Cntrl
PLCB1 OE

PTPRN2 and PLCβ1 Promote Migration through Actin Remodeling by Cofilin

I next explored whether the cofilin localization changes observed upon depletion of PLCβ1 or PTPRN2 result in altered cofilin activity. Cofilin regulates migration by severing F-actin filaments to generate free barbed ends. The production of free barbed ends by cofilin is a necessary precursor for the assembly of actin filaments driving membrane protrusion, and enhanced abundance of free barbed ends correlates with increased actin polymerization (Carlsson, 2006; Chan et al., 2000). Cofilin is only able to bind and sever actin when not bound to PI(4,5)P2, as the binding sites for actin and PI(4,5)P2 overlap and are mutually exclusive. To determine whether the decreased cytoplasmic cofilin I observed in cancer cells with depletion of PTPRN2 and PLCβ1 led to a reduction in cellular cofilin activity, I performed barbed end assays. In the barbed end assay, cells are partially permeabilized and incubated with labeled actin monomers. The actin monomers are only able to incorporate into free barbed ends. Unbound actin monomers are washed away, and cells are fixed and stained for immunofluorescence. The amount of free barbed ends can be quantified by measuring the amount of labeled actin monomer present in the cells. Measurement of the number of free barbed ends in the breast cancer cells revealed that cells depleted of PTPRN2 or PLCβ1 contained significantly fewer free barbed ends relative to control cells, as quantified by the incorporation of labeled actin monomers (Figure 4.24). These results suggest that PLCβ1 and PTPRN2 regulate breast cancer cell actin polymerization through decreased membrane PI(4,5)P2 abundance and increased cofilin activity.

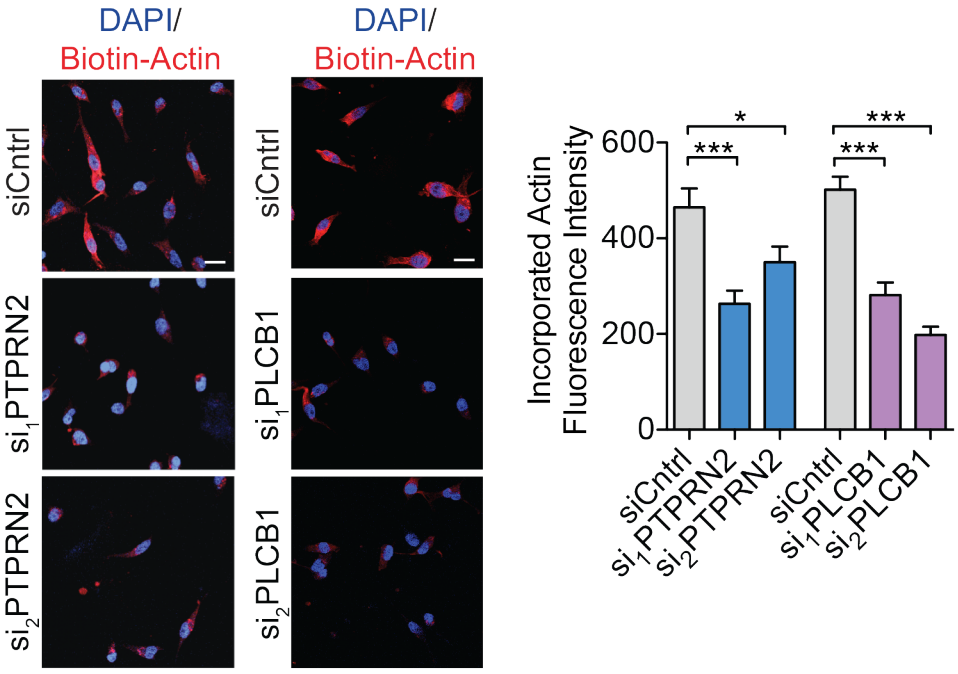

Figure 4.24. PTPRN2 and PLCβ1 mediate cofilin activity.

LM2 cells transfected with siRNA targeting PTPRN2, PLCβ1, or control siRNA were partially permeabilized and incubated with biotin-actin monomers. Cells were stained for incorporated biotin-actin monomers using Streptavidin-555 (red) and DAPI (blue). Right, quantification of mean fluorescence intensity of incorporated biotin-actin monomers. N = 100 cells/group. Scale bar, 20 μm. Data are represented as mean ± S.E.M. *p<0.05, ***p<0.001.

Given the changes in cofilin localization and activity observed upon PLCβ1 and PTPRN2 modulation, we next asked whether these changes in cofilin localization alter the actin cytoskeleton in cancer cells. Interestingly, cells depleted of PTPRN2 or PLCβ1 exhibited reduced F-actin signal as visualized by immunofluorescence (Figure 4.25a). This change in staining intensity was independent of total actin protein abundance as measured by western blotting (Figure 4.22), suggesting that these cells possessed similar quantities of actin monomers, but less filamentous actin in the setting of PTPRN2 or

PLCβ1 knockdown. Conversely, PTPRN2 or PLCβ1 overexpression significantly increased cellular F-actin staining intensity (Figure 4.25b). The weak actin filament network seen upon PTPRN2 or PLCβ1 depletion is consistent with the migration defects observed in these cells, since actin filament polymerization capacity at the leading edge is necessary for cellular migration and invasion (Ghosh et al., 2004). These findings are also consistent with the increased membrane-associated (inactive) cofilin in these cells, since cofilin activity is necessary for the generation of new actin filaments.

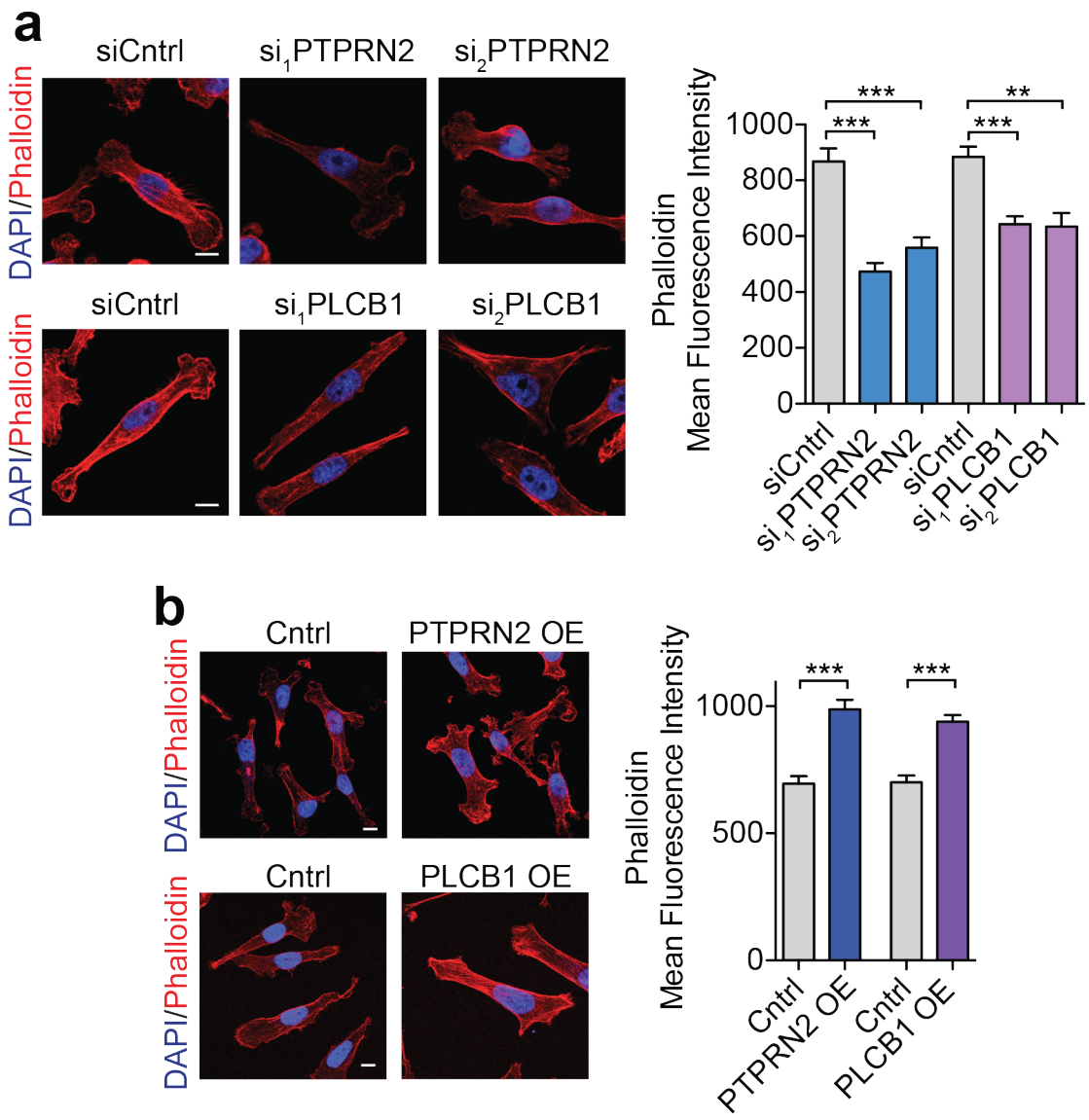

Figure 4.25. PTPRN2 and PLCβ1 expression affects actin polymerization.

a, b. LM2 cells transfected with siRNA targeting PTPRN2, PLCβ1, or control siRNA (**a**) and MDA-MB-231 cells overexpressing PTPRN2, PLCβ1, or a control vector (**b**) were stained with phalloidin (red) and DAPI (blue) and analyzed using fluorescence microscopy. Right, mean fluorescence intensity quantification of whole cell phalloidin signal. N = 40 cells/group. Scale bar, 10 μm. Data are represented as mean ± S.E.M. **p<0.01, ***p<0.001.

The above findings reveal PTPRN2 and PLCβ1 to regulate actin dynamics, decreasing the levels of plasma membrane PI(4,5)P2 to increase active cytoplasmic cofilin to drive metastatic migration. To test whether cofilin acts downstream of PLCβ1/PTPRN2-mediated PI(4,5P)2 dynamics and metastatic migration, I performed epistasis experiments. Partial knockdown of cofilin using RNA-interference abrogated the effects of PTPRN2-mediated enhancement of migration and metastatic colonization, consistent with cofilin being necessary for the effects (Figure 4.26a-c). In the setting of PTPRN2 overexpression, cofilin depletion decreased migration by cancer cells by greater than 70%. Similarly, cofilin depletion prevented enhanced migration capacity induced by PLCβ1 overexpression (Figure 4.26d). Consistent with cofilin as necessary for cell motility, depletion of cofilin reduced the ability of control cells to migrate, but to a lesser extent than cells with PTPRN2 or PLCβ1 overexpression, indicating that cofilin is acting in part through the PTPRN2/PLCβ1 pathway.

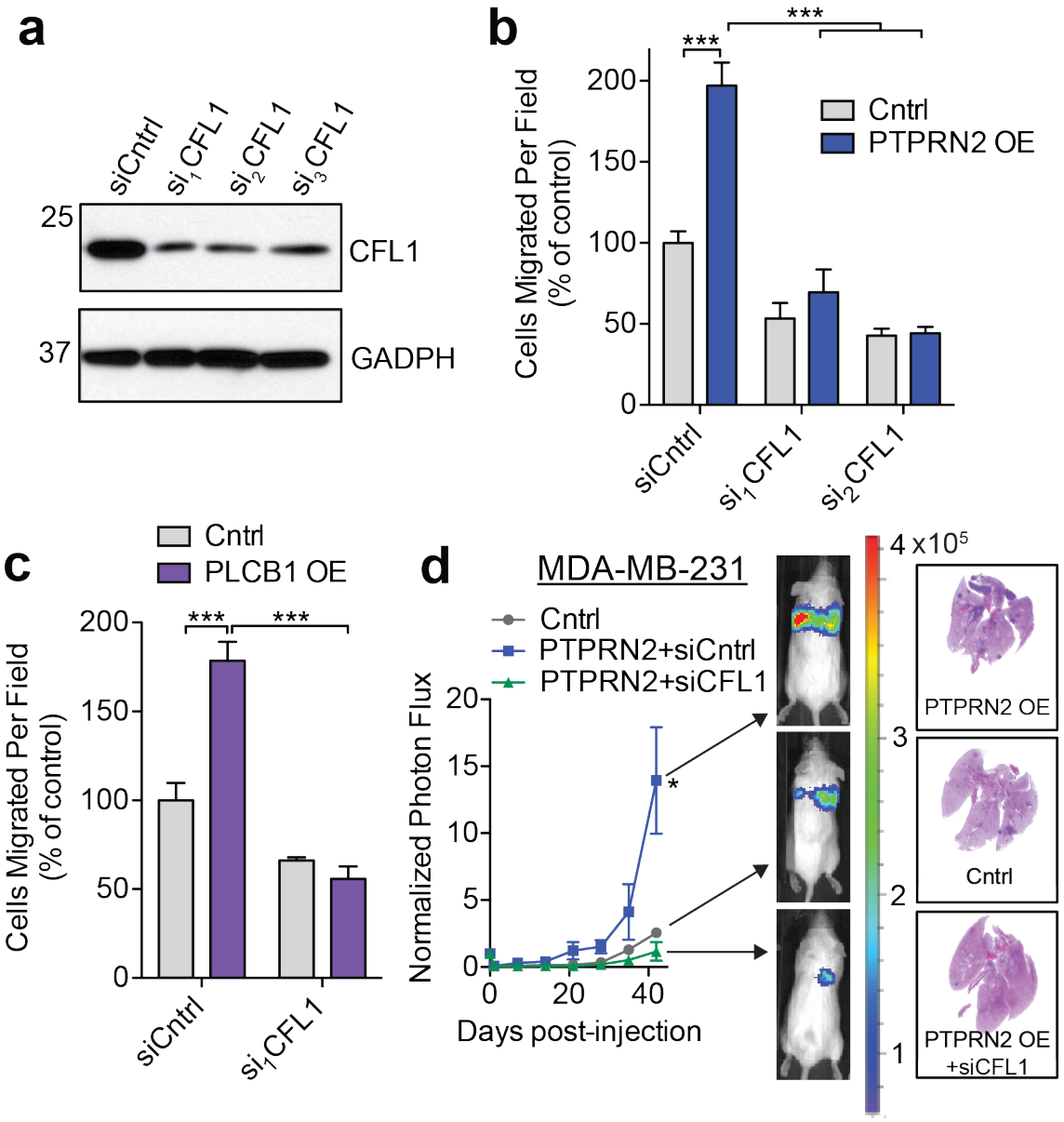

Figure 4.26. Cofilin is required for PTPRN2- and PLCβ1-mediated metastasis.

a. Western blot analysis of CFL1 in MDA-MB-231 cells transfected with siRNAs targeting CFL1. GAPDH was used as a loading control.

b, c. MDA-MB-231 cells were transfected with siRNAs targeting CFL1 or a control siRNA in the setting of control or PTPRN2 (**b**) or PLCβ1 (**c**) overexpression and subjected to the migration assay. N = 5 inserts/group.

c. Bioluminescence imaging quantification of 40,000 MDA-MB-231 cells as in (**b**). Right, representative lung histology. N = 5 mice/group.

Data are represented as mean ± S.E.M. *p<0.05, ***p<0.001.

I hypothesized that PTPRN2 and PLCβ1 act upstream of cofilin by regulating cofilin's localization through modulating plasma membrane PI(4,5)P2 levels. Cells depleted of either enzyme exhibited increased levels of plasma membrane PI(4,5)P2 and increased membrane-associated cofilin. Given that the activation of cofilin depends on its release from PI(4,5)P2, a constitutively membrane-associated mutant of cofilin should not be able to respond to changes in plasma membrane PI(4,5)P2 levels mediated by PLCβ1 or PTPRN2. To generate a continuously membrane-associated form of cofilin, I fused the N-terminal sequence of Lck, a Src tyrosine kinase to cofilin. This sequence is myristoylated and inserted into the plasma membrane (Zlatkine et al., 1997). Addition of this sequence has been demonstrated as sufficient to target proteins to the plasma membrane. Cells transfected with cofilin-Lck exhibited increased cofilin localization to the plasma membrane relative to cells transfected with wild-type cofilin (Figure 4.27). In cells overexpressing either PLCβ1 or PTPRN2, endogenous cofilin was depleted using siRNA targeting the 3'UTR, and cofilin was re-expressed as either wild-type cofilin or membrane-anchored cofilin-Lck. Cells with replacement expression of wild-type cofilin exhibited PTPRN2 and PLCβ1-mediated increases in migration. However, restoring cofilin expression with membrane-anchored cofilin-Lck abolished the ability of PTPRN2 or PLCβ1 to increase migration (Figure 4.27a, b). These findings indicate that metastatic migration driven by PTPRN2 and PLCβ1 is accomplished through active, non-PI(4,5)P2 membrane-associated cofilin.

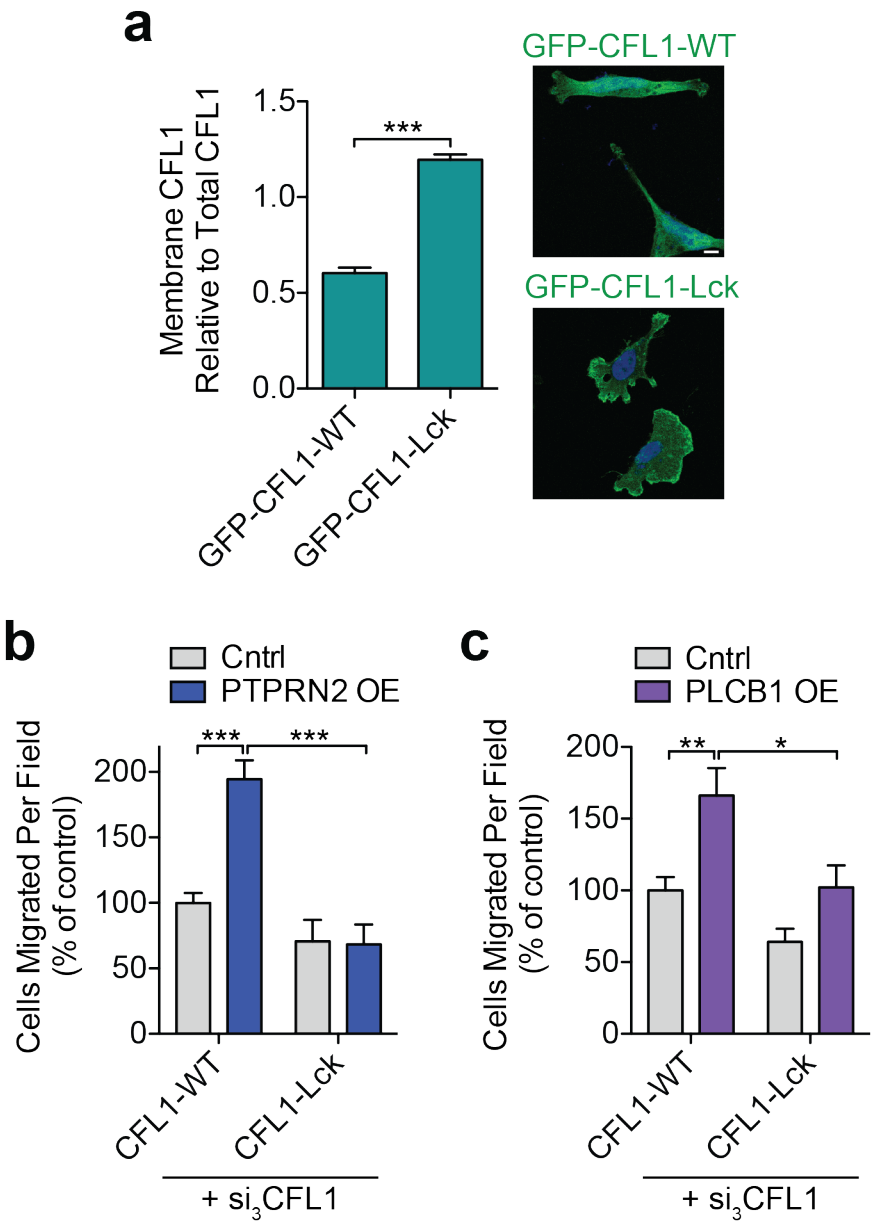

Figure 4.27. Membrane-fused cofilin abrogates PTPRN2 and PLCβ1 effects.

a. MDA-MB-231 were transfected with siRNA targeting the 3'UTR of *CFL1* to deplete endogenous CFL1 and further transfected with plasmids encoding either GFP-CFL1-WT or GFP-CFL1-Lck (green) and immunostained with DAPI (blue). Left, quantification of membrane GFP-CFL1. Right, representative images. N=50 cells/group. Scale bar, 10 μm.

b, c. MDA-MB-231 cells overexpressing PTPRN2 (**b**) or PLCβ1 (**c**) were transfected as in (**a**) and subjected to the migration assay. N = 5 inserts/group.

Data are represented as mean ± S.E.M. *p<0.05, **p<0.01, ***p<0.001.

Our findings support a model wherein PTPRN2 and PLCβ1 abundance increases in highly metastatic breast cancer cells. PTPRN2 and PLCβ1 convergently reduce the levels of PI(4,5)P2 in the plasma membrane, dissociating cofilin from the membrane and enabling it to sever cytoplasmic actin to drive actin assembly, metastatic migration, and colonization.

CHAPTER V: DISCUSSION

Overview of Findings

Phosphoinositide regulator proteins may drive cancer progression by manipulating the lipids governing the cellular processes that give rise to metastatic phenotypes. In this thesis, I describe the molecular mechanisms of three proteins, PITPNC1, PTPRN2, and PLCβ1, which regulate the levels of PIs in cancer cells to promote metastasis. In the final chapter of this thesis, I summarize the findings from Chapters II-IV, address additional considerations on the mechanisms of these proteins, synthesize findings from both projects, and discuss the therapeutic potential of targeting these pathways.

We first identified PITPNC1 as a robust driver of metastasis in melanoma, breast, and colon cancer through functional studies and clinical data analysis. Notably, *PITPNC1* expression increased significantly in triple negative breast cancer, a subtype of breast cancer for which targeted adjuvant therapy is currently lacking. We furthermore identified multiple pathways by which PITPNC1 expression may be increased in cancer cells. PITPNC1 was initially identified as a target of the metastasis suppressor miRNA, miR-126, and we discovered PITPNC1 was also targeted by a second metastasis suppressor miRNA, miR-335. Additionally, *PITPNC1* is amplified in nearly half of breast tumors due to a common amplification within chromosome 17q where it is located.

We then investigated the molecular mechanism of PITPNC1-mediated metastasis, and found that PITPNC1 binds to PI4P in the trans Golgi network (TGN), bringing its binding partners, RAB1B and 14-3-3 proteins to the Golgi. The PITPNC1/RAB1B

protein complex increases PI4P abundance in the Golgi, and we propose this occurs through the recruitment of PI4KA to the TGN by RAB1B. PI4KA increases the TGN abundance of PI4P, and GOLPH3 binds to the additional PI4P, inducing tensile forces on the Golgi through GOLPH3's binding to MY018A and the actin cytoskeleton. The elongated Golgi ribbon induced by these forces facilitates secretion, leading to enhanced release of secreted factors. We identified a set of pro-metastatic genes whose secretion required PITPNC1: ADAM10, FAM3C, HTRA1, MMP1, and PDGFA (Figure 5.1).

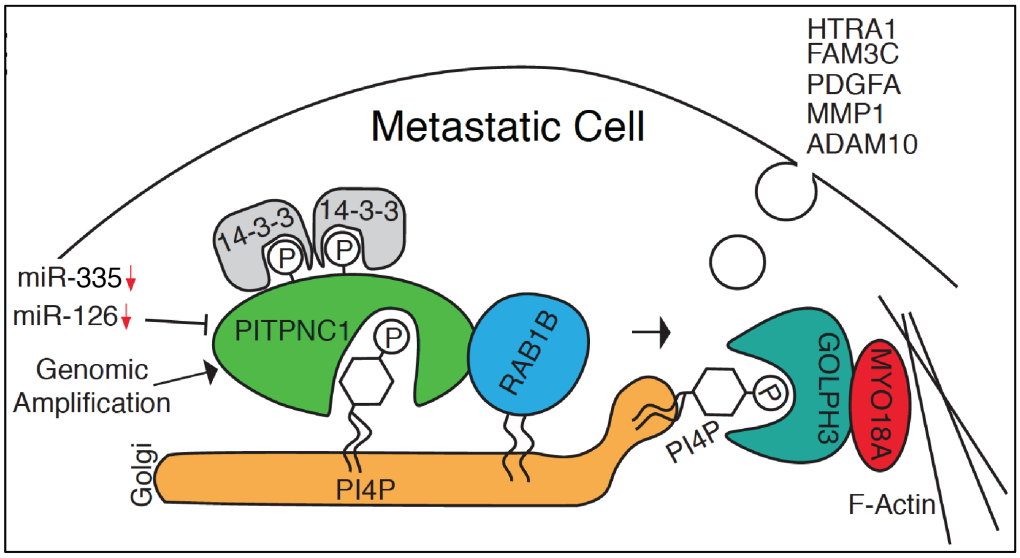

Adapted from Halberg, N, Sengelaub, CA*, et al. In Revision at Cancer Cell.*

Figure 5.1. PITPNC1-mediated metastatic secretion though recruitment of RAB1B to the *trans* Golgi.

PITPNC1 expression is augmented in highly metastatic cells due to genomic amplification and loss of miR-126- and miR-335-mediated repression. PITPNC1 binds 14-3-3 and RAB1B, and localizes to the Golgi due to its binding of PI4P. Recruitment of RAB1B to the Golgi enhances PI4P abundance, increasing tensile stretching of the Golgi by GOLPH3. The elongated Golgi morphology enhances secretion of a set of pro-antigenic and pro-metastatic factors.

PTPRN2 and PLCβ1 were initially identified as putative targets of a metastasis suppressor miRNA, miR-335. Increased expression of PTPRN2 and PLCβ1 was found to clinically correlate with metastatic relapse and worse overall survival in breast cancer in breast cancer patients. PTPRN2 and PLCβ1 convergently target PI(4,5)P2 in the plasma membrane of breast cancer cells. These enzymes act in two independent manners: PTPRN2 dephosphorylates PI(4,5)P2 while PLCβ1 hydrolyzes the lipid. The action of these enzymes decreases the abundance of PI(4,5)P2 in the plasma membrane, releasing cofilin from the membrane to the cytoplasm. Cofilin in the cytoplasm binds and severs actin, generating increased actin polymerization and enhancing cellular motility. Enhanced cellular motility driven by PTPRN2 and PLCβ1 promotes metastatic migration, especially at early stages in the metastatic cascade (Figure 5.2).

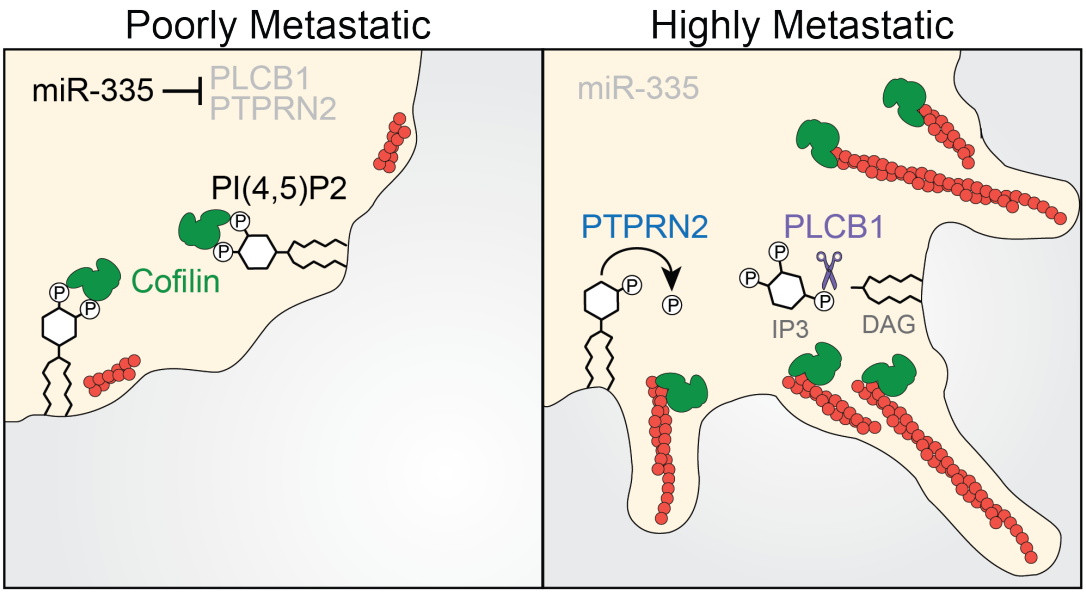

Adapted from Sengelaub, CA et al. In Revision at EMBO J.

Figure 5.2. PTPRN2- and PLCβ1-mediated metastatic migration through PI(4,5)P2-dependent actin remodeling.

PTPRN2 and PLCβ1 expression is increased in highly metastatic breast cancer cells due to loss of translational repression by miR-335. PTPRN2 and PLCβ1 deplete PI(4,5)P2 in the plasma membrane. PI(4,5)P2 binds cofilin to inhibit its activity, and loss of PI(4,5)P2 increases cofilin actin-severing activity to promote metastatic migration.

Considerations on the Mechanism of PITPNC1-mediated Metastasis

PITPNC1 belongs to the RdgB class of PITP transfer proteins (PITP family class II), which is generally less well characterized than the class I proteins, PITPα and PITPβ. PITPα and PITPβ have been found to bind and transfer unmodified phosphoinositide (PI) and phosphatidyl choline (PC). Previous work by other researchers implicated PITPNC1 as binding and transferring phosphatidic acid (PA) (Garner et al., 2012). The physiological implication of this activity is unclear; although the researchers suggest that PITPNC1 may transfer PA to the endoplasmic reticulum for synthesis of PI. In our biochemical and cellular analyses, we did not detect binding of PITPNC1 to PA.

Additionally, PITPNC1 exhibited localization to the TGN in breast cancer cells, an organelle enriched in PI4P. PITPNC1 localization to the TGN was dependent upon PI4P, as depletion of PI4P by Golgi-localized SAC1 reduced PITPNC1 abundance in the Golgi and increased PITPNC1 in the cytoplasm. Furthermore, the defects in secretion we observe upon depletion of PITPNC1 are consistent with a role for PITPNC1 in the Golgi. PI4P thus represents a new substrate for the PITP domain, as previous PITP domain substrates have been limited to PI, PC, and PA.

Future studies will be required to determine what role, if any, the lipid transfer capacity of PITPNC1 serves in metastatic cells. Nils Halberg previously observed that recombinant PITPNC1 is capable of transferring PI4P between vesicles *in vitro*, however with much lower efficiency relative to the transfer of PI by PITPα. Several possible functions of PITPNC1 transfer of PI4P are considered as follows. First, it is possible that PITPNC1 may localize PI4P to proposed "microdomains" within the TGN where exocytic budding is thought to occur (De Matteis and Luini, 2008). PI4P recruits proteins required for vesicle budding at these sites in the TGN. Another possibility is that PITPNC1 maintains PI4P localization in the TGN. The Golgi is a dynamic organelle undergoing continual anterograde and retrograde transport of cargo. PITPNC1 may bind to PI4P to prevent PI4P retrograde transport to the *cis* Golgi, maintaining enrichment of PI4P in the TGN. Lastly, a new role for lipid transfer domains as lipid-presenting proteins has recently been suggested. The lipid transfer protein TIPE3 was demonstrated to not only transfer PI(4,5)P2, but also present PI(4,5)P2 to PI3K, increasing the generation of PIP3 through optimal orientation of the substrate (Fayngerts et al., 2014). This suggests

that PITPNC1 could also present PI4P to PI4P-binding proteins, although the physiological role of this activity would need to be determined.

In our proposed mechanism of PITPNC1-mediated secretion, PITPNC1 binds and recruits RAB1B to the Golgi. RAB1B in turn recruits PI4KA to the Golgi, increasing the abundance of PI4P in the TGN. In addition to its role in recruiting PI4KA, RAB1B also enhances secretion through activating ADP ribosylation factor 1 (ARF1). Secretory vesicles are formed by the recruitment of various cytoplasmic proteins, a process that is initiated by ARF1. ARF1 is activated by conversion from a GDP-bound form to GTP-bound state by the guanine nucleotide exchange factor (GEF) GBF1. RAB1B has been found to recruit GBF1 from the cytoplasm to the Golgi where it activates ARF1, inducing vesicle formation at the TGN (Dumaresq-Doiron et al., 2010; Monetta et al., 2007). Consequently, PITPNC1-mediated recruitment of RAB1B to the TGN may promote metastatic secretion through two methods: RAB1B recruiting PI4KA and RAB1B activating ARF1. Interestingly, 14-3-3 proteins have also been shown to recruit BARS and PI4KB to the Golgi to regulate Golgi carrier formation and vesicular budding and fission (Valente et al., 2012). In addition to bringing RAB1B to the Golgi, PITPNC1 may also increase 14-3-3 Golgi abundance to facilitate secretion.

Considerations on the Mechanism of PTPRN2 and PLCβ1-mediated Metastasis

PTPRN2 and PLCβ1 deplete PI(4,5)P2 from the plasma membrane, which promotes actin remodeling and migration. This is accomplished through the activation of cofilin, which is inhibited as a result of its binding to membrane PI(4,5)P2. Loss of

PI(4,5)P2 allows cofilin to move to the cytoplasm where it modifies actin filaments. Through fluorescence recovery after photobleaching (FRAP) experiments, cofilin has been shown to bind PI(4,5)P2 transiently, with fast on- and off-rates (van Rheenen et al., 2007). Therefore, the increase in cytoplasmic cofilin upon PI(4,5)P2 depletion is not the result of direct release of cofilin by PTPRN2 or PLCβ1, but rather the lower on-rate of cofilin binding to PI(4,5)P2 as a result of the lower PI(4,5)P2 concentration at the plasma membrane. Cofilin activation is highly sensitive to alterations in PI(4,5)P2 levels by PTPRN2 and PLCβ1.

Cofilin activity must be carefully temporally and spatially controlled to promote optimal formation of plasma membrane protrusions and subsequent migration. Indeed, excess cofilin activation can inhibit actin dynamics (Wang et al., 2007). Although the mechanisms by which PTPRN2 and PLCβ1 enzymatic activities are controlled were not studied in this thesis, several modes of regulation are possible. First, we noted that both PTPRN2 and PLCβ1 frequently localize to one edge of the plasma membrane, potentially corresponding to the leading edge of the cancer cell. Restricted localization of these proteins would thus generate restricted cofilin activation, promoting directional migration. However, future work will be required to determine how the localization of PTPRN2 and PLCβ1 to the leading edge is established.

In addition to polarized localization of PTPRN2 and PLCβ1, the enzymatic activity of each protein may be temporally restricted. As a transmembrane protein, PTPRN2 is transported to the plasma membrane and then recycled back to the Golgi in a cyclical manner. Since PTPRN2 is not constitutively localized to the plasma membrane,

it is only able to dephosphorylate PI(4,5)P2 during one part of its cellular trafficking cycle, restricting its activity.

PLCβ1 activity is temporally restricted by its requirement for external activation. The PLCβ family is activated by heterotrimeric G proteins, and PLCβ1 is specifically activated by the $G_q\alpha$ subunits. In order to activate PLCs, heterotrimeric G proteins must first be activated by G protein-coupled receptors (GPCRs) which act as GEFs to exchange GDP to GTP bound to the G protein. GPCRs are activated by small molecules such as hormones, cytokines, and peptides. $G_q\alpha$ -coupled GPCRs are activated by several molecules that have been implicated in cancer, including CXC chemokines (implicated in metastatic angiogenesis), bradykinin (identified as a growth factor in multiple cancer types), angiotensin II (promotes migration and proliferation in breast and lung cancer), and endothelin-1 (overexpressed in multiple cancer types, promotes survival and migration) (Rhee, 2001). The fact that these molecules must be present to activate PLCβ1 restricts its enzymatic activity. The localization of these activating molecules in the microenvironment may perhaps also provide a chemotactic directional effect on cellular migration.

PLCβ1 activity is further temporally restricted by the length of G protein activation. Activated G proteins contain intrinsic GTPase activity, quickly inactivating the signaling cascade. Interestingly, PLCβ enzymes possess GTPase stimulating activity, or the ability to increase the rate of inactivation of the G protein to prevent constitutive activation of enzymatic activity (Rebecchi and Pentyala, 2000). Thus PLCβ1 limits its own activity, consistent with the need for temporal control of PI(4,5)P2 depletion and cofilin activation. In PLCδ, a homolog of PLCβ1, decreasing concentrations of PI(4,5)P2

reduced enzymatic activity *in vitro*, indicating that the PI(4,5)P2 substrate itself may also serve to modulate the activity of the enzyme (Cifuentes et al., 1993). This represents an additional route by which the enzymatic activity of PLCβ1 may be limited, to allow for controlled activation of cofilin without depleting membrane PI(4,5)P2 necessary for other cellular processes.

A recent study on PTPRN2 suggested a role for PTPRN2 in resistance to apoptosis, specifically in the setting of high cell density (Sorokin et al., 2015). We did not observe changes in the cellular proliferation rates of cancer cells with either depletion or overexpression of PTPRN2. However, staining for caspase markers and Ki67 in these cells will be required to conclusively eliminate this hypothesis. Nuclear-localized PLCβ1 has also been implicated in cell proliferation. Products of the PLC reaction, DAG and IP3, activate PKC, which in turn activates cell cycle proteins (Faenza et al., 2000). However we did not observe PLCβ1 localization to the nucleus in the breast cancer cells utilized in this work, nor did we observe changes in cellular proliferation rates upon PLCβ1 depletion or overexpression.

miR-126 and miR-335 Regulation of PITPNC1, PTPRN2, and PLCB1

PITPNC1, *PTPRN2*, and *PLCB1* were initially identified as putative targets of miR-126 and miR-335. These miRNAs are silenced in highly metastatic breast cancer cells, and reconstituting their expression reduces metastatic colonization capacity (Tavazoie et al., 2008). Expression of these miRNAs is repressed by independent mechanisms. Work by Kim Png, a previous graduate student in the laboratory, revealed

that miR-335 is silenced by two independent mechanisms in highly metastatic breast cancer cells. Copy number analysis demonstrated that one allele is genetically deleted in multiple metastatic derivative sublines, while methylation-specific PCR showed that the miR-335 is also epigenetically silenced through promoter hypermethylation (Png et al., 2011).

Png did not find evidence of genomic deletion or promoter hypermethylation in the silencing of miR-126 in highly metastatic breast cancer cells. Work by Png and Claudio Alarcon, a postdoctoral fellow in the laboratory, determined that miR-126 expression is silenced in part due to a defect in its processing. Although highly metastatic cells exhibit low levels of mature miR-126, they possess an increased quantity of pri- and pre-miR-126. The pri form of a microRNA is the initial transcript transcribed by RNA polymerase II. The pri-miRNA is bound by DCGR8 and cleaved by the ribonuclease Drosha to generate the pre-miRNA. The pre-miRNA is then exported from the nucleus. In the cytoplasm, the pre-miRNA is cleaved by Dicer to generate the mature miRNA (Kim, 2005). The expression of pre-miR-126 but not mature miR-126 in the metastatic cells suggests defects in nuclear export of pre-miR-126 or in recognition and cleavage by Dicer. Further work is needed to precisely determine the underlying cause of this processing defect.

Png, Halberg, and I established PITPNC1 as targeted by both miR-126 and miR-335. Future studies will be required to determine if *PTPRN2* and *PLCB1* are directly or indirectly targeted by miR-335. Analysis of the coding sequences and 3'UTRs of *PTPRN2* and *PLCB1* did not reveal any sequences with the required 6-nucleotide complementarity to the 3p arm of miR-335, however several regions showed 5- and 4-

nucleotide complementarity. The miRNA 6-nucleotide seed sequence must be entirely complimentary to the target gene transcript in order for the RISC complex to degrade the transcript (Grimson et al., 2007). However, 4- and 5-nucleotide sequence complementarity is still sufficient for miRNA binding that can inhibit translation through steric hindrance, reducing protein levels of a target gene. Several regions of 6-nucleotide complementarity in both *PTPRN2* and *PLCB1* were identified for the 5' arm of miR-335. Heterologous luciferase reporter assays in conjunction with mutational analysis will be required to determine if miR-335-5p directly targets these genes. Additionally, it cannot be excluded that miR-335 is indirectly regulating expression of these genes through modulation of an RNA binding protein or transcription factor.

Implications for Lipid Regulators in Metastatic Progression

Given the requirement for careful regulation of PIs, it is notable that the expression of *PITPNC1*, *PTPRN2*, and *PLCB1* are all regulated by miRNA-induced translational repression in metastatic breast cancer cells, which results in modulation of gene expression, but not complete depletion or aberrant activation. Cancer cells frequently exhibit dramatic changes that lead to gene silencing, including genetic deletions or epigenetic silencing such as DNA methylation or chromatin modification, or gene activation, such as promoter hypermethylation or gene copy number amplification. Additionally, cancer cells undergo frequent mutations which may repress gene product expression by inducing nonsense-mediated decay of gene transcripts, or increase gene product effects by constitutively activating protein activity. In contrast, miRNA overexpression or silencing decreases or increases gene expression within a small

dynamic range. This modulation of gene expression is particularly important for PI regulator proteins, since the abundance and localization of PIs is tightly controlled within cells.

We have shown that although PITPNC1 binds to PI4P, its binding capacity is weaker than other PI4P binding proteins, such as FAPP1. This potentially allows PITPNC1 to recruit RAB1B to the Golgi without preventing the binding of secretion effector proteins to PI4P, which would disrupt cellular secretion and eventually lead to cell death. Essentially, PITPNC1's weak binding capacity enables it to facilitate secretion without permanently affecting the abundance, localization, or action of PI4P.

Conversely, PTPRN2 and PLCβ1 both deplete PI(4,5)P2. As described above, the enzymatic activity of these proteins must be restricted since PI(4,5)P2 is crucial in other cellular processes. For example, PI(4,5)P2 is the precursor to PI(3,4,5)P3, a key PI in cancer proliferation (Bunney and Katan, 2010). We have shown that PTPRN2 and PLCβ1 deplete PI(4,5P)2 by approximately 30%, leaving remaining lipid for other cellular activities. However, it cannot be excluded that PTPRN2 and PLCβ1-mediated depletion of this lipid may impact other processes in addition to cofilin activation. PI(4,5)P2 is involved in membrane trafficking through both exocytosis and endocytosis (Martin, 2001; Zoncu et al., 2007). PI(4,5)P2 serves as a docking site for proteins involved in Ca^{2+}-triggered vesicle exocytosis, however depletion of this lipid has also been demonstrated to be necessary for secretion in mast cells (Hammond et al., 2006). A similar process has been reported to occur in endocytosis, where PI(4,5)P2 recruits

clathrin or other coat proteins, but the lipid must be removed for vesicle fission to complete (Chang-Ileto et al., 2011). While our findings focus on the role of PTPRN2 and PLCβ1-mediated depletion of PI(4,5)P2 on actin dynamics and migration, they do not exclude other effects on the above cellular processes, which may also contribute to metastatic phenotypes.

Metastatic Secretion

Secretion is a required phenotype in multiple steps of the metastatic cascade, including secretion of proteases to degrade the ECM allowing for cancer cell invasion, and secretion of attractive factors for cancer cell proliferation and angiogenesis. PITPNC's ability to promote metastasis in melanoma, breast, and colon cancers is surprising given the diversity of tissues in the primary site and metastatic site of these cancers. However, the ability to invade, colonize a metastatic niche, and induce angiogenesis is required for metastasis in all solid tumor cancers. In addition to establishing PITPNC1 as a robust mediator of metastatic secretion, we identified Golgi elongation as a previously un-described morphological feature of highly metastatic cells. Given the importance of secretion in the metastatic cascade, enhanced secretion is likely a feature of highly metastatic subpopulations in other solid tumor types, and future studies are needed to determine if Golgi elongation correlates with metastatic capacity across a broad spectrum of cancers.

We identified a set of five proteins that exhibited PITPNC1-dependence for their secretion. However, given the effects of PITPNC1 on Golgi morphology, it is likely that

PITPNC1 affects global secretion in metastatic cells and is not limited to the secretion of a subset of proteins. MMP1, ADAM10, FAM3C, PDGFA, and HTRA were identified in our SILAC secretome as exhibiting the greatest change in secreted abundance upon depletion of PITPNC1, but mass spectrometry identified 40 proteins whose abundance changed by at least 1.5-fold. As this data was collected three years ago, repeating this experiment with improved mass spectrometry protocols and equipment could reveal novel pro-metastatic secreted factors. Furthermore, it would be interesting to determine whether these five proteins serve pro-metastatic functions in melanoma and colon cancer cells, or whether secretome profiling in these cells would reveal a novel set of secreted pro-metastatic proteins.

Golgi elongation is mediated through the actin cytoskeleton, suggesting a secondary role for PTPRN2 and PLCβ1 in mediating metastatic secretion. The weak actin cytoskeleton observed upon depletion of PTPRN2 or PLCβ1, reflecting defects in actin polymerization, would affect tensile forces on the Golgi leading to a condensed Golgi and impairing secretion. Future experiments are needed to measure the length of the Golgi upon PTPRN2 or PLCβ1 depletion and overexpression to determine if Golgi morphology and secretory capacity is a consequence of PI(4,5)P2-mediated actin dynamics. PTPRN2 has been previously demonstrated to regulate insulin secretion in pancreatic beta cells, although the molecular mechanism is unknown (Wasmeier and Hutton, 1996). A possible explanation is that PTPRN2 regulates actin dynamics in these cells through PI(4,5)P2 depletion, altering Golgi morphology to enhance insulin secretion.

Potential for Therapeutic Targeting of PITPNC1, PTPRN2, and PLCβ1

PITPNC1, PTPRN2, and PLCβ1 have the potential to be therapeutically targeted at three levels: restoring miRNA-126 or miR-335 expression, inhibiting the activities of these enzymes, or inhibiting effector proteins downstream of these enzymes. The clinical application of miRNA-based therapies is hindered by the short half-life of miRNAs *in vivo* and difficulties in delivering miRNAs to targeted tissues (Broderick and Zamore, 2011). Even if the miRNA were successfully delivered to target cells, a single dose would not be sufficient to restore sustained miRNA expression and tumor suppression. Instead viral delivery of miRNAs represents a more promising avenue of therapeutic development, as it would allow for continuous restoration of expression. Several studies have demonstrated efficacy of using adeno-associated virus (AAV) to drive expression of a given miRNA, restoring miRNA expression and preventing tumor growth in murine models of liver and lung cancer, as well as preventing metastatic colonization by colon cancer (Kota et al., 2009; Loo et al., 2015; Miyazaki et al., 2012). Viral delivery of miRNAs has the potential to deliver specific and continuous level of expression, however AAV as a delivery vehicle for therapeutic treatments is currently still under clinical development and testing.

Targeting the PITPNC1, PTPRN2, or PLCβ1 directly with small molecular inhibitors represents an additional option for therapeutic targeting. For PITPNC1, a small molecule inhibitor could bind within its PITP domain, preventing PITPNC1's ability to bind PI4P in the Golgi. As we showed in our cell biological experiments, PITPNC1's ability to bind PI4P is critical for its pro-metastatic effects. A study recently identified a

class of small molecules, nitrophenyl(4-(2-methoxyphenyl)piperazin-1-yl)methanones (NPPMs), with the ability to inhibit the PI transfer activity of the major yeast PITP, Sec14 (Nile et al., 2014). *In silico* docking studies projected that the NPPMs bind within Sec14's hydrophobic lipid binding pocket, and NPPM binding would prevent binding of PI or PC. This study represented the first validated inhibitors against PITP domains and established the PITP domain as pharmacologically targetable. Future studies are needed to determine if NPPMs are capable of inhibiting PITPNC1 PI4P-binding activity, but this study creates promise for future drug discovery targeting PITPNC1.

An alternate method of targeting PITPNC1 would be through inhibiting its interaction with 14-3-3 proteins. 14-3-3 proteins bind to PITPNC1, blocking a PEST degradation sequence within PITPNC1's cytoplasmic tail. In the absence of 14-3-3 binding, PITPNC1 has a much shorter half-life in cells. Protein-protein interactions may be inhibited by peptides, but use of peptides as therapeutics faces many challenges including poor metabolic stability, poor cell permeability, and rapid clearance. Inhibiting protein-protein interactions by a small molecule is highly difficult due to the complex structure of proteins compared to the relatively simple structure of small molecules. Surprisingly, one study identified a compound, BV02 (2-(2,3-Dihydro-1,5-dimethyl-3-oxo-2-phenyl-1H-pyrazol-4-yl)-2,3-dihydro-1,3-dioxo-1H-isoindole-5-carboxylic acid), which is able to inhibit the interaction between 14-3-3 and Bcr-Abl protein kinase (Mancini et al., 2011). Screening for compounds that block the PITPNC1-14-3-3 interaction may reveal additional therapeutic targets against PITPNC1.

One possible method to identify small molecule inhibitors of the PITPNC1/14-3-3 interaction in a high-throughput format is an in-cell western assay, which is allows for

quantification of protein levels in whole cells using immunofluorescence. In this assay, cancer cells would be seeded in microtiter plates and incubated with various compounds. After treatment, cells would be fixed, permeabilized, incubated with anti-PITPNC1 and a control antibody, and finally incubated with infrared-conjugated secondary antibodies. An infrared imaging system would measure PIPTNC1 protein levels and control protein levels for normalization. A small molecule that inhibits the 14-3-3 binding to PITPNC1 would be expected to decrease PITPNC1 levels, without changing levels of a control protein or changing cell viability. This screen would identify a set of primary hits, which would be validated for their ability to directly disrupt the PITPNC1/14-3-3 interaction in a biochemical secondary assay. In the secondary assay, we would combine hits from the first screen with purified 14-3-3 protein and a rhodamine-labeled peptide comprising PITPNC1's 14-3-3 binding sequence and measure fluorescence polarization (FP). In cases where a small molecule inhibitor successfully disrupts the PITPNC1 peptide/14-3-3 interaction, the free peptide would exhibit lower FP compared to the larger FP of the peptide/14-3-3 complex.

PITPNC1 regulates the secretion of a set of pro-metastatic and pro-angiogenic proteins, and these proteins also represent potential therapeutic targets. Secreted proteins are therapeutically advantageous compared to intracellular proteins since they may be targeted by systemically administered antibodies. Although antibodies are expensive to produce, they possess a longer half-life and higher specificity than non-biological drugs. One example of a therapeutic antibody targeting a secreted protein is bevacizumab, which binds vascular endothelial growth factor A (VEGF-A) to prevent angiogenesis. However bevacizumab has demonstrated mixed efficacy, prolonging survival in patients

with metastatic colon, lung, or renal cancers, but not breast cancer (Ferrara et al., 2004; Montero et al., 2012). Since PITPNC1 facilitates the secretion of multiple proteins, this treatment approach would require multiple therapeutic antibodies.

Although there are many drugs that inhibit kinases, the discovery of cell permeable and orally bioavailable phosphatase and phospholipase inhibitors has proven a much more difficult task. Several compounds have been discovered that inhibit PTP and PLC domains, although no specific *in vivo* inhibitors for PTPRN2 or PLCβ1 currently exist. Small molecule inhibitors of PTP domains typically mimic the structure of phosphotyrosine, the natural substrate of PTP domains, but are rendered non-hydrolyzable. A popular target for drug discovery is PTP1B, a PTP found to promote Type II diabetes (Johnson et al., 2002). The catalytic site of PTP1B has so far proven intractable to specific small molecule inhibitors due to the highly conserved nature of the PTP domain. Since PTPRN2 contains a non-canonical PTP domain, it may be easier to identify specific inhibitors.

Prior to the discovery of PTPRN2's activity against PI(4,5)P2, one research group "back mutated" several residues in the PTPRN2 catalytic domain to the canonical PTP residues. These mutations created PTP activity, which was used as the readout in a screen for catalytic inhibitors. The group identified derivatives of 2-(oxalylamino)benzoic acid as inhibitors of mutant PTPRN2 recombinant protein (Drake et al., 2003). Future experiments are needed to determine if these compounds inhibit wild-type PTPRN2's lipid phosphatase activity and thus would be candidates for optimization for use *in vivo*.

A potent inhibitor of PLCy, U73122 (1-(6-((17β-3-methoxyestra-1,3,5(10)-trien-17-yl)amino)hexyl)-1H-pyrrole-2,5-dione), has been used in many studies to dissect the role of this enzyme in cellular processes. However, U73122 has little activity against PLCβ1 (Hou et al., 2004), suggesting that the divergence among the PLC family could sufficiently allow for an inhibitor specific to PLCβ1.

Given the importance of cofilin in many cell types, targeting cofilin would be clinically unfeasible. Cells must maintain a balance of cofilin activity in order to maintain their actin cytoskeletons and thus structural integrity. However, our clinical and experimental findings suggest that increasing plasma membrane PI(4,5)P2 may prevent metastasis. One method to achieve this is increasing the activity of PIP5K, although the mechanisms by which PIP5K isoforms are regulated are not well characterized. Overall, PITPNC1, PTPRN2, and PLCβ1 represent viable novel targets for the development of anti-metastatic treatments.

MATERIALS AND METHODS

Animal Experiments

All animal experiments were conducted in accordance to a protocol approved by the Institutional Animal Care and Use Committee at The Rockefeller University. Mice were housed 5 mice/cage at a 12-hour day-night cycle with free access to tap water and food pellets. Six- to eight-week old age-matched female NOD-SCID mice were used for lung and liver metastasis assays. For lung metastatic colonization assays, luciferase reporter-labeled cells at the number indicated were suspended in 100μL PBS and injected via the tail vein. For liver metastasis assays, luciferase reporter-labeled breast cancer cells were resuspended in 50μl of a 1:1 ratio of Matrigel and PBS and injected into the spleens of six-week old age-matched female NOD-SCID mice. After injection into the spleen, a splenectomy was then performed to prevent the growth of a tumor in the spleen. Seven- to eight- week old age-matched female Balb/c mice were used for 4T1 lung metastasis assay.

Lung or liver colonization was measured once per week by non-invasive bioluminescence imaging. Mice were anesthetized and injected retro-orbitally with 100μL luciferin (15 mg/mL). Imaging was performed between 2 and 5 minutes after injection with a Xenogen IVIS system and analyzed with Living Image software (Xenogen).

Cell Lines

The MDA-MB-231 breast cancer cell line and its metastatic derivatives, 293T cells, LS174T-LvM3 colorectal cells, and 4T1 cells were cultured with Dulbecco's modified Eagles' medium (DMEM) supplemented with 10% Fetal Bovine Serum (FBS). LS174T-LvM3 subline was derived from the human LS174 colon cancer line through rounds of *in vivo s*election (Loo et. al., 2015). The MeWo melanoma cell line (ATCC) was maintained according to ATCC guidelines in DMEM supplemented with 10% FBS. BT-549 and HCC-1806 cell lines (ATCC) were maintained according to ATCC guidelines in RPMI medium supplemented with 10% FBS. MDA-MB-468 cells (ATCC) were cultured in DMEM medium containing 10% FBS. Human umbilical vein endothelial cells (HUVEC) (ATCC) were maintained according to ATCC guidelines in EGM-2 media (Lonza) supplemented with 2% FBS.

Cell Transfections

Transient transfection of siRNAs (Integrated DNA Technologies, sequences in Table 6.1) was performed using Lipofectamine 2000 (Life Technologies) according to the manufacturer's protocol. Cells were seeded for invasion and migration assays or subjected to the tail vein metastasis assay 48 hours post-transfection.

Immunofluorescence was conducted 72 hours post-transfection.

Transient transfection of plasmids into cells was conducted using Lipofectamine 2000 according to the manufacturer's protocol. Cells were used for immunofluorescence, migration, or invasion assays 24 hours post-transfection.

Table 6.1. siRNA Sequences

Control	CGUUAUCGCGUAUAUACGCGAU
PITPNC1 #1	CCACAGACGCACCCGAAUU
PITPNC1 #2	CGAUGAAAUUCCAGAGCGC
GOLPH3	GCUUGUGGAAUGAGACGUA
MMP1	GGAGGUAUGAUGAAUAUAA
RAB1B	GCCAGCGAGAACGUCAAU
PTPRN2 #1	CCUACUGAGCGGACAGAAAGAAGCC
PTPRN2 #2	GGCAUUGAGCAAGCUAUGAGGGUCC
PLCB1 #1	CGCUAAGAAAUAAUUGAUGGAGCCA
PLCB1 #2	GGCGUUAAUCAUAAAGAAGCAAGAA
CFL1 #1	GCAAGCAAACUGCUACGAGGAGGUC
CFL1 #2	ACGACAUGAAGGUGCGUAAGUCUUC
CFL1 #3 (3'UTR targeting)	CUCAUGGAAGCAGGACCAGUAAGGG

Generation of Constructs for Knockdown and Overexpression Cell Lines

For generation of retrovirus, 293T cells were seeded onto a 10cm plates. 12μg of Gag/Pol vector, 6μg of VSVG vector, and 12μg of the appropriate plasmid were then co-transfected into the 293T cells using 60μL of Lipofectamine 2000 transfection reagent (Life Technologies) according to the manufacturer's protocol. After 5 hours, the media was replaced with fresh antibiotic-free DMEM supplemented with 10% FBS. At 72 hours post-transfection, the virus was harvested by spinning for 5 min at 400 x g to pellet cellular debris. The supernatant was decanted through a 0.45μm filter.

For generation of lentivirus, 293T cells were transfected using the third generation lentiviral packaging system (Dull et al., 1998). 3μg of each of the 3 packaging vectors

and 9μg of the appropriate shRNA plasmid were transfected into cells using 60μl of Lipofectamine 2000 transfection reagent according to the manufacturer's protocol. The virus was collected as above for lentiviral production.

Cancer cells were transduced with virus in the presence of 10μg/mL of polybrene (Millipore). After 16 hours, the media was changed to DMEM supplemented with 10% FBS and the appropriate antibiotic was added for selection.

Primers used to clone overexpression constructs are listed in Table 6.2. shRNA sequences are listed in Table 6.3. Mutagenesis was performed using QuikChange Lightning Multi Site-Directed Mutagenesis Kit (Agilent Technologies) according to the manufacturer's protocol. Mutagenesis primer sequences are listed in Table 6.4.

The Sac1-K2A construct was a gift from Dr. Peter Mayinger, University of Oregon (Rohde et al., 2003). For PI(4,5)P2 depletion experiments, LYN11-FRB-mcherry (Addgene plasmid # 38004) and PJ-INPP5E (Addgene plasmid # 38001) were gifts from Robin Irvine (Hammond et al., 2012). For cofilin replacement experiments, pEGFP-N1 human cofilin WT was a gift from James Bamburg (Addgene plasmid # 50859) (Garvalov et al., 2007).

Table 6.2. Cloning Primers

PITPNC1 Vector: pBABE-puro	F: CCGGCCTACGTAATGCTGCTGAAAGAGTACCG
	R: CCGGCCGAATTCTTACTCAGATTTGGGCCGACA
PITPNC1-GFP Vector: pBABE-puro	F: CCGGCCAAGCTTATGCTGCTGAAAGAGTACCGG
	R: CCGGCCCTCGAGCTCAGATTTGGGCCGACA
PITPNC1-GST Vector: pGEX-6p-1	F: CCGGCCGAATTCCTGCTGAAAGAGTACCGGATC
	R: CCGGCCCTCGAGTTACTCAGATTTGGGCCGACA
PITPNC1-Flag Vector: pBABE-puro	F: CCGGCCTACGTAATGCTGCTGAAAGAGTACCG
	R:CCGGCCGAATTCTTACTTGTCGTCATCGTCTTTGT AGTCCTCAGATTTGGGCCGACATG
FAPP1-PH Vector: pGEX-6p-1	F: CCGGCCGAATTCATGGAGGGGGTGTTGTACAA
	R:CCGGCCCTCGAGTCACCTTGTATCAGTCAAACAT G
PTPRN2 Vector: pBABE-puro	F: CCGGCCGAATTCGGGCCGCCGCTCCCGCTGCTG
	R: CCGGCCCTCGAGTCACTGGGGAAGGGCCTTGAG
PLCB1 Vector: pBABE-puro	F: CCGGCCTACGTAATGGCCGGGGCTCAACCCGGA
	R: CCGGCCGTCGACTCACAGAGGAGTATCAAATTC
CFL1-Lck Vector: pEGFP-N1	F:CCGGCCGAATTCATGGGATGCGTCTGCTCAAGCG CCTCCGGTGTGGCTGTC
	R:CCGGCCGGATCCCGGGATAACAAAGGCTTGCCCT CCAGGGAG
PIP5K1A C-terminal FLAG Vector: pBABE-puro	F: CCGGCCTACGTAATGGCGTCGGCCTCCTCCGGG
	R:CCGGCCGTCGACTTACTTGTCGTCATCGTCTTTGT AGTCATGGGTGAACTCTGACTCTGC

Table 6.3. shRNA Sequences

Control	CCGGCAACAAGATGAAGAGCACCAACTCGAGTTGGTGCTCTTCATCTTGTTGTTTTT
PITPNC1#1	CCGGCGGGTGTATCTCAACAGCAAACTCGAGTTTGCTGTTGAGATACACCCGTTTTTG
PITPNC1#2	CCGGCAATGGATGAAGTCCGAGAATCTCGAGATTCTCGGACTTCATCCATTGTTTTTG
ADAM10	CCGGGCAGGTTCTATCTGTGAGAAACTCGAGTTTCTCACAGATAGAACCTGCTTTTT
FAM3C	CCGGGATGCAAGTTTAGGAAATCTACTCGAGTAGATTTCCTAAACTTGCATCTTTTTG
HTRA	CCGGCGGTGAAGTGATTGGAATTAACTCGAGTTAATTCCAATCACTTCACCGTTTTTG
PDGFA	CCGGGAATCCGGATTATCGGGAAGACTCGAGTCTTCCCGATAATCCGGATTCTTTTTTG
PTPRN2 #1	CCGGAGGTGCTAAAGAGATTGATATCTCGAGATATCAATCTCTTTAGCACCTTTTTT
PTPRN2 #2	CCGGCGACGATGATAGACTTTACCACTCGAGTGGTAAAGTCTATCATCGTCGTTTTT

Table 6.4. Mutagenesis Primers

PITPNC1 T58E	F:CCCTCACCATGGCAATGGGCAGTTCGAAGAGAAGCGGGTGTATCTCAACAGCA
	R:TGCTGTTGAGATACACCCGCTTCTCTTCGAACTGCCCATTGCCATGGTGAGGG
PITPNC1 N88F	F:ATTTTATGTGACAGAGAAGGCTTGGTTCTATTATCCCTACACAATTACAGAAT
	R:ATTCTGTAATTGTGTAGGGATAATAGAACCAAGCCTTCTCTGTCACATAAAAT
PITPNC1 S274A	F:TCTTCCGTCCGCAGTGCGCCTTCTGCCGCTCCATCCACCCCTCTCTCCACA
	R:TGTGGAGAGAGGGGTGGATGGAGCGGCAGAAGGCGCACTGCGGACGGAAGA
PITPNC1 S299A	F:CCCAAAGATCGGCCCCGGAAAAAGGCCGCCCCAGAAACTCTCACACTTCCA
	R:TGGAAGTGTGAGAGTTTCTGGGGCGGCCTTTTTCCGGGGCCGATCTTTGGG
PTPRN2 C945A	F:GCCGTTCTTGTCCAATAATTGTTCATGCCAGTGACGGTGCAG
	R:CTGCACCGTCACTGGCATGAACAATTATTGGACAAGAACGGC
PLCB1 H331Q	F:ATTTCATTAATTCCTCGCAAAACACCTACCTCACAGCTG
	R:CAGCTGTGAGGTAGGTGTTTTGCGAGGAATTAATGAAAT

RNA Extraction and Real-Time Quantitative PCR (RT-qPCR)

Total RNA was collected from cells using the Total RNA Purification Kit (Norgen Biotek) according to the manufacturer's protocol. For quantification of mRNA,

1μg of total RNA was reverse transcribed using the cDNA First-Strand Synthesis Kit (Life Technologies). Approximately 50ng of the resulting cDNA was then mixed with SYBR green PCR Master Mix (Applied Biosystems) and appropriate primers. Quantitative mRNA expression data was obtained using an ABI Prism 7900HT Real-Time PCR System (Applied Biosystems). HPRT was used as an endogenous control for normalization. Primer sequences are listed in Table 6.5.

Table 6.5. Quantitative PCR Primers

PITPNC1	F: GCGCTACTACAAAGAATCTGAGG
	R: GAGCACATGATAGGCTGATGAC
ADAM10	F: AGCAACATCTGGGGACAAAC
	R: CCCAGGTTTCAGTTTGCATT
FAM3C	F: ATCTCAAAAGCTTGCCCTGA
	R: AAATGGTGCCACATCTCCTC
MMP1	F: AGGTCTCTGAGGGTCAAGCA
	R: AGTTCATGAGCTGCAACACG
HTRA1	F: TGGAATCTCCTTTGCAATCC
	R: CCTTCAGCTCTTTGGCTTTG
PDGFA	F: ACACGAGCAGTGTCAAGTGC
	R: ACCTCACATCCGTGTCCTCT
PTPRN2	F: GGCCAAAGGTGCTAAAGAGA
	R: TGTCAGCGCGAACTCAAA
PLCB1	F: TCTGGAATGCAGGTTGTCAG
	R: GCCACTCTTCCCGTTGTATT
CFL1	F: TGTCAAGATGTGCCAGATAA
	R: GCCCAGAAGATAAACACCAGAT
PIP5K1A	F: CGGCCCGATGATTACTTGTAT
	R: CGTCGCTGGACACATAGAATAG

Matrigel Invasion Assay

Cancer cells were grown to 70% confluence and then the medium was changed to 0.2% FBS DMEM for 16 hours. BioCoat Matrigel invasion chambers (Corning) were hydrated with 0.2% DMEM media for 2 hours prior to use. Cells were seeded into invasion chambers at 50,000 cells per well in quintuplicate and incubated at 37°C for 20 hours. Inserts were rinsed in PBS, and the apical side of the insert was gently scraped to remove non-invaded cells. Inserts were fixed in 4% paraformaldehyde in PBS for 15 minutes at 37°C. The inserts were excised and mounted with VECTASHIELD HardSet Mounting Medium with DAPI (Vector Laboratories). Invaded cells were imaged using an inverted fluorescence microscope (Zeiss Axiovert 40 CFL). Four images at 10X magnification were taken for each insert and quantified using Fiji software.

Endothelial Recruitment Assay

50,000 cancer cells were seeded into 24-well plates approximately 24 hours prior to the start of the assay. HUVEC cells were serum-starved in EGM-2 media (Lonza) supplemented with 0.2% FBS for 20 hours. Cancer cells were washed with PBS and 1 mL 0.2% FBS EGM-2 medium was added to each well. Each well was then fitted with a 3.0μm HTS Fluoroblock trans-well migration insert (BD Falcon). 80,000 HUVECs, resuspended in 0.5 mL of starvation media, were seeded into each insert and incubated at 37°C for 20 hours. The inserts were processed and analyzed as described above for the Matrigel invasion assay.

Trans-well Migration Assay

Cancer cells were grown to 70% confluence and medium changed to 0.2% FBS DMEM media for 16 hours. Cells were seeded into 3.0μm PET trans-well migration inserts (Corning) in quintuplicate at 100,000 cells per well in 0.2% FBS DMEM. Inserts were processed and analyzed as described above for the Matrigel invasion assay.

Scratch Assay

Cancer cells seeded in triplicate were grown to 90% confluence in 6-well plates and then starved for 16 hours in 0.2% FBS DMEM. A scratch through the cell monolayer was made using a 1000μL pipet tip. Four images of each well were taken after the scratch was made (0 h) and 24h later. Images were analyzed using ImageJ (NIH) to quantify the scratch area covered by cancer cells.

Proliferation Assay

20,000 cancer cells were seeded in triplicate for each time point in 6-well plates and counted after 1, 3, and 5 days using a hemocytometer.

Luciferase Reporter Assay

The full-length 3'UTR's and CDS's of *PITPNC1, PTPRN2,* and *PLCB1* were cloned into the psiCheck2 dual luciferase reporter vector (Promega). MDA-MB-231 cells were transfected with the respective specific reporter construct. 30 hours after transfection, the cells were lysed and the ratio of renilla to firefly luciferase expression was determined using the dual luciferase assay (Promega).

Flag Immunoprecipitation

MDA-MB-231 cells retrovirally transduced to express Flag-tagged PITPNC1 were lysed in TNET buffer (50mM Tris, 150mM NaCl, 1mM EDTA, 1% Triton X-100, pH 7.4). Following centrifugation at 20,000 x g for 15 minutes the supernatant was mixed with magnetic anti-flag beads (Sigma) and left to rotate end over end at 4°C for 5 hours. Immunoprecipitated material was washed twice in PBS before eluting the bound protein complexes by addition of 3X Flag peptide (Sigma). Immunoprecipitated material was analyzed by mass spectrometry and western blotting.

Protein Production

cDNA of human PITPNC1 and the FAPP-PH domain was cloned into the pGEX-6P-1 vector (GE Healthcare Biosciences) and transformed into BL21(DE3) cells (Agilent Technologies). Cells were grown in LB medium supplemented with 100μg/mL ampicillin to OD_{600} = 0.6 at 37°C. Isopropyl-B-D-thiogalactaside (IPTG, Sigma) was added to 0.2mM and incubation was continued at 18°C overnight. Cells were collected by centrifugation and resuspended in 50mM Tris-HCl, 150mM NaCl, 2mM DTT, pH 7.5 plus protease inhibitors (Roche). The lysate was sonicated and spun down at 6,000 x g for 20 minutes at 4°C. Protein was further purified from the supernatant using the Pierce GST Spin Purification kit (Thermo Scientific) according to the manufacturer's instructions.

Lipid Overlay Assay

Nitrocellulose membranes were spotted with the indicated lipids (Echelon Biosciences). The membranes were blocked in 3% FFA-free BSA (Sigma-Aldrich) and incubated with 1μg recombinant PITPNC1 protein overnight at 4°C. PITPNC1 was detected using anti-GST antibody (Cell Signaling Technologies) and HRP-conjugated anti-rabbit antibody (Invitrogen).

Liposome Pull-Down Assay

The assay was performed as previously described (He et al., 2009). Solutions of phosphatidylcholine, phosphatidylethanolamine and phosphoinositides (65/24/4) were dried under argon. The lipids were resuspended in lipid transfer buffer (10mM HEPES pH 7.4, 150mM NaCl) for a total 4mM total lipid and incubated at 65°C for 1 hour. The lipids were frozen in liquid nitrogen and thawed at 37°C three times. Resulting liposomes were pelleted by centrifugation at 25,000 x g for 20 minutes at 22°C. Pelleted liposomes were resuspended in lipid transfer buffer and mixed with 4μg recombinant protein. After a 30 minute incubation at room temperature the liposomes were collected by centrifugation (25,000 x g for 20 minutes at 22°C) and levels of PITPNC1 in the supernatant and pellet were detected by SDS-PAGE followed by SimplyBlue staining (Invitrogen). The liposome-bound fraction was determined as PITPNC1 protein levels in the pellet compared to the supernatant.

Immunofluorescence

Immunocytochemical detection of PI4P was performed as previously described (Hammond et al., 2009b). Cells were fixed in 4% paraformaldehyde/PBS for 15 minutes at room temperature, washed, and permeabilized for 5 minutes with 20μM digitonin. Blocking and all subsequent staining steps were carried out in 5% goat serum/PBS. The following primary antibodies were also used: anti-p230 (BD Biosciences), FAPP-PH-GST (recombinant protein), anti-GM130 (BD Biosciences), anti-GOLPH3 (Abcam), anti-RAB1B (Proteintech), anti-TGN46 (AbD Serotec), anti-Flag (Sigma) and anti-GST (Cell Signaling). Cells were rinsed, stained with DAPI (4',6-diamidino-2-phenylindole), and mounted with ProLong Gold (Life Technologies).

Immunocytochemical detection of PI(4,5)P2 was performed as previously described (Hammond et al., 2009b). Cells were fixed in 4% paraformaldehyde, 0.2% glutaraldehyde in PBS for 15 minutes at room temperature, washed, and then chilled on ice. Cells were blocked and permeabilized for 45 minutes in 5% goat serum, 50mM NH4Cl, 0.5% saponin, 20mM Pipes pH 6.8, 137mM NaCl, 2.7mM KCl. Subsequent steps were carried out in this buffer with reduction of saponin to 0.1%. Cells were incubated with anti-PI(4,5)P2 IgM antibody (Echelon Biosciences), followed by Biotinylated anti-IgM antibody (Vector Laboratories), and detected using Streptavidin Alexa Fluor-labeled tertiary antibody (Life Technologies). Cells were post-fixed in 2% paraformaldehyde for 10 minutes on ice, before warming to room temperature. Cells were rinsed, stained with DAPI, and mounted with ProLong Gold (Life Technologies).

For immunocytochemical detection of CFL1 or FLAG, cells were fixed in 4% paraformaldehyde/PBS for 15 minutes at room temperature, rinsed, and permeabilized for

5 minutes with 0.3% Triton-X. Blocking and incubation with antibodies was conducted in 5% goat serum/PBS. Anti-CFL1 antibody (Cell Signaling Technologies) or anti-FLAG (Sigma) was detected using the appropriate Alexa Fluor-labeled secondary antibody (Life Technologies). Cells were stained with DAPI and mounted in ProLong Gold (Life Technologies).

Immunofluorescence of phalloidin was performed using Alexa Fluor-555 and Alexa Fluor-647 Phalloidin (Life Technologies) according to the manufacturer's protocol.

Microscopy

Fluorescence images were acquired on an inverted TC5 SP5 laser scanning confocal microscope. Image analysis was performed using Fiji software.

To measure lipid/protein contents in the *trans* Golgi compartments, the *trans* Golgi markers (p230, TGN46) were thresholded and the magic wand tool (ImageJ) was used to demarcate the trans-Golgi compartments. Mean signal intensity of the lipid/protein was then measured in the demarcated compartment.

Golgi extent was calculated as the length of p230-covered nucleus relative to the nuclear circumference multiplied by 100.

For quantification of released PI4P-containing vesicles in the Golgi exit assay, *trans* Golgi PI4P abundance was subtracted from whole cellular PI4P abundance and divided by the cell area. The data was then normalized to the time 0 value.

To measure mean signal intensity in the membrane compartment, the cell was thresholded and the outline of the cell selected using the magic wand tool. The outline

was reduced by 1μm to form an inner band, and mean signal intensity of this area between the outer and inner band was recorded.

For whole cell phalloidin content, the cell was thresholded and the outline of the cell selected using the magic wand tool. The mean signal intensity of the signal over the area of the cell was recorded.

To measure incorporation of biotin-actin monomers in the barbed end assay, the cell was thresholded in the phalloidin signal channel and the outline of the cell selected using the magic wand tool. The mean signal intensity of the streptavidin signal over the area of the cell was recorded.

Transmission Electron Microscopy

Cells were fixed in 4% paraformaldehyde and 2.5% glutaraldehyde in 0.075M sodium cacodylate buffer pH 7.4 for 30 minutes. Subsequently, cells were washed in the buffer, post-fixed with 1% osmium tetra-oxide for 1 hour, stained en bloc with 2% uranyl acetate for 30 minutes, dehydrated by a graded series of ethanol, depletion of ethanol with propylene oxide, infiltrated with a resin (Electron Microscope Sciences) and embedded with the resin. After polymerization at 60°C for 48 hours, ultra-thin sections were cut, post-stained with 2% uranyl acetate and 1% lead citrate and visualized by electron microscopy (100CX JEOL) with the digital imaging system XR41-C (Advantage Microscopy Technology).

Stable Isotope Labeling of Amino acids in Culture (SILAC) LC-MS/MS Experiment

Cells were grown in DMEM-Flex media contained in the SILAC Protein ID & Quantitation Kit (Invitrogen) for 7 days according to the manufacturer's instructions. Media was changed to serum-free DMEM-Flex media 16 hours prior to collection of conditioned media. Conditioned media was 0.2μM-filtered to remove dead cells, and concentrated 100x using Amicon Ultra-15 centrifugal filter units (Millipore). Reduced and alkylated proteins were separated by 1D gel electrophoresis, stained by SimplyBlue (Invitrogen), and protein bands were excised and trypsinized (Promega), following published protocol (Shevchenko et al., 1996). Extracted peptides were desalted on a trap column following separation using a 12cm/75μm reversed phase C18 column (Nikkyo Technos Co., Ltd.). The resolving gradient, increasing from 10% B to 45% B in 45 minutes (A: 0.1% Formic Acid, B: Acetonitrile/0.1% Formic Acid), was delivered at 300 nL/min. The liquid chromatography setup (Dionex) was connected to an Orbitrap XL (Thermo Scientific) operated in CID top-7-mode. Acquired data was searched against a forward and a reversed (Elias et al., 2005) human data base (ipi.HUMAN v3.87) appended with common contaminants (Bunkenborg et al., 2010) and quantified using MaxQuant version 1.2.2.5 (Cox et al., 2011). Tandem MS data were queried using full tryptic constraint allowing for a maximum of 3 missed cleavages. Oxidation of methiones and N-terminal acetylation of protein was allowed. Cysteines were treated as being fully carbamidomethylated. Matched peptides fulfilling a False Discovery Rate of 1% or lower were accepted as valid matches.

Label Free Quantification LC-MS/MS experiment

Co-immunoprecipitated and 3x-FLAG eluted proteins were trypsinized in-solution overnight. Peptides were desalted using homemade Empore C18 columns prior to being analyzed by LC-MS/MS (Dionex 3000 HPLC coupled to Orbitrap XL, Thermo Scientific). The mass spectrometer was operated in a high/low mode. Peptides were separated at 300nL/min using a gradient increasing from 10% B to 45% B in 120 minutes (A: 0.1% Formic Acid, B: Acetonitrile/0.1% Formic Acid). Generated LC-MS/MS data were queried against UniProt's complete Human Proteome (July 2014) and quantified using MaxQuant 1.5.0.30. In short, Peptide Spectrum Match false discovery rate was set to 1% while protein false discovery rate was set to 1%. A total of 563 proteins were matched. Match between runs were used for the label free quantification. Generated label free quantification values were analyzed using Perseus 1.5.0.9. All LFQ values were log2 transformed and filtered, requiring that a given protein was matched in two of the three replicates. An excellent correlation was measured between replicate samples (r^2 of 0.98 for each condition). Missing LFQ values were imputed (width: 0.3, down shift: 1.8). Differences between the two conditions were assessed by a 2-sample t-test using a permutation based FDR cut-off of $p < 0.05$. In addition to PITPNC1, several 14-3-3 protein isoforms and RAB1B were found to be significantly different between the two samples. RAB1B was matched with 6, 8, and 9 peptide spectrum matches (PSMs) in bait samples versus 2, 1 and 2 PSMs in control.

Western Blot Analysis

Membrane and membrane-associated proteins were isolated from cells using the ProteoExtract native membrane and membrane-associated protein extraction kit (EMD Millipore) according to the manufacturer's instructions. Whole cell lysate was prepared by lysing cells in RIPA buffer containing protease and phosphatase inhibitors (Roche). Conditioned media was collected from cell incubated in serum-free media for 16 hours. Collected media was 0.2μm-filtered to remove dead cells and concentrated 20-fold using spin filter columns (Millipore). Proteins were separated using SDS-PAGE gels (Life Technologies) and transferred to PVDF membrane (Millipore). The following antibodies were used for protein detection: anti-FAM3C (Abcam), anti-MMP1 (Acris Antibodies), anti-HTRA1 (Sigma), anti-PDGFA (Acris Antibodies), anti-ADAM10 (Millipore), anti-RAB1B (Proteintech), anti-GOLPH3 (Abcam), anti-CFL1 (Cell Signaling Technologies,), anti-EGFR (Cell Signaling Technologies), anti-PTPRN2 (Sigma,), anti-PLCB1 (Sigma), anti-β-actin (Sigma), anti-GAPDH (Cell Signaling Technologies). To image loading control proteins, blots were stripped using Restore Western Blot stripping buffer (Thermo Scientific) according to the manufacturer's protocol followed by incubation with appropriate primary antibodies. Bound antibody was detected using the appropriate HRP-conjugated secondary antibodies (Life Technologies). Densitometry analysis of blots was performed using ImageJ (NIH).

Addition of Exogenous PI(4,5)P2

Exogenous PI(4,5)P2 was performed using the Shuttle PIP kit (Echelon Biosciences) according to the manufacturer's instructions. PI(4,5)P2-diC16 and Carrier 2

(Histone H1) were solubilized in water to 500μM concentration. Carrier 2 and PI(4,5)P2 were combined in a 1:1 ratio (100μM concentration each) and incubated for 15 minutes at room temperature. The complex was added to cells for 1 hour at a final concentration of 10μM. Treated cells were then subjected to immunofluorescence, migration, or metastatic colonization assays.

Barbed End Assay

Barbed end assay was performed with slight modifications as previously described (Chan et al., 1998). Biotin-G-actin (Cytoskeleton, Inc.) was prepared as monomers according to the manufacturer's instructions. Permeabilizing buffer was prepared as 20mM Hepes, 138mM KCl, 4mM MgCl2, 3mM EGTA, 0.04 g/L saponin, 1mM ATP, and 1% BSA. Cells were starved for 3 hours in 0% FBS DMEM. Cells were treated with addition of serum for 5 minutes, and then incubated in permeabilizing buffer containing 0.2μM biotin-G-actin for 1 minute at 37°C. Cells were rinsed in PBS and fixed for 15 minutes in 4% paraformaldehyde/PBS. Cells were blocked in 5% goat serum/PBS for 30 minutes, followed by incubation with Streptavidin-conjugated Alexa Fluor-555 and Phalloidin Alex Fluor-647 (Life Technologies) in blocking buffer for 30 minutes. Cells were counter-stained with DAPI and mounted using Prolong Gold (Life Technologies).

Histology

Lungs were prepared by intravenous perfusion of PBS followed by 4% paraformaldehyde/PBS and infusion of paraformaldehyde via the trachea. Removed lungs were embedded in paraffin, sectioned in 5μm thick slices, and stained with hematoxylin and eosin.

Analysis of clinical data sets

Published data generated by the TCGA Research Network (http://cancergenome.nih.gov/)(Cancer Genome Atlas, 2012) was used to obtain RNA-Seq expression values for PTPRN2 and PLCB1 in breast cancer patients. Values were converted to z-scores and averaged to determine the PTPRN2 and PLCB1 combined gene signature. Each sample was classified as positive for the gene signature if the signal was above the median signal for the population.

Published microarray data from GSE17536 was used to obtain probe-level expression values for PITPNC1 in colorectal cancer patients. Each sample was classified as PITPNC1 positive if the signal was above the median signal for the population.
KM Plot data from the breast cancer database (version 2014) (Gyorffy et al., 2010) was analyzed using JetSet probes only (Li et al., 2011a). Expression of each gene was calculated using the auto-selected best cutoff. Each sample was classified as positive for the selected gene expression if the signal was above the designated cutoff.

Statistical analyses and general methods

All statistical analysis was performed using Graphpad Prism 5. For each figure, center bars represent the mean and error bars represent S.E.M. Populations were determined to be normally distributed by the Kolmogorov-Smirnov normality test, and unpaired Student's one-tailed t-test was used to determine significance. F test was performed to compare variances, and Welch's correction was included for populations where the variances differed significantly. For populations where $N < 5$ or populations were not normally distributed, one-tailed Mann-Whitney test was used to determine significance. For Kaplan-Meir survival analysis, a Log-rank (Mantel-Cox) test was used. Symbols were used as follows: $*P < 0.05$, $**P < 0.01$, $***P < 0.001$. $P < 0.05$ was considered statistically significant.

For *in vitro* and cellular experiments, no statistical method was used to predetermine sample size. The investigators were not blinded to allocation during experiments and outcome assessment. *In vitro* experiments and imaging experiments were performed a minimum of three independent times with separate culture preparations and imaged in individual sessions. Western blots were conducted three times using independent sample preparations.

For animal experiments, no statistical method was used to predetermine sample size. The investigators were not blinded to allocation during experiments and outcome assessment. Mice were randomized into groups prior to injection. Pre-established criteria for exclusion included accidental death before completion of the experiment for causes unrelated to the experiment or significant outlier as calculated by sample values greater than two standard deviations from the mean.

REFERENCES

Agranoff, B.W., Bradley, R.M., and Brady, R.O. (1958). The enzymatic synthesis of inositol phosphatide. J Biol Chem *233*, 1077-1083.

Andreasen, P.A., Kjoller, L., Christensen, L., and Duffy, M.J. (1997). The urokinase-type plasminogen activator system in cancer metastasis: a review. Int J Cancer *72*, 1-22.

Andrianantoandro, E., and Pollard, T.D. (2006). Mechanism of actin filament turnover by severing and nucleation at different concentrations of ADF/cofilin. Mol Cell *24*, 13-23.

Apte, S.S., Fukai, N., Beier, D.R., and Olsen, B.R. (1997). The matrix metalloproteinase-14 (MMP-14) gene is structurally distinct from other MMP genes and is co-expressed with the TIMP-2 gene during mouse embryogenesis. J Biol Chem *272*, 25511-25517.

Aslakson, C.J., and Miller, F.R. (1992). Selective events in the metastatic process defined by analysis of the sequential dissemination of subpopulations of a mouse mammary tumor. Cancer Res *52*, 1399-1405.

Balla, A., Tuymetova, G., Barshishat, M., Geiszt, M., and Balla, T. (2002). Characterization of type II phosphatidylinositol 4-kinase isoforms reveals association of the enzymes with endosomal vesicular compartments. J Biol Chem *277*, 20041-20050.

Balla, A., Tuymetova, G., Tsiomenko, A., Varnai, P., and Balla, T. (2005). A plasma membrane pool of phosphatidylinositol 4-phosphate is generated by phosphatidylinositol 4-kinase type-III alpha: studies with the PH domains of the oxysterol binding protein and FAPP1. Mol Biol Cell *16*, 1282-1295.

Balla, T. (2013). Phosphoinositides: tiny lipids with giant impact on cell regulation. Physiol Rev *93*, 1019-1137.

Barford, D., Das, A.K., and Egloff, M.P. (1998). The structure and mechanism of protein phosphatases: insights into catalysis and regulation. Annual review of biophysics and biomolecular structure *27*, 133-164.

Beroukhim, R., Mermel, C.H., Porter, D., Wei, G., Raychaudhuri, S., Donovan, J., Barretina, J., Boehm, J.S., Dobson, J., Urashima, M., *et al*. (2010). The landscape of somatic copy-number alteration across human cancers. Nature *463*, 899-905.

Bonazzi, M., Spano, S., Turacchio, G., Cericola, C., Valente, C., Colanzi, A., Kweon, H.S., Hsu, V.W., Polishchuck, E.V., Polishchuck, R.S., *et al*. (2005). CtBP3/BARS drives membrane fission in dynamin-independent transport pathways. Nat Cell Biol *7*, 570-580.

Broderick, J.A., and Zamore, P.D. (2011). MicroRNA therapeutics. Gene Ther *18*, 1104-1110.

Brown, F.D., Rozelle, A.L., Yin, H.L., Balla, T., and Donaldson, J.G. (2001). Phosphatidylinositol 4,5-bisphosphate and Arf6-regulated membrane traffic. J Cell Biol *154*, 1007-1017.

Bunkenborg, J., Garcia, G.E., Paz, M.I., Andersen, J.S., and Molina, H. (2010). The minotaur proteome: avoiding cross-species identifications deriving from bovine serum in cell culture models. Proteomics *10*, 3040-3044.

Bunney, T.D., and Katan, M. (2010). Phosphoinositide signalling in cancer: beyond PI3K and PTEN. Nat Rev Cancer *10*, 342-352.

Cai, T., Hirai, H., Zhang, G., Zhang, M., Takahashi, N., Kasai, H., Satin, L.S., Leapman, R.D., and Notkins, A.L. (2011). Deletion of Ia-2 and/or Ia-2beta in mice decreases insulin secretion by reducing the number of dense core vesicles. Diabetologia *54*, 2347-2357.

Cancer Genome Atlas, N. (2012). Comprehensive molecular portraits of human breast tumours. Nature *490*, 61-70.

Cao, J., Cai, J., Huang, D., Han, Q., Yang, Q., Li, T., Ding, H., and Wang, Z. (2013). miR-335 represents an invasion suppressor gene in ovarian cancer by targeting Bcl-w. Oncol Rep *30*, 701-706.

Carlsson, A.E. (2006). Stimulation of actin polymerization by filament severing. Biophys J *90*, 413-422.

Caromile, L.A., Oganesian, A., Coats, S.A., Seifert, R.A., and Bowen-Pope, D.F. (2010). The neurosecretory vesicle protein phogrin functions as a phosphatidylinositol phosphatase to regulate insulin secretion. J Biol Chem *285*, 10487-10496.

Chan, A.Y., Bailly, M., Zebda, N., Segall, J.E., and Condeelis, J.S. (2000). Role of cofilin in epidermal growth factor-stimulated actin polymerization and lamellipod protrusion. J Cell Biol *148*, 531-542.

Chan, A.Y., Raft, S., Bailly, M., Wyckoff, J.B., Segall, J.E., and Condeelis, J.S. (1998). EGF stimulates an increase in actin nucleation and filament number at the leading edge of the lamellipod in mammary adenocarcinoma cells. J Cell Sci *111 (Pt 2)*, 199-211.

Chang-Ileto, B., Frere, S.G., Chan, R.B., Voronov, S.V., Roux, A., and Di Paolo, G. (2011). Synaptojanin 1-mediated PI(4,5)P2 hydrolysis is modulated by membrane curvature and facilitates membrane fission. Dev Cell *20*, 206-218.

Cheang, M.C., Chia, S.K., Voduc, D., Gao, D., Leung, S., Snider, J., Watson, M., Davies, S., Bernard, P.S., Parker, J.S., *et al*. (2009). Ki67 index, HER2 status, and prognosis of patients with luminal B breast cancer. J Natl Cancer Inst *101*, 736-750.

Chiang, A.C., and Massague, J. (2008). Molecular basis of metastasis. N Engl J Med *359*, 2814-2823.

Cifuentes, M.E., Honkanen, L., and Rebecchi, M.J. (1993). Proteolytic fragments of phosphoinositide-specific phospholipase C-delta 1. Catalytic and membrane binding properties. J Biol Chem *268*, 11586-11593.

Condeelis, J., and Segall, J.E. (2003). Intravital imaging of cell movement in tumours. Nature Reviews Cancer *3*, 921-930.

Condeelis, J., Singer, R.H., and Segall, J.E. (2005). The great escape: when cancer cells hijack the genes for chemotaxis and motility. Annual review of cell and developmental biology *21*, 695-718.

Conley, M.E., Rohrer, J., and Minegishi, Y. (2000). X-linked agammaglobulinemia. Clinical reviews in allergy & immunology *19*, 183-204.

Cox, J., Neuhauser, N., Michalski, A., Scheltema, R.A., Olsen, J.V., and Mann, M. (2011). Andromeda: a peptide search engine integrated into the MaxQuant environment. J Proteome Res *10*, 1794-1805.

D'Angelo, G., Vicinanza, M., Di Campli, A., and De Matteis, M.A. (2008). The multiple roles of PtdIns(4)P -- not just the precursor of PtdIns(4,5)P2. J Cell Sci *121*, 1955-1963.

De Matteis, M.A., and Luini, A. (2008). Exiting the Golgi complex. Nat Rev Mol Cell Biol *9*, 273-284.

Dippold, H.C., Ng, M.M., Farber-Katz, S.E., Lee, S.K., Kerr, M.L., Peterman, M.C., Sim, R., Wiharto, P.A., Galbraith, K.A., Madhavarapu, S., *et al*. (2009). GOLPH3 bridges phosphatidylinositol-4- phosphate and actomyosin to stretch and shape the Golgi to promote budding. Cell *139*, 337-351.

Dove, S.K., Dong, K., Kobayashi, T., Williams, F.K., and Michell, R.H. (2009). Phosphatidylinositol 3,5-bisphosphate and Fab1p/PIKfyve underPPIn endo-lysosome function. Biochem J *419*, 1-13.

Drake, P.G., Peters, G.H., Andersen, H.S., Hendriks, W., and Moller, N.P. (2003). A novel strategy for the development of selective active-site inhibitors of the protein tyrosine phosphatase-like proteins islet-cell antigen 512 (IA-2) and phogrin (IA-2beta). Biochem J *373*, 393-401.

Dugan, J.M., deWit, C., McConlogue, L., and Maltese, W.A. (1995). The Ras-related GTP-binding protein, Rab1B, regulates early steps in exocytic transport and processing of beta-amyloid precursor protein. J Biol Chem *270*, 10982-10989.

Dull, T., Zufferey, R., Kelly, M., Mandel, R.J., Nguyen, M., Trono, D., and Naldini, L. (1998). A third-generation lentivirus vector with a conditional packaging system. J Virol *72*, 8463-8471.

Dumaresq-Doiron, K., Savard, M.F., Akam, S., Costantino, S., and Lefrancois, S. (2010). The phosphatidylinositol 4-kinase PI4KIIIalpha is required for the recruitment of GBF1 to Golgi membranes. J Cell Sci *123*, 2273-2280.

Egeblad, M., and Werb, Z. (2002). New functions for the matrix metalloproteinases in cancer progression. Nat Rev Cancer *2*, 161-174.

Elias, J.E., Haas, W., Faherty, B.K., and Gygi, S.P. (2005). Comparative evaluation of mass spectrometry platforms used in large-scale proteomics investigations. Nat Methods *2*, 667-675.

Ellis, I.O., Galea, M., Broughton, N., Locker, A., Blamey, R.W., and Elston, C.W. (1992). Pathological prognostic factors in breast cancer. II. Histological type. Relationship with survival in a large study with long-term follow-up. Histopathology *20*, 479-489.

Faenza, I., Matteucci, A., Manzoli, L., Billi, A.M., Aluigi, M., Peruzzi, D., Vitale, M., Castorina, S., Suh, P.G., and Cocco, L. (2000). A role for nuclear phospholipase Cbeta 1 in cell cycle control. J Biol Chem *275*, 30520-30524.

Farmer, H., McCabe, N., Lord, C.J., Tutt, A.N., Johnson, D.A., Richardson, T.B., Santarosa, M., Dillon, K.J., Hickson, I., Knights, C., *et al*. (2005). Targeting the DNA repair defect in BRCA mutant cells as a therapeutic strategy. Nature *434*, 917-921.

Fayngerts, S.A., Wu, J., Oxley, C.L., Liu, X., Vourekas, A., Cathopoulis, T., Wang, Z., Cui, J., Liu, S., Sun, H., *et al*. (2014). TIPE3 is the transfer protein of lipid second messengers that promote cancer. Cancer Cell *26*, 465-478.

Feng, R., Chen, X., Yu, Y., Su, L., Yu, B., Li, J., Cai, Q., Yan, M., Liu, B., and Zhu, Z. (2010). miR-126 functions as a tumour suppressor in human gastric cancer. Cancer Lett *298*, 50-63.

Ferrara, N., Hillan, K.J., Gerber, H.P., and Novotny, W. (2004). Discovery and development of bevacizumab, an anti-VEGF antibody for treating cancer. Nat Rev Drug Discov *3*, 391-400.

Fidler, I.J. (1970). Metastasis: guantitative analysis of distribution and fate of tumor embolilabeled with 125 I-5-iodo-2'-deoxyuridine. J Natl Cancer Inst *45*, 773-782.

Filipowicz, W., Bhattacharyya, S.N., and Sonenberg, N. (2008). Mechanisms of post-transcriptional regulation by microRNAs: are the answers in sight? Nature reviews Genetics *9*, 102-114.

Formolo, C.A., Williams, R., Gordish-Dressman, H., MacDonald, T.J., Lee, N.H., and Hathout, Y. (2011). Secretome signature of invasive glioblastoma multiforme. J Proteome Res *10*, 3149-3159.

Foulkes, W.D., Smith, I.E., and Reis-Filho, J.S. (2010). Triple-negative breast cancer. N Engl J Med *363*, 1938-1948.

Fu, H., Subramanian, R.R., and Masters, S.C. (2000). 14-3-3 proteins: structure, function, and regulation. Annual review of pharmacology and toxicology *40*, 617-647.

Fujiwara, T., Oda, K., Yokota, S., Takatsuki, A., and Ikehara, Y. (1988). Brefeldin A causes disassembly of the Golgi complex and accumulation of secretory proteins in the endoplasmic reticulum. J Biol Chem *263*, 18545-18552.

Gao, H., Chakraborty, G., Lee-Lim, A.P., Mo, Q., Decker, M., Vonica, A., Shen, R., Brogi, E., Brivanlou, A.H., and Giancotti, F.G. (2012). The BMP inhibitor Coco reactivates breast cancer cells at lung metastatic sites. Cell *150*, 764-779.

Garner, K., Hunt, A.N., Koster, G., Somerharju, P., Groves, E., Li, M., Raghu, P., Holic, R., and Cockcroft, S. (2012). Phosphatidylinositol transfer protein, cytoplasmic 1 (PITPNC1) binds and transfers phosphatidic acid. J Biol Chem *287*, 32263-32276.

Garner, K., Li, M., Ugwuanya, N., and Cockcroft, S. (2011). The phosphatidylinositol transfer protein RdgBbeta binds 14-3-3 via its unstructured C-terminus, whereas its lipid-binding domain interacts with the integral membrane protein ATRAP (angiotensin II type I receptor-associated protein). Biochem J *439*, 97-111.

Garvalov, B.K., Flynn, K.C., Neukirchen, D., Meyn, L., Teusch, N., Wu, X., Brakebusch, C., Bamburg, J.R., and Bradke, F. (2007). Cdc42 regulates cofilin during the establishment of neuronal polarity. J Neurosci *27*, 13117-13129.

Ghosh, M., Song, X., Mouneimne, G., Sidani, M., Lawrence, D.S., and Condeelis, J.S. (2004). Cofilin promotes actin polymerization and defines the direction of cell motility. Science *304*, 743-746.

Giancotti, F.G. (2013). Mechanisms governing metastatic dormancy and reactivation. Cell *155*, 750-764.

Gligorijevic, B., Wyckoff, J., Yamaguchi, H., Wang, Y., Roussos, E.T., and Condeelis, J. (2012). N-WASP-mediated invadopodium formation is involved in intravasation and lung metastasis of mammary tumors. J Cell Sci *125*, 724-734.

Godi, A., Di Campli, A., Konstantakopoulos, A., Di Tullio, G., Alessi, D.R., Kular, G.S., Daniele, T., Marra, P., Lucocq, J.M., and De Matteis, M.A. (2004). FAPPs control Golgi-to-cell-surface membrane traffic by binding to ARF and PtdIns(4)P. Nat Cell Biol *6*, 393-404.

Gong, M., Ma, J., Guillemette, R., Zhou, M., Yang, Y., Yang, Y., Hock, J.M., and Yu, X. (2014). miR-335 inhibits small cell lung cancer bone metastases via IGF-IR and RANKL pathways. Molecular cancer research : MCR *12*, 101-110.

Gorbatyuk, V.Y., Nosworthy, N.J., Robson, S.A., Bains, N.P., Maciejewski, M.W., Dos Remedios, C.G., and King, G.F. (2006). Mapping the phosphoinositide-binding site on chick cofilin explains how PIP2 regulates the cofilin-actin interaction. Mol Cell *24*, 511-522.

Grimson, A., Farh, K.K., Johnston, W.K., Garrett-Engele, P., Lim, L.P., and Bartel, D.P. (2007). MicroRNA targeting specificity in mammals: determinants beyond seed pairing. Mol Cell *27*, 91-105.

Gronborg, M., Kristiansen, T.Z., Iwahori, A., Chang, R., Reddy, R., Sato, N., Molina, H., Jensen, O.N., Hruban, R.H., Goggins, M.G., *et al*. (2006). Biomarker discovery from pancreatic cancer secretome using a differential proteomic approach. Mol Cell Proteomics *5*, 157-171.

Guo, C., Sah, J.F., Beard, L., Willson, J.K., Markowitz, S.D., and Guda, K. (2008). The noncoding RNA, miR-126, suppresses the growth of neoplastic cells by targeting phosphatidylinositol 3-kinase signaling and is frequently lost in colon cancers. Genes Chromosomes Cancer *47*, 939-946.

Gyorffy, B., Lanczky, A., Eklund, A.C., Denkert, C., Budczies, J., Li, Q., and Szallasi, Z. (2010). An online survival analysis tool to rapidly assess the effect of 22,277 genes on breast cancer prognosis using microarray data of 1,809 patients. Breast Cancer Res Treat *123*, 725-731.

Haas, A.K., Yoshimura, S., Stephens, D.J., Preisinger, C., Fuchs, E., and Barr, F.A. (2007). Analysis of GTPase-activating proteins: Rab1 and Rab43 are key Rabs required to maintain a functional Golgi complex in human cells. J Cell Sci *120*, 2997-3010.

Hama, H., Schnieders, E.A., Thorner, J., Takemoto, J.Y., and DeWald, D.B. (1999). Direct involvement of phosphatidylinositol 4-phosphate in secretion in the yeast Saccharomyces cerevisiae. J Biol Chem *274*, 34294-34300.

Hamada, S., Satoh, K., Fujibuchi, W., Hirota, M., Kanno, A., Unno, J., Masamune, A., Kikuta, K., Kume, K., and Shimosegawa, T. (2012). MiR-126 acts as a tumor suppressor in pancreatic cancer cells via the regulation of ADAM9. Molecular cancer research : MCR *10*, 3-10.

Hammond, G.R., Dove, S.K., Nicol, A., Pinxteren, J.A., Zicha, D., and Schiavo, G. (2006). Elimination of plasma membrane phosphatidylinositol (4,5)-bisphosphate is required for exocytosis from mast cells. J Cell Sci *119*, 2084-2094.

Hammond, G.R., Fischer, M.J., Anderson, K.E., Holdich, J., Koteci, A., Balla, T., and Irvine, R.F. (2012). PI4P and PI(4,5)P2 are essential but independent lipid determinants of membrane identity. Science *337*, 727-730.

Hammond, G.R., Schiavo, G., and Irvine, R.F. (2009a). Immunocytochemical techniques reveal multiple, distinct cellular pools of PtdIns4P and PtdIns(4,5)P(2). Biochem J *422*, 23-35.

Hammond, G.R., Schiavo, G., and Irvine, R.F. (2009b). Immunocytochemical techniques reveal multiple, distinct cellular pools of PtdIns4P and PtdIns(4,5)P(2). Biochem J *422*, 23-35.

Hanahan, D., and Weinberg, R.A. (2011). Hallmarks of cancer: the next generation. Cell *144*, 646-674.

Haqq, C., Nosrati, M., Sudilovsky, D., Crothers, J., Khodabakhsh, D., Pulliam, B.L., Federman, S., Miller, J.R., 3rd, Allen, R.E., Singer, M.I., *et al*. (2005). The gene expression signatures of melanoma progression. Proc Natl Acad Sci U S A *102*, 6092-6097.

Harris, W.A., and Stark, W.S. (1977). Hereditary retinal degeneration in Drosophila melanogaster. A mutant defect associated with the phototransduction process. J Gen Physiol *69*, 261-291.

He, J., Vora, M., Haney, R.M., Filonov, G.S., Musselman, C.A., Burd, C.G., Kutateladze, A.G., Verkhusha, V.V., Stahelin, R.V., and Kutateladze, T.G. (2009). Membrane insertion of the FYVE domain is modulated by pH. Proteins *76*, 852-860.

Hou, C., Kirchner, T., Singer, M., Matheis, M., Argentieri, D., and Cavender, D. (2004). In vivo activity of a phospholipase C inhibitor, 1-(6-((17beta-3-methoxyestra-1,3,5(10)-trien-17-yl)amino)hexyl)-1H-pyrrole-2,5-di one (U73122), in acute and chronic inflammatory reactions. J Pharmacol Exp Ther *309*, 697-704.

Johnson, T.O., Ermolieff, J., and Jirousek, M.R. (2002). Protein tyrosine phosphatase 1B inhibitors for diabetes. Nat Rev Drug Discov *1*, 696-709.

Joyce, J.A., and Pollard, J.W. (2009). Microenvironmental regulation of metastasis. Nat Rev Cancer *9*, 239-252.

Kallioniemi, O.P., Kallioniemi, A., Kurisu, W., Thor, A., Chen, L.C., Smith, H.S., Waldman, F.M., Pinkel, D., and Gray, J.W. (1992). ERBB2 amplification in breast cancer analyzed by fluorescence in situ hybridization. Proc Natl Acad Sci U S A *89*, 5321-5325.

Kessenbrock, K., Plaks, V., and Werb, Z. (2010). Matrix metalloproteinases: regulators of the tumor microenvironment. Cell *141*, 52-67.

Kim, V.N. (2005). MicroRNA biogenesis: coordinated cropping and dicing. Nat Rev Mol Cell Biol *6*, 376-385.

Kota, J., Chivukula, R.R., O'Donnell, K.A., Wentzel, E.A., Montgomery, C.L., Hwang, H.W., Chang, T.C., Vivekanandan, P., Torbenson, M., Clark, K.R., *et al*. (2009). Therapeutic microRNA delivery suppresses tumorigenesis in a murine liver cancer model. Cell *137*, 1005-1017.

Lan, M.S., Wasserfall, C., Maclaren, N.K., and Notkins, A.L. (1996). IA-2, a transmembrane protein of the protein tyrosine phosphatase family, is a major autoantigen in insulin-dependent diabetes mellitus. Proc Natl Acad Sci U S A *93*, 6367-6370.

Lazaro-Dieguez, F., Jimenez, N., Barth, H., Koster, A.J., Renau-Piqueras, J., Llopis, J.L., Burger, K.N., and Egea, G. (2006). Actin filaments are involved in the maintenance of Golgi cisternae morphology and intra-Golgi pH. Cell motility and the cytoskeleton *63*, 778-791.

Li, Q., Birkbak, N.J., Gyorffy, B., Szallasi, Z., and Eklund, A.C. (2011a). Jetset: selecting the optimal microarray probe set to represent a gene. BMC Bioinformatics *12*, 474.

Li, X., Zhang, Y., Zhang, H., Liu, X., Gong, T., Li, M., Sun, L., Ji, G., Shi, Y., Han, Z., *et al*. (2011b). miRNA-223 promotes gastric cancer invasion and metastasis by targeting tumor suppressor EPB41L3. Molecular cancer research : MCR *9*, 824-833.

Liu, J., Carmell, M.A., Rivas, F.V., Marsden, C.G., Thomson, J.M., Song, J.J., Hammond, S.M., Joshua-Tor, L., and Hannon, G.J. (2004). Argonaute2 is the catalytic engine of mammalian RNAi. Science *305*, 1437-1441.

Liu, P., Cheng, H., Roberts, T.M., and Zhao, J.J. (2009). Targeting the phosphoinositide 3-kinase pathway in cancer. Nat Rev Drug Discov *8*, 627-644.

Loo, J.M., Scherl, A., Nguyen, A., Man, F.Y., Weinberg, E., Zeng, Z., Saltz, L., Paty, P.B., and Tavazoie, S.F. (2015). Extracellular metabolic energetics can promote cancer progression. Cell *160*, 393-406.

Lu, J., Li, Q., Xie, H., Chen, Z.J., Borovitskaya, A.E., Maclaren, N.K., Notkins, A.L., and Lan, M.S. (1996). Identification of a second transmembrane protein tyrosine phosphatase, IA-2 beta, as an autoantigen in insulin-dependent diabetes mellitus: Precursor of the 37-kDa tryptic fragment. P Natl Acad Sci USA *93*, 2307-2311.

Lu, P., Weaver, V.M., and Werb, Z. (2012). The extracellular matrix: a dynamic niche in cancer progression. J Cell Biol *196*, 395-406.

Luo, J.M., Yoshida, H., Komura, S., Ohishi, N., Pan, L., Shigeno, K., Hanamura, I., Miura, K., Iida, S., Ueda, R., *et al*. (2003). Possible dominant-negative mutation of the SHIP gene in acute myeloid leukemia. Leukemia *17*, 1-8.

Magistrelli, G., Toma, S., and Isacchi, A. (1996). Substitution of two variant residues in the protein tyrosine phosphatase-like PTP35/IA-2 sequence reconstitutes catalytic activity. Biochem Biophys Res Commun *227*, 581-588.

Mancini, M., Corradi, V., Petta, S., Barbieri, E., Manetti, F., Botta, M., and Santucci, M.A. (2011). A new nonpeptidic inhibitor of 14-3-3 induces apoptotic cell death in chronic myeloid leukemia sensitive or resistant to imatinib. J Pharmacol Exp Ther *336*, 596-604.

Martin, T.F. (2001). PI(4,5)P(2) regulation of surface membrane traffic. Curr Opin Cell Biol *13*, 493-499.

Martoglio, A.M., Tom, B.D., Starkey, M., Corps, A.N., Charnock-Jones, D.S., and Smith, S.K. (2000). Changes in tumorigenesis- and angiogenesis-related gene transcript abundance profiles in ovarian cancer detected by tailored high density cDNA arrays. Molecular medicine *6*, 750-765.

Mayinger, P. (2012). Phosphoinositides and vesicular membrane traffic. Biochim Biophys Acta *1821*, 1104-1113.

Mehta, Z.B., Pietka, G., and Lowe, M. (2014). The cellular and physiological functions of the Lowe syndrome protein OCRL1. Traffic *15*, 471-487.

Milligan, S.C., Alb, J.G., Jr., Elagina, R.B., Bankaitis, V.A., and Hyde, D.R. (1997). The phosphatidylinositol transfer protein domain of Drosophila retinal degeneration B protein is essential for photoreceptor cell survival and recovery from light stimulation. J Cell Biol *139*, 351-363.

Minn, A.J., Gupta, G.P., Siegel, P.M., Bos, P.D., Shu, W., Giri, D.D., Viale, A., Olshen, A.B., Gerald, W.L., and Massague, J. (2005). Genes that mediate breast cancer metastasis to lung. Nature *436*, 518-524.

Miyazaki, Y., Adachi, H., Katsuno, M., Minamiyama, M., Jiang, Y.M., Huang, Z., Doi, H., Matsumoto, S., Kondo, N., Iida, M., *et al*. (2012). Viral delivery of miR-196a ameliorates the SBMA phenotype via the silencing of CELF2. Nat Med *18*, 1136-1141.

Moasser, M.M. (2007). The oncogene HER2: its signaling and transforming functions and its role in human cancer pathogenesis. Oncogene *26*, 6469-6487.

Monetta, P., Slavin, I., Romero, N., and Alvarez, C. (2007). Rab1b interacts with GBF1 and modulates both ARF1 dynamics and COPI association. Mol Biol Cell *18*, 2400-2410.

Montero, A.J., Escobar, M., Lopes, G., Gluck, S., and Vogel, C. (2012). Bevacizumab in the treatment of metastatic breast cancer: friend or foe? Current oncology reports *14*, 1-11.

Mosesson, Y., Mills, G.B., and Yarden, Y. (2008). Derailed endocytosis: an emerging feature of cancer. Nat Rev Cancer *8*, 835-850.

Naba, A., Clauser, K.R., Lamar, J.M., Carr, S.A., and Hynes, R.O. (2014). Extracellular matrix signatures of human mammary carcinoma identify novel metastasis promoters. eLife *3*, e01308.

Nash, G.F., Turner, L.F., Scully, M.F., and Kakkar, A.K. (2002). Platelets and cancer. The Lancet Oncology *3*, 425-430.

Nile, A.H., Tripathi, A., Yuan, P., Mousley, C.J., Suresh, S., Wallace, I.M., Shah, S.D., Pohlhaus, D.T., Temple, B., Nislow, C., *et al*. (2014). PITPs as targets for selectively interfering with phosphoinositide signaling in cells. Nat Chem Biol *10*, 76-84.

Ojala, P.J., Paavilainen, V., and Lappalainen, P. (2001). Identification of yeast cofilin residues specific for actin monomer and PIP2 binding. Biochemistry *40*, 15562-15569.

Ozaki, S., DeWald, D.B., Shope, J.C., Chen, J., and Prestwich, G.D. (2000). Intracellular delivery of phosphoinositides and inositol phosphates using polyamine carriers. Proc Natl Acad Sci U S A *97*, 11286-11291.

Paget, S. (1889). The distribution of secondary growths in cancer of the breast. 1889. Cancer Metastasis Rev *8*, 98-101.

Patarroyo, M., Tryggvason, K., and Virtanen, I. (2002). Laminin isoforms in tumor invasion, angiogenesis and metastasis. Semin Cancer Biol *12*, 197-207.

Pencheva, N., Tran, H., Buss, C., Huh, D., Drobnjak, M., Busam, K., and Tavazoie, S.F. (2012). Convergent multi-miRNA targeting of ApoE drives LRP1/LRP8-dependent melanoma metastasis and angiogenesis. Cell *151*, 1068-1082.

Perl, A.K., Wilgenbus, P., Dahl, U., Semb, H., and Christofori, G. (1998). A causal role for E-cadherin in the transition from adenoma to carcinoma. Nature *392*, 190-193.

Perou, C.M., Sorlie, T., Eisen, M.B., van de Rijn, M., Jeffrey, S.S., Rees, C.A., Pollack, J.R., Ross, D.T., Johnsen, H., Akslen, L.A., *et al*. (2000). Molecular portraits of human breast tumours. Nature *406*, 747-752.

Plutner, H., Cox, A.D., Pind, S., Khosravi-Far, R., Bourne, J.R., Schwaninger, R., Der, C.J., and Balch, W.E. (1991). Rab1b regulates vesicular transport between the endoplasmic reticulum and successive Golgi compartments. J Cell Biol *115*, 31-43.

Png, K.J., Halberg, N., Yoshida, M., and Tavazoie, S.F. (2012). A microRNA regulon that mediates endothelial recruitment and metastasis by cancer cells. Nature *481*, 190-194.

Png, K.J., Yoshida, M., Zhang, X.H., Shu, W., Lee, H., Rimner, A., Chan, T.A., Comen, E., Andrade, V.P., Kim, S.W., *et al*. (2011). MicroRNA-335 inhibits tumor reinitiation and is silenced through genetic and epigenetic mechanisms in human breast cancer. Genes Dev *25*, 226-231.

Pollack, V.A., and Fidler, I.J. (1982). Use of young nude mice for selection of subpopulations of cells with increased metastatic potential from nonsyngeneic neoplasms. J Natl Cancer Inst *69*, 137-141.

Polyak, K. (2011). Heterogeneity in breast cancer. J Clin Invest *121*, 3786-3788.

Psaila, B., and Lyden, D. (2009). The metastatic niche: adapting the foreign soil. Nat Rev Cancer *9*, 285-293.

Rakha, E.A., and Ellis, I.O. (2009). Triple-negative/basal-like breast cancer: review. Pathology *41*, 40-47.

Ramazzotti, G., Faenza, I., Gaboardi, G.C., Piazzi, M., Bavelloni, A., Fiume, R., Manzoli, L., Martelli, A.M., and Cocco, L. (2008). Catalytic activity of nuclear PLC-beta(1) is required for its signalling function during C2C12 differentiation. Cell Signal *20*, 2013-2021.

Rebecchi, M.J., and Pentyala, S.N. (2000). Structure, function, and control of phosphoinositide-specific phospholipase C. Physiol Rev *80*, 1291-1335.

Rhee, S.G. (2001). Regulation of phosphoinositide-specific phospholipase C. Annual review of biochemistry *70*, 281-312.

Rohde, H.M., Cheong, F.Y., Konrad, G., Paiha, K., Mayinger, P., and Boehmelt, G. (2003). The human phosphatidylinositol phosphatase SAC1 interacts with the coatomer I complex. J Biol Chem *278*, 52689-52699.

Romero, N., Dumur, C.I., Martinez, H., Garcia, I.A., Monetta, P., Slavin, I., Sampieri, L., Koritschoner, N., Mironov, A.A., De Matteis, M.A., *et al*. (2013). Rab1b overexpression modifies Golgi size and gene expression in HeLa cells and modulates the thyrotrophin response in thyroid cells in culture. Mol Biol Cell *24*, 617-632.

Saarikangas, J., Zhao, H., and Lappalainen, P. (2010). Regulation of the actin cytoskeleton-plasma membrane interplay by phosphoinositides. Physiol Rev *90*, 259-289.

Sahai, E., and Marshall, C.J. (2002). RHO-GTPases and cancer. Nat Rev Cancer *2*, 133-142.

Samuels, Y., Wang, Z., Bardelli, A., Silliman, N., Ptak, J., Szabo, S., Yan, H., Gazdar, A., Powell, S.M., Riggins, G.J., *et al*. (2004). High frequency of mutations of the PIK3CA gene in human cancers. Science *304*, 554.

Scott, K.L., Kabbarah, O., Liang, M.C., Ivanova, E., Anagnostou, V., Wu, J., Dhakal, S., Wu, M., Chen, S., Feinberg, T., *et al*. (2009). GOLPH3 modulates mTOR signalling and rapamycin sensitivity in cancer. Nature *459*, 1085-1090.

Shevchenko, A., Wilm, M., Vorm, O., and Mann, M. (1996). Mass spectrometric sequencing of proteins silver-stained polyacrylamide gels. Anal Chem *68*, 850-858.

Simonsen, A., Lippe, R., Christoforidis, S., Gaullier, J.M., Brech, A., Callaghan, J., Toh, B.H., Murphy, C., Zerial, M., and Stenmark, H. (1998). EEA1 links PI(3)K function to Rab5 regulation of endosome fusion. Nature *394*, 494-498.

Slamon, D.J., Clark, G.M., Wong, S.G., Levin, W.J., Ullrich, A., and McGuire, W.L. (1987). Human breast cancer: correlation of relapse and survival with amplification of the HER-2/neu oncogene. Science *235*, 177-182.

Slamon, D.J., Leyland-Jones, B., Shak, S., Fuchs, H., Paton, V., Bajamonde, A., Fleming, T., Eiermann, W., Wolter, J., Pegram, M., *et al*. (2001). Use of chemotherapy plus a monoclonal antibody against HER2 for metastatic breast cancer that overexpresses HER2. N Engl J Med *344*, 783-792.

Smid, M., Wang, Y., Zhang, Y., Sieuwerts, A.M., Yu, J., Klijn, J.G., Foekens, J.A., and Martens, J.W. (2008). Subtypes of breast cancer show preferential site of relapse. Cancer Res *68*, 3108-3114.

Smith, I.E., and Dowsett, M. (2003). Aromatase inhibitors in breast cancer. N Engl J Med *348*, 2431-2442.

Smrcka, A.V., Hepler, J.R., Brown, K.O., and Sternweis, P.C. (1991). Regulation of polyphosphoinositide-specific phospholipase C activity by purified Gq. Science *251*, 804-807.

Sorlie, T., Perou, C.M., Tibshirani, R., Aas, T., Geisler, S., Johnsen, H., Hastie, T., Eisen, M.B., van de Rijn, M., Jeffrey, S.S., *et al*. (2001). Gene expression patterns of breast carcinomas distinguish tumor subclasses with clinical implications. Proc Natl Acad Sci U S A *98*, 10869-10874.

Sorokin, A.V., Nair, B.C., Wei, Y., Aziz, K.E., Evdokimova, V., Hung, M.C., and Chen, J. (2015). Aberrant Expression of proPTPRN2 in Cancer Cells Confers Resistance to Apoptosis. Cancer Res *75*, 1846-1858.

Sotiriou, C., and Pusztai, L. (2009). Gene-expression signatures in breast cancer. N Engl J Med *360*, 790-800.

Suh, B.C., and Hille, B. (2008). PIP2 is a necessary cofactor for ion channel function: how and why? Annual review of biophysics *37*, 175-195.

Takano, N., Owada, Y., Suzuki, R., Sakagami, H., Shimosegawa, T., and Kondo, H. (2003). Cloning and characterization of a novel variant (mM-rdgBbeta1) of mouse M-rdgBs, mammalian homologs of Drosophila retinal degeneration B gene proteins, and its mRNA localization in mouse brain in comparison with other M-rdgBs. J Neurochem *84*, 829-839.

Tavazoie, S.F., Alarcon, C., Oskarsson, T., Padua, D., Wang, Q., Bos, P.D., Gerald, W.L., and Massague, J. (2008). Endogenous human microRNAs that suppress breast cancer metastasis. Nature *451*, 147-152.

Taylor, S.J., Chae, H.Z., Rhee, S.G., and Exton, J.H. (1991). Activation of the beta 1 isozyme of phospholipase C by alpha subunits of the Gq class of G proteins. Nature *350*, 516-518.

Tilley, S.J., Skippen, A., Murray-Rust, J., Swigart, P.M., Stewart, A., Morgan, C.P., Cockcroft, S., and McDonald, N.Q. (2004). Structure-function analysis of human [corrected] phosphatidylinositol transfer protein alpha bound to phosphatidylinositol. Structure *12*, 317-326.

Tsujita, K., Itoh, T., Ijuin, T., Yamamoto, A., Shisheva, A., Laporte, J., and Takenawa, T. (2004). Myotubularin regulates the function of the late endosome through the gram domain-phosphatidylinositol 3,5-bisphosphate interaction. J Biol Chem *279*, 13817-13824.

Turhani, D., Krapfenbauer, K., Thurnher, D., Langen, H., and Fountoulakis, M. (2006). Identification of differentially expressed, tumor-associated proteins in oral squamous cell carcinoma by proteomic analysis. Electrophoresis *27*, 1417-1423.

Unwin, R.D., Craven, R.A., Harnden, P., Hanrahan, S., Totty, N., Knowles, M., Eardley, I., Selby, P.J., and Banks, R.E. (2003). Proteomic changes in renal cancer and co-ordinate demonstration of both the glycolytic and mitochondrial aspects of the Warburg effect. Proteomics *3*, 1620-1632.

Valente, C., Turacchio, G., Mariggio, S., Pagliuso, A., Gaibisso, R., Di Tullio, G., Santoro, M., Formiggini, F., Spano, S., Piccini, D., *et al*. (2012). A 14-3-3gamma dimer-based scaffold bridges CtBP1-S/BARS to PI(4)KIIIbeta to regulate post-Golgi carrier formation. Nat Cell Biol *14*, 343-354.

van den Bout, I., and Divecha, N. (2009). PIP5K-driven PtdIns(4,5)P2 synthesis: regulation and cellular functions. J Cell Sci *122*, 3837-3850.

van Rheenen, J., Song, X., van Roosmalen, W., Cammer, M., Chen, X., Desmarais, V., Yip, S.C., Backer, J.M., Eddy, R.J., and Condeelis, J.S. (2007). EGF-induced PIP2 hydrolysis releases and activates cofilin locally in carcinoma cells. J Cell Biol *179*, 1247-1259.

Venter, D.J., Tuzi, N.L., Kumar, S., and Gullick, W.J. (1987). Overexpression of the c-erbB-2 oncoprotein in human breast carcinomas: immunohistological assessment correlates with gene amplification. Lancet *2*, 69-72.

Vicinanza, M., D'Angelo, G., Di Campli, A., and De Matteis, M.A. (2008). Function and dysfunction of the PI system in membrane trafficking. EMBO J *27*, 2457-2470.

Vu, T.H., and Werb, Z. (2000). Matrix metalloproteinases: effectors of development and normal physiology. Genes Dev *14*, 2123-2133.

Wang, W., Eddy, R., and Condeelis, J. (2007). The cofilin pathway in breast cancer invasion and metastasis. Nat Rev Cancer *7*, 429-440.

Wang, W., Goswami, S., Lapidus, K., Wells, A.L., Wyckoff, J.B., Sahai, E., Singer, R.H., Segall, J.E., and Condeelis, J.S. (2004). Identification and testing of a gene

expression signature of invasive carcinoma cells within primary mammary tumors. Cancer Res *64*, 8585-8594.

Wang, X., Tang, S., Le, S.Y., Lu, R., Rader, J.S., Meyers, C., and Zheng, Z.M. (2008). Aberrant expression of oncogenic and tumor-suppressive microRNAs in cervical cancer is required for cancer cell growth. PLoS One *3*, e2557.

Wang, Y.J., Wang, J., Sun, H.Q., Martinez, M., Sun, Y.X., Macia, E., Kirchhausen, T., Albanesi, J.P., Roth, M.G., and Yin, H.L. (2003). Phosphatidylinositol 4 phosphate regulates targeting of clathrin adaptor AP-1 complexes to the Golgi. Cell *114*, 299-310.

Wasmeier, C., and Hutton, J.C. (1996). Molecular cloning of phogrin, a protein-tyrosine phosphatase homologue localized to insulin secretory granule membranes. Journal of Biological Chemistry *271*, 18161-18170.

Wilson, P.M., Labonte, M.J., and Lenz, H.J. (2010). Molecular markers in the treatment of metastatic colorectal cancer. Cancer journal *16*, 262-272.

Winter, J., Jung, S., Keller, S., Gregory, R.I., and Diederichs, S. (2009). Many roads to maturity: microRNA biogenesis pathways and their regulation. Nat Cell Biol *11*, 228-234.

Wong, C.C., Wong, C.M., Tung, E.K., Au, S.L., Lee, J.M., Poon, R.T., Man, K., and Ng, I.O. (2011). The microRNA miR-139 suppresses metastasis and progression of hepatocellular carcinoma by down-regulating Rho-kinase 2. Gastroenterology *140*, 322-331.

Wyckoff, J., Wang, W., Lin, E.Y., Wang, Y., Pixley, F., Stanley, E.R., Graf, T., Pollard, J.W., Segall, J., and Condeelis, J. (2004). A paracrine loop between tumor cells and macrophages is required for tumor cell migration in mammary tumors. Cancer Res *64*, 7022-7029.

Yabuta, T., Shinmura, K., Tani, M., Yamaguchi, S., Yoshimura, K., Katai, H., Nakajima, T., Mochiki, E., Tsujinaka, T., Takami, M.*, et al*. (2002). E-cadherin gene variants in gastric cancer families whose probands are diagnosed with diffuse gastric cancer. Int J Cancer *101*, 434-441.

Yamaguchi, H., Yoshida, S., Muroi, E., Kawamura, M., Kouchi, Z., Nakamura, Y., Sakai, R., and Fukami, K. (2010). Phosphatidylinositol 4,5-bisphosphate and PIP5-kinase Ialpha are required for invadopodia formation in human breast cancer cells. Cancer Sci *101*, 1632-1638.

Yan, Z., Xiong, Y., Xu, W., Gao, J., Cheng, Y., Wang, Z., Chen, F., and Zheng, G. (2012). Identification of hsa-miR-335 as a prognostic signature in gastric cancer. PLoS One *7*, e40037.

Yanaihara, N., Caplen, N., Bowman, E., Seike, M., Kumamoto, K., Yi, M., Stephens, R.M., Okamoto, A., Yokota, J., Tanaka, T., *et al*. (2006). Unique microRNA molecular profiles in lung cancer diagnosis and prognosis. Cancer Cell *9*, 189-198.

Yeo, B., Turner, N.C., and Jones, A. (2014). An update on the medical management of breast cancer. BMJ *348*, g3608.

Yoder, M.D., Thomas, L.M., Tremblay, J.M., Oliver, R.L., Yarbrough, L.R., and Helmkamp, G.M., Jr. (2001). Structure of a multifunctional protein. Mammalian phosphatidylinositol transfer protein complexed with phosphatidylcholine. J Biol Chem *276*, 9246-9252.

Yonezawa, N., Homma, Y., Yahara, I., Sakai, H., and Nishida, E. (1991). A Short Sequence Responsible for Both Phosphoinositide Binding and Actin Binding Activities of Cofilin. Journal of Biological Chemistry *266*, 17218-17221.

Zlatkine, P., Mehul, B., and Magee, A.I. (1997). Retargeting of cytosolic proteins to the plasma membrane by the Lck protein tyrosine kinase dual acylation motif. J Cell Sci *110 (Pt 5)*, 673-679.

Zoncu, R., Perera, R.M., Sebastian, R., Nakatsu, F., Chen, H., Balla, T., Ayala, G., Toomre, D., and De Camilli, P.V. (2007). Loss of endocytic clathrin-coated pits upon acute depletion of phosphatidylinositol 4,5-bisphosphate. Proc Natl Acad Sci U S A *104*, 3793-3798.

The American Cancer Society, Key Statistics in Breast Cancer. (2015). <http://www.cancer.org/cancer/breastcancer/detailedguide/breast-cancer-key-statistics>.

National Cancer Institute, Surveillance Epidemiology, and End Results Program. SEER Stat Fact Sheets: Breast Cancer. (2015). <http://seer.cancer.gov/statfacts/html/breast.html>.